

**LABORATORY ANALYSIS OF SETTLING VELOCITIES OF
WASTEWATER PARTICLES IN SEAWATER
USING HOLOGRAPHY**

Thesis by

Rueen-Fang Theresa Wang

In Partial Fulfillment of the Requirements

for the Degree of

Doctor of Philosophy

California Institute of Technology

Pasadena, California

1988

Submitted May 23, 1988

© 1988

Rueen-Fang Theresa Wang

All rights reserved

ACKNOWLEDGMENTS

First and foremost, I would like to thank my advisor, Professor Norman H. Brooks. This dissertation would never have come to be without his supporting and guiding hand. Also, I would like to thank Dr. Robert C. Y. Koh for his stimulating discussions and many constructive suggestions and criticisms. The following professors kindly serve on my examination committee: Allan J. Acosta, Richard C. Flagan, E. John List and James J. Morgan. I thank them for their time and help through my course of study.

Appreciation also goes to Dr. Tim J. O'Hern who taught me the experimental techniques of holography and helped me started on the design of my own system. I would like to thank John Yee-Keung Ngai, my best friend at Caltech. His friendship and words of encouragement helped me through the most difficult time in my study. Technically, he introduced me to the fancy world of computation, discussed my problems, and made available to me his computer for my research work. I am grateful to my brothers, Yuan-Fang and Jih-Fang, who taught me the fundamentals of digital image processing and helped me build the interface and image analysis routines which greatly simplified the image processing task in this research.

The assistance of Elton Daly, Joe Fontana, Rich Eastvedt and Hai Duc Vu at the Keck Lab Shop is of particular importance in the construction and troubleshooting of the experimental apparatus. The continuing friendship and help of Joan Mathews, Luise Betterton, Rayma Harrison, Gunilla Hastrup, Elaine Granger, and Sandy Brooks are greatly valued. I would like to thank Nancy Tomer, whose professional skill and agreeable personality make my thesis preparation much easier. I also thank personnel of the County Sanitation Districts of Orange and Los Angeles Counties for providing sludge and effluent samples. Special thanks go to Professor

Nobuo Mimura for his interest in this work as well as his valuable discussions and suggestions. For all my friends and colleagues, especially Liyuan Liang and David Walker, I thank them for their support and understanding.

I gratefully acknowledge the financial support provided by the United States National Oceanic and Atmospheric Administration (Grants no.NA80RAD0055 and NA81RAC00153), the County Sanitation Districts of Orange County, the County Sanitation Districts of Los Angeles County, the Andrew W. Mellon Foundation, the William and Flora Hewlett Foundation and EQL gifts.

I cannot express in words my feeling for my family whose love and devotion never fail to encourage me and propel me through my study, and to whom, I dedicate this dissertation.

ABSTRACT

Ocean discharge of treated sewage and digested sludge has been a common practice for the disposal of municipal and industrial wastewaters for years. Since the particles in the discharge cause much of the adverse effect on the marine environment, the transport processes and the final destinations of particles and the associated pollutants have to be studied to evaluate the environmental impact and the feasibility of disposal processes. The settling velocity of particles and the possible coagulation inside the discharge plume are among the most important factors that control the transport of particles.

A holographic camera system was developed to study the settling characteristics of sewage and sludge particles in seawater after simulated plume mixing with possible coagulation. Particles were first mixed and diluted in a laboratory reactor, which was designed to simulate the mixing conditions inside a rising plume by varying the particle concentration and turbulent shear rate according to predetermined scenarios. Samples were then withdrawn from the reactor at different times for size and settling velocity measurements. Artificial seawater without suspended particles was used for dilution.

An in-line laser holographic technique was employed to measure the size distributions and the settling velocities of the particles. Doubly exposed holograms were used to record the images of particles for the fall velocity measurement. Images of individual particles were reconstructed and displayed on a video monitor. The images were then digitized by computer for calculating the equivalent diameter, the position of the centroid, the deviations along the principal axes, and the orientation of particles. A special analysis procedure was developed to eliminate sampling biases in the computation of cumulative frequency distributions. The principal advantages of this new technique over the conventional settling column (used in the early part of this research) are that: (1) the coagulation and settling processes can be uncoupled by use of extremely small concentrations (less than 2 mg/l) in the

holographic sample cell, and (2) the individual particle sizes and shapes can be observed for correlation with measured fall velocities.

Four sets of experiments were conducted with blended primary/secondary effluent from the County Sanitation Districts of Los Angeles County and the digested primary sludge from the County Sanitation Districts of Orange County (proposed deep ocean outfall) using different mixing processes. Experimental results show that the sludge and effluent particles have very similar settling characteristics, and that particle coagulation is small under the simulated plume mixing conditions used in these experiments. The median and 90-percentile fall velocities and the fractions of particles with fall velocities larger than 0.01 *cm/sec* of the digested primary sludge and the effluent are summarized in the following table. The experimental results from the conventional settling column are also included for comparison. In general, the holographic technique indicates slower settling velocities than all the previous investigations by other procedures.

Sample Description	median <i>w</i> <i>cm/sec</i>	90%ile <i>w</i> <i>cm/sec</i>	% with <i>w</i> > 0.01 <i>cm/sec</i>
Measurements by the holographic technique			
Digested primary sludge, CSDOC	0.0004	0.003	2.5
Effluent, CSDLAC	< 0.0001	0.001	1.7
Measurements by the conventional settling column (average)			
Digested primary sludge, CSDOC (at 500:1 dilution)	0.0002 – 0.002	0.04 – 0.05	14 – 43

TABLE OF CONTENTS

<i>Acknowledgments</i>	iii
<i>Abstract</i>	v
<i>List of Tables</i>	xi
<i>List of Figures</i>	xiii
<i>Notation</i>	xx
1. Introduction	1
2. Literature Review	6
2.1 Particle Coagulation inside a Plume	6
2.1.1 Turbulence Coagulation	8
2.1.2 Floc Breakup by Turbulence	15
2.1.3 Coagulating Reactor	18
2.2 Settling Velocity Measurements	21
2.2.1 Experimental Technique	22
2.2.2 Settling Velocity Measurements for Sewage Particles	23
2.2.3 Data Interpretation for Settling Column Measurements with Particle Coagulation	26
2.2.4 Conventional Settling Column Experiment	28
2.2.5 Velocity Measurement by Holographic Technique	31
2.3 Summary	33
3. Experimental Setup and Procedures	34
3.1 Design of the Coagulating Reactor	35
3.1.1 Time History of the Dilution and the Energy Dissipation Rate of a Discharging Sewage Plume	35
3.1.1.1 Proposed Sludge Outfall for CSDOC	36

3.1.1.2	Effluent Outfall of CSDLAC	40
3.1.2	Design of a CFSTR with Variable Input Flow Rate and Stirring Speed	43
3.1.3	Calibration of the Coagulating Reactor	50
3.2	Design of the Settling Experiment—Holographic Technique	50
3.2.1	Design of the Holographic Camera System	53
3.2.1.1	Design Considerations	55
3.2.1.2	Holographic Camera System—Recording	57
3.2.1.3	Holographic Camera System—Reconstruction	62
3.2.2	Image Analysis System	63
3.2.3	Size and Velocity Measurements Using the In-line Holographic Camera System	69
3.2.4	Calibration of the Holographic Camera System	69
3.2.5	Design of the Settling Cell	72
3.2.6	Experimental Error	76
3.3	Experimental Procedure	79
3.3.1	Sample Preparation	81
3.3.2	Coagulation and Sampling	83
3.3.3	Settling Experiment	85
3.3.3.1	Filtration	85
3.3.3.2	Size Distribution Measurement	86
3.3.3.3	Settling Velocity Measurement	86
4.	Experimental Results	90
4.1	Data Analysis	90
4.1.1	Size Distribution	91
4.1.2	Settling Velocity of Individual Particles	93
4.1.3	Settling Velocity Distribution	94
4.1.3.1	Sampling Problems	94
4.1.3.2	Settling Velocity Distribution Derived from the Measurement of Settling Velocity	97
4.1.3.3	Conditional Settling Velocity Distribution Derived from the Measurement of Settling Velocity	99
4.1.3.4	Settling Velocity Distribution Derived from the Measurements of Size and Settling Velocity	101
4.2	Experimental Results	101
4.2.1	Run 1—Digested Primary Sludge (CSDOC), Simple Mixing	103

4.2.1.1	Size Distribution	103
4.2.1.2	Run 1a—Settling Velocity Distribution Measured in Seawater	104
4.2.1.3	Run 1b—Settling Velocity Distribution Measured in Fresh Water	105
4.2.2	Run 2—Effluent (CSDLAC), Simple Mixing	114
4.2.2.1	Size Distribution	114
4.2.2.2	Settling Velocity Distribution	114
4.2.3	Run 3—Digested Primary Sludge (CSDOC), Plume Mixing . .	115
4.2.3.1	Size Distribution	120
4.2.3.2	Settling Velocity Distribution at $t = 0''$	121
4.2.3.3	Settling Velocity Distribution at $t = 5'40''$	121
4.2.4	Run 4—Effluent (CSDLAC), Plume Mixing	124
4.2.4.1	Size Distribution	134
4.2.4.2	Settling Velocity Distribution at $t=4'30''$	134
4.3	Summary	135
5.	Discussion	143
5.1	Limitations of the Experimental Technique	143
5.1.1	Definition of the Equivalent Diameter	143
5.1.2	Particles with Equivalent Diameter Smaller than $10 \mu m$. . .	147
5.1.3	Accuracy of the Size Distribution	147
5.1.4	Accuracy of the Settling Velocity Distribution	148
5.1.5	Time Limitation	152
5.2	Degree of Coagulation	154
5.2.1	Comparison with Gibbs and Hopkins' Results	157
5.2.2	Time Scale of Plume Mixing	161
5.3	Relationship between Particle Size and Fall Velocity	161
5.3.1	Shape of Sewage Particles	162
5.3.2	Orientation of Particles during Settling	164
5.3.3	Density of Sludge Particles	165
5.3.4	Comparison with Gibb's Measurements	166
5.4	Settling Velocity Distribution	167
5.4.1	Comparison with the Measurements by Conventional Settling Column	171
5.4.2	Comparison with Measurements by Faisst (1976,1980)	172
5.4.3	Comparison with Measurements by Gibbs (1984)	172

5.4.4 Comparison with Measurements by Ozturgut and Lavelle (1984)	175
5.4.5 Comparison with Measurements by Lavelle <i>et al.</i> (1987)	177
5.4.6 Fractions of Particles with Fast Settling Velocities	180
5.5 Possible Field Application	182
6. Summary and Conclusion	187
6.1 Summary of Experimental Results	187
6.2 Recommendations for Future Work	191
6.2.1 Research	191
6.2.2 Improvements of the Experimental Technique	192
References	194
Appendices	
A. Interpretation of Settling Column Measurements of Sludge	204
B. Effects of Initial Mixing on the Apparent Fall Velocity	
Distributions Using Conventional Settling Columns	237
C. Particle Image Analysis	250

LIST OF TABLES

Table	Page
3.2.1 Design requirements of the holographic camera system for various particle diameters	58
3.2.2 Calibration of the scaling factor for image analysis	72
3.2.3 Calibration of the settling velocity measurements with PSL particles	76
3.2.4 Expected maximum error in fall velocity measurements for different velocity ranges	79
3.3.1 Time schedule for recording holograms for settling analysis	88
4.2.1 Summary of experimental parameters for the measurements of sludge and effluent particles (Concentrations given are suspended solids in the samples tested.) ...	102
4.2.2 Summary of the number of particles and sample volume measured for the hologram recorded for each sample taken at different times during plume mixing experiment of the D.P.S. (CSDOC)	124
4.2.3 Summary of the number of particles and sample volume measured for the hologram recorded for each sample taken at different times during plume mixing experiment of the effluent (CSDLAC)	135
5.2.1 Summary of the particle number concentrations (normalized to 1000:1 dilution) at different times during plume mixing experiment for the D.P.S. (CSDOC)	156
5.2.2 Summary of the particle number concentrations (normalized to 100:1 dilution) at different times during plume mixing experiment for the effluent (CSDLAC)	157
5.4.1 Summary of the settling velocity distributions for D.P.S. (CSDOC) and effluent (CSDLAC)	170
5.4.2 Summary of the settling velocity distributions for coagulated	

	sludges: the New Jersey Middlesex sludge and the digested sludge from the City of Philadelphia by Gibbs (1984)	176
5.4.3	Summary of the fractions of particles with fall velocities larger than 0.01 <i>cm/sec</i> for different effluent and sludges.....	183
C.1	Summary of the experimental data for Run 3—D.P.S. (CSDOC) at $t = 0''$	257
C.2	Summary of the experimental data for Run 4—Effluent (CSDLAC) at $t = 4'30''$	264

LIST OF FIGURES

Figure	Page
3.1.1 Time history of plume mixing calculated for the proposed deep sludge outfall for the County Sanitation Districts of Orange County, $Q = 0.131 \text{ m}^3/\text{sec}$, $B = 0.0340 \text{ m}^4/\text{sec}^3$, and $M = 0.105 \text{ m}^4/\text{sec}^2$, (a) dilution versus time, (b) energy dissipation rate versus time	41
3.1.2 Time history of plume mixing calculated for the existing 120-in effluent outfall for the County Sanitation Districts of Los Angeles County, $Q = 9.66 \text{ m}^3/\text{sec}$, $B = 0.00185 \text{ m}^4/\text{sec}^3$, (a) dilution versus time, (b) energy dissipation rate versus time	44
3.1.3 Schematic diagram of the coagulating reactor	47
3.1.4 The average energy dissipation rate $\bar{\epsilon}$ versus the rotation speed of the paddle for the reactor shown in Figure 3.1.3 derived from the $\Phi-Re$ curve (Rushton <i>et al.</i> , 1950) for $10^2 < Re < 5 \times 10^3$	48
3.1.5 Input flow rate versus time calculated for the reactor shown in Figure 3.1.3 for: CSDOC (—), CSDLAC (- - -)	49
3.1.6 Photograph of the coagulating reactor	51
3.1.7 Calibration of the flowmeters (a) FP-1/2-27-G-10/27, (b) FP-3/8-25-G-5/36	52
3.1.8 Calibration of the variable speed motor	53
3.1.9 Calibration of the dilution history inside the reactor, (Lines are the calculated dilution history and symbols are the measured suspended solids concentrations at different times.)	

	(a) CSDOC, (b) CSDLAC	54
3.2.1	Schematic diagram of the optical arrangement to record and reconstruct holograms	59
3.2.2	Photograph of the recording system	60
3.2.3	Photograph of the reconstruction system	60
3.2.4	The image processing system	66
3.2.5	Photographs of the double images of a D.P.S. particle, $A_p=849 \mu m^2$, $d_{equ}=32.5 \mu m$, $\frac{len_v}{d_{equ}}=1.19$, $\frac{len_h}{d_{equ}}=1.06$, $\frac{max_v}{d_{equ}}=1.13$, $\frac{max_h}{d_{equ}}=0.98$, $\frac{\sigma_{major}}{d_{equ}}=0.32$, $\frac{\sigma_{minor}}{d_{equ}}=0.25$, $\theta = 167^\circ$, $l_v = 116 \mu m$, $\Delta t = 5.23 \text{ sec}$, $w_s = 2.22 \times 10^{-3} \text{ cm/sec}$ (a) original image, (b) digitized images (after thresholding)	67
3.2.6	The magnification of the auxiliary viewing system	71
3.2.7	Determination of the scaling factor as a function of the position of TV camera y : (a) the ratio of the equivalent diameter measured at different y 's to that measured at $y = 170 \text{ mm}$, (b) the scaling factor versus the position of TV camera	73
3.2.8	Photograph of the settling cell	74
3.2.9	Settling velocity measurements for PSL particles by the holographic camera system; the crosses show the mean values of diameter d and velocity w and the length of the tick marks corresponds to $\pm\sigma$	77
3.3.1	Flow chart of the experimental procedure	80
4.1.1	Settling of particles in the cell	96
4.2.1	Size distribution ($d \geq 10 \mu m$) of the D.P.S. (CSDOC) after coagulation with a magnetic stirrer at 250 mg/l for 20 min , measured by holographic technique	104
4.2.2	Settling velocity versus equivalent diameter for the D.P.S (CSDOC) measured in seawater after coagulation with a magnetic stirrer at 250 mg/l for 20 min	106
4.2.3	Settling velocity distribution ($d \geq 10 \mu m$) of the D.P.S. (CSDOC) measured in seawater after coagulation with a magnetic stirrer at 250 mg/l for 20 min , derived from the settling measurement alone: (a) density distribution, (b) cumulative distribution	107
4.2.4	Conditional settling velocity distribution ($d \geq 10 \mu m$) of the	

	D.P.S. (CSDOC) measured in seawater after coagulation with a magnetic stirrer at 250 <i>mg/l</i> for 20 <i>min</i>	108
4.2.5	Settling velocity distribution ($d \geq 10 \mu m$) of the D.P.S. (CSDOC) measured in seawater after coagulation with a magnetic stirrer at 250 <i>mg/l</i> for 20 <i>min</i> , derived from the measurements of both size and velocity: (a) density distribution, (b) cumulative distribution.....	109
4.2.6	Settling velocity versus equivalent diameter for the D.P.S. (CSDOC) measured in fresh water after coagulation with a magnetic stirrer at 250 <i>mg/l</i> for 20 <i>min</i>	110
4.2.7	Settling velocity distribution ($d \geq 10 \mu m$) of the D.P.S. (CSDOC) measured in fresh water after coagulation with a magnetic stirrer at 250 <i>mg/l</i> for 20 <i>min</i> , derived from the settling measurement alone: (a) density distribution, (b) cumulative distribution.....	111
4.2.8	Conditional settling velocity distribution ($d \geq 10 \mu m$) of the D.P.S. (CSDOC) measured in fresh water after coagulation with a magnetic stirrer at 250 <i>mg/l</i> for 20 <i>min</i>	112
4.2.9	Settling velocity distribution ($d \geq 10 \mu m$) of the D.P.S. (CSDOC) measured in fresh water after coagulation with a magnetic stirrer at 250 <i>mg/l</i> for 20 <i>min</i> , derived from the measurements of both size and velocity: (a) density distribution, (b) cumulative distribution.....	113
4.2.10	Size distribution ($d \geq 10 \mu m$) of the effluent (CSDLAC) after coagulation with a magnetic stirrer at 57 <i>mg/l</i> for 25 <i>min</i> , measured by holographic technique.....	115
4.2.11	Settling velocity versus equivalent diameter for the effluent (CSDLAC) measured in seawater after coagulation with a magnetic stirrer at 57 <i>mg/l</i> for 25 <i>min</i>	116
4.2.12	Settling velocity distribution ($d \geq 10 \mu m$) of the effluent (CSDLAC) measured in seawater after coagulation with a magnetic stirrer at 57 <i>mg/l</i> for 25 <i>min</i> , derived from the settling measurement alone: (a) density distribution, (b) cumulative distribution.....	117
4.2.13	Conditional settling velocity distribution ($d \geq 10 \mu m$) of the effluent (CSDLAC) measured in seawater after coagulation with a	

	magnetic stirrer at 57 mg/l for 25 min.....	118
4.2.14	Settling velocity distribution ($d \geq 10 \mu m$) of the effluent (CSDLAC) measured in seawater after coagulation with a magnetic stirrer at 57 mg/l for 25 min, derived from the measurements of both size and velocity: (a) density distribution, (b) cumulative distribution.....	119
4.2.15	Size distributions ($d < 10 \mu m$) of the D.P.S. (CSDOC) at different times of plume mixing, measured by the gravimetric technique	122
4.2.16	Size distributions ($d \geq 10 \mu m$) of the D.P.S. (CSDOC) at different times of plume mixing, measured by the holographic technique	123
4.2.17	Settling velocity versus equivalent diameter for the D.P.S (CSDOC) measured in fresh water at $t = 0''$	125
4.2.18	Settling velocity distribution ($d \geq 10 \mu m$) of the D.P.S. (CSDOC) measured in fresh water for the sample withdrawn at $t = 0''$, derived from the settling measurement alone: (a) density distribution, (b) cumulative distribution.....	126
4.2.19	Conditional settling velocity distribution ($d \geq 10 \mu m$) of the D.P.S. (CSDOC) measured in fresh water for the sample withdrawn at $t = 0''$	127
4.2.20	Settling velocity distribution ($d \geq 10 \mu m$) of the D.P.S. (CSDOC) measured in fresh water for the sample withdrawn at $t = 0''$, derived from the measurements of both size and velocity: (a) density distribution, (b) cumulative distribution.....	128
4.2.21	Settling velocity versus equivalent diameter for the D.P.S (CSDOC) measured in seawater for the sample withdrawn at $t = 5'40''$	129
4.2.22	Settling velocity distribution ($d \geq 10 \mu m$) of the D.P.S. (CSDOC) measured in seawater for the sample withdrawn at $t = 5'40''$, derived from the settling measurement alone: (a) density distribution, (b) cumulative distribution.....	130
4.2.23	Conditional settling velocity distribution ($d \geq 10 \mu m$) of the D.P.S. (CSDOC) measured in seawater for the sample withdrawn at $t = 5'40''$	131
4.2.24	Settling velocity distribution ($d \geq 10 \mu m$) of the D.P.S. (CSDOC)	

	measured in seawater for the sample withdrawn at $t = 5'40''$, derived from the measurements of both size and velocity: (a) density distribution, (b) cumulative distribution.....	132
4.2.25	Revised dilution history of the plume mixing experiment for the effluent (CSDLAC): original design (—), revised design (- - -), and experiment measurements(\times)	133
4.2.26	Size distributions ($d \geq 10 \mu m$) of the effluent (CSDLAC) at different times of plume mixing, measured by holographic technique	136
4.2.27	Settling velocity versus equivalent diameter for the effluent (CSDLAC) measured in fresh water for the sample withdrawn at $t = 4'30''$	137
4.2.28	Settling velocity distribution ($d \geq 10 \mu m$) of the effluent (CSDLAC) measured in fresh water for the sample withdrawn at $t = 4'30''$, derived from the settling measurement alone: (a) density distribution, (b) cumulative distribution.....	138
4.2.29	Conditional settling velocity distribution ($d \geq 10 \mu m$) of the effluent (CSDLAC) measured in fresh water at $t = 4'30''$	139
4.2.30	Settling velocity distribution ($d \geq 10 \mu m$) of the effluent (CSDLAC) measured in fresh water for the sample withdrawn at $t = 4'30''$, derived from the measurements of both size and velocity: (a) density distribution, (b) cumulative distribution.....	140
5.1.1	Scanning electron micrographs of sludge particles (digested primary sludge from the County Sanitation Districts of Orange County): (a) uncoagulated particles, (b) a coagulated particle	145
5.1.2	Size distributions ($d \geq 10 \mu m$) of the repeated measurements of the same sample from: (a) the same hologram, (b) different hologram of the same sample.....	149
5.1.3	Size distributions ($d \geq 10 \mu m$) of a diluted effluent sample (0.68 mg/l) at different times: (a) $t = 0''$, (b) after being stored for 36 hr	155
5.2.1	The relationship of the coagulation rate constant, k , min^{-1} as a function of turbulent shear rate at different solids concentrations of sludge (from Gibbs, 1984)	159

5.2.2	The relationship of the equilibrium time as a function of turbulent shear rate at different solids concentrations of sludge (from Gibbs, 1984).....	160
5.3.1	Examples of $\frac{\sigma_{major}}{d_{equ}}$ and $\frac{\sigma_{minor}}{d_{equ}}$ for sewage particles (a) D.P.S. (CSDOC)—Run 3, (b) effluent (CSDLAC)—Run 4	163
5.3.2	Orientation (in two-dimensional plane) of particles during settling (θ is the angle between the horizontal axis and the major principal axis of particles on the hologram plane which is perpendicular to the optical axis)	164
5.3.3	The relationship of settling velocity at 20°C and diameter of coagulated sludge flocs for anaerobic digested sludge from Wilmington; sludge was coagulated in seawater at the turbulent shear rate of 2 sec ⁻¹ (—) and 5 sec ⁻¹ (- - -) (from Gibbs, 1984).....	168
5.4.1	Settling velocity distributions for the entire sewage samples derived from the holographic measurements and the filtration analysis: Δ —effluent (CSDLAC, Run 4), \square —D.P.S. (CSDOC, Run 3, $t = 0''$), and \times —D.P.S. (CSDOC, Run 3, $t = 5'40''$).....	169
5.4.2	Settling velocity distributions of the D.P.S. (CSDOC) measured by the conventional settling column technique (each run has two lines representing the distributions measured at 60 and 120 cm from the bottom of the settling column): (a) selected results from Appendix A; (b) selected results from Appendix B compared with the hologram results shown on Figure 5.4.1	173
5.4.3	Settling velocity distributions for different sludge samples measured by Faisst (1976, 1980) with the settling column technique: (a) shallow column (2 l graduated cylinder), single-depth sampling at 15 cm below the surface; (b) tall column (171 cm), two-depth sampling at 30 and 90 cm from the bottom	174
5.4.4	Settling velocity distribution ($d < 64 \mu m$) for the effluent sample from the Municipality of Metropolitan Seattle. This distribution is derived for settling velocities calculated according to Stokes' law with the measured densities and sizes of particles. The density of the heavy fraction (40% by volume), which is not measured, is assumed to be 1.4 g/cm ³ (○) and 2.65 g/cm ³ (△)	

	(from Ozturgut and Lavelle, 1984)	178
5.4.5	Settling velocity distributions for different sludges: (a) cumulative distributions by weight for the coarse fraction ($d > 63 \mu m$), (b) cumulative distributions by volume for the fine fraction ($d < 63 \mu m$) (from (Lavelle <i>et al</i> , 1987)	181
C.1	Definitions of the equivalent diameter d_{equ} , the angle θ , and the other length scales used to characterize the shape of particle images	252
C.2	$\frac{len_v}{d_{equ}}$ versus d_{equ} for D.P.S (CSDOC)—Run 3, $t = 0''$ (\square), and effluent (CSDLAC)—Run 4, $t = 4'30''$ (\times).....	255
C.3	$\frac{len_v}{len_h}$ versus d_{equ} for D.P.S (CSDOC)—Run 3, $t = 0''$ (\square), and effluent (CSDLAC)—Run 4, $t = 4'30''$ (\times).....	255
C.4	$\frac{max_v}{max_h}$ versus d_{equ} for D.P.S (CSDOC)—Run 3, $t = 0''$ (\square), and effluent (CSDLAC)—Run 4, $t = 4'30''$ (\times).....	256
C.5	$\frac{\sigma_{major}}{\sigma_{minor}}$ versus d_{equ} for D.P.S (CSDOC)—Run 3, $t = 0''$ (\square), and effluent (CSDLAC)—Run 4, $t = 4'30''$ (\times).....	256

NOTATION

Symbol	Definition
	Roman symbols
<i>A</i>	shape factor
<i>A_p</i>	area of a particle
<i>a</i>	cross section area of the settling cell
<i>B</i>	initial buoyancy flux
<i>b_w</i>	velocity profile $\frac{1}{e}$ -width
<i>C</i>	floc strength constant
<i>C₀</i>	initial particle concentration
<i>C₁</i>	solids concentration of the coagulating particles
<i>C(z, t)</i>	particle concentration at depth <i>z</i> and time <i>t</i>
<i>CFSTR</i>	continuous flow stirred tank reactor
<i>CSDLAC</i>	County Sanitation Districts of Los Angeles County
<i>CSDOC</i>	County Sanitation Districts of Orange County
<i>D</i>	<ul style="list-style-type: none"> • diffusion coefficient of particles, $\frac{kT}{3\pi\mu d}$ (2.1.1) • impeller diameter (2.1.3) (3.1.2) • diameter of the outfall pipeline (3.1.1)
<i>D.P.S.</i>	digested primary sludge
<i>d</i>	<ul style="list-style-type: none"> • maximum dimension of an object (3.2.1) • particle diameter
<i>d_v</i>	volumetric average diameter
<i>d_{equ}</i>	equivalent diameter, the diameter of a circle with the same area of the test particles
<i>d_{max}</i>	maximum stable floc size
<i>E</i>	ambient density gradient, $-\frac{1}{\rho} \frac{d\rho}{dz}$
<i>E_k</i>	local kinetic energy flux of a plume
<i>e</i>	void ratio of particles
<i>F_D</i>	drag force
<i>F_G</i>	submerged weight of particles

$F(w)$	cumulative settling velocity distribution (based on particle volume)
f	focal length of the microscope objective
$f(w)$	probability density function of fall velocity w (based on particle volume)
$f(w d)$	conditional probability density function of fall velocity w for a particular particle size d (based on particle volume)
G	shear rate, $\sqrt{\frac{\epsilon}{\nu}}$
g	gravitational acceleration constant
g'	$g \frac{\Delta\rho}{\rho}$
$g(z)$	the initial volume distribution of particles inside the layer H
H	<ul style="list-style-type: none"> • depth of the liquid in a reactor (3.1.2) • initial thickness of particles in the settling cell (4.1.3.1)
h	height of the observing window (holographic film)
$I(x, y)$	an image function
k	<ul style="list-style-type: none"> • Boltzmann constant, $1.380 \times 10^{-16} \text{ erg}/^\circ K$ (2.1.1) • proportionality constant, $\frac{4\phi}{\pi}$ (3.1.2) • coagulation rate constant, min^{-1} (5.2.1)
K_B	floc breakup rate coefficient
K_p	performance parameter characterizing the stirring arrangement
K_s	proportionality coefficient between the turbulence energy spectrum and the diffusion coefficient
K_1	proportional constant
L	<ul style="list-style-type: none"> • Eulerian macroscale of turbulence • length of the diffuser (3.1.1.2) • distance between the microscope objective and the TV camera (3.2.4) • distance between the water surface and the center of the observing window (4.1.3.1)
l	turbulence integral scale
l_b	buoyancy length scale, $\frac{B}{U_A^3}$
l'_b	length scale describing the height of rise of a plume in a stagnant and stratified fluid, $\frac{B^{1/4}}{(gE)^{3/8}}$
l_p	characteristic length scale of particles
l_v	particle settling distance measured between two images within a time Δt

len_v, len_h	vertical and horizontal dimensions of the bounding box enclosing the image of a particle
M	<ul style="list-style-type: none">• initial momentum flux (3.1.1)• overall magnification of the holographic system (3.2.4)• number of particle with diameter in the size range d_j to d_{j+1} inside a hologram (4.1.3.3)
$M(t)$	the mass collected inside a settling column up to time t
M_{tot}	total mass of particles added into the settling column
m	<ul style="list-style-type: none">• floc breakup rate exponent (2.1.1)• specific momentum flux of a buoyant jet (3.1.1)
m_a	magnification from the auxiliary viewing system
m_i	reconstruction magnification
m_o	recording magnification
m_{TV}	magnification of the TV camera
max_v, max_h	lengths of the longest scan lines contained in a particle along the directions of principal axes
N	<ul style="list-style-type: none">• collision rate between particles in (2.1.1)• rotation speed (3.1.2)• far-field number, $\frac{z\lambda}{D^2}$ (3.2.1)• total number of particle in a hologram (4.1.3.2)
N_{1F}	collision rate between primary particles and flocs
N_x	the horizontal dimension of a digitized image field
N_y	the vertical dimension of a digitized image field
n	stable floc size exponent
n_i	particle number concentration
P	power input to the reactor
$p(d)$	probability density function of size d (based on particle volume)
Q	initial volume flux
q	initial discharge per unit length, $\frac{Q}{L}$
R	<ul style="list-style-type: none">• $r_1 + r_2$ (2.1.1)• $\frac{\mu\beta^{1/2}}{m^{5/4}}$ (3.1.1)
R_F	radius of flocs
R_p	plume Richardson number, 0.577
Re	Reynolds number
r_i	radius of particles
r	radial distance from the axis of a buoyant jet
$S_c(z)$	centerline dilution at distance z from the outfall

T	<ul style="list-style-type: none"> • temperature (2.1.1) • torque applied on the impeller shaft (2.1.3) • tank diameter (3.1.2)
t	time
t_{exp}	exposure time
U_a	ambient current
u	fluid velocity
u_{pq}	pq-th central moment of a particle
u'_{pq}	normalized pq-th central moment of a particle
u_r	relative velocity between particles
u_*	pipe shear velocity
$\overline{u'^2}$	mean square velocity fluctuation
$\sqrt{\overline{u'^2}}$	turbulent root-mean-square velocity
V	volume of the fluid in the reactor
V_d	volume analyzed inside a hologram for particles of diameter d
$V_L(t)$	total particle volume observed inside the window at time t
V_{tot}	total particle volume suspended inside the layer H on top of the settling cell at time $t = 0$
W	stability ratio
w	settling velocity of particles
$w(r, z)$	time-averaged velocity profile of a buoyant jet
$\bar{w}(t)$	average fall velocity of particles inside a hologram recorded at time t
$w_m(z)$	time-averaged centerline velocity of a buoyant jet
x	mixed liquor suspended solids concentration
\bar{x}, \bar{y}	the centroid position of a particle
$y_{0.5w_m}$	lateral distance from the plume axis to where $w = 0.5w_m(z)$
z	<ul style="list-style-type: none"> • vertical distance from the plume exit (3.1.1) • sampling depth from the water surface in (2.2.1) (4.1.1) • distance between objects and the recording plane (3.2.1)

Greek symbols

α	<ul style="list-style-type: none"> • collision efficiency (2.1) • coagulation rate constant (2.2.4) • entrainment coefficient (3.1.1)
α_j	entrainment coefficient of a pure jet, 0.0535 ± 0.0025
α_p	entrainment coefficient of a pure plume, 0.0833 ± 0.0042

β	<ul style="list-style-type: none"> • coagulation rate parameter (2.2.2) (2.2.3) • specific buoyancy flux of a buoyant jet (3.1.1)
β_{ds}	coagulation rate parameter for the coagulation induced by differential settling
β_{sh}	coagulation rate parameter for the coagulation induced by shear
β_b	coagulation rate parameter for the coagulation induced by Brownian motion
Δl_h	horizontal displacement due to the film movement
Δl_v	vertical displacement due to the film movement
Δt	time between two exposures
Δt_f	time between two adjacent frames
$\Delta \rho$	<ul style="list-style-type: none"> • density difference between particles and fluid $\rho_p - \rho_f$ (2.1.1) • density difference between seawater and sludge (3.1.1)
ϵ	energy dissipation rate
ϵ_o	effective mean energy dissipation rate
$\bar{\epsilon}$	average energy dissipation rate
η	Kolmogorov microscale of length, $\frac{\nu^{3/4}}{\epsilon^{1/4}}$
θ	angle between the x-axis of the image plane and the principal axes of a particle
θ_m	time-averaged density anomaly along the plume axis
Λ	local width of the plume
λ	<ul style="list-style-type: none"> • =1.16, λb_w is the concentration profile $\frac{1}{e}$-width (3.1.1) • wavelength of the illuminating light (3.2.1) (4.1.1)
ν	kinematic viscosity of fluid
μ	<ul style="list-style-type: none"> • dynamic viscosity of fluid • volume flux of a buoyant jet (3.1.1)
ρ_f	density of fluid
ρ_p	density of particles
σ	standard deviation of settling velocities of PSL particles (3.2.5)
$\sigma_{major}^2, \sigma_{minor}^2$	second moments in the principal axes directions for observed particles
τ	relaxation time, $\frac{2r^2 \rho_p}{9\mu}$
Φ	power number, $\frac{P}{\rho N^3 D^5}$
ω	angular velocity

1. INTRODUCTION

The oceans have served as media for the disposal of municipal and industrial wastes for many years (Duedall *et al.*, 1983). At the present time, most municipal wastewaters are treated to different degrees before the effluent is discharged into inland or coastal waters. The treatment of wastewater produces sewage sludge, which contains much of the waste material and pollutants in the wastewaters. Disposal of sewage sludge presents another potential environmental problem.

Several alternatives of disposal of digested sewage sludge are available, e.g., landfill, incineration, and ocean discharge (NRC, Commission on Physical Sciences, Mathematics, and Resources, 1984). Landfill and incineration require prior extraction of water from the sludge mixture, which is an expensive process. Furthermore, incineration can cause air pollution, and land disposal can lead to groundwater contamination. For coastal areas, ocean disposal may sometimes be a more attractive alternative, not only because it is less expensive than land disposal or incineration, but also because the impacts on the environment may be less significant.

The environmental impact of discharging effluent or digested sludge into the oceans depends on many factors such as the composition of the raw sewage, the degree of treatment provided, the design of the outfall or barging systems, and

the characteristics of the receiving water. Small particles cause much of the adverse effects of marine disposal of treated effluent or digested sludge. For instance, they decrease the light penetration into the water column (Peterson, 1974), an effect which is not only aesthetically displeasing but also can decrease the rate of photosynthesis—the primary productivity of the oceans. Solid particles in sewage are of particular concern because toxic metals and refractory organic compounds are predominately contained within the particles or adsorbed at the surfaces of particles (e.g. Morel *et al.*, 1975; Faisst, 1976; Pavlou and Dexter, 1979). Oxidizable particulate sludge could deplete oxygen and increase dissolved trace metal and sulfide concentrations in the water column (Jackson, 1982). Accumulation of particles on the ocean bottom may alter the chemistry of the sediments, and concentrate organic matter and toxic substances which are harmful to the natural benthic community. Fine particles and the associated pollutants may also be carried away by currents and taken up by zooplankton. Hence, we need to predict the fate of sewage particles and the associated pollutants in order to evaluate the environmental impacts of ocean discharge and to help design the disposal systems.

The distribution of sewage wastes in the ocean after they are discharged is governed by many physical, chemical, and biological processes (Brooks *et al.*, 1985). The settling velocities of sewage and sludge particles are among the most important factors that control the transport of particles and determine the impacts of the discharge on the marine environment. (Kavanaugh and Leckie, 1980; Koh, 1982). However, the settling velocities may be altered by particle coagulation in the plume discharging into seawater. When sewage is mixed with seawater, the high ionic strength of the seawater destabilizes the particles (Stumm and Morgan, 1981). If particles are brought together by the turbulent mixing inside the discharge plume,

they can stick to each other. This coagulation process can modify the size, shape, structure, density, and the settling velocity of particles. However, both the particle concentration and the turbulence intensity decrease rapidly during the rise of the plume. Consequently in the later stage of plume mixing, the small particle concentration and the low turbulence intensity will prevent any further significant coagulation. Hence, it is important to understand what the settling velocity distributions of sewage particles are, and how these distributions are affected by the coagulation inside a discharge plume.

The objective of this dissertation is to study the settling characteristics of sewage particles introduced into seawater with possible coagulation. A two-step experiment was devised to simulate the particle coagulation inside the discharge plume, and then to measure the settling velocities of particles.

A laboratory reactor was designed to simulate the mixing conditions in a rising plume. However, the conditions which affect the particle coagulation inside a plume are too complicated to be faithfully reproduced in the laboratory. Based on the analysis of different models of turbulence coagulation and floc breakage, it was concluded that the most important factors which control the coagulation inside a plume are the particle concentration and the turbulent shear (the square root of the ratio of energy dissipation rate to viscosity of seawater). In the experiments, an attempt was made to produce the correct time history of the energy dissipation rate and dilution (or concentration) to be similar to that of a possible plume. As the coagulating experiment progressed, samples were withdrawn from the reactor at different times and diluted immediately with filtered artificial seawater to suppress further coagulation. Measurements of the settling velocities and the size distributions were then performed for these diluted samples (concentration ≤ 2 mg/l).

A conventional settling column was first used in this study to measure the settling velocities of sewage particles, as presented in Wang *et al.*, 1984 (see Appendix A). With the solids concentrations used in the settling tests ranging from 50 to 250 *mg/l*, coagulation and settling took place simultaneously inside the settling column. Experimental results showed a combined effect of settling and coagulation which cannot be distinguished from each other. We concluded that the conventional settling column is inadequate for our purpose. It was decided to use sludge samples of sufficiently high dilution ($\geq 10^4 : 1$) during fall velocity measurements to avoid the interference of coagulation. This high dilution ratio decreases the particle concentration and reduces the collision rate—hence the effect of coagulation. However, due to the low solids concentration, conventional techniques for solids analysis, such as the gravimetric and absorbance methods, are not able to provide measurements with enough accuracy. Hence, a new experimental method based on a holographic technique was developed to measure the settling velocities and size distributions for sewage particles larger than 10 μm .

Since sewage particles have very small settling velocities ($\ll 1.0 \text{ cm/sec}$), a special settling cell was designed to eliminate the influence of convection currents. This settling cell consists of two parts: a rectangular lucite box with two parallel windows made of high quality optical glass and a funnel on top. Samples were introduced from the top and allowed to settle in quiescence by gravity. A collimated laser light, travelling through the cell, interferes with the light scattered by the settling particles. The interference patterns, recorded on a high resolution film, were reconstructed to create the three dimensional images of particles for analysis.

The particle size distribution was obtained by counting the number of particles and measuring their sizes inside a small volume in the settling cell. Particle velocities

were measured from doubly exposed holograms on which double images of particles were recorded. The travel distance and the time between two exposures were used to calculate the fall velocity. The settling velocity distributions were then derived from the size distributions and the fall velocity measurements of individual particles.

We conducted four sets of experiments with the effluent from the County Sanitation Districts of Los Angeles County (CSDLAC) and digested primary sludge (D.P.S.) from the County Sanitation Districts of Orange County (CSDOC). Both simple mixing and simulated plume mixing were used for particle coagulation. These experiments illustrate the procedures for measuring the size and velocity distributions of sewage particles with the holographic technique. The results show that the D.P.S. and effluent particles have similar settling characteristics and that coagulation appears to be insignificant under the conditions simulated. With the new procedure, it is possible to study the settling characteristics in detail for different sewage particles under different mixing conditions. Hence, this study contributes to a better understanding of the ocean disposal process by providing basic information on fall velocity which is needed for numerical modeling of the fate of particles (Koh, 1982).

The remainder of this dissertation is organized as follow: Chapter 2 reviews the theoretical and experimental works on turbulent coagulation and settling velocity measurement. Chapter 3 explains the equipment design and the experimental procedure. Chapter 4 presents the experimental results. Chapter 5 discusses their implication and significance and compares them with the settling velocity measurements by the conventional settling column and by other people. Chapter 6 contains the conclusions and the recommendation for future work, including possible improvements in the techniques as well as research directions.

2. LITERATURE REVIEW

In this chapter, mechanisms that determine coagulation are studied and compared to identify the dominant coagulation factors in the discharge plume and to help set the simulation criteria. Possible configurations of the coagulating reactors are reviewed and the selected design is outlined.

To study the settling velocity, we begin with a review of the existing techniques for measuring the fall velocities of particles. Relevant research on estimating the settling characteristics of sewage particles is reviewed. We then present our experimental results of using the conventional settling column to measure the fall velocities of sewage particles. Based on the review and our study, it was concluded that a modified settling column with holographic technique for particle analysis is the most suitable design. Hence, a review of velocity measurements using holography is given at the end.

2.1 Particle Coagulation inside a Plume

There are two important factors in determining particulate coagulation, and both have to be favorable for coagulation to occur. First, particles have to be destabilized so that they can stick to each other upon contact. Second, particles

have to be brought together by transport processes. The destabilization of particles can be explained by physical models, i.e. double layer theory, and chemical models (Stumm and Morgan, 1981). The destabilization effect can be expressed in term of the collision efficiency α (which is the reciprocal of the stability ratio (W)) measured as the fraction of collisions which lead to permanent agglomeration. Particle transport may take place as a result of Brownian motion, laminar shear, turbulent motion, or differential sedimentation (Friedlander, 1977). The collision of particles as a result of the transport process is expressed in terms of the collision functions, which determine the particle collision rate under different transport mechanisms (e.g. Valioulis, 1983).

In this dissertation, instead of studying the coagulation of sewage particles under different chemical conditions and mixing histories, our objective is to understand the coagulation of sewage particles under certain specified conditions, i.e., the conditions inside the discharge plumes. Hence, in our experiments, we maintained the chemical conditions similar to those in the ocean by using artificial seawater (prepared according to Lyman and Fleming's recipe in Riley and Skirrow, 1965) as the coagulating medium. The same chemical species, the same pH value and the same ionic strength as in real seawater were maintained. Furthermore, as a first setup to understand the coagulation of sewage particles, the effects of naturally occurring particles and organic matter in the real seawater were excluded, and the artificial seawater was filtered through a 0.4- μm Nuclepore membrane before use.

The mixing processes inside a plume are complicated and inhomogeneous. The axial velocity, turbulent intensities (axial and radial), and particle concentration vary across the width of a plume and decrease with the distance from the source (Papanicolaou, 1984). Hence, the coagulation induced by the plume mixing is

expected to be very complicated. Different coagulation mechanisms are examined in the following sections. Based on the theories and experimental works on particle coagulation, the dominant factors that determine the coagulation in a plume are identified and employed to control the coagulation experiment.

2.1.1 Turbulence coagulation

Turbulence affects coagulation through two different mechanisms—collisions induced by the motion of particles *with* the fluid, and collisions induced by the motion of particles *relative to* the fluid (Saffman and Turner, 1956; Hidy and Brock, 1970). For particles with length scale smaller than the characteristics length scale of small eddies (Kolmogorov microscale of length $\eta = \sqrt[4]{\frac{\nu^3}{\epsilon}}$), inhomogeneity in the turbulence flow causes neighboring particles to possess different velocities, and hence, induces collisions among particles. Secondly, particles move relative to the fluid because the inertia of particles is not the same as the equivalent volume of the fluid. Again, this relative motion can induce collisions if particles are of different inertia, e.g., different densities.

Let us consider small particles which have the length scale smaller than that of small eddies ($d \ll \eta$), and the relaxation time ($\tau = \frac{2r^2\rho_p}{9\mu}$ for small spherical particles obeying Stokes' law) less than the time scale of small eddies, $\tau \ll \sqrt{\frac{\nu}{\epsilon}}$. If the distortion of the flow field due to the presence of particles is neglected, and the turbulence is isotropic, the collision rate between particles of similar sizes is given as the following equation (Saffman and Turner, 1956; Hidy and Brock, 1970):

$$N = 2\sqrt{2\pi}R^2n_1n_2 \left[\left(1 - \frac{\rho_f}{\rho_p}\right)^2 (\tau_1 - \tau_2)^2 \left(\overline{\frac{Du}{Dt}}\right)^2 + \frac{1}{3} \left(1 - \frac{\rho_f}{\rho_p}\right)^2 (\tau_1 - \tau_2)^2 g^2 + \frac{1}{9} R^2 \frac{\epsilon}{\nu} \right]^{1/2} \quad (2.1.1)$$

where

$R = r_1 + r_2$; r_1, r_2 are radii of particles

$n_1, n_2 =$ particle number concentration

$\rho_f, \rho_p =$ density of fluid and particles

$\tau_i = \frac{2r_i^2\rho_p}{9\mu}$, relaxation time ($i = 1, 2$)

$\epsilon =$ energy dissipation rate

When Reynolds number is large, $\left(\overline{\frac{Du}{Dt}}\right)^2$ can be approximated by $1.3\nu^{-1/2}\epsilon^{3/2}$ (Batchelor, 1951).

In the above equation, the third term in the brackets represents the coagulation effects induced by the spatial variation of velocities in the fluid (or the collisions due to the motion of particles *with* the fluid). The first term shows the effects of turbulent acceleration and the second term shows the effects of the gravity (or the collisions due to the motion of particles *relative to* the fluid). The relative importance of these different coagulation mechanisms in a turbulent flow can be evaluated by comparing three terms in Eqn. 2.1.1. For particles with similar sizes, the ratios are as follows:

$$\frac{\text{inertia of particles}}{\text{turbulent shear}} \approx \frac{0.6(\rho_p - \rho_f)^2(r_1 - r_2)^2\sqrt{\epsilon}}{\rho_f^2\sqrt{\nu^3}} \quad (2.1.2)$$

$$\frac{\text{gravity}}{\text{turbulent shear}} \approx \frac{0.15(\rho_p - \rho_f)^2g^2(r_1 - r_2)^2}{\epsilon\nu\rho_f^2} \quad (2.1.3)$$

Before we use these ratios to estimate the relative importance of different coagulation mechanisms inside a plume, we must check if the assumptions made in deriving these equations are satisfied by the coagulating conditions for the sewage particles in a plume. The size of the sludge particles ranges from submicron up to about $60 \mu m$, with majority of particles smaller than $10 \mu m$ and volume-averaged diameter around $20 \mu m$ (Faisst, 1976). The density range of particles is from 1.02 to $1.7 g/cm^3$ (Faisst, 1980; Ozturgut and Lavelle, 1984). The energy dissipation rate inside the plume is about 1 to $100 cm^2/sec^3$ (Figure 3.1.1). If we take $r_1 - r_2 = 10 \mu m$, and $\epsilon = 30 cm^2/sec^3$, we get the Kolmogorov microscale of length and time as $125 \mu m$ and $0.016 sec$, respectively. For $\rho_p = 1.05 g/cm^3$ and $d = 20 \mu m$, the relaxation time of particles is $2.3 \times 10^{-5} sec$. These numbers satisfy the requirements of the time and length scales in deriving the equations.

When the Reynolds number (Re) of the flow field is very large, there exists a *local isotropy* for small scale eddies (Tennekes and Lumley, 1972). For sewage outfall jets, the Reynolds numbers are in general larger than 1×10^5 , so the assumption of local isotropy of the flow field can be applied. We can then calculate the ratios between different coagulation mechanisms according to the above equations and get 0.0008 for Eqn 2.1.2, and 0.1 for Eqn. 2.1.3. Therefore, it is concluded that the turbulent shear is the dominant one among these three processes.

When particles get smaller, the collisions induced by their Brownian motion become significant. Hence, Brownian coagulation should be considered for small particles. The effects due to the Brownian motion and the turbulent shear can be compared based on the collision time scales (Valioulis and List, 1984): $(ndD)^{-1}$ for Brownian motion, and $(nd^3\sqrt{\frac{\epsilon}{\nu}})^{-1}$ for turbulent shear, where n is particle number concentration, d is the diameter of particles, and $D = \frac{kT}{3\pi\mu d}$ is the diffusion coefficient of particles. The relative importance of the Brownian coagulation to turbulent shear coagulation is:

$$\frac{\text{Brownian motion}}{\text{turbulent shear}} \approx \frac{D\sqrt{\nu}}{d^2\sqrt{\epsilon}} \quad (2.1.4)$$

Under the conditions of sewage discharge, the typical temperature is about $10^\circ C$ and the energy dissipation rate is around $30 \text{ cm}^2/\text{sec}^3$ inside the plume, turbulent shear will be the dominant coagulating mechanism for particles larger than $0.5 \mu m$.

Finally, in addition to the turbulence-induced shear, mean flow shear can also contribute to the collisions of particles. The mean velocity profile for a plume follows the following equation (Papanicolaou, 1984):

$$w(r, z) = w_m(z)e^{-80(r/z)^2} \quad (2.1.5)$$

$$w_m(z) = 3.85\sqrt[3]{\frac{B}{z}} \quad (2.1.6)$$

where $w_m(z)$ is the time-averaged centerline velocity, B the buoyancy flux, r the radial distance from the axis, and z axial distance from the plume exit. Based on this equation, we can calculate the maximum mean flow shear rate as:

$$\left| \frac{\partial w}{\partial r} \right|_{max} = \left| \frac{\partial w}{\partial r} \right|_{r/z=0.08} = 30 \sqrt[3]{\frac{B}{z^4}} \quad (2.1.7)$$

As mentioned before, the turbulent shear is proportional to $\sqrt{\frac{\epsilon}{\nu}}$. From dimensional analysis, we have $\epsilon \propto \frac{B}{z^2}$, so the turbulent shear is proportional to $\sqrt{\frac{B}{\nu z^2}}$. The coagulation induced by these two mechanisms can be compared according to the following equation:

$$\frac{\text{mean flow shear}}{\text{turbulent shear}} \approx \frac{\nu^{1/2}}{B^{1/6} z^{1/3}} \quad (2.1.8)$$

For the proposed deep ocean disposal of sludge for Orange County (Brooks *et al.*, 1985), B is $0.034 \text{ m}^4/\text{sec}^3$ for a flow rate of 3.0 mgd ($0.131 \text{ m}^3/\text{sec}$), Eqn. 2.1.8 gives a value of 0.008 for $z \geq 1 \text{ cm}$. The coagulation induced by the mean flow shear is much smaller than that induced by the turbulent shear. Therefore, we can conclude that the most important coagulation mechanism for sewage particles inside a discharge plume is the turbulent shear. In the following, theoretical and experimental works on the turbulent coagulation are reviewed.

Argaman and Kaufman (1970) have developed a model for turbulent flocculation. Their model is based on the hypothesis that particles suspended in a turbulent fluid experience random motion which can be characterized by an appropriate diffusion coefficient. The effective diffusivity is a function of the turbulence field,

and can be expressed in terms of the mean-square-velocity-fluctuation, $\overline{u'^2}$, and the particle size. The collision rate predicted by their model is as the equation: $N_{1F} = 4\pi K_s R_F^3 n_1 n_F \overline{u'^2}$, where K_s is a proportionality coefficient expressing the effect of the turbulence energy spectrum on the diffusion coefficient, n_1, n_F are the number concentrations of the primary particles and flocs, and R_F is the radius of the flocs. Based on the experimental measurements, they concluded that $\overline{u'^2}$ depends on the total energy dissipation in the system. It can be estimated by the equation: $\overline{u'^2} = K_p G$, where K_p is the performance parameter characterizing the stirring arrangement, and G is the rms velocity gradient which is related to the average energy dissipation by $G = \sqrt{\epsilon/\nu}$.

Delichatsios and Probst (1975) have also developed a turbulent coagulation model by applying simple binary collision mean-free path concepts to calculate the collision rate based on the statistical nature of the turbulent flow. The interaction among particles, the gravitational force and the breakup of particles due to turbulence are neglected in their model. Particles are assumed to follow the turbulent motion, and only binary collisions are considered because of the assumption of low volume concentration ($\leq 3\%$). The collision rate is calculated to be: $N = 1/2 n^2 \pi d^2 u_r$, where u_r is the the relative velocities between particles. They assumed that u_r is approximately equal to the root-mean-square relative turbulent velocity between two points separated by a distance of the particle diameter. Based on the Kolmogorov theory of isotropic turbulence, they derived the following relations:

$$\begin{aligned}
 u_r &= \sqrt{\epsilon/15\nu}d, & d < \eta \\
 u_r &= 1.37\sqrt[3]{\epsilon d}, & d > \eta \\
 u_r &\approx \sqrt[3]{\epsilon L}, & d \sim L
 \end{aligned}
 \tag{2.1.9}$$

where ϵ is the energy dissipation rate, η the Kolmogorov microscale, L the Eulerian macroscale of turbulence, and d particle diameter. They measured the coagulation rate of colloidal particles inside a fully developed turbulent pipe flow. The experimental results show good agreement with their theoretical prediction for particles with sizes smaller than the Kolmogorov microscale.

Cleasby (1984) has reviewed some of the flocculation kinetic models for turbulent flow and re-analyzed the experimental data of Argaman and Kaufman (1970). He suggested that the important eddies that cause flocculation are about the size of the flocculated particles. He also summarized the control parameters for flocculation induced by different sized eddies. It is concluded that the root-mean-square velocity gradient $G = \sqrt{\bar{\epsilon}/\nu}$ ($\bar{\epsilon}$ is the average energy dissipation rate) is a valid parameter for describing the flocculation only for particles smaller than the Kolmogorov microscale of turbulence. For larger particles, $\bar{\epsilon}^{2/3}$ should be used to correlate coagulation with turbulence.

As mentioned above, the size of sewage particles is smaller than the Kolmogorov microscale, η , inside a discharge plume. Based on different models on turbulent coagulation, it can be concluded that the controlling parameters are the number concentration of particles and $\sqrt{\bar{\epsilon}/\nu}$ (or the energy dissipation rate of the turbulence since ν is constant). However, although turbulent shear can bring particles together to coagulate, it can also break up the agglomerates. Coagulation observed is actually

a balance between particle aggregation and breakup. To better simulate the real coagulation process, we need to understand the floc breakage mechanisms under turbulence as well. In the following, we will survey some of the models of breakage of flocs under turbulence.

2.1.2 Floc breakup by turbulence

Thomas (1964) has given a detailed discussion of the mechanisms of rupture of solid aggregates in a turbulent flow. He postulated that the basic mechanism leading to aggregate deformation and rupture can be ascribed to an instantaneous pressure difference on opposite sides of the floc. This pressure difference is created by the random velocity fluctuation of the turbulence flow. The effect of floc breakage increases with the energy dissipation rate, ϵ .

Argaman and Kaufman (1970) have done experiments to illustrate that in a stirred reactor, the average size of flocs is related to the mean square velocity fluctuations ($\overline{u'^2}$) by the equation $R_F = \frac{K_1}{\overline{u'^2}}$, where R_F is the average size of the flocs, K_1 is a constant. Considering the stripping of individual primary particles from the surface of flocs as the most important mechanism of floc breakage, they suggested that the rate of releasing primary particles due to floc breakage depends on the surface shear, the floc size, and the size of the primary particles. The shear stress depends on $\overline{u'^2}$, which is empirically related to the rms velocity gradient G .

Parker *et al.* (1972) have considered two mechanisms for floc breakup in the literature: surface erosion of primary particles, and bulgy deformation (floc splitting). For the surface erosion model, they argued that eddies which are large enough to entrain a floc produce zero relative velocity and no surface shear. Eddies which are much smaller than the floc result in little surface shear. Eddies with length

scale similar to the floc diameter create the maximum relative velocity and maximum surface shear. This model better suits the inorganic chemical flocs which have relatively homogeneous internal bonding and can be approximately as loose aggregations of primary particles. This model predicts that the maximum stable floc size follows the relation: $d_{max} = \frac{C}{G^n}$, and the primary particle erosion rate follows the equation: $\frac{dn_1}{dt} = K_B x G^m$, where C is the floc strength constant, n is the stable floc size exponent, n_1 is number concentration of primary particles, K_B is the floc breakup rate coefficient, x is the mixed liquor suspended solids concentration, and m the floc breakup rate exponent. They obtained n and m as 2 and 4 for inertial convection range, and 1 and 2 for viscous dissipation range, respectively. For biological flocs such as activated sludge, they suggested the model of filament breakage to explain the floc breakage due to tensile failure to yield two floc fragments. Again, they derived the expression of the size of the maximum stable floc as $d_{max} \propto G^{1/2}$ for both inertial convective and viscous dissipation subranges.

Tomi and Bagster (1978ab) calculated the upper size limit of aggregates inside a stirred tank under fully developed turbulent flow. They assumed that the yield stress of an aggregate is independent of its size, and the flow field is characterized by the average energy dissipation rate, $\bar{\epsilon}$, and the viscosity, ν . From both theoretical and experimental studies, they showed that when both viscous and inertial effects are important ($d_{max} \sim \eta$), the optimum floc size decreases with the intensity of agitation by the relation: $d_{max} \propto \bar{\epsilon}^{-1/2}$.

Tambo and Hozumi (1979) used clay-aluminum flocs to study the characteristic features of floc strength. In the viscous subrange ($d_{max} \ll \eta$), the maximum stable size was observed to follow the equation $d_{max} \propto \epsilon_o^{-0.38 \sim -0.33}$, where $\bar{\epsilon}$ is the total mean energy dissipation rate and ϵ_o is the effective mean energy dissipation rate

$= 0.1 - 0.2\bar{\epsilon}$. Similar results were obtained by Leentvaar and Rebhun (1983). They studied the strength of ferric hydroxide flocs and found out the dominant breakup mechanism is the surface erosion process. Their experimental results follow the relation: $d_{max} \propto \bar{\epsilon}^{-\gamma}$, and γ ranges from 0 to 1.

Summarizing the previous work on the breakage of flocs under a turbulent flow, we can infer that the breaking effects depend on the length scale of the coagulating particles and the energy dissipation rate.

Based on the above discussion of coagulation and floc breakage, it is concluded that for sludge particles ($d \leq 20 \mu m$), the energy dissipation rate and the particle number concentration are the most important parameters in determining particulate coagulation in a plume. Since the collision rate is a nonlinear function of the particle concentration and the energy dissipation rate, the coagulation should depend on the spatial distributions of these two factors (Clark, 1985). Hence, the better ways to study the coagulation of particles inside a plume are either to sample the sewage plume directly in the field or to generate a small scale plume in the laboratory.

Unless an adequate *in situ* test facility is available, field sampling is infeasible because of the possible change of sample characteristics during the collection, transportation, and storage before the laboratory analysis. Besides, we have no control of the field conditions. There are so many variables involved in a field test that we may not be able to understand and explain what is observed. Hence, a laboratory scale experiment is preferred to start with.

The major difficulty of using a laboratory scale plume to simulate the coagulation process is the change in the time scale. To simulate the fluid motion in a discharge plume, the Froude number should be preserved and the Reynolds number should be large enough to maintain the turbulence. Under Froude similarity,

the time scale should be proportional to the square root of the length scale. For example, if the model is 100 times smaller than the real plume, the coagulation time should be 10 times shorter. Since coagulation is a time-dependent process (not related to Froude similarity), the change of time scale will affect the results significantly. Hence, it is infeasible to use a small scale model of a plume to simulate coagulation. What we need is really a coagulating device which can generate the same particle concentrations and energy dissipation rate as in an actual plume under the actual time scale. In the following, we briefly survey the design of coagulating devices.

2.1.3 Coagulating reactor

Any apparatus which can create velocity gradients is a possible candidate for use as a coagulating reactor. The stirred tank reactor (jar-test apparatus) and the Couette reactor (concentric rotating cylinders) are widely employed in studying the coagulation of different kinds of particles.

A stirred tank reactor consists of a container and a mixing impeller driven by a variable-speed motor. A torque meter is coupled between the motor and the stirring shaft to measure the torque. The power input to the reactor (P) is calculated based on the equation: $P = T\omega$, where T is the torque on the impeller shaft, and ω is the angular velocity. The average energy dissipation rate $\bar{\epsilon}$ and the mean velocity gradient G are calculated as follow: $G = \sqrt{\frac{\bar{\epsilon}}{\nu}} = \sqrt{\frac{P}{\rho\nu V}}$, where V is the volume of the fluid. These two factors, $\bar{\epsilon}$ and G , were used extensively to correlate the coagulation data, and were also widely adopted as design parameters for flocculating devices (e.g. Birkner and Morgan, 1968; Argaman and Kaufman, 1970).

A Couette reactor is made of two concentric cylinders which can rotate relative to each other. Laminar shear can be produced inside the annular gap. The mean shear G can be calculated directly from the dimensions and the rotation speed of these two cylinders (van Duuren, 1968; Hunt, 1980). If the gap between cylinders is small, the Couette reactor can provide a nearly uniform shear rate. The settling of particles during coagulating experiments with Couette reactor can be avoided by using a horizontal axis design (e.g. Gibbs, 1982).

Fully developed turbulent pipe flow can also be used as a coagulating device (Delichatsios and Probst, 1975). The turbulent characteristics of pipe flow are well known, and the flow is nearly isotropic and homogeneous at the core of the pipe. The energy dissipation rate at the core of the pipe can be calculated from the diameter of the pipe and the pipe shear velocity u_* (Hinze, 1975).

An oscillating grid is yet another way to generate turbulence in a water tank (Linden, 1971). The turbulence characteristics have been measured in the laboratory (Thompson and Turner, 1975; Hopfinger and Toly, 1976). The turbulent root-mean-square velocity $\sqrt{u'^2}$, the turbulence integral scale l , and the energy dissipation rate $\bar{\epsilon}$ ($\bar{\epsilon} \propto \frac{\sqrt{u'^2}^3}{l}$) at a point inside the tank depend on the geometry, the frequency and stroke of the grid, as well as the distance of the point from the grid. At a short distance away from the grid, the turbulence intensity is nearly isotropic and homogeneous across the planes parallel to the grid. The intensity decreases with the distance from the grid.

Other possible coagulating devices include baffled mixers, small-bore tubes, granular filters and fluidized beds. Detailed discussions of the reactor design can be found in Ives's work (1977).

The turbulence intensity in a plume is both anisotropic and inhomogeneous. None of the existing coagulators is capable of reproducing the plume turbulence faithfully. In this research, we simplified the simulation by considering only the spatial average of the particle concentration and the energy dissipation rate across the width of the plume. We can calculate the average particle concentration and energy dissipation rate as functions of the plume height based on the equations governing the plume motion (Fischer *et al.*, 1979; List and Morgan, 1984). Furthermore, if we let the reference frame move at the centerline velocity of the plume, the change of the concentration and the energy dissipation rate with respect to the height of the plume becomes the change with respect to time. Then a coagulating device which generates similar history of the spatially averaged concentration and energy dissipation rate can satisfy our requirement.

This approach is intended to establish only order of magnitudes without allowing for heterogeneous effects. The real turbulent conditions inside a plume involve large fluctuations of velocity and concentration (with a positive correlation between them) and fluctuating path lines along which the coagulation may not be represented by the mean streamlines. Furthermore, it may be noted that the time of travel along mean streamlines is the minimum along the centerline, but approaches a large value at the dilute (non-coagulating) edges of a plume. Here, the centerline velocity was chosen to establish the time scale, although it may underestimate the effective coagulation times for the outer parts of a plume.

Among all the reactors, the stirred tank with variable input-output flow, i.e. the continuous flow stirred tank reactor (CFSTR), is the simplest design which approximately satisfies the requirements. Hence, a baffled stirred tank was selected as a coagulating device in this study. For a stirred tank, the turbulence intensity

and the average energy dissipation rate are related to the tank geometry and the rotation speed of the impeller at large Reynolds number (Schwartzberg and Treybal, 1968; Levins and Glastonbury, 1972; Günkel and Weber, 1975). The power characteristics of various kinds of impellers with vessels of different geometry have been studied extensively (e.g., Rushton *et al.*, 1950; Leentvaar and Ywema, 1979; Foust *et al.*, 1980). When the Reynolds number is larger than 1×10^5 , local isotropic turbulence exists and the power number Φ is constant ($\Phi = \frac{P}{\rho N^3 D^5}$, D is impeller diameter, and N is the rotation speed). These well researched data on the power characteristics of the tank were used to determine the configuration of the reactor and to calculate the energy dissipation rate.

2.2 Settling Velocity Measurements

The samples extracted from the coagulating reactor, whether coagulated or not, were used to measure settling velocity distribution of the sewage and sludge particles. In this section, the techniques for measuring the settling velocities are reviewed first, followed by discussion of the previous measurements of the settling velocities of sewage and sludge particles. A conventional settling column was used in the early stage of this study, and the results are presented in Appendices A and B. These results illustrate that the conventional settling column is infeasible for studying settling characteristics of sewage particles independent of coagulation. The problem arises because the initial concentrations required by the measuring techniques (typically greater than 50 mg/l) are high enough to induce significant coagulation over the many hours duration of the settling experiment. To overcome this difficulty, a holographic technique was developed as explained in Chapter 3.

2.2.1 Experimental technique

Settling velocities of particles can be measured directly inside a settling column, or estimated indirectly from size and density measurements of the settling particles (Ozturgut and Lavelle, 1984).

There are two different methods to measure the fall velocities with a settling column. One is to introduce particles from the top of the settling column filled with water, and measure the travelling time and distance of each individual particle. Particles can be observed using a microscope (Gibbs, 1982), or photographic technique (Chase, 1979; Kawana and Tanimoto, 1979), or holographic technique (Carder, 1979). To measure the fall velocity distribution using this top-feeding method, all particles have to be observed and either the number, or the volume, or the mass of particles is recorded at a fixed distance from the water surface. For example, an electrobalance can be mounted inside the settling column to measure the collected mass as a function of time (Gibbs, 1982). The cumulative velocity distribution $F(w)$ is then calculated as $\frac{M(z/w)}{M_{tot}}$, where $M(t)$ is the collected mass up to time t , M_{tot} is the total mass of the sample added into the settling column and z is the distance between the balance and the water surface.

The other approach is to start with a uniform particle suspension inside the settling column. If the particle concentration is low enough so that the interference among particles can be neglected, the accumulative velocity distribution, $F(w)$, can be derived as: $F(w) = \frac{C(z, z/w)}{C_0}$, where z is the sampling depth from the water surface, $C(z, t)$ is the particle concentration at depth z and time t , and C_0 is initial particle concentration. When particle coagulation takes place during settling, the distribution curves obtained at different depths are not the same. McLaughlin

(1958, 1959) suggested that the effect of coagulation is to increase the local mean settling velocity and the rate of change of local removal, i.e. $\frac{\partial^2 C(z, t)}{\partial t^2}$. Based on his experimental results, the coagulation effect, which was measured by a multiple-depth settling apparatus, was observed to increase with depth.

If the second approach is used, particle concentration is the only parameter that needs to be measured. The measurements can be obtained by taking samples from the column at fixed depths and analyzing the samples using a gravimetric technique (Faisst, 1976), or an absorbance method (Hunt, 1980), or a Coulter counter (Ozturgut and Lavelle, 1986; Lavelle *et. al*, 1986; Tennant *et. al*, 1987). If the settling velocities of individual particles are sought, a holographic technique can be applied to obtain *in situ* measurements without withdrawing samples from the settling column (Carder and Meyers, 1980).

2.2.2 Settling velocity measurements for sewage particles

Sedimentation of sludge or sewage effluent in seawater or salt water was studied by Brooks (1956), Myers (1974), and Morel *et al.* (1975). These works have been summarized and compared by Faisst (1976). He concluded that though the experimental conditions and the solids-capture technique were different, the measured settling velocities fall in the range from 1×10^{-5} to $3 \times 10^{-2} \text{ cm/sec}$. Faisst also carried out sedimentation experiments for different sludge samples with two different settling apparatus—a shallow column (a standard 2-l graduated cylinder) and a tall column (a 10-l plexiglass tube with side sampling ports). The shallow column tests were performed using digested primary sludge (D.P.S.) from the County Sanitation Districts of Los Angeles County (CSDLAC) at different dilution ratios (500:1, 200:1, and 50:1). Based on the sedimentation curves from previous studies and the

shallow column tests, he concluded that increasing the dilution ratio decreases the coagulation and, hence, the apparent sedimentation rate.

Faisst (1980) has also performed four multi-depth sampling sedimentation experiments using sludges from the Hyperion Plant (City of Los Angeles), CSDLAC, and the County Sanitation Districts of Orange County (CSDOC) with the tall column at 100:1 dilution. Particle coagulation during settling was confirmed by the difference of fall velocity distributions observed at two different depths. The distribution curves shift in the direction of larger velocities at the deeper sampling port. His results also show that the fall velocity distribution curves are different for sludges from different sources. The median fall velocities range from 1×10^{-4} to 5×10^{-3} *cm/sec*.

Herring (1980) has conducted settling velocity measurement for effluent from CSDOC, CSDLAC and San Diego in 1-l graduated cylinders. He used a dilution ratio in the order of 100:1, which is similar to the dilution ratio of the wastewater plumes in the ocean. Unfiltered seawater was used in his experiment to provide the interaction between natural particles and effluent particles. Because of the very diluted particle concentration in his experiments, he used several cylinders in parallel to measure $C(z,t)$. Experiments were stopped at designated sampling times, the 50 ml samples at the bottom of the cells were removed by siphoning and the particle concentrations of the remaining suspensions were measured by gravimetric method. He concluded that about 40% particles by weight in the effluent from CSDOC have fall velocities larger than 10^{-2} *cm/sec*. The percentage drops to about 15 % for the effluents from San Diego and CSDLAC.

Hunt and Pandya (1984) studied the coagulation and settling of sewage particles with a Couette reactor under laminar shear. The sewage samples used were

anaerobically digested primary and waste-activated sludge from the East Bay Municipal Utility District, Oakland, California. They assumed that particles are coagulated by a combination of Brownian motion, fluid shear and differential sedimentation. These processes aggregate particles from the initial size up to a size where settling becomes dominant. Particles are then removed from the fluid volume by settling, i.e., $\frac{\partial C(z,t)}{\partial t} = -\beta C^2(z,t) = w \frac{\partial C(z,t)}{\partial z}$. At different times, they measured particle concentrations at two different depths simultaneously to obtain the rate parameter, β , and the aggregate settling velocity, w . Their data indicate that the concentration of sludge in the Couette reactor decreases following the second-order kinetics. The sludge removal rate parameter, β , has a range from 1.0×10^{-6} to $9.1 \times 10^{-6} \text{ l/mg sec}^{-1}$ for $G = 0$ to 8 sec^{-1} at an initial concentration of 100 mg/l . Settling velocities of aggregate are from 2.8×10^{-3} to $1.1 \times 10^{-2} \text{ cm/sec}$ under the same conditions. Both β and w increase with shear rates as expected for a suspension dominated by coagulation.

Ozturgut and Lavelle (1984) developed a different technique to derive the settling velocity distributions for the fraction of the sewage particles with diameters less than $64 \mu\text{m}$. Instead of measuring the settling velocity directly, they first measured the wet density and the size distribution, and then calculated the settling velocity distributions based on the Stokes' law. This technique was used for particles with densities lower than 1.4 g/cm^3 and settling velocities larger than $3.6 \times 10^{-5} \text{ cm/sec}$.

In their experiment, the effluent was first wet sieved through a $64\text{-}\mu\text{m}$ mesh sieve, and then settled for 77 hr in a 12 cm high container. The material collected in the lower 2 cm of the container ($\sim 187 \text{ mg/l}$) was then introduced into the top of a density stratified column ($\frac{1}{\rho} \frac{d\rho}{dz} \cong 0.4 \text{ m}^{-1}$). After 171 hr , samples were withdrawn. The fluid density (equal to the density of the particles in it) was measured by a

hydrometer, and the particle size distributions were determined by a Coulter counter (1.0–64 μm).

For a 24-hr composite effluent sample from the Municipality of Metropolitan Seattle, they found that 8.5% by weight of particles with diameter larger than 64 μm , and within which, 83.1% by weight with $\rho \leq 1.4 \text{ g/cm}^3$. For particles smaller than 64 μm , 27% by volume have $\rho \leq 1.01 \text{ g/cm}^3$, 33% by volume have $1.02 < \rho < 1.4 \text{ g/cm}^3$, and 40% by volume have $\rho \geq 1.4 \text{ g/cm}^3$. For particles smaller than 64 μm , the median fall velocity (by volume) is around $1.5 \times 10^{-3} \text{ cm/sec}$.

2.2.3 Data interpretation for settling column measurements with particle coagulation

If particles coagulate inside a settling column, the curves of $\frac{C(z,t)}{C_0}$ versus $\frac{z}{t}$ can no longer be considered as the accumulative fall velocity distribution. Instead, these curves illustrate a combined results of coagulation and settling. In the following, different models for data interpretation are reviewed.

Using different approaches, Hunt (1980), and Morel and Schiff (1983) have arrived at the same conclusion that the overall particle removal by coagulation and settling has a second-order dependence on the particle concentration, i.e., $\frac{dC(t)}{dt} = -\beta C(t)^2$, where $C(t)$ is the solids concentration at time t , and β is a constant characterizing the frequency of particle collision. In deriving this relation, Hunt assumed that a single coagulation mechanism dominates a subrange of particle size: Brownian motion for the smaller sizes, shear for the intermediate sizes, and differential sedimentation for the largest sizes. He also assumed that the particle size distribution is in a dynamic steady state, which implies the existence of a constant

flux of particle volume through the distribution. This flux is equal to the rate of formation of small particles by coagulation and the rate of removal of large particles by sedimentation.

From a different point of view, Morel and Schiff considered the coagulation as the rate-limiting step in the overall sedimentation process. It was assumed that small particles coagulate but have zero net settling velocity; while big particles, formed by coagulation, settle infinitely fast. Previous sedimentation column data by Brooks (1956), Myers (1974), Morel *et al.* (1975), and Faisst (1979) were reanalyzed and interpreted as coagulation kinetics rather than the distribution of settling velocities. They derived a β of $2 \times 10^{-7} \text{sec}^{-1} \text{mg}^{-1} \text{l}$ within half an order of magnitude.

Farley and Morel (1986) combined analytical, numerical, and laboratory studies to examine the kinetic behavior of sedimentation in a settling column. They derived an expression for the rate of mass removal of solids in the column as $\frac{dC(t)}{dt} = -\beta_{ds}C^{2.3} - \beta_{sh}C^{1.9} - \beta_bC^{1.3}$. The first term accounts for the coagulation induced by the differential settling, the second for the shear, and the third for the Brownian motion.

Their results from numerical simulation illustrated a nonuniform reduction in the characteristic size distribution—the removal of large particles by settling is faster than the replenishment from small particles by coagulation when total mass concentration decreases. This result is inconsistent with Morel and Schiff's assumption in deriving the 2nd-order coagulation kinetic for sedimentation column (1983). Their numerical simulation results also contradict Hunt's assumptions (1980). The coagulation volume flux is not constant across the size distribution, and the coagulation of particles within a small size interval is controlled by more than one

collision mechanism as mass concentration is reduced. Their numerical simulation confirmed that the characteristic rates of solids removal can be described by power law dependencies on mass concentration and that the exponent is dependent on the mode of coagulation.

Farley and Morel also performed settling column experiments under quiescent environment with particles of high density. Metallic copper particles ($\rho = 8.9 \text{ g/cm}^3$), and goethite ($\rho = 4.5 \text{ g/cm}^3$) were used to test the proposed rate law for total mass removal. The observed results are in good agreement with the proposed power law prediction. The three sedimentation rate coefficients (β_b , β_{sh} , and β_{ds}) were determined as functions of system parameters based on a semiempirical solution which shows consistent results with laboratory observations.

2.2.4 Conventional settling column experiment

Conventional settling columns were used in the early stage of our research to study the settling behavior of sewage particles in seawater (see Appendix A for reproduction of Wang, Koh, and Brooks (1984) for detailed results). Two 10-liter plexiglass columns, 9 cm I.D. \times 2 m with five side-sampling ports, were used as the settling apparatus. All experiments were performed under quiescent condition without shear. Two different techniques were employed to measure the particle concentration. One is the gravimetric method (Faisst, 1976,1980) which weighs the collected mass of particles retained on the 0.4- μm Nuclepore membrane (Nuclepore Corporation, Pleasanton, California) after filtration. The other technique measures the absorbance of chemically treated samples. The absorbance readings can then be correlated to the mass concentration of particles (Dubois *et al.*, 1956; Bradley and Krone, 1971; Hunt, 1980).

Twenty-six tests were performed for different sludge and effluent samples in filtered artificial seawater; results are presented as apparent fall velocity distributions, i.e., $\frac{C(z,t)}{C_0}$ versus $\text{Log}\left(\frac{z}{t}\right)$ (Appendix A). Based on these data, it can be concluded that the apparent fall velocity distributions are affected by the types of sewage or sludge used, the initial dilution of sewage, the treatment processes, and the time when sewage was collected at the treatment plant. Effects from both settling and particulate coagulation were observed to influence the downward transport of particles. Hence, the conventional settling column results are, in fact, measurements of the combined effects of settling and particulate coagulation.

We also developed a simple conceptual model to illustrate that the conventional settling column experiment is unable to distinguish the effects of settling from those of coagulation. This simple model simulates a hypothesized settling and coagulation process in a conventional settling column (see Appendix A). Only two types of particles were considered: coagulating particles and settling particles. Coagulating particles are small and with negligible settling velocities. Settling particles, which are coagulated from smaller coagulating particles, are assumed to have a single settling velocity. The expression of n^{th} order kinetics with a constant rate coefficient was assumed for the coagulating particles, i.e., the rate follows the expression: $r_1 = -\frac{dC_1}{dt} = \alpha C_1^n$, where r_1 is the coagulation rate, α is the rate constant, and C_1 is the solids concentration of the coagulating particles. This simplified model shows that the observed results from the conventional settling column can be interpreted either as the pure settling of a group of particles with different velocities, or as the settling of particles of a constant velocity which are coagulated from smaller particles at the rate mentioned above.

Different models for interpreting the settling and coagulation processes inside the conventional settling columns were also developed by McLaughlin (1958, 1959), Morel and Schiff (1983), Hunt and Pandya (1984), Lo and Weber (1984), and Farley (1984). Although their model predictions agree well with their experimental results, their models cannot be extended directly to field applications because of much greater depths and settling times to reach the bottom. Since the experimental conditions in the settling columns are different from those in the ocean, the resulting coagulation-settling process in the ocean may be quite different from what are observed in the laboratory. It is difficult to incorporate the parameters such as β , which are derived from the laboratory experiments based on the settling column model, to describe the transport processes in the ocean. For more reliable fall velocity data, it is essential to design an experimental setup which can measure settling velocity distributions independently.

Dilution can decrease particle number concentration, thereby reducing the collision rate. In our settling velocity measurements of digested sludge, samples with low particle concentration, i.e., high dilution ratio (with total dilution ratio $\geq 10^4$ and concentration $\leq 2 \text{ mg/l}$), were used to prevent coagulation. This extremely low solids concentration renders the traditional gravimetric and absorbance methods infeasible. Among the techniques for measuring low particle concentrations, the Coulter counter was discarded because of the possibility of breaking flocs during sampling and measurement. Among the *in situ* measuring methods, the holographic technique was preferred to photographic and microscopic examination because it can provide a larger depth of field. Hence, an in-line holographic camera system was applied for measuring the settling velocities. In the following section, a brief review of velocity measurements using the holographic technique is given.

2.2.5 Velocity measurement by holographic technique

Holography is a photographic process which is used to record and regenerate three-dimensional information. A hologram records complete information of a light wave field, i.e., both amplitude and phase (Collier *et al.*, 1971; Caulfield, 1979). What is recorded by a hologram is basically an interference pattern resulting from the interference of two coherent light waves: a reference wave, and an objective wave reflected or scattered by the test object. During the reconstruction, a hologram acts as a diffraction grating, through which the light diffracts and regenerates two three-dimensional images of the original test object. These images can then be analyzed in detail. There are considerable amounts of research focused on the fundamental principles of this technique and its application. Recent reviews provide useful guides to this technique (Thompson, 1974; Trolinger, 1975; Thompson and Dunn, 1980).

The holographical technique provides a number of useful features for studying the dynamics of particles. It can simultaneously record a large three-dimensional particle field with information on sizes, shapes and spatial positions of individual particles. Compared to conventional photography, it provides a larger depth of field without sacrificing the resolution. Motion analysis, i.e., estimating the velocity, acceleration and trajectory of particles, can be easily done by using multiple-exposed holograms (Brenden, 1981; Stanton *et al.*, 1984).

Different methods proposed for velocity measurements with holographic techniques can be classified into four categories (Boettner and Thompson, 1973). The first type allows the particles to move during the recording so that the resultant images show streaks with length proportional to the velocity of particles. The second method is to record series of holograms at preset time intervals. Coordinates

of particles with respect to a fixed reference point can be derived from every hologram; the displacements and velocities of particles can then be calculated based on the positions of particles in different holograms and the time between recording (Carder, 1979). The third method is to use the double-exposure technique to record the sample volume twice on a single hologram. The reconstructed holograms show double images of every particle. The velocities of particles can be calculated from the time between exposures and the relative distances between the double images (Trolinger *et al.*, 1968, 1969; Fourney *et al.*, 1969; Boettner and Thompson, 1973; Belz and Menzel, 1979; Brenden, 1981). The fourth technique is the same as the third one during recording process, i.e., to record doubly exposed holograms. However, instead of analyzing the reconstructed images, the displacements and velocities are measured on the optical Fourier-transform plane (Ewan, 1979ab, 1980; Malyak and Thompson, 1984).

Since holograms record the interference patterns, the visibility of the interference fringes can be degraded by the movement of the object during recording. Without the special design such as the synchronized moving reference beam (Dyes *et al.*, 1970), the observation of the streaks can be difficult. Furthermore, it cannot measure particle size and shape. The last approach works well for spherical particles of uniform size or for particles of some known size distribution. However, it cannot be applied directly to the irregular and nonhomogeneous sewage particles. The third method is better than the second one because it requires less time for data analysis. Hence, doubly exposed holograms were used to measure the settling velocities of sewage particles in this study.

2.3 Summary

To measure the settling velocity distribution of sewage or digested sludge particles in seawater, it was decided to use a double-exposure holographic technique. This technique permits direct measurement of individual particle velocity without the ambiguity of settling column data caused by coagulation during the tests. Coagulation in this research is simulated separately in a special mixing reactor before the settling measurements. The experimental setup and procedures are presented in detail in the next chapter.

3. EXPERIMENTAL SETUP AND PROCEDURES

In this chapter, we discuss the experimental techniques for studying the settling characteristics of the sewage particles in seawater under the influence of coagulation. When sludge is mixed with seawater after being discharged through a pipeline, the strong turbulence, the relatively high concentration of suspended solids at the beginning of the plume rise, and the high ionic strength of seawater together provide the opportunity for particle coagulation. This coagulation process may modify the size, shape, structure, density, and, hence, the settling velocity of sludge particles. However, both the concentration and the turbulence intensity decrease rapidly during the rise of the discharge plume. Consequently in the later stage of plume mixing, the low solids concentration and turbulence intensity prevent any further significant coagulation.

From the above discussion, it is clear that coagulation may play a major role in determining the distribution of the settling velocities of sludge particles. Hence, experimental techniques have to be designed to study the possible change of fall velocity distribution as a result of coagulation in the plume mixing. In the past, a settling column was used extensively as an apparatus to measure the fall velocity distributions of a variety of particles including sewage particles (Brooks, 1956;

Myers, 1974; Morel, 1975; Faisst, 1976, 1980). It was employed again in this study and proven to be inadequate for our purposes (see Appendix A). A new experimental design that approximately simulates the coagulation inside the rising plume and then measures the settling velocity distribution was developed in this study. The design of the new experimental apparatus and procedures are discussed in this chapter.

3.1 Design of the Coagulating Reactor

As discussed in the previous chapter, the conditions which determine the coagulation of sewage particles inside a discharge plume are too complicated to be faithfully reproduced in the laboratory. Among all the parameters which affect the coagulation, only the most important ones—time, dilution and energy dissipation rate—were controlled for the simulation. One should be aware that what happens inside this coagulating reactor does not reflect exactly that inside a real discharge plume. Nonetheless, this experiment does provide a basis for comparison and makes it possible to predict the behavior of particles in the field based on the laboratory study.

3.1.1 Time history of the dilution and the energy dissipation rate of a discharge sewage plume

To simulate the coagulation inside a rising plume, first we need to know how the dilution and the energy dissipation rate change with depth. Two outfall systems were selected for simulation: one was the proposed sludge disposal plan of Orange County (Brooks *et al.*, 1985), and the other was the existing effluent outfall of Los Angeles County. The case of sludge discharge is discussed next.

3.1.1.1 Proposed sludge outfall for CSDOC

When sludge is discharged from the end of an outfall pipe, it rises and mixes with surrounding seawater in the form of a buoyant jet. Due to the ambient density stratification, the plume stops rising after reaching its neutral buoyancy and is then carried away by ambient current. The dilution ratio of a sludge plume at this equilibrium height is so large ($> 10^3 : 1$) that particle coagulation becomes insignificant and the settling characteristics of sewage particles remain practically unchanged afterwards. Hence, our laboratory coagulator was designed to simulate the mixing history of a sewage plume from the pipe exit to the equilibrium height.

For the proposed Orange County sludge outfall, the ambient density gradient is approximately linear ($E = -\frac{1}{\rho} \frac{d\rho}{dz} \cong 1.5 \times 10^{-6} \text{ m}^{-1}$), and the ambient current, U_A , has a median speed around 7 cm/sec . It is presumed that the digested sludge will be diluted with effluent to a concentration of about $10,000 \text{ mg/l}$, and that the relative density difference, $\frac{\Delta\rho}{\rho}$, between seawater and the sludge mixture at the exit of the outfall will be 26.5×10^{-3} . The diameter, D , of the outfall pipe will be about 18 in (0.457 m). The design flow rate, Q , of sludge-effluent mixture will be selected in the range from 3.0 to 12.0 mgd (0.131 to $0.526 \text{ m}^3/\text{sec}$), corresponding to a buoyancy flux, $B = g \frac{\Delta\rho}{\rho} Q$, of 0.0340 to $0.137 \text{ m}^4/\text{sec}^3$ and a momentum flux, $M = \frac{4}{\pi} \frac{Q^2}{D^2}$, of 0.105 to $1.69 \text{ m}^4/\text{sec}^2$. Following Wright's work (1977, 1984) on the fluid dynamics of a buoyant jet in a stratified cross-flow, different characteristic length scales were calculated for the discharge plume based on the design parameters. It was found that $\frac{M^{3/4}}{B^{1/2}}$, ranging from 1.00 to 4.00 m , is much smaller than $\frac{B^{1/4}}{(gE)^{3/8}}$, ranging from 27.9 to 39.4 m , indicating that the buoyancy flux will dominate the buoyant

jet in the near field, well before the plume reaches its equilibrium height. Hence, considering a sludge plume driven by only the buoyancy flux, the effects of the ambient current were compared with the effects of the ambient density gradient by the use of the characteristic buoyancy length scales, l_b and l'_b . The result is that $l'_b = \frac{B^{1/4}}{(gE)^{3/8}} = 27.9 - 39.4 \text{ m}$ is substantially less than $l_b = \frac{B}{U_A^3} = 99 - 399 \text{ m}$, which suggests that the general behavior of this sludge plume in the near field is the same as that of a buoyant plume in a nonflowing stratified field.

Based on the above discussion, the equations that govern the motion of a vertical turbulent buoyant jet in a density-stratified environment were used to calculate the dilution and the energy dissipation rate inside a plume. The equations are (Fischer *et al.*, 1979):

$$\frac{d}{dz} (\pi b_w^2 w_m) = 2\pi \alpha b_w w_m \quad (3.1.1)$$

$$\frac{d}{dz} \left(\frac{\pi}{2} b_w^2 w_m^2 \right) = \pi g \lambda^2 b_w^2 \theta_m \quad (3.1.2)$$

$$\frac{d}{dz} \left(\frac{\pi g \lambda^2 b_w^2 w_m \theta_m}{1 + \lambda^2} \right) = -g E \pi b_w^2 w_m \quad (3.1.3)$$

with the initial conditions:

$$[\pi b_w^2 w_m]_{z=0} = Q' = 2Q \quad (3.1.4)$$

$$\left[\frac{\pi}{2} b_w^2 w_m^2 \right]_{z=0} = M \quad (3.1.5)$$

$$\left[\pi g \frac{\lambda^2}{1 + \lambda^2} b_w^2 w_m \theta_m \right]_{z=0} = B \quad (3.1.6)$$

In these equations, z is the vertical distance from the exit of the pipe, $w_m(z)$ is the time-averaged vertical velocity on the axis of the buoyant jet; $\theta_m(z) = \frac{\rho_a - \bar{\rho}}{\rho_0}$

is the time-averaged density anomaly caused by the jet along the axis of the jet; $\lambda = 1.16$, where b_w is the velocity profile $\frac{1}{e}$ -width and λb_w the concentration profile $\frac{1}{e}$ -width; Q is the initial volume flux; $Q' = 2Q$ is the flow flux of the plume at the end of zone of flow establishment; M is the initial momentum flux; B is the initial buoyancy flux; $E = -\frac{1}{\rho_0} \frac{d\rho}{dz}$ is the ambient density gradient; and α is the entrainment coefficient calculated from the following equations:

$$\alpha = \alpha_j \exp \left[\ln \left(\frac{\alpha_p}{\alpha_j} \right) \left(\frac{R}{R_p} \right)^2 \right] \quad (3.1.7)$$

$$R = \frac{\mu \beta^{1/2}}{m^{5/4}} = \left[\frac{4\sqrt{2\pi} \lambda^2}{(1 + \lambda^2)} \left(\frac{g b_w \theta_m}{w_m^2} \right) \right]^{1/2} \quad (3.1.8)$$

where R_p is the plume Richardson number with the value of 0.557, α_j is the entrainment coefficient of a pure jet with the value of 0.0535 ± 0.0025 , and α_p is the entrainment coefficient of a pure plume with the value of 0.0833 ± 0.0042 , μ is the volume flux, β the buoyancy flux, and m the momentum flux at distance z .

The time for the sludge plume to travel from the pipe exit to the equilibrium height can be estimated by multiplying both sides of Eqn. 3.1.2 with w_m , taking derivatives with respect to z , and multiplying with w_m again. Together with Eqn. 3.1.3, we have:

$$\frac{d^2}{dt^2} \left(\frac{\pi}{2} b_w^2 w_m^2 \right) = -2(1 + \lambda^2) g E b_w^2 w_m^2 \quad (3.1.9)$$

By solving Eqn. (3.1.9), we obtained the expression of travelling time to be $\frac{\pi}{\sqrt{2(1 + \lambda^2)gE}}$. The travelling time, which depends only on the ambient density

gradient, is 370 sec in this case. Equations (3.1.1) to (3.1.3) can be simplified again as follows:

$$\frac{dw_m}{dz} = -2\alpha \frac{w_m}{b_w} + 2g\lambda^2 \frac{\theta_m}{w_m} \quad (3.1.10)$$

$$\frac{db_w}{dz} = 2\alpha - g\lambda^2 \frac{b_w\theta_m}{w_m^2} \quad (3.1.11)$$

$$\frac{d\theta_m}{dz} = -\frac{1 + \lambda^2}{\lambda^2} E - 2\alpha \frac{\theta_m}{b_w} \quad (3.1.12)$$

with the corresponding initial conditions

$$[w_m]_{z=0} = \frac{2M}{Q'} \quad (3.1.13)$$

$$[b_w]_{z=0} = \sqrt{\frac{Q'^2}{2\pi M}} \quad (3.1.14)$$

$$[\theta_m]_{z=0} = \frac{1 + \lambda^2}{\lambda^2} \frac{B}{Q'g} \quad (3.1.15)$$

These equations were solved numerically to give w_m , b_w and θ_m as functions of the distance z . The independent variable, distance z , can be converted to time t by substituting $t = \int \frac{dz}{w_m}$ for the corresponding z . The average dilution was then calculated using $\frac{\pi b_w^2 w_m}{Q}$ †. The energy dissipation rate was estimated from the equation derived for a turbulent plume by List and Morgan (1984) as: $\frac{\bar{\epsilon}\Lambda^3}{E_k} = 0.25$,

† It is preferred to use centerline dilution instead of the average dilution for sludge outfall. Hence, the dilution history used in this study is equivalent to the centerline dilution history of a sludge outfall with the same buoyancy flux but smaller initial concentration as 5600 mg/l ($= \frac{10000 \text{ mg/l}}{1.78}$).

where $\bar{\epsilon}$ is the local mean dissipation rate, Λ is the local width of the plume, and E_k is the local flux of kinetic energy in the plume at height z . In this study, we used * $\Lambda = 2b_w$ and $E_k = 0.5\pi b_w^2 w_m^3 = (0.5w_m^2)(\pi b_w^2 w_m)$. The calculated time history of dilution and energy dissipation rate are plotted in Figure 3.1.1. Because of the many assumptions, these curves can only be considered approximate representatives, intended to establish the correct order of magnitudes.

3.1.1.2 Effluent outfalls of CSDLAC

The largest of the three multiport effluent outfalls of Los Angeles County at Whites Point was used as the basis for simulation; the inside diameter is 120 *in* (3.05 *m*), and there are 743 discharge ports along a line diffuser. The length of the diffuser, L , is 4440 *ft* (1354 *m*), the depth of discharge ranges 165 to 190 *ft* (50.3 to 57.9 *m*), and the design average flow, Q , is 341 *ft*³/*sec* (9.66 *m*³/*sec*) (Fischer *et al.*, 1979). The suspended solids concentration of the effluent is about 60 *mg/l*. If we assume $g' = g \frac{\Delta\rho}{\rho}$ is 0.26 *m/sec*², the buoyancy flux $B = g' \frac{Q}{L}$ is 0.00185 *m*³/*sec*³. Under non-stratified (winter) conditions, the time for the plume to travel to the ocean surface was estimated to be 270 *sec* by dividing the average depth of the diffusers by the centerline velocity, $w_m = 1.66B^{1/3} = 0.204$ *m/sec*, of the plume.

* If w^3 is integrated across the plume, assuming a Gaussian profile, the result is $E_k = \frac{\pi}{6} b_w^2 w_m^3$, which would have been a better value than $\frac{\pi}{2} b_w^2 w_m^3$ used here. Hence the $\bar{\epsilon}$ used in this study may be three times too large and the coagulation rate may be too large by a factor of $\sqrt{3}$. However, the definite effects on coagulation are still unresolved due to the inhomogeneity of turbulence shear inside the plume and the coagulating reactor as well as the difference in turbulence structure of the plume and the available laboratory reactors.

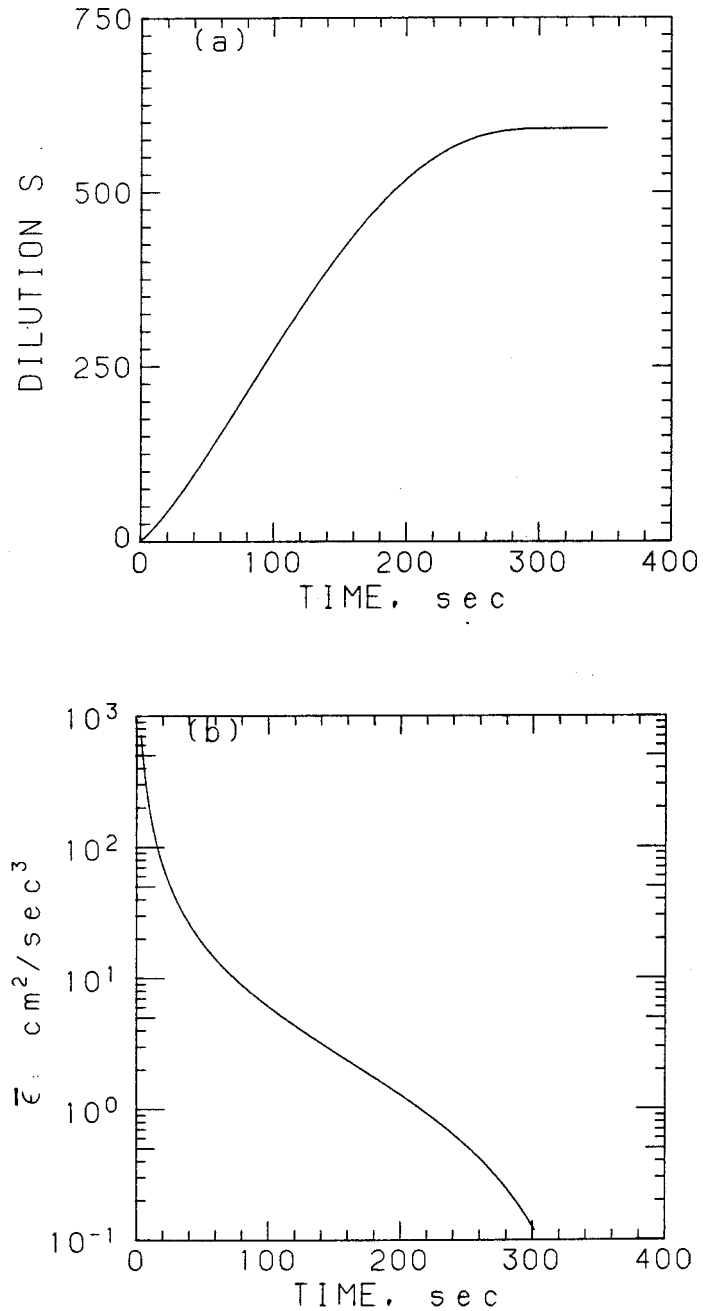


Figure 3.1.1 Time history of plume mixing calculated for the proposed deep sludge outfall for the County Sanitation Districts of Orange County, $Q = 0.131 \text{ m}^3/\text{sec}$, $B = 0.0340 \text{ m}^4/\text{sec}^3$, and $M = 0.105 \text{ m}^4/\text{sec}^2$, (a) dilution versus time, (b) energy dissipation rate versus time

The dilution ratio was calculated according to the solution for a two-dimensional plume in an uniform and motionless environment:

$$S_c(z) = 0.38 \frac{g'^{1/3} z}{q^{2/3}} \quad (3.1.16)$$

where $S_c(z)$ is the centerline dilution at distance z from the outfall; $g' = g \frac{\Delta\rho}{\rho}$, where ρ is the density of the effluent and $\Delta\rho$ the density difference between the ambient fluid and the effluent; and $q = \frac{Q}{L}$ is the initial discharge per unit length. Eqn. 3.1.16 was rewritten as $S_c = \frac{0.63g't}{B^{1/3}}$ by combining with the relation $w_m = \frac{z}{t} = 1.66B^{1/3}$ for a plane plume. Since the thickness of the sewage field above a diffuser was found to be 30% of the depth under the unstratified situation (Koh, 1983), this plume formula should be used to calculate the dilution only to the height of 70 % of the water depth ($z = 38.5 \text{ m}$, $t = 190 \text{ sec}$), and the dilution beyond 38.5 m should remain roughly constant at the calculated value of $S = 250$.

The energy dissipation rate was estimated from the result of the energy balance of a plane plume derived from the turbulence model by Hossain and Rodi (1982). The average energy dissipation rate approximately follows the equation $\bar{\epsilon} \simeq 0.013 \left(\frac{w_m^3}{y_{0.5w_m}} \right)$; where w_m is the velocity at plume axis, $y_{0.5w_m}$ is the lateral distance from the plume axis to where $w = 0.5w_m$. Assuming a Gaussian profile for the velocity, we obtained $y_{0.5w_m} = 0.83b_w$. Therefore, with $b_w = 0.116z$, $z = w_m t$ and $w_m = 1.66B^{1/3}$, this equation was rearranged as follows:

$$\bar{\epsilon} \simeq 0.013 \frac{w_m^3}{0.83b_w} = 0.013 \frac{w_m^3}{0.83(0.116)w_m t} = 0.37 \frac{B^{2/3}}{t} \quad (3.1.17)$$

The resulting dilution ratio and the energy dissipation rate as functions of time are shown in Figure 3.1.2. Although these approximate relationships represent only one condition (mean flow, no stratification, and rise along the centerline), they give the correct order of magnitudes. The outfall diffuser was idealized as a simple line plume neglecting initial momentum flux and individual jets before merging.

The above calculations show that the dilution ratio increases and the energy dissipation rate decreases with time for both outfall systems. The next step is to design a laboratory scale reactor inside which the time history of particle concentrations and energy dissipation rates are simulated according to the above calculations.

3.1.2 Design of a CFSTR with variable input flow rate and stirring speed

A continuous flow stirred tank reactor (CFSTR) was designed to generate the desired dilution and mixing history. For a stirred tank, the dimensionless power number $\Phi = \frac{P}{\rho N^3 D^5}$, in general, depends on the Reynolds number ($Re = \frac{ND^2}{\nu}$), the Froude number, and the geometry of the mixing device, where N is the rotation speed of the impeller, D is the impeller diameter. The geometry of the mixing device is defined by the shape and the diameter of the impeller, the diameter of the tank, the height of the liquid, the position of the impeller inside the tank, and the number and the width of the baffles. If geometric similarity of the mixing device is preserved and vortexing is prevented by baffles, the power number depends only on the Reynolds number (e.g. Rushton *et al.*, 1950). The average energy dissipation rate inside the tank is expressed as:

$$\bar{\epsilon} = \frac{kN^3D^5}{T^2H} \quad (3.1.18)$$

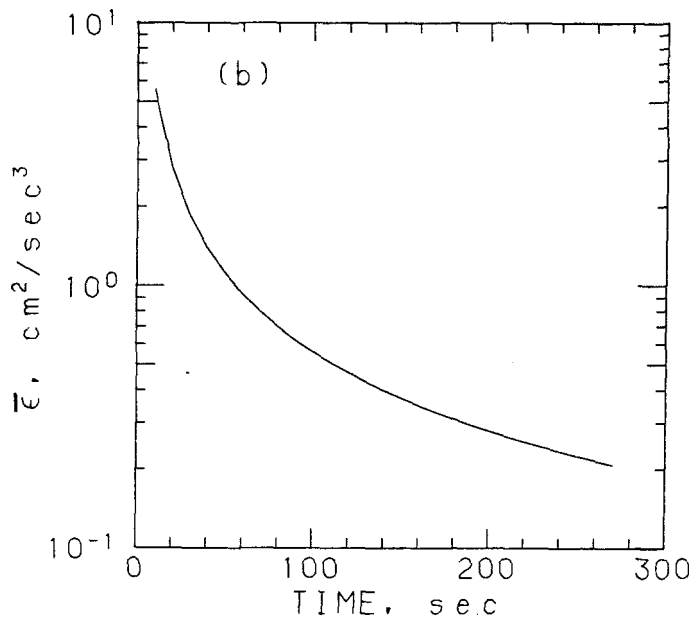
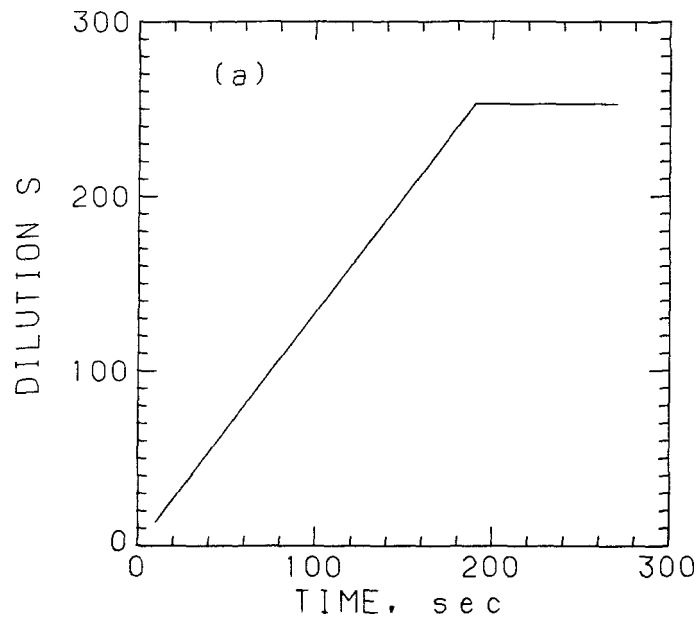


Figure 3.1.2 Time history of plume mixing calculated for the existing 120-in effluent outfall for the County Sanitation Districts of Los Angeles County, $Q = 9.66 \text{ m}^3/\text{sec}$, $B = 0.00185 \text{ m}^4/\text{sec}^3$, (a) dilution versus time, (b) energy dissipation rate versus time

where N is the rotation speed in *rps*, H is the depth of the liquid, T is the tank diameter, and $k = \frac{4\Phi}{\pi}$ is a proportionality constant.

Since the power characteristics, Φ versus Re , of various kinds of impellers with vessels of different geometry have been studied extensively (e.g., Rushton *et al.*, 1950; Leentvaar and Ywema, 1979; Foust *et al.*, 1980), Eqn. 3.1.18 was used to calculate the average energy dissipation rate. The configuration of the reactor was determined by weighing a number of requirements.

The volume of the reactor should be larger than 2000 *ml* to provide enough samples for later settling measurements. Most of the reactors studied before have equal diameter and height, so the diameter of the reactor should be no less than 14 *cm*. Furthermore, larger $\frac{D}{T}$ ratio provide better mixing for a stirrer tank. If $\frac{D}{T}$ is set to be at least 1/3, D should be larger than 4.7 *cm*. Under the condition $T = H = 3D \geq 14\text{cm}$, we calculated the energy dissipation rate to be $\bar{\epsilon} = 0.047\Phi N^3 D^2$ from Eqn. 3.1.18. In order to meet the required energy dissipation rate, which ranges from 0.1 to 100 cm^2/sec^3 , and, at the same time, maintain high enough Reynolds number to keep flow turbulent (small ΦN^3 and large N), an impeller with relatively small power number should be used. Therefore, a two-blade paddle was chosen for its small power number and its simple structure.

The dimensions of the reactor and the impeller were designed to be $T = H = 3D = 6 \text{ in } (15.24 \text{ cm})$ (Figure 3.1.3). Based on this configuration, the power number Φ is constant and equal to 1.8 and $\bar{\epsilon} = 2.16N^3$ for $Re \geq 5 \times 10^3$, and the corresponding rotation speed and average energy dissipation rate are 1.9 *rps* and 14.8 cm^2/sec^3 respectively. When $Re < 5 \times 10^3$, the power number is no longer constant, but varies with Re . For Re ranging from 10^2 to 5×10^3 (N from 0.038 to 1.9 *rps*), power number Φ changes from 1.6 to 1.8. To obtain the energy dissipation

rate at different rotation speed in this Re range, we first calculated the Reynolds number, then read the power number from the Φ versus Re curve, and applied Eqn. 3.1.18 to get $\bar{\epsilon}$. The result is shown in Figure 3.1.4. The linear regression line shows that the relation between the energy dissipation rate and the rotation speed of the impeller follows the empirical equation: $\bar{\epsilon} = 1.91N^{3.05}$, where $\bar{\epsilon}$ is in cm^2/sec^3 , and N is in rps .

A Bodine motor (Model 527, Bodine Electric Co., Chicago, Illinois) with a Minarik adjustable speed controller (Model SL-15, Minarik Electric Company, Los Angeles, California) provides a range of rotation speeds from 7.5 to 250 rpm , corresponding to an energy dissipation rate ranging from 0.0034 to 148 cm^2/sec^3 .

The dilution ratio or the particle concentration inside the reactor was controlled by adjusting the flow rate of the dilution water into and out of the reactor. The flow rate was calculated based on mass balance as: $V \left(\frac{1}{S} \frac{dS}{dt} \right)$, where V is the volume of the reactor, and S is the dilution ratio at time t . The required flow rate as a function of time is shown in Figure 3.1.5 for the case of sludge disposal of CSDOC and the case of the effluent outfall of CSDLAC respectively.

Based on the dilution history, the computed flow rate in the first 30 seconds is so large (or the residence time so short) that most of the particles are flushed away before they are well mixed. This makes the dilution higher than what it should be. This large inflow of dilution water also generates more turbulence than is needed. Hence, instead of starting with a pure sludge sample inside the reactor and diluting the sample with a huge quantity of seawater, dilution for the first 20 seconds was achieved by injecting a small sludge jet into a reactor full of seawater. The paddle was then turned on to mix the surface layer resulting from the sludge jet with the rest of the water in the container. The mixture inside the reactor reached the

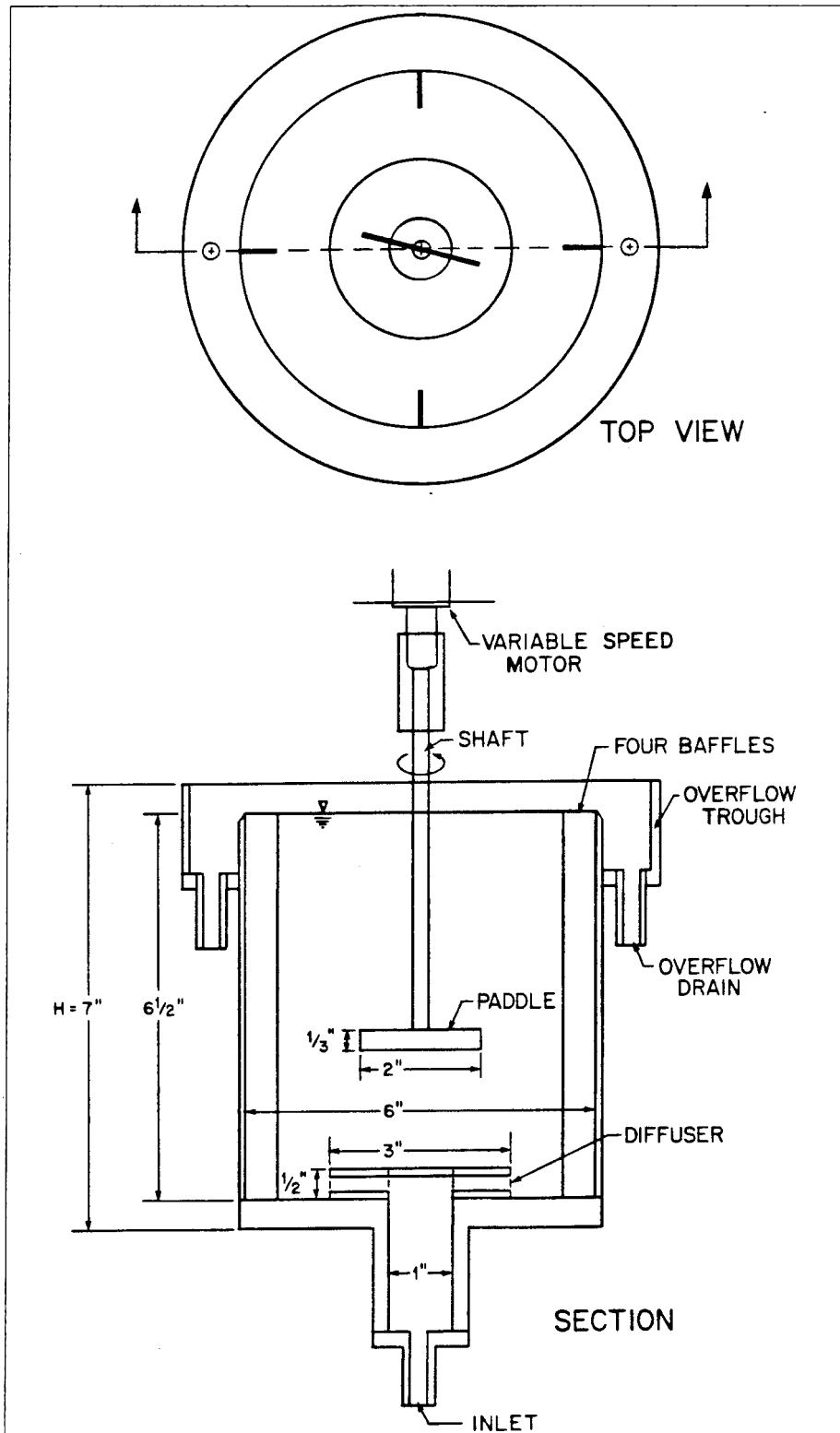


Figure 3.1.3 Schematic diagram of the coagulating reactor

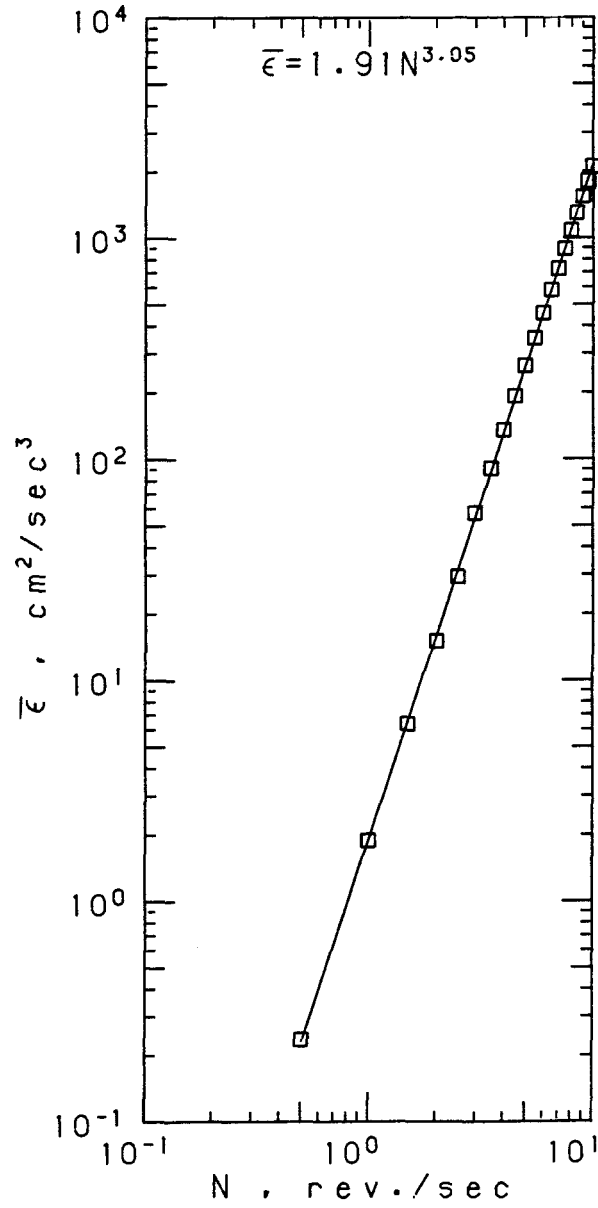


Figure 3.1.4 The average energy dissipation rate $\bar{\epsilon}$ versus the rotation speed of the paddle for the reactor shown in Figure 3.1.3 derived from the $\Phi-Re$ curve (Rushton *et al.*, 1950) for $10^2 < Re < 5 \times 10^3$

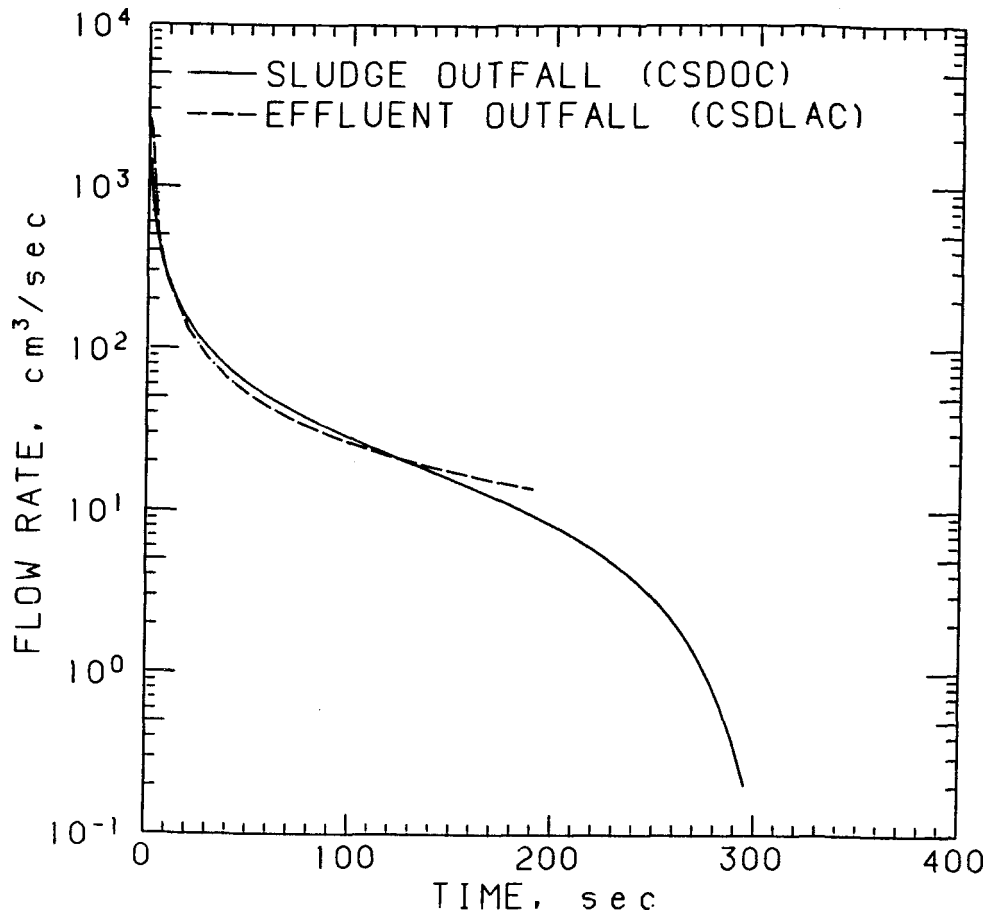


Figure 3.1.5 Input flow rate versus time calculated for the reactor shown in Figure 3.1.3 for: CSDOC (—), CSDLAC (- - -)

desired dilution at the end of 30 seconds. After the first 30 seconds, the flow rate and the rotating speed of the paddle were adjusted every 10 seconds according to the pre-calculated history.

The required flow rate after the first 30 sec ranges from 85 down to 0.2 cm³/sec. Filtered artificial seawater, which was stored in two 5-gal carboys, supplied the dilution water to the reactor through plastic tubing. The dilution water, flowing down by gravity, went separately through two valves and flowmeters in parallel before

entering the reactor. The input flow was controlled by adjusting two Whitey regulating valves (Whitey Co., Highland Heights, Ohio) according to the reading of the connected flowmeters. The larger flowmeter (Model FP-1/2-27-G10/27, Fisher & Porter, Warminster, Pennsylvania) covers the range from 10 to 100 *ml/sec* and the smaller one (Model FP-3/8-25-G-5/36, Fisher & Porter) from 0.1 to 10 *ml/sec*. The clean seawater entered the reactor at the bottom through a diffuser to minimize the disturbance and to ensure a uniform inflow. After mixing with the sewage suspension inside the reactor, the excess mixture left the container over the circular weir (Figure 3.1.3). The reactor was made of lucite for visual inspection. A photograph of the complete system is presented in Figure 3.1.6.

3.1.3 Calibration of the coagulating reactor

The two flowmeters were calibrated with artificial seawater by measuring the volume of water collected within a certain period of time. Calibration results are shown in Figure 3.1.7. Rotation speed of the variable speed motor was calibrated by counting the number of revolutions per minute for the slow speed range (≤ 120 *rpm*) and by using the strobe light for the fast speed range (≥ 100 *rpm*) (Figure 3.1.8). The dilution history of the modified mixing process was checked by measuring the suspended solids concentrations of samples withdrawn from the reactor at different times. As shown in Figure 3.1.9, the dilution history was very close to the designed value.

3.2 Design of the Settling Experiment—Holographic Technique

The major difficulties in designing a system to measure the settling velocities of sewage particles are the slow settling velocities (< 0.1 *cm/sec*), and the small particle concentrations (≤ 2 *mg/l*) required to prevent the interference of coagulation.

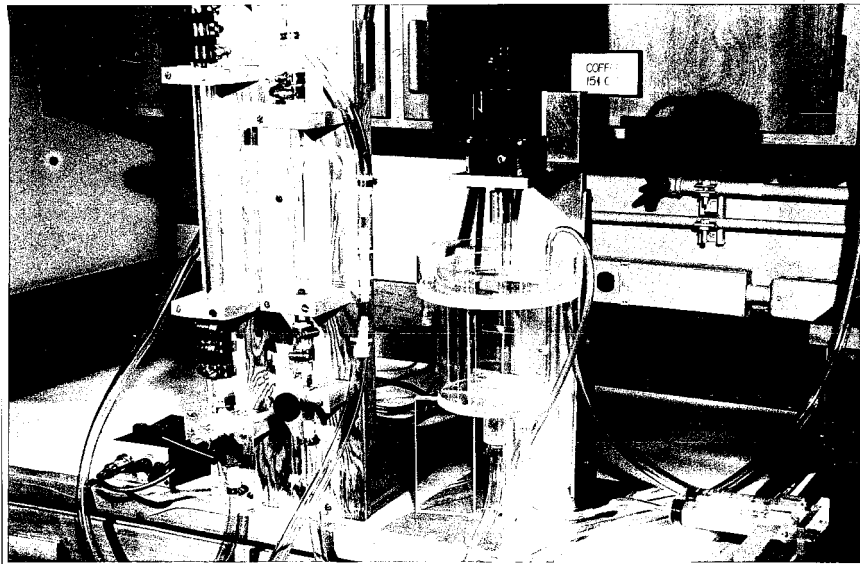


Figure 3.1.6 Photograph of the coagulating reactor

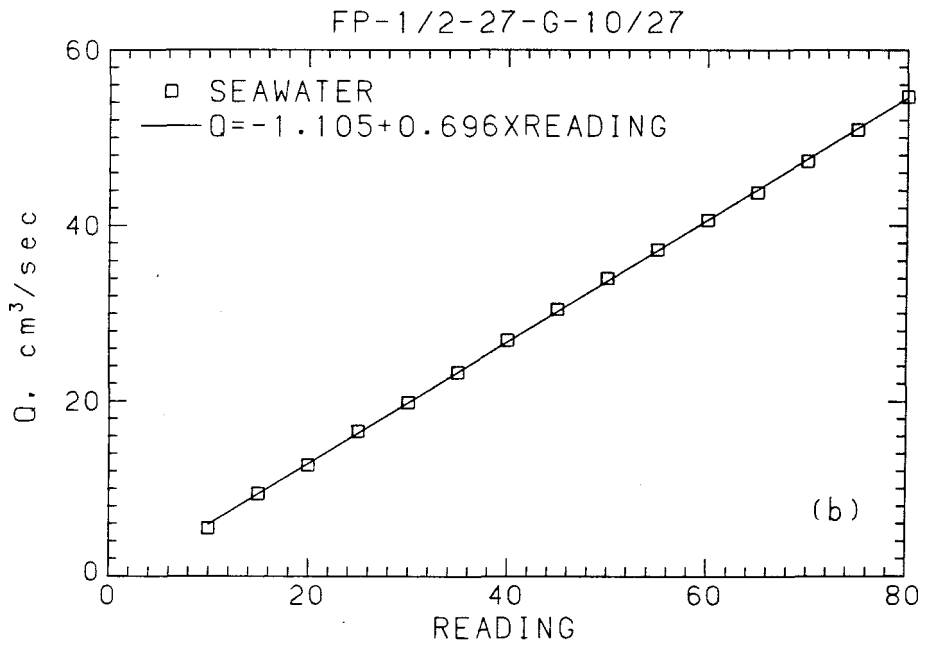
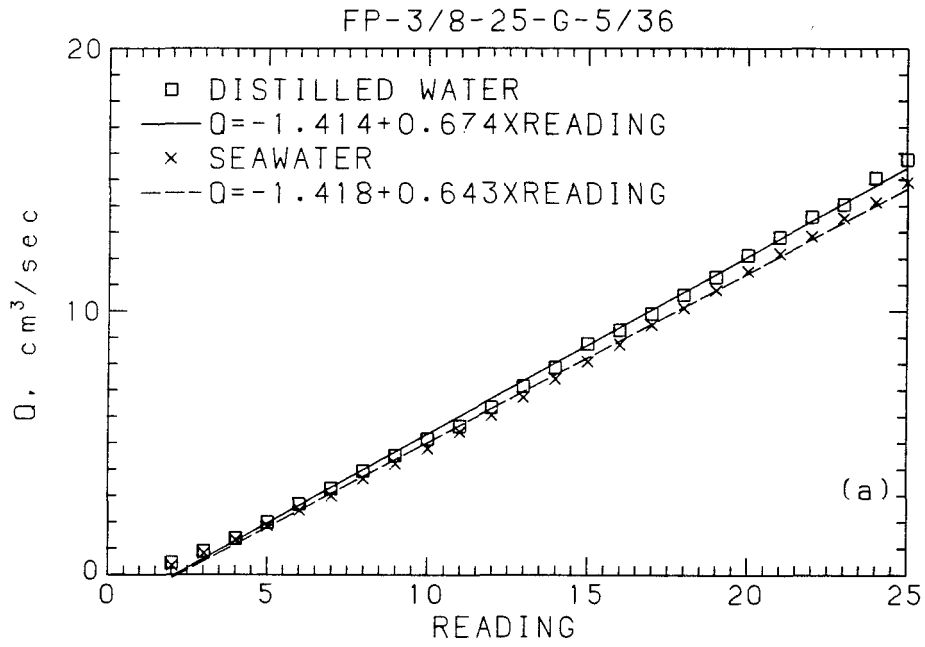


Figure 3.1.7 Calibration of the flow meters (a) FP-1/2-27-G-10/27, (b) FP-3/8-25-G-5/36

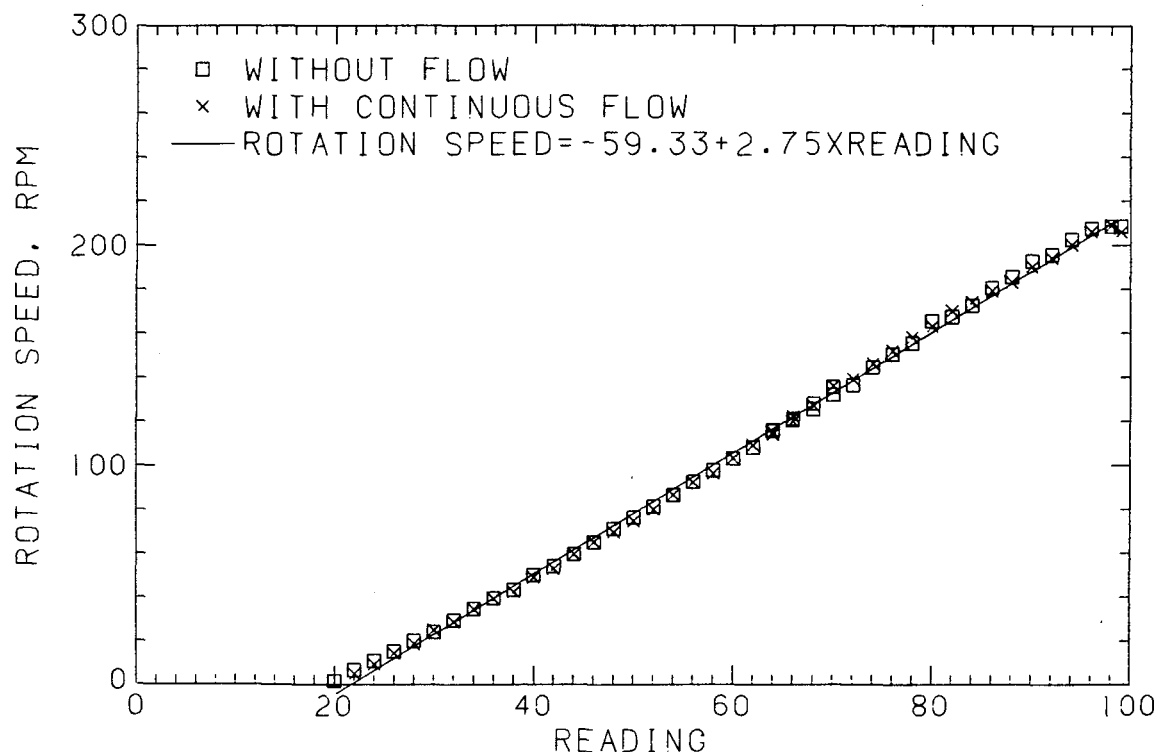


Figure 3.1.8 Calibration of the variable speed motor

The holographic technique makes it possible to work with very dilute suspensions. At the range of the fall velocities considered, 0.0001 to 0.1 *cm/sec*, both the temperature variation and the process of introducing particles into the settling cell can create disturbances which may be of a magnitude similar to, or even greater than, that of the settling velocities of particles. Special experimental designs and procedures used to overcome these problems are presented in this section.

3.2.1 Design of the holographic camera system

An in-line Fraunhofer (far-field) hologram is a record of the interference pattern of the collinear coherent background and the Fraunhofer diffraction pattern of an

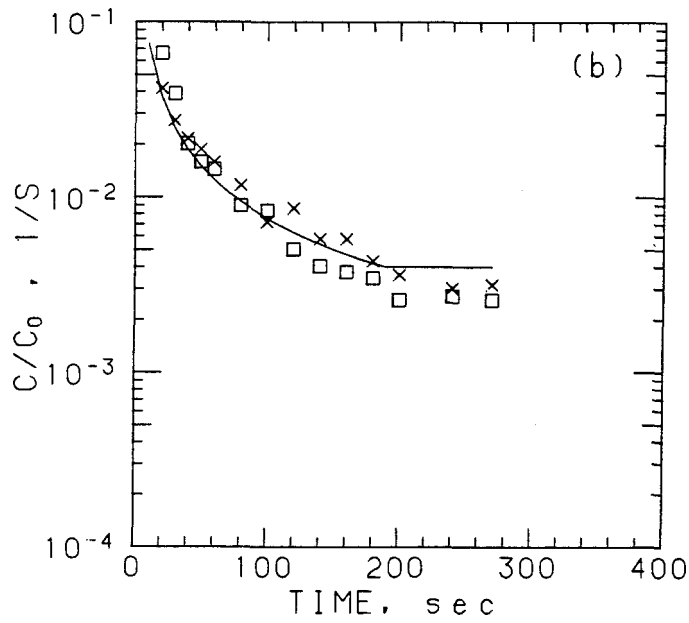
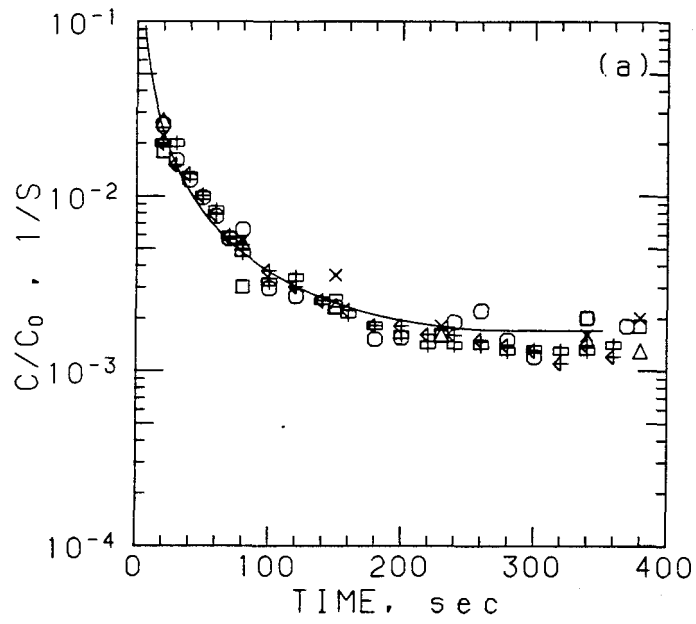


Figure 3.1.9 Calibration of the dilution history inside the reactor, (Lines are the calculated dilution history and symbols are measured suspended solids concentrations at different times.) (a) CSDOC, (b) CSDLAC

object formed in the far-field (e.g. Thompson, 1979). An in-line Fraunhofer hologram is created by passing a coherent light through a volume of particles; part of the incident light is diffracted by the particles and the remainder passes through the volume unscattered. The unscattered (reference) light interferes with the scattered (object) light, and the resulting interference pattern is recorded on a photographic medium. In our experiment, an in-line holographic system was preferred over other holographic configurations for its simple arrangement, which requires fewer optical components. An in-line system is also less sensitive to vibration, and puts less constraints on the coherence of the light source, and the resolution of the recording material (Cartwright *et al.*, 1980).

3.2.1.1 Design considerations

Several design criteria must be satisfied to make good in-line holograms. A sufficient amount of light, at least 80%, must pass through the sample volume undiffracted to serve as the reference beam (Trolinger, 1975), which implies the applicable particle size range and number concentration are limited. For a monodisperse system, the number concentration should be kept lower than $3 \times 10^3 / \text{cm}^{-3}$ for 100 μm particles and $3 \times 10^5 / \text{cm}^{-3}$ for 10 μm particles (Witherow, 1979). The distance, z , between objects and the recording plane should meet the far-field requirement, i.e., $z \geq \frac{d^2}{\lambda}$, where d is the maximum dimension of the object, and λ is the wavelength of the light (Thompson, 1974). Although the far-field number, $N = \frac{z\lambda}{d^2}$, can be as high as 2058 (Witherow, 1979), the practical rule is to use N less than 100 (Trolinger, 1975).

Spatial coherence of the reference beam is critical in obtaining large, high resolution holograms, while temporal coherence of the object and the reference

beams is needed in providing large depth of field. The coherence length of the illuminating light should be longer than the maximum path difference between reference and object beams, which can be estimated for an in-line system as $16N\lambda$ (Cartwright *et al.*, 1980). A holographic system should be designed to ensure that the spatial and temporal coherence of the illuminating beams are not the limiting factors in determining the resolution, the dimension, and the depth of the field of the holograms (Thompson, 1979). The single mode operation of a laser, which results in a Gaussian beam intensity profile and a uniphase wavefront, provides the highest degree of spatial and temporal coherence (O'Shea *et al.*, 1978), hence, can usually satisfy the coherence requirement.

If the spatial and temporal coherence of illumination are not the limiting factors as mentioned above, the resolution of holograms depends on the resolution and the dimensions of the recording material (e.g. Thompson, 1974). The film must be able to record a sufficient portion of the Fraunhofer diffraction pattern associated with particles—the central maximum and, in general, three side lobes of the fringes. Hence, the half width of the film should be at least equal to $4Nd = \frac{4z\lambda}{d}$, and the required resolution of the film can be estimated from the maximum angular spatial frequency as $\frac{8\pi}{d}$ (e.g. Cartwright *et al.*, 1980).

In addition to the requirement on the resolution, the interference pattern must remain stationary during recording. The movement of the fringes by a small fraction of the spatial period could reduce the contrast of the recorded fringes and deteriorate the image quality upon reconstruction. Since the positions of the interference patterns are determined by the relative phases of the objective and reference light waves at the recording plane, all the optical components that can affect the path length of the waves should remain still within a small fraction of the wavelength

of the illuminating light ($< 0.5\lambda$) (Kurtz *et al.*, 1979). This requirement on high stability can be satisfied by using an isolation table, or short recording time, or both. The displacement of individual particles during the recording should be less than one-tenth of its diameter, which puts an upper limit on the exposure time, $t_{exp} \leq \frac{d}{10v}$, where v is the velocity of particle with diameter d (e.g. Thompson *et al.*, 1967).

3.2.1.2 Holographic camera system—recording

From the above discussion, we estimated some of the design parameters, such as far-field distance, the dimensions and the resolution of the film, and the maximum exposure time for different particle sizes (Table 3.2.1). If we considered particles with dimension from 10 to 250 μm , the far-field distance should be arranged between 2.0 to 32 cm . The half width of the recording film should be larger than 6 mm and the resolution of the film should be higher than 2500 $lines/mm$, so a 35 mm high resolution holographic film was chosen as the recording material. Furthermore, the exposure time should be less than $\frac{1}{50}$ sec . Based on these parameters, we determined the diameter of the beam and the power of the laser, and selected other optical components such as the lenses, filters, shutter, film holder, and mounting units. An in-line holographic camera system was then constructed to record the motion of sludge particles during settling. Figure 3.2.1 shows the block diagram of this system, and Figure 3.2.2 shows the configuration of the recording system.

All optical components of this system are mounted on a 3 m long optical rail manufactured by Melles Griot (Irvine, California). A 10 $ft \times 20 in \times 1 in$ aluminum jig plate is used as the support for the whole system. A 5 mW He-Ne laser (Uniphase Model 1105P, Uniphase Co., Sunnyvale, California) is used as the light source to

Table 3.2.1 Design requirements of the holographic camera system for various particle diameters

Particle Diameter (μm)	Far-field Distance (Note 1) (cm)	Film Resolution (Note 2) ($lines/mm$)	Film Half Width (Note 3) (mm)	Maximum t_{exp1} (Note 4) (sec)	Maximum t_{exp2} (Note 5) (sec)	Maximum t_{exp} (Note 6) (sec)
5	0.001-8.1	5026	30.0	1.47	1.64	1.47
10	0.004-32.5	2500	1.5	0.73	13.12	0.73
25	0.025-206	1005	6.0	0.29	205	0.29
50	0.1-813	500	3.0	0.15	1640	0.15
75	0.22-1856	335	2.0	0.10	5540	0.10
100	> 0.4	251	1.5	0.073	13100	0.07
250	> 2.5	100	1.0	0.029	25600	0.03

Note 1 Required far-field distance = $N \frac{d^2}{\lambda}$, $N = 0.25-2058$ (allowable range), $\lambda = 632.8 \text{ nm}$

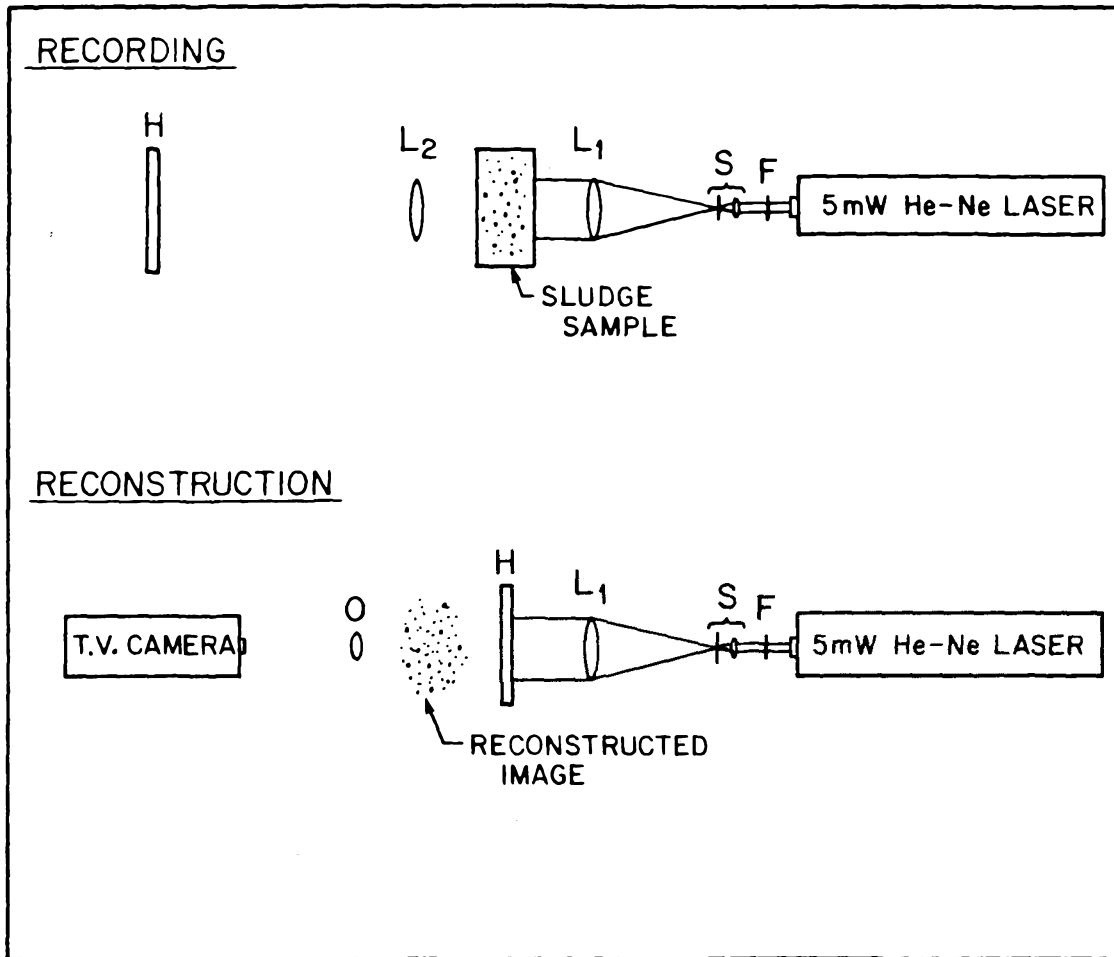
Note 2 Minimum required film resolution = $\frac{8\pi}{d}$

Note 3 Minimum required film half width = $4Nd$, $N = \frac{z}{d^2/\lambda}$, z is assumed to be 6 cm

Note 4 Calculated from the settling velocity of particles: $t_{exp1} = \frac{d}{10w}$, where $w = \frac{g}{18\mu}(\rho_p - \rho_w)d^2$, $\rho_p = 1.05 \text{ g/cm}^3$, and $\rho_w = 1.025 \text{ g/cm}^3$

Note 5 Calculated from the Brownian motion of particles: $t_{exp2} = \frac{d^2}{200D}$, where D is the diffusion coefficient of particles

Note 6 The smaller one of t_{exp1} and t_{exp2}



- F: Neutral density filter (to control the exposure level of the hologram)
- S: Spatial filter (to clean the laser beam): comprises a microscope objective ($f = 1.0 \text{ mm}$) and a pinhole ($10 \mu\text{m}$)
- L₁: Collimating lens (to expand laser beam)
- H: Holographic film (mounted inside a 35mm camera during recording and mounted on the x,y,z-translating stage during reconstruction)
- L₂: Magnification lens for small particles (not included in this study)
- O: Microscope objective (to focus and magnify the reconstructed images)

Figure 3.2.1 Schematic diagram of the optical arrangement to record and reconstruct holograms

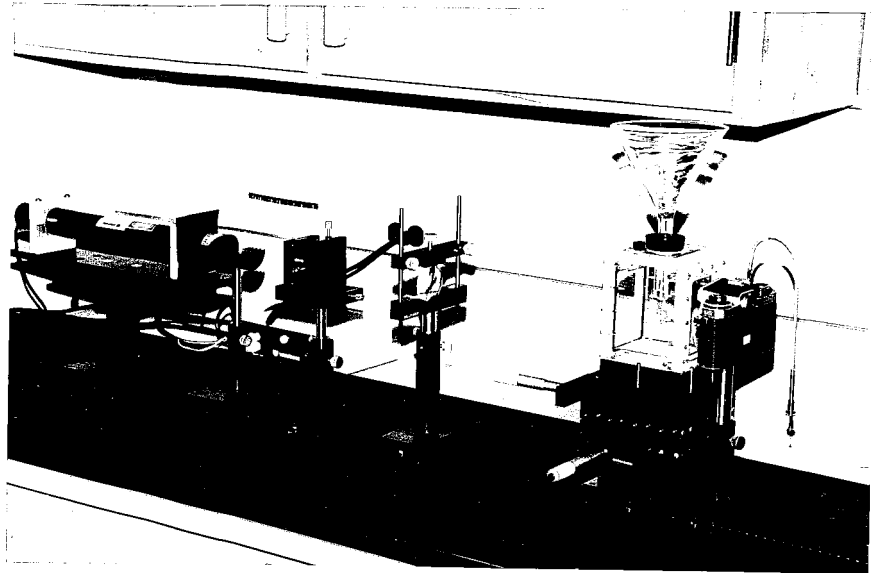


Figure 3.2.2 Photograph of the recording system

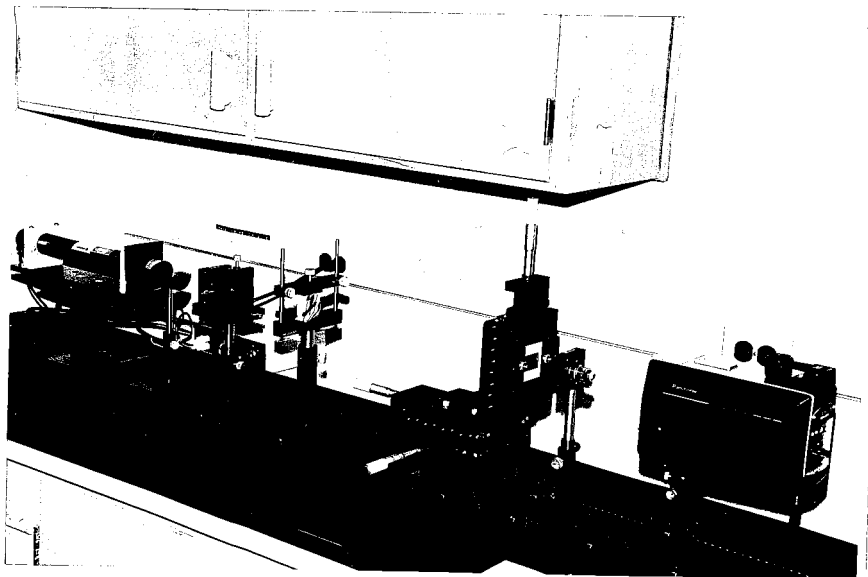


Figure 3.2.3 Photograph of the reconstruction system

provide both objective and reference beams. A set of neutral density filters (optical density = 0.4, 0.6, and 1.0, Melles Griot) is used to adjust the exposure level of the recording film according to the speed of the films and the concentrations of the samples. A spatial filter (Ealing Co., South Natick, Massachusetts), which comprises a microscope objective (focal length = 4.0 *mm*) and a pinhole (diameter = 10 μm), is included to filter out stray light and to maintain a smooth beam irradiance distribution, which is crucial in making good holograms.

During the recording of holograms, the parallel laser beam from the He-Ne laser was focused by the microscope objective of the spatial filter and filtered by the small pinhole at the focal point of the objective. This focusing process converted the parallel beam to a divergent beam. Since a parallel beam (plane wave) has the advantage of maintaining a constant magnification ratio across the whole hologram, this filtered divergent beam was again collimated back to a parallel beam of 50 *mm* diameter by a collimating lens (focal length = 190 *mm*, diameter = 2 *in* (5.08 *cm*), Optics for Research, Caldwell, New Jersey). This parallel light beam then travelled through the settling cell. Part of the beam was scattered by particles in the cell and became the objective beam. The unscattered portion of the laser light, serving as the reference beam, interfered with the object beam, and the interference patterns were recorded on the films as holograms.

Three different Kodak films, SO-253, SO-173, and 649F, with resolution equal to or higher than 2500 *lines/mm* were used to record the particle field (Gladden and Leighty, 1979). A 35*mm* (Nikon FE) camera body with a focal plane shutter was used to hold the film as well as to control the exposure time. The holographic

films were processed within 8 *hr* after exposure. The developing chemicals and procedures followed the manufacturer's recommendation (Eastman Kodak Company, 1976, 1984).

3.2.1.3 Holographic camera system—reconstruction

Figure 3.2.3 shows the configuration of the recording system. The same laser beam was used to reconstruct three-dimensional images from holograms. The settling cell was replaced by an x,y,z-translating stage (Daedal, Inc., Harrison City, Pennsylvania) for mounting holograms. The laser beam, travelling through the hologram, was diffracted to regenerate two three-dimensional images, a real and a virtual image, of the particles inside the settling cell at the opposite sides of the hologram. The real image was used for hologram reconstruction. The reconstructed images of particles were focused using a focusing unit, which consists of a microscope objective (10× magnification, Zeiss, West Germany) and a video camera (Panasonic PK-400, Panasonic Company, Secaucus, New Jersey). The microscope objective is used to magnify the particle images, and the video camera is used to catch the images for display. Since the television (TV) monitor cannot accept signals directly from the video camera, a video cassette recorder (VCR) is connected between the camera and TV monitor.

Both the microscope objective and the camera are mounted on a 75 *cm* long optical rail (Melles Griot), which, in turn, is mounted on the 3 *m* rail. This setup enables us to change the relative position of the objective and the camera, or to move them as a unit at fixed separation. The distance between the video camera and the microscope objective determines the magnification ratio of the display and

the size of the field of view. The longer the distance is, the larger the magnification ratio and the smaller the field of view, and vice versa.

In our experiment, focusing images of particles in the reconstructed three-dimensional holograms was achieved by adjusting the three micrometers on the x,y,z-translating stage and the position of the 75 cm rail. In general, we started with the micrometers at a special (x_0, y_0, z_0) setting. With the x and y setting of the micrometers unchanged, we moved the z-micrometer or the 75 cm rail through a predetermined depth, Δz , to search for the images of particles. After this small volume, $\Delta x \Delta y \Delta z$, was examined, we advanced to the next x-y frame by adjusting the x and y-micrometers and went through the same depth Δz . This procedure was repeated until either a sufficiently large number of particles was measured or the whole hologram was examined. The size of the viewing volume was then calculated from the position readings of the micrometers and the rail. The size and velocity of particles were either measured directly on the TV screen or measured with a computer analysis program.

3.2.2 Image analysis system

Although it is possible to analyze the reconstructed images of particles directly on a TV screen, this manual analysis is inefficient and time-consuming. For particles of irregular shapes, manual examination can provide only a rough estimate of particle size. It is also inevitably subject to human error during the analysis. To improve the accuracy and the speed of data analysis, fully or partially automated reconstruction systems have been utilized by various people (e.g. Bexon *et al.*, 1976; Belz *et al.*, 1979; Haussmann and Lauterborn, 1980). Those systems basically

include a computer, a video camera for image scanning, a video I/O interface for digitizing and displaying images, and some image processing software.

The state-of-the-art in computing and image acquisition technologies allows real-time processing of focused images reconstructed from holograms. However, it is still difficult to automatically focus the images of particles. One approach is to digitize successive x-y planes along the z direction. If there is an image of a particle within a $\Delta x \Delta y \Delta z$ volume, the plane where this particle is in focus can be identified by comparing the image brightness, edge gradients, etc. in successive planes (e.g. Payne *et al.*, 1984). This procedure demands a lot of processing and storage. Hence, Stanton *et. al.* (1984) developed a non-image plane scheme for analyzing spherical particles which requires only three x-y planes to be digitized along the z-direction. However, since sludge particles have very irregular shape and complicated boundary configuration, which make the image processing difficult even at the in-focus plane, we decided to focus images manually and then digitize them for computer analysis.

The image processing system developed in this study is for digitizing, storing, and processing the focused images to automatically calculate the size and velocity of particles. A low cost frame grabber DT2803 (Data Translation, Inc., Marlboro, MA) with spatial resolution of 256×256 and 64 gray levels is used as the video I/O interface. It consists of a high speed (1/30 *sec*) flash A/D converter for image input and eight software-selectable input look-up tables which can be programmed for specific applications.

The frame grabber digitizes the color video signals (in NTSC format) after filtering the signals through a 3.58 MHz filter. Each screen is then formatted into 240 lines, each line into 256 pixels. The intensity of each pixel is represented by the corresponding gray level. The range of possible shades of gray is quantified

into 64 levels which is encoded with 8 bits. Hence, each pixel occupies a single byte of memory space. The 64 kilobyte on-board frame-store memory is mapped into the PC memory area where it can be accessed over the PC bus. The digitized images can be displayed on the monitor after passing through user-selectable output look-up tables and a D/A converter for color or monochrome output.

A Compaq portable personal computer (Compaq Computer Corp., Houston, Texas), which is an IBM PC compatible with 256K RAM and two floppy disk drives, is used as the processing host. Video signals from the TV camera are first divided into two, one of which is connected to the input jack on the digitizing board. The output digitized images from the board and the original video signals that do not go through digitizing board are connected by a 75Ω VCR/TV/FM switch, which is then connected to the TV monitor (Figure 3.2.4). By selecting the setting of the switch, we can decide which image, original or digitized, is displayed on the TV monitor.

Either the original images or the digitized images can be used to manually focus the images of particles. After the image of one particle is in focus, simple thresholding is applied to the whole screen to filter out the background noise from the input image. Thresholding is an operation which maps a gray level image into a binary one. Assume that the intensity of the input image varies from 0 to N . A "threshold" is an intensity level and the intensities higher than the threshold are mapped to a single intensity (say 1) and the intensities lower than the threshold are mapped to another intensity (say 0). The intensity threshold is changed in real time by redefining the contents of the selected output look-up table. Switching alternately the display of the thresholded and the original images, we can determine the optimum threshold for a particular image, and then use a cursor on the screen

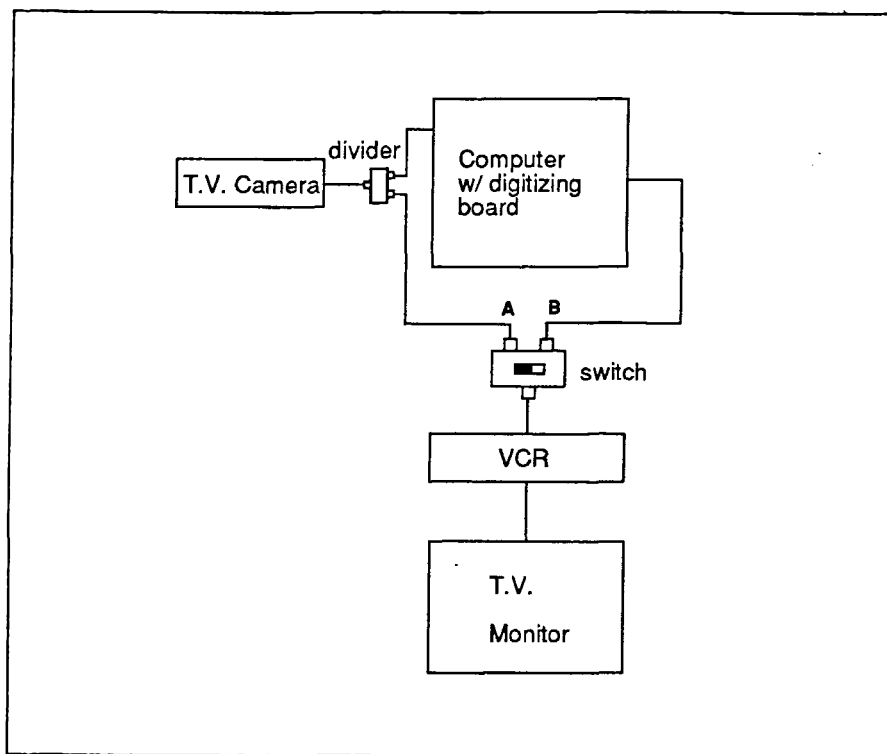


Figure 3.2.4 The image processing system

to mark the region occupied by the particle that is to be analyzed by the image analysis program (Figure 3.2.5).

The thresholding operation for locating particles was chosen over other image processing techniques, such as convolutions, for its speed, simplicity in implementation, and the fact that it provides the best possible results for our application. As mentioned before, sludge particles do not have well defined shapes, and their image boundaries can be very complicated and fussy. Images of small particles (with dimension less than $20 \mu m$) may become very hard to distinguish from background noise, partially because of the low resolution of the imaging components, i.e., film, TV camera, and digitizing board, and partially because of the speckle effect of the holograms.

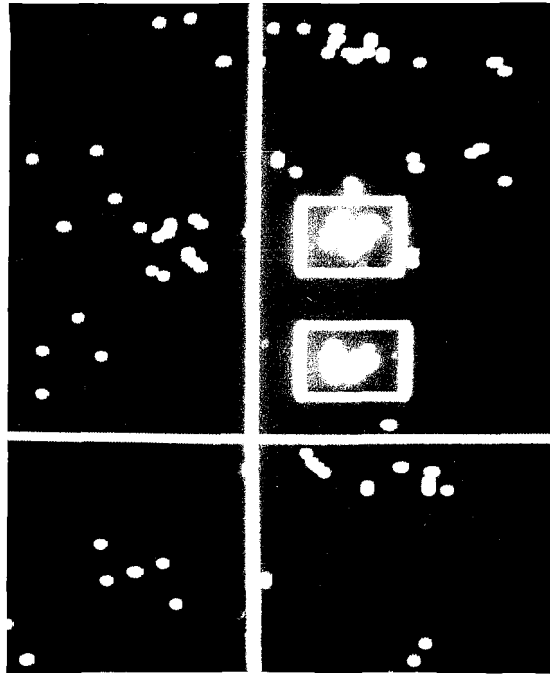
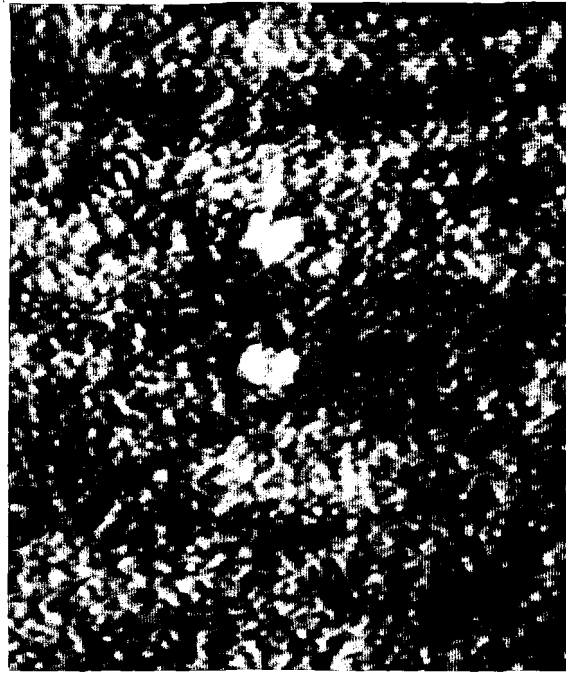


Figure 3.2.5 Photographs of the double images of a D.P.S. particle, $A_p=849 \mu m^2$,
 $d_{equ}=32.5 \mu m$, $\frac{len_v}{d_{equ}}=1.19$, $\frac{len_h}{d_{equ}}=1.06$, $\frac{max_v}{d_{equ}}=1.13$, $\frac{max_h}{d_{equ}}=0.98$,
 $\frac{\sigma_{major}}{d_{equ}}=0.32$, $\frac{\sigma_{minor}}{d_{equ}}=0.25$, $\theta = 167^\circ$, $l_v = 116 \mu m$, $\Delta t = 5.23 \text{ sec}$,
 $w_s = 2.22 \times 10^{-3} \text{ cm/sec}$, (a) original image, (b) digitized images
(after thresholding)

Transform techniques, such as low and high pass filtering for region and boundary detection, have limitations in determining the shapes for irregular particles. Low-pass filtering attenuates high-frequency information. It averages out the noise, but at the same times blurs the edges. High-pass filtering, which makes high-frequency information more prominent, enhances the edges as well as the noise. Image processing routines based on edge detection and edge tracing have also been developed. However, experience showed that edge tracing takes a much longer time than thresholding to locate sludge particles, and it does not necessarily give better results. Especially for particles with complicated shapes, tracing routines had difficulties in following the boundaries and gave poor estimates on the size and shape of particles.

An image processing software module was developed in Turbo Pascal specially for this research. The module provides the options of continuously digitizing the camera input, acquiring and analyzing a single frame, acquiring and storing a single frame into the disk, retrieving data from disk, and analyzing and displaying the images of particles onto the screen. After simple thresholding was used to find the boundary of particles for the reconstructed images, the software module calculated, for every particle, the area (A_p), the equivalent diameter ($d_{equ} = \sqrt{\frac{4A_p}{\pi}}$), the directions of the principal axes ($\theta =$ the angle between the major principal axis and the horizontal axis on the image plane), the vertical and horizontal lengths of the bounding box (len_v, len_h), the maximum dimensions along the principal axes (max_v, max_h), and the second moments in the principal directions ($\sigma_{major}^2, \sigma_{minor}^2$). For doubly exposed holograms, this image analysis program also calculated the positions of the centroids and the displacement between the centroids for the double

images of particles to estimate the settling velocities. The detailed calculation procedures are summarized in Appendix C; an example is given in Figure 3.2.5.

3.2.3 Size and velocity measurements using the in-line holographic camera systems

Singly exposed holograms were used for counting the number of particles and measuring their sizes inside a small volume in the settling cell. The total volume analyzed was calculated from the travelling distances of the micrometers on the x,y,z-translating stage. Particle size distributions were derived from these measurements.

Doubly exposed holograms were used to measure the settling velocities of particles in the following manner: After sludge samples were introduced into the settling cell, particles were left to settle by gravity in a quiescent medium. As particles travelled downward through the observing window, doubly exposed holograms were recorded. The time between two exposures, Δt , was measured by manually starting and stopping a stopwatch when the two exposures were made for each film. The reconstructed holograms showed double images of every particle recorded. Displacement between the two exposures was measured, and the settling velocity was calculated as the quotient of travel distance divided by the time between the exposures.

3.2.4 Calibration of the holographic camera system

The overall magnification of the holographic system, i.e. the ratio of the size of the particle image displayed on the TV screen to its actual size, is given by $M = m_o m_i m_a$, where m_o is the recording magnification, m_i the reconstruction

magnification, and m_a the magnification from the auxiliary viewing system, e.g. microscope, enlarging lens, and the electronic magnification of the camera (Bexon, 1973). A parallel beam (plane wave) is used in both the recording and the reconstruction of holograms in our system, so m_o and m_i are both unity. The magnification of the TV camera is fixed, so the only factor that can affect the magnification ratio of the image is the distance between the microscope objective and the TV camera. Hence, the magnification is given by $M = m_a = m_{TV} \frac{L-f}{f}$, where L is the distance between the microscope objective and the TV camera, f the focal length of the objective, and m_{TV} the magnification of the TV camera (Figure 3.2.6). In addition to the magnification ratio, a scaling factor that relates the particle size as calculated by the analysis program (in number of pixels) and the real physical scale of the particles (in μm) needed to be calibrated.

Standard polystyrene latex particles (PSL, Duke Scientific Corp., Palo Alto, California) with sizes of 100, 50, 20 μm were used to calibrate the magnification ratio and the scaling factor as functions of the distance between the objective microscope and the video camera. The microscope objective is fixed on one end ($\sim 0 mm$) of the 75 *cm* rail, and the camera is moved along the rail to change the distance between these two. The adjustable distance is about 57 *cm* corresponding to the positions of the camera on the 75 *cm* rail from 80 to 650 *mm*. Although larger distance provides higher magnification, the deterioration of the images with the increasing distance limits the usable distance ranges (camera position from 110 to 250 *mm*). The optimum position of the TV camera was found by experience to be 170 *mm*.

Singly exposed holograms were recorded and analyzed for several suspensions of PSL particles. For every particle size, at least 100 particles were observed and

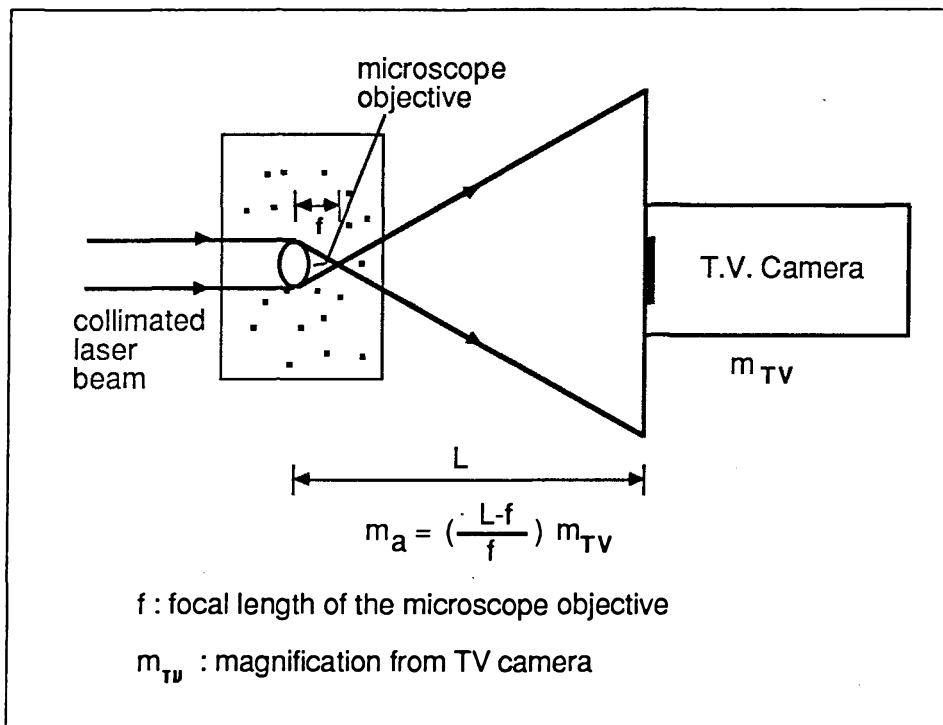


Figure 3.2.6 The magnification of the auxiliary viewing system

measured with the image analysis system at the optimum setting, which was used most often (TV camera at 170 mm). The measured sizes were compared with the manufacturer's data for PSL particles to give the magnification ratio as $390 \pm 5 \%$ and the scaling factor as $4.26 \pm 2 \%$ for this particular setting (Table 3.2.2). The standard deviations of size measurements for 100, 50 and 20 μm PSL particles are the same as those specified by the manufacturer, which suggests that the errors in the size measurements by this holographic system are very small. The magnification ratio and the scaling factor for other settings were derived by comparing the measured dimensions of the same set of particles against those measured at the

Table 3.2.2 Calibration of the scaling factor for image analysis

Diameter (μm)		Measured values [†]		Scaling factor	Measured number
mean	$\frac{\sigma}{\text{mean}}$	mean	$\frac{\sigma}{\text{mean}}$		
99.1	4.8%	22.889	4.8%	4.33	177
49.4	5.1%	11.613	5.2%	4.25	153
19.1	5.8%	4.552	6.7%	4.20	100

† in number of pixels

Scaling factor = $4.26 \pm 2\%$

standard setting (Figure 3.2.7a), and the scaling factor as a function of the camera position is shown in Figure 3.2.7b.

3.2.5 Design of the settling cell

The settling cell consists of two parts: a rectangular lucite box ($6.35 \text{ cm} \times 7.62 \text{ cm} \times 10.16 \text{ cm}$ high, 492 ml) with two parallel windows made of high quality optical glass, and a funnel on the top (Figure 3.2.8). To minimize the disturbance and the convection current resulting from the act of introducing the sample and from temperature variations, water inside the settling cell was stratified to suppress vertical mixing. Seawater of different densities was prepared by adding different amounts of sodium chloride to the artificial seawater. Six solutions with density from 1.021 to 1.028 g/cm^3 were used. Stratification was established by carefully feeding these solutions into the cell. Possible vertical mixing during the feeding process was minimized by transferring the salt solutions onto a plastic plate floating on the water surface. The stratified cell was left for at least 8 hours to stabilize, resulting in a density gradient of about 0.07 m^{-1} in the vertical direction along which the particles settle.

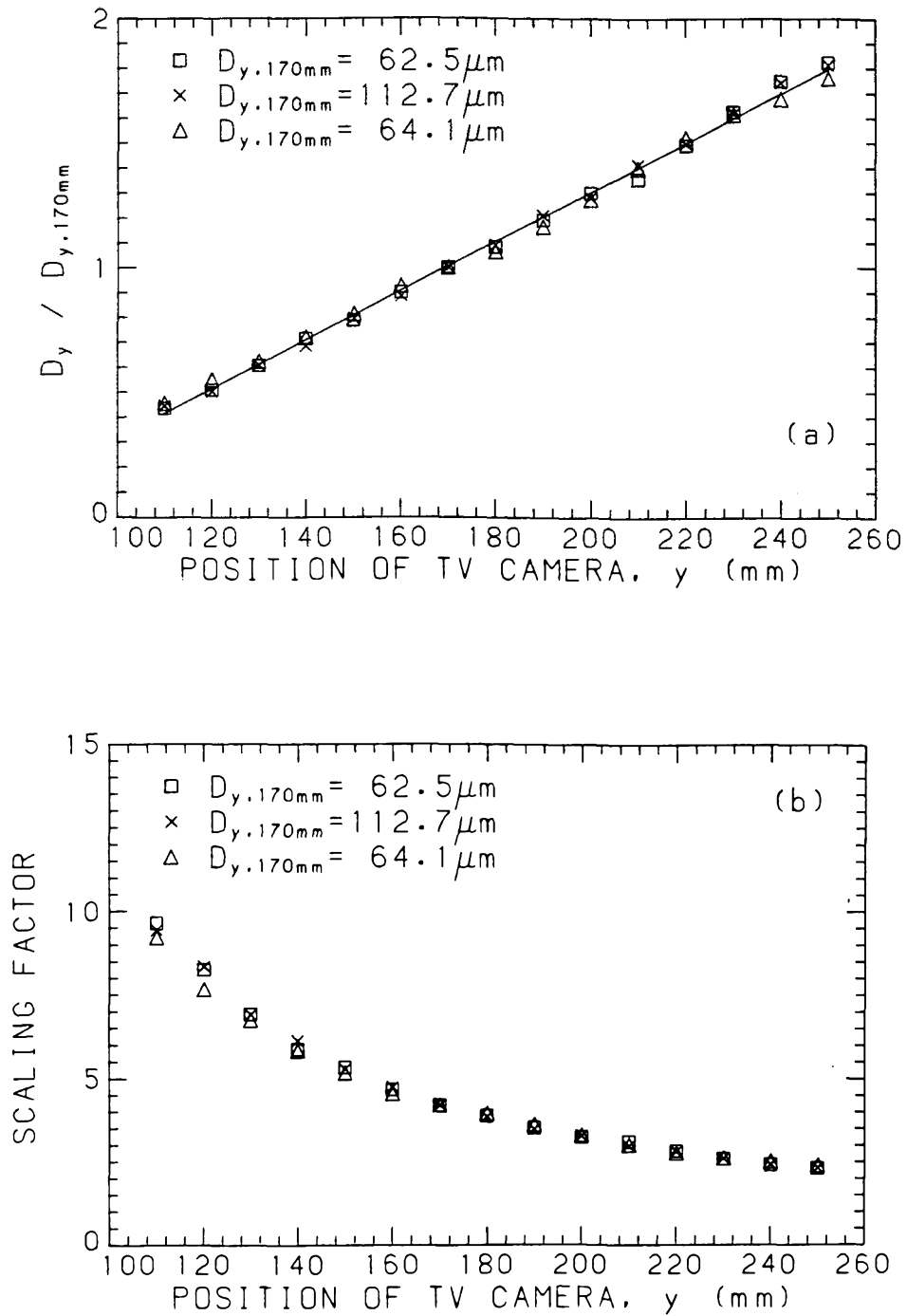


Figure 3.2.7 Determination of the scaling factor as a function of the position of TV camera y : (a) the ratio of the equivalent diameter measured at different y 's to that measured at $y = 170$ mm, (b) the scaling factor versus the position of TV camera

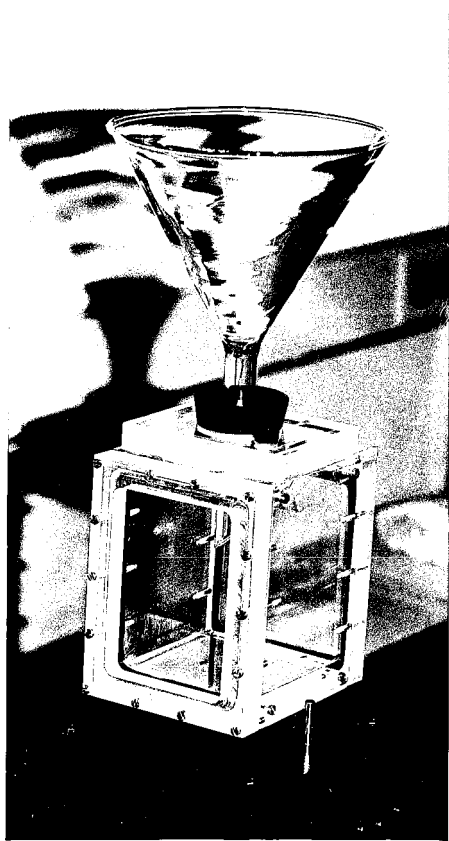


Figure 3.2.8 Photograph of the settling cell

The same caution was exercised when introducing sludge samples into the funnel, i.e., samples were transferred onto the floating plate instead of into the water directly. The small diameter of the funnel neck, about 1 *cm*, also helped speed up the die off of the turbulence. Furthermore, since the bulk density of samples is larger than that of seawater because of the suspended particles contained in the sample, this density difference will also influence the settling velocities of particles. Hence, the temperature of the samples was raised about 2°C to compensate for this effect and to prevent convective overturning in the funnel. The distance between the water surface, where samples were introduced, and the measuring window was about 18 *cm* in the settling cell.

To verify that the above procedures can effectively diminish convection currents so that we can observe the undisturbed settling velocities, a calibration process was performed with standard PSL particles of known density ($\rho = 1.05 \text{ g/cm}^3$) and size (10, 20, 30, and 40 μm). Since these PSL particles are spherical, their settling velocities can be calculated according to Stokes' law, $w = \frac{g}{18\mu} \Delta\rho d^2$. The diameter and density values specified by the manufacturer were used in the calculation. The settling velocity measurement was done at a temperature of $20 \pm 0.5^\circ\text{C}$, so the kinematic viscosity of seawater at 20°C, i.e. 0.011 cm^2/sec , was used. The density of seawater was measured as 1.025 g/cm^3 , so the dynamic viscosity μ was calculated to be 0.0113 $\text{g cm}^{-1}\text{sec}^{-1}$ (1.025×0.011).

Both the calculated and measured fall velocities are summarized in Table 3.2.3. Calibration results illustrate that the settling velocities, which range from 1×10^{-4} to $1 \times 10^{-2} \text{ cm/sec}$, measured by this experimental setup match closely the theoretical predictions. The crosses in Figure 3.2.9 show the mean values of d and w for large samples ($N \sim 30 - 100$) and the length of the tick marks corresponds to $\pm\sigma$. The

Table 3.2.3 Calibration of the settling velocity measurements with PSL particles

Diameter, μm		Calculated w^\dagger , cm/sec		Measured w , cm/sec		Measured number
mean	$\frac{\sigma}{\text{mean}}$	mean	$\frac{\sigma}{\text{mean}}^\dagger$	mean	$\frac{\sigma}{\text{mean}}$	
99.1	4.8 %	0.012	9.6 %	0.0112	7.0 %	27
49.4	5.1 %	0.0029	10.2 %	0.0031	9.0 %	83
19.1	5.8 %	0.00044	11.6 %	0.00042	7.5 %	95
9.6	5.2 %	0.00011	10.4 %	0.00013	15.0 %	42

† calculated from the σ of particle diameter

‡ calculated from Stokes' law with $\rho_p = 1.05 \text{ g/cm}^3$ and $\rho_w = 1.025 \text{ g/cm}^3$

mean standard deviations of the settling velocity measurements for PSL particles are within reasonable agreement with calculated values based on the diameters and densities given by the manufacturer. It is thus concluded that the convection currents were eliminated.

3.2.6 Experimental error

If we assume that there is no image distortion during the recording and reconstruction processes, the error in the size and velocity measurements can be attributed mainly to the fluctuation of the analog signals during image scanning, image focusing, and edge determination during thresholding. It is difficult to decompose the error effect induced by each individual process, so the combined effect was examined by repeating the size measurements for the same particle. Due to limited resolution of the digitizing board, errors in size measurements are higher for the smaller particles than for the larger ones. Errors in size measurements can be as high as 10 % for particles around $10 \mu m$, and about 5 % for particles larger than $20 \mu m$.

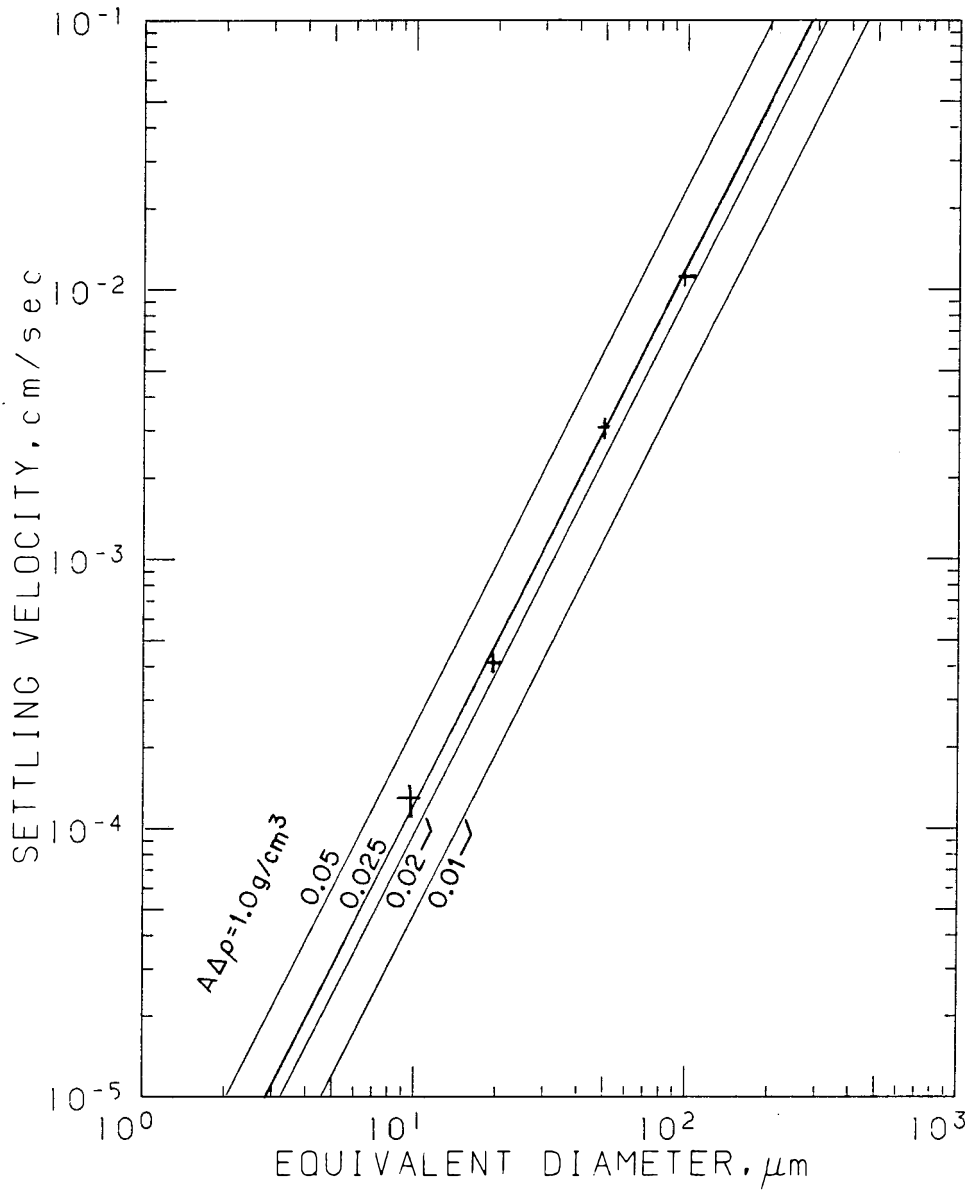


Figure 3.2.9 Settling velocity measurements for PSL particles by the holographic camera system; the crosses show the mean values of diameter d and velocity w and the length of the tick marks corresponds to $\pm\sigma$

The maximum errors in velocity measurements were estimated using the equation:

$$\frac{d(w)}{w} = \frac{d(l_v)}{l_v} + \frac{d(\Delta t)}{\Delta t} \quad (3.2.1)$$

where w is the settling velocity, l_v is the measured settling distance within a time Δt . Similarly, we repeated the measurements of the distance between two images of the same particles and obtained the maximum $d(l_v)$ to be $2.6 \mu m$. During recording, Δt was adjusted to make l_v larger than $100 \mu m$. Hence, the expected maximum error from the distance measurement should be less than 3 %.

As mentioned before, Δt was measured by a stopwatch, which was manually operated to record the time difference between two exposures. Special tests were performed to estimate $d(\Delta t)$. Under complete darkness, a stopwatch was set in front of the 35 mm camera with a flash. The same procedure for recording doubly exposed holograms was repeated except that the film was rewound between the two exposures. When the film was exposed by flash, the time on the stopwatch in front of the camera was recorded on the film. Then, Δt was derived from the time difference between that recorded on the film and that measured by the stopwatch in hand.

The maximum $d(\Delta t)$ was found to be 0.1 sec. The range of Δt used in the settling test was from 1 to 200 sec. Therefore, the expected maximum $\frac{d(\Delta t)}{\Delta t}$ was 10 % for fast settling particles ($w \geq 5 \times 10^{-2} \text{ cm/sec}$), which required short time

Table 3.2.4 Expected maximum error in fall velocity measurements for different velocity range

$w_s(cm/sec)$	$\frac{d(l_v)}{l_v}$	$\frac{d(\Delta t)}{\Delta t}$	$\frac{d(w_s)}{w_s}$
$\geq 5.0 \times 10^{-2}$	3 %	10 %	13 %
2.5×10^{-2}	3 %	5 %	8 %
1.0×10^{-2}	3 %	3 %	6 %
2.0×10^{-3}	3 %	1 %	4 %
1.0×10^{-3}	3 %	0.5 %	3.5 %
1.0×10^{-4}	3 %	0.1 %	3.1 %

between exposures, and decreased to less than 0.5 % for particles with fall velocity smaller than $1 \times 10^{-3} cm/sec$ (Table 3.2.4).

Since fall velocities depend on the fluid viscosity ($w \propto \mu^{-1}$), which changes with temperature, another source of error is the temperature variation during settling analysis. For this study, temperature of the seawater inside the settling cell was not controlled and the change in temperature during experiment was observed to be within $\pm 0.5^\circ C$. For seawater with salinity $34^\circ/_{\infty}$, the dynamic viscosity μ decreases from 0.010698 to 0.009757 $g cm^{-1}sec^{-1}$ for the temperature increase from 20 to $24^\circ C$ (Riley and Skirrow, 1975). Hence, the corresponding $\frac{d(\mu)}{\mu}$ for $\pm 0.5^\circ C$ temperature change in this range is about 2.4 %, which is small enough to be considered secondary.

3.3 Experimental Procedure

The experimental procedure can be divided into three steps: sample preparation, coagulation experiment, and settling experiment (Figure 3.3.1). In the following sections, we discuss these three steps in greater detail.

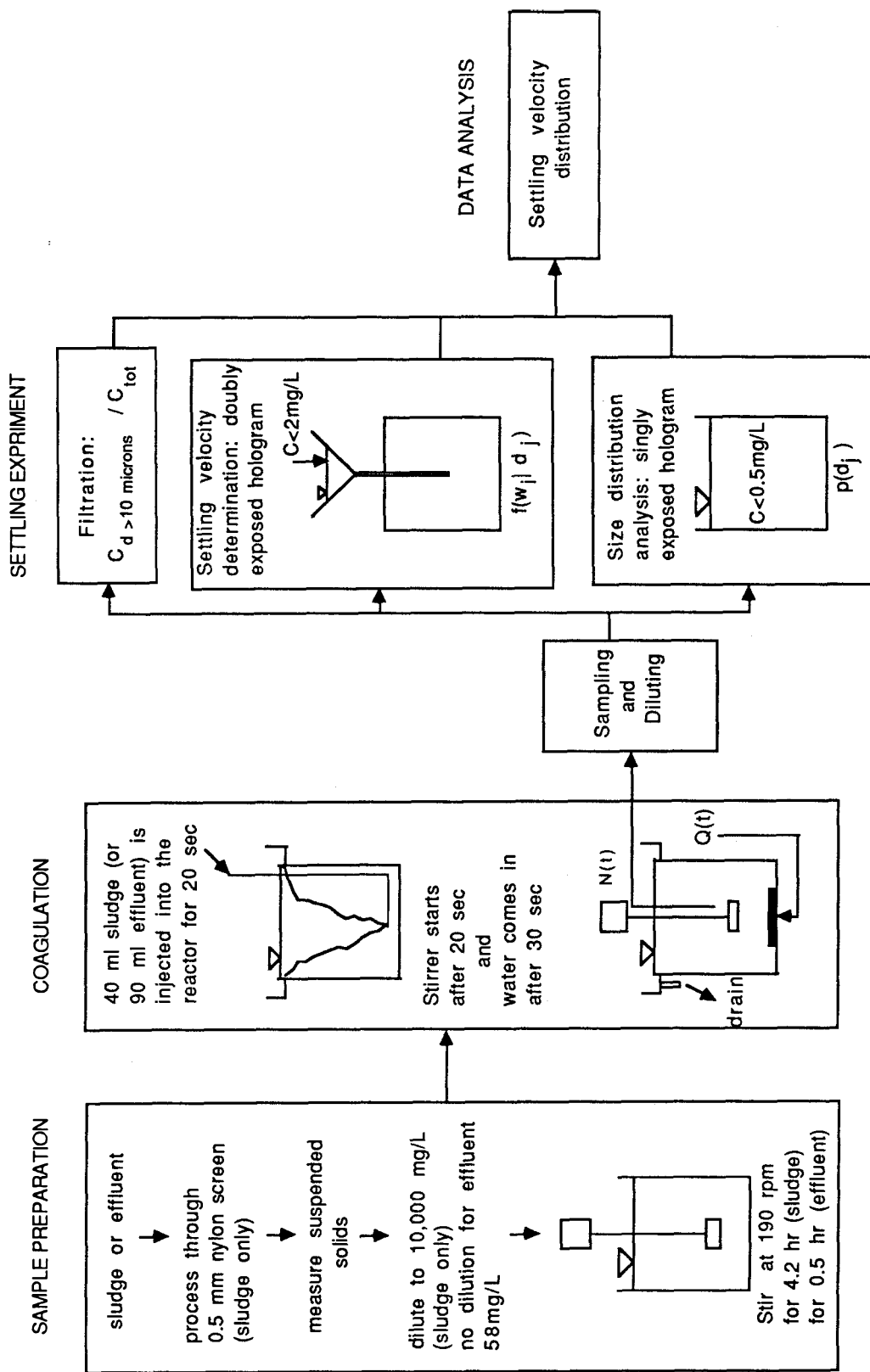


Figure 3.3.1 Flow chart of the experimental procedure

3.3.1 Sample preparation

At this stage, raw sewage samples, taken from the treatment plant, were prepared for the coagulation experiment; the suspended solids concentration and particle size distribution were measured to provide initial conditions of the coagulation experiment. Sludge samples were first filtered through a 0.5-*mm* nylon screen to remove coarse material to avoid clogging the 6-*mm* sludge injecting tube in the coagulating reactor during the feeding process. The solids concentrations were measured by vacuum filtration of the diluted samples separately through two Nuclepore membranes with different pore size, 10 μm and 0.4 μm . This filtering process measured the mass of total suspended solids (i.e., the mass retained on the 0.4 μm membranes) as well as that of the solids with diameter larger than 10 μm , which is the resolution limit of our holographic camera system. The initial size distribution for particles larger than 10 μm was obtained by recording and analyzing singly exposed holograms of diluted sewage samples.

For the proposed sludge outfall for Orange County (CSDOC), it was not possible to closely simulate the expected plume behavior because many engineering design decisions have not been made by CSDOC, and an application for a discharge permit has not been made. In the Clean Water Act Amendments of 1987, the legislative authority was given for discharge of only 50 % of the sludge solids from CSDOC plants, or approximately 70 metric tons (dry solids) per day. The concentration of the solids at the end of the pipe will depend on (a) the initial concentration of solids in the mixed sludge and (b) how much effluent is premixed with the sludge to maintain the desired flow characteristics in the pipeline. If the discharge was to be 3.0 *mgd* (0.131 m^3/s), then the solids concentration would have

to be 6,200 *mg/l* (0.62 %) to yield a throughput of 70 tons/day. For these experiments, the initial solids concentration of sludge was taken as 10,000 *mg/l*, and the samples were diluted with deionized distilled water as needed to achieve this value. For example, if the suspended solids of a sample of digested primary sludge is 25,000 *mg/l*, then 1.5 parts of deionized distilled water are added to achieve the required dilution ratio of 2.5. (The suspended solids in the treated effluent used for pre-dilution at CSDOC may be neglected.)

When the deep outfall project is designed, it may be necessary to redo these tests with the designated discharge conditions, both with respect to concentration and buoyancy-driven mixing in the plume (i.e. the dilution history). However, the concentration chosen is believed to be upper limit while the flow discharge may well be higher than 3 *mgd*, depending on the pipe diameter selected. Considering the combined effects of initial concentration and time histories of dilution and turbulent shear, the scenario chosen probably results in more coagulation effect than will occur in the future prototype discharge; nevertheless, the tests should be repeated when prototype candidates are established.

The effluent from CSDLAC has much less solids concentration (~ 60 *mg/l*), and does not contain those coarse materials that can clog the injecting tube. Hence, the effluent sample was not treated through the nylon screen, nor was it diluted for the coagulation experiment.

For the case of the proposed outfall of digested primary sludge for CSDOC, the length of the discharge pipeline is designed to be about 12 *km* long and the average velocity inside the pipe (0.46 *m* in diameter) is about 0.79 *m/sec* for 3 *mgd* (0.131 *m*³/*sec*) discharge. The travelling time for the sludge inside the pipeline is about 4.2 *hr* ($=12000/0.79=15190$ *sec*) Hence, the diluted sludge was stirred with the

paddle at 190 rpm ($\bar{\epsilon} \sim 64 \text{ cm}^2/\text{sec}^3$) for about 4.2 hr to simulate the transporting process inside the outfall pipeline. For the effluent outfall of CSDLAC, the length of outfall is 7440 ft (2268 m), the pipe diameter is 120 in (3.05 m), and the design flow rate is 341 ft³/sec (9.66 m³/sec). The corresponding travelling time is about half an hour (2268/1.32=1718 sec), so the effluent was stirred at the same speed for about half an hour before the coagulation experiment.

3.3.2 Coagulation and sampling

At the beginning of the coagulation experiment, the coagulating reactor was filled with filtered artificial seawater. A small amount of the pre-processed sludge sample or raw effluent sample was then injected into the reactor from the bottom of the reactor as a small vertical buoyant jet, which entrained and mixed with the surrounding seawater when rising up to the surface. Because the density of the surrounding seawater is higher than that of the sewage, this sewage jet formed a diluted sewage layer occupying roughly the upper half of the reactor when the injection procedure was completed; the same was also true for the sludge. The paddle was then started to generate the turbulence needed for mixing and coagulation. To ensure complete mixing before any overflow over the weir, the inflow of seawater was delayed for a few seconds. At the end of this time period, the rotation speed of the paddle and the flow rate of the dilution water started to follow the predesigned values.

The initial injected sewage volume was determined in such a way that the dilution ratio after the complete mixing of the injected sludge and the seawater in the reactor was the same as that calculated for a particular plume at the corresponding time. For example, to simulate the sludge disposal process proposed for

Orange County, 40 *ml* of sludge sample was injected into the reactor during the first 20 *sec* of the experiment. The stirrer started at the end of the first 20 *sec* to mix the surface layer with the clean seawater in the reactor for 10 *sec*, and the flow of dilution seawater was started at the end of the first 30 *sec*. According to the calculated mixing history, the dilution ratio is 67 at 30 *sec*. The total volume of the reactor is 2600 *ml*, so $2600 \text{ ml}/67 \sim 40 \text{ ml}$ sludge is needed to achieve the desired dilution ratio. After the initial jet mixing stage, which was the first 30 *sec* in the case with sludge samples, the flow rate of the dilution water and the rotation speed of the paddle were adjusted every 10 *sec* following the pre-calculated schedule (Figure 3.1.1). The whole coagulation process lasted for 6 *min* and 20 *sec*.

In simulating the coagulation for the effluent outfall, about 90 *ml* of effluent was injected into the reactor during the first 20 *sec*. Stirring started at the end of the first 20 *sec* for another 20 *sec* before the dilution water started. This resulted in a dilution ratio of 30 at the end of the first 40 *sec* (lower than the design value, 55, at the end of the first 40 *sec*), and the whole coagulation process lasted for 4 *min* and 30 *sec*.

As the experiment progressed, samples were withdrawn from the reactor at different times. Since the coagulated flocs are very delicate and fragile, special caution was exercised in sampling. For sludge, samples were withdrawn from the center of the reactor with wide-mouth pipettes (opening diameter $> 1 \text{ cm}$) and transferred into containers filled with filtered artificial seawater. Samples were diluted immediately to a concentration less than 2 *mg/l* to suppress further coagulation. Effluent samples, with very small initial concentration (60 *mg/l* as compared to 10,000 *mg/l* for sludge), required a large volume of water, 2 *l*, which is about 77 % of the reactor volume, to be withdrawn for the subsequent size and settling velocity measurements

for each sample. Hence, to get the coagulation history at several time instants for effluent samples, the coagulation experiments were repeated many times. Each time the experiment was stopped at a prespecified sampling time. Water in the reactor was then siphoned out from the reactor through a plastic tubing, with 0.5 in (1.3 cm) inside diameter, directly into storage bottles without further dilution. These samples were then used for size and settling velocity analysis.

3.3.3 Settling experiment

To obtain the fall velocity distribution, every sample has to go through three different analyses: filtration, size distribution measurement, and settling velocity measurement.

3.3.3.1 Filtration

The purpose of filtration is to obtain the total solids concentration and the percentage of solids (by weight) with diameter larger than 10 μm . Samples of known volume were filtered separately through 10- μm and 0.4- μm Nuclepore membranes. Filtration results from the 0.4- μm membranes gave the mass of all suspended solids, while the filtration results from the 10- μm membranes gave the mass of particles with diameter larger than 10 μm . The ratio of the measured masses on 10- μm and the 0.4- μm membranes was the fraction of solids in the sewage with diameter larger than 10 μm .

The mass of the particles left on the membrane, or the solids loading, is critical in this filtration process. If the solids loading is too high, the pores on the membrane may be clogged and retain particles which otherwise will pass through. On the other hand, if the loading is too low, the accumulated mass may not be measured

accurately. The accuracy of the weighing process determined the minimum solids loading. By weighing the same membranes several times, we obtained the maximum difference among measurements to be less than 0.05 *mg*. This finding suggests that the accuracy of the weighing process is within 0.05 *mg*, so the collected solids mass should be kept higher than this value to ensure enough accuracy. The solids loadings that will clog the membranes can be estimated from the manufacturer's data (Faisst, 1976), or tested directly by filtration. Our experience indicated that the optimal range of the solids loading was around 0.5 *mg* for the 10- μm membrane and between 1 and 2 *mg* for the 0.4- μm membrane. Hence, for sludge and effluent samples, the volume used for filtration was adjusted to fit these ranges.

3.3.3.2 Size distribution measurement

To obtain the size distribution of particles larger than 10 μm of sewage samples, samples were first diluted to a concentration of less than 0.5 *mg/l* before being introduced into the cell for holograms recording. Dilution is necessary because that the images of particles get cluttered, and become hard to distinguish at high particle concentration. After the samples were introduced into the cell, singly exposed holograms were recorded. A small volume in the settling cell was reconstructed and the size of a large number of sewage particles inside this volume was measured. The size of the volume was calculated using the reading of the micrometers on the x,y,z-translating stage.

3.3.3.3 Settling velocity measurement

For the settling experiment, a density-stratified settling cell was prepared well in advance. Layers of water with slightly decreasing salt concentration (and density)

were carefully added into the cell, which was then left to stabilize for at least 8 *hr* before the experiment (see Sec. 3.2.5 for details). A sludge sample of 20 *ml* (concentration ~ 2 *mg/l*), or an effluent sample of 40 *ml* (concentration ~ 0.5 *mg/l*), was introduced from the top of the cell. A timer was started after the feeding of the samples to monitor the elapsed time.

Recording of holograms started three minutes after the sample was introduced. Doubly-exposed holograms were recorded according to the pre-calculated schedule (Table 3.3.1). The elapsed time and the time between the two exposures were recorded for every hologram. At the beginning of the settling experiment, particles with relatively high velocities were observed in the recording window. Hence, holograms were recorded fairly frequently (at a rate of one hologram every 30 *sec*), and the time interval between two exposures on the same film was small (≤ 1 *sec*). As the experiment progressed, particles with increasingly smaller velocities were observed, and both the time interval between exposures and the recording frequency decreased. The whole experiment lasted for 48 hours, and covered a velocity range from 1×10^{-4} to 0.05 *cm/sec*.

The size and velocity measurements were carried out by examining the reconstructed images of particles from the recorded holograms. After the images of particles were focused manually, the image analysis program automatically performed thresholding of the focused images and calculated various measurements, such as size and velocity, of particles as described in Sec. 3.2.2.

In presenting the experimental data in Chapter 4, the equivalent diameter, $d_{equ} = \sqrt{\frac{4A_p}{\pi}}$, was used to classify particles and to correlate particle sizes and their settling velocities. Results from the settling measurements are presented in

Table 3.3.1 Time schedule for recording holograms for settling analysis

Δt^\dagger , <i>sec</i>	t^\ddagger , <i>min</i>
~ 1	2'30", 2'45", 3', 3'15", 3'35", 3'55" 4'15", 4'40", 5'05", 5'30", 6'00",
1 - 1.25	6'40", 7'20", 8'
1 - 1.6	8'50", 9'40"
1 - 2	10'30", 11'30"
1 - 2.5	12'30", 13'45", 15'
1 - 3	16'15", 17'45", 19'20"
1 - 4	21', 23'
1 - 5	25', 27'30", 30'
1.3 - 6.3	32'30", 35'40", 38'50"
2 - 8	42, 46
2 - 10	50, 55
2.5 - 12.5	60, 66, 72, 78
3 - 15	84, 92
4 - 20	100, 110, 120
5 - 25	130, 142.5
6 - 31	155, 170.5, 186
8 - 40	201.5, 221.5, 241.5
10 - 50	261.5, 286.5, 306.5
13 - 63	331.5, 363, 394.5
16 - 79	426, 466
20 - 100	506, 556, 606
25 - 125	656, 718.5
31 - 156	781, 859, 937
40 - 200	1015, 1115, 1215
50 - 250	1315, 1440
63 - 313	1565, 1721, 1877
80 - 397	2033, 2231, 2429
100 - 500	2627

† Time interval between double exposures

‡ Time at which holograms are taken (measured from the time when samples were placed into the funnel)

two ways: the $w - d$ graphs, which show the relations between particle sizes and the settling velocities, and the distribution curves (probability density functions and cumulative distributions). The procedures used to derive the fall velocity distributions are discussed in Sec. 4.1. For $w - d$ plots, d_{equ} is used as the abscissa. In addition, several lines calculated from the Stokes' law, $w = A \frac{g}{18\mu} \Delta\rho d_{equ}^2$, with different values of $A\Delta\rho$ are depicted in the same graphs, in which A is the shape factor of particles. The use of d_{equ} and A will be discussed in detail in Chapter 5.

4. EXPERIMENTAL RESULTS

In this chapter, the technique used to derive the size and fall velocity distributions from the experimental data is first introduced. The experimental conditions and results are presented next.

4.1 Data Analysis

In this section, the detailed reconstruction procedures required to obtain reliable size distributions within the shortest time are introduced, followed by a discussion of the method used to calculate the probability density function of particle size from the experimental data. The next is a description of the technique for calculating the fall velocity of individual particles from the holograms.

There are two different ways to calculate fall velocity distributions from the experimental data: (1) Fall velocity distributions can be derived using only the data from settling velocity measurements, i.e., the settling velocities of individual particles. (2) They can also be estimated by combining the separate measurements of size and fall velocity. The procedures to calculate velocity distributions according to both methods are addressed.

Both size distributions and fall velocity distributions are calculated based on particle volume.

4.1.1 Size distribution

Singly exposed holograms were recorded and analyzed to provide information on size distributions based on particle volume for different samples. Similar to the particle size analysis by microscopy, time and operator fatigue limit the number of particles that can be counted by hologram reconstruction. To maximize sampling reliability and minimize the number of measurements, a procedure known as “stratified sampling” was employed (e.g. Yamate and Stockham, 1979). Basically, “stratified sampling” means that since number concentration of smaller particles is higher than that of larger ones, a smaller volume is analyzed for sizing smaller particles, while a larger volume is used for larger particles.

The above procedure is necessary even if counting every particle in the hologram could be accomplished through patience and tedious work. As mentioned in the previous chapter, we can move either the 75 *cm* rail or the z-micrometer in the z direction to focus the images of particles within a particular x-y frame. The distance, Δz , over which a particle can be observed, is roughly proportional to $\frac{d^2}{\lambda}$, where d is the size of the particle and λ the wavelength of the illuminating light (Stanton *et al.*, 1984). Hence, even though the 75 *cm* rail with 1 *mm* position accuracy is sufficient for particles with dimension larger than 30 μm , the z-micrometer, which has position accuracy of 10 μm , should be used in focusing the images of smaller particles with smaller Δz . The 75 *cm* rail can be moved much more easily and faster than the micrometer. Analyzing larger particles with this rail saves time since a larger volume needs to be examined.

The reconstruction volume of each hologram is about 10.6 cm^3 . For each hologram, we first scanned through a small three-dimensional volume in the hologram (0.2 to 0.8 cm^3) by adjusting the x,y,z-micrometers with the 75 cm rail at a fixed position. All particles inside this volume with equivalent diameter equal to or larger than $10 \mu\text{m}$ were measured until the total number exceeded 200. Following the same observation procedure, we went through another volume of about 0.7 to 3.2 cm^3 searching for all particles larger than $20 \mu\text{m}$ until we had more than 100 particles. Then with the z-micrometer fixed, the 75 cm rail and the x,y-micrometers were used to examine a volume of about 1.4 to 7.0 cm^3 for particles larger than $30 \mu\text{m}$. It took one to two days to analyze one singly exposed hologram to obtain the size distribution of a particular sample. The total volume examined ranges from 3.0 to 10.0 cm^3 , and the total number counted ranges from 400 to 800 for each hologram analyzed.

We measured the equivalent diameter and recorded the appropriate sample volume of each group of particles based on the above analysis. To construct the size distribution, we divided the possible size range from 10 to $250 \mu\text{m}$ into 14 subranges. Each subrange covers the diameter ranging from d_j to d_{j+1} , and d_j 's were determined in such a way as to maintain $\Delta \text{Log}(d_j) = \text{Log}(d_{j+1}) - \text{Log}(d_j) = \text{constant}$ between adjacent subranges. Hence, using 10 steps per log cycle we have:

$$d_j (\mu\text{m}) = 10^{1+0.1(j-1)}, \quad j = 1, 15 \quad (4.1.1)$$

If V_d is the examined volume for particles with diameter d , the probability density function, $p(d_j)$, of the size distribution based on particle volume can be calculated according to the following equation:

$$p(d_j) = \frac{\sum_{d_j \leq d \leq d_{j+1}} (d^3/V_d)}{(d_{j+1} - d_j) \sum_{total} (d^3/V_d)} \quad (4.1.2)$$

4.1.2 Settling velocity of individual particles

Settling velocities of individual particles were measured from doubly exposed holograms. Upon reconstruction, double images of particles were focused; the averaged equivalent diameter and the distance between the centroids of the two images were measured.

When the doubly exposed hologram was recorded, the shutter, not the film, had to be rewound between two exposures to reactive the shutter. This process may slightly change the position of the film in both vertical (0 to 20 μm) and horizontal directions (0 to 200 μm). For each hologram, the double images of dust particles on the optical windows were also analyzed to give the vertical and horizontal displacements due to the film movement, i.e., Δl_v and Δl_h . Since the settling of particles induces only the vertical displacement of images, the horizontal displacement must result from the film movement. The vertical displacement due to the film movement should be added to or subtracted from the vertical distances measured between two images in calculating fall velocities. If the film movement increases the settling distance, the vertical correction, Δl_v , is negative, and vice versa. Taking l_v as the distance measured between two images and Δt as the time difference between exposures, we can calculate the settling velocity as:

$$w = \frac{l_v + \Delta l_v}{\Delta t} \quad (4.1.3)$$

4.1.3 Settling velocity distribution

One of the main objectives of our experiment is to obtain the settling velocity distributions based on the particle volume for different types of sewage particles. From the settling velocity measurements described in the previous section, we obtained the information on both sizes and fall velocities of a group of particles. If these particles are representative, we can derive the fall velocity distribution based on particle volume directly from the measurements as:

$$f(w_i) = \frac{\sum_{w_i \leq w \leq w_{i+1}} d^3}{(w_{i+1} - w_i) \sum_{total} d^3} \quad (4.1.4)$$

However, this equation gives a biased result because the probability of sampling particles of a certain size and velocity is not uniform for all velocity and size ranges, but depends on the fall velocity of particles, the initial position of particles in the settling cell, and the time of recording holograms. Hence, the size and fall velocity distributions, as calculated directly from the observed particles in the measuring window from settling velocity measurements, are different from the true distributions of the samples that are introduced into the settling cell. In the following, we discuss this biased sampling problems in detail as well as the procedures used to counteract the sampling bias in the velocity distribution data.

4.1.3.1 Sampling problems

There are two important length scales and three time scales which work together to determine the range of the velocities that can be measured using this holographic technique. The length scales are the vertical dimension of the recorded

field ($h = 1.5 \text{ cm}$) and the distance between the water surface and the observation window ($L \sim 18 \text{ cm}$). The time scales are the time between two exposures on the same frame, Δt , the time between two adjacent frames, Δt_f , and the time t when holograms are recorded.

Currently the camera system is under manual control; there is a low limit on Δt and Δt_f . The shortest Δt is about 1 *sec*, and the shortest Δt_f is about 30 *sec*. Particles with velocities fast enough to travel the entire recording field between two exposures ($\sim 1.5 \text{ cm/sec}$) will be lost or exposed only once on films. This implies that particles with velocities faster than 1.5 cm/sec cannot be measured. Similarly, particles with velocities fast enough to travel across the entire recording field between two successive frames ($\sim 0.05 \text{ cm/sec}$) may or may not be observed. Hence, we can catch some of the particles in this category, but not all of them.

Although the time interval between frames was continuously adjusted to minimize the chance of recording the same set of particles twice, it is still possible for particles with settling velocities less than 0.05 cm/sec to stay in the field of view long enough to appear in two successive frames and, hence, to be counted more than once. Particles having such slow fall velocities that they fail to reach the observing window before the end of the experiment will not be recorded. At the present time, the settling experiments lasted for 48 *hr* and the smallest observable velocity is about $1 \times 10^{-4} \text{ cm/sec}$.

Another difficulty in obtaining representative samples arises from the separation of particles during settling because of different fall velocities. Let us assume that particles start to fall down from an uniform layer of thickness, H , at the top of the settling cell at time $t = 0$ as shown in Figure 4.1.1. For particles with fall velocities in the range of w to $w + \Delta w$, the thickness of this layer increases with

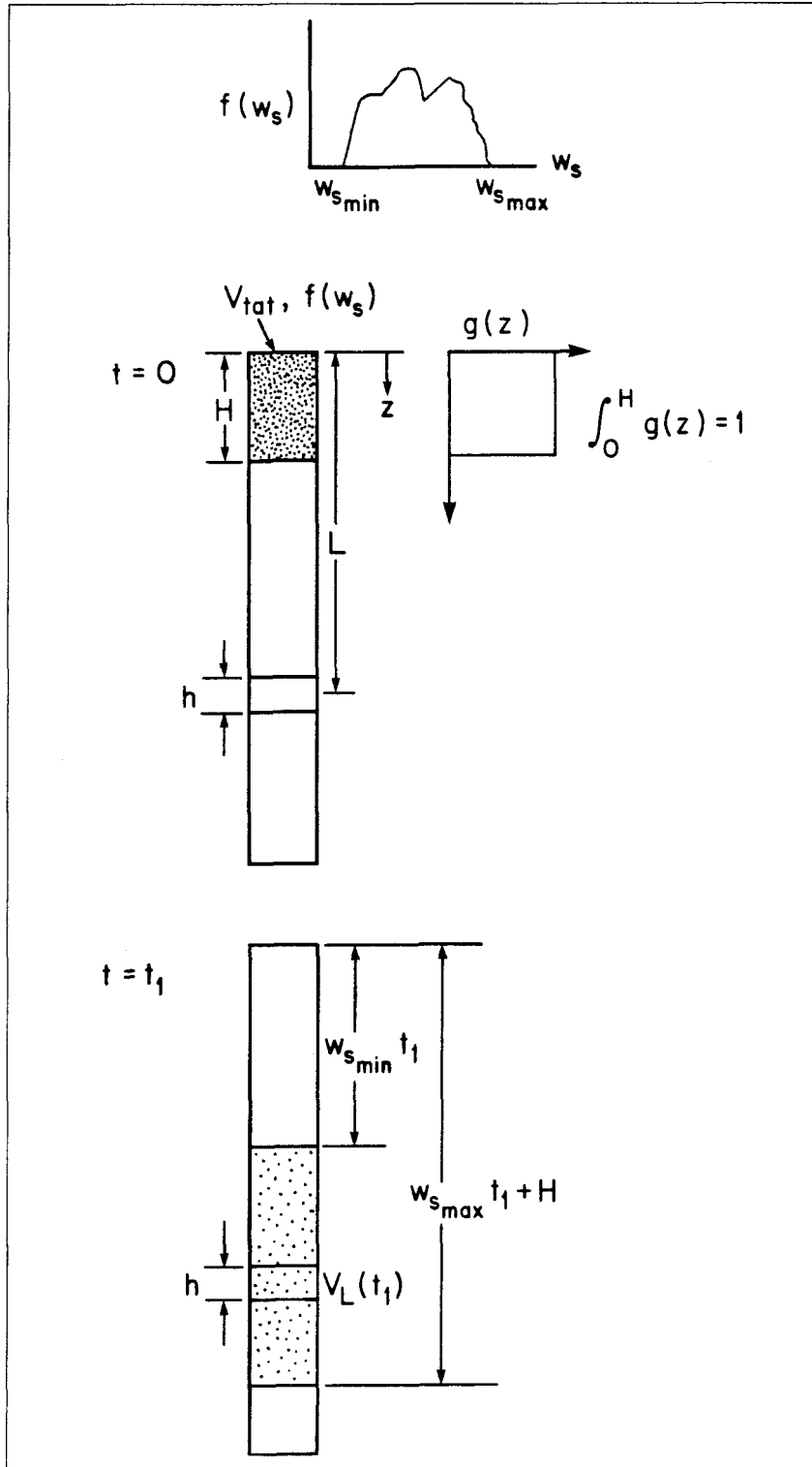


Figure 4.1.1 Settling of particles in the cell

time according to $H + t\Delta w$. During the settling of particles, particles are also rearranging themselves inside this layer—particles with velocities closer to w tend to cluster on the top of this layer, and particles with velocities closer to $w + \Delta w$ on the bottom of this layer. Hence, the particle concentration inside this layer decreases accordingly. However, the sampling volume, ha (a is the area of the cross section of the settling cell), does not change with time. Therefore, the number of particles that can be recorded by a hologram depends not only on their initial concentration, but also on the time when the hologram is recorded.

4.1.3.2 Settling velocity distribution derived from the measurement of settling velocity

From the discussion above, we conclude that velocity distributions calculated from Eqn. 4.1.4 are incorrect and a different technique used to derive unbiased fall velocity distributions is needed and will be introduced here.

Consider Figure 4.1.1 which depicts a group of particles with total particle volume of V_{tot} suspended inside the layer H on top of the settling cell at time $t = 0$. The volume distribution of particles inside the layer H is described by $g(z)$, and $\int_0^H g(z)dz = 1$. We assume these particles have a fall velocity distribution, $f(w)$, which is independent of the position z . Then, at time t , the total particle volume that will be observed within the recording field, i.e., from $z = L - 0.5h$ to $z = L + 0.5h$, can be calculated according to the following equation:

$$V_L(t) = \int_0^H V_{tot} g(z) dz \int_{(L-z-0.5h)/t}^{(L-z+0.5h)/t} f(w) dw \quad (4.1.5)$$

where L is the distance between the water surface and the center of the observing window, and h is the height of the sampling volume. If we assume that $f(w)$ does not change dramatically over the velocity range from $\frac{L-z-0.5h}{t}$ to $\frac{L-z+0.5h}{t}$, it can be approximated by $f\left(\frac{L-z}{t}\right)$. Then Eqn. 4.1.5 can be simplified as:

$$V_L(t) = V_{tot} \frac{h}{t} \int_0^H g(z) f\left(\frac{L-z}{t}\right) dz \quad (4.1.6)$$

To further simplify the above equation, it is assumed that the initial distribution of particles inside the layer h is nearly uniform, so $g(z) \simeq \frac{1}{H}$. Hence, we have:

$$\begin{aligned} V_L(t) &\simeq V_{tot} \frac{h}{t} \frac{1}{H} \int_0^H f\left(\frac{L-z}{t}\right) dz \\ &\simeq V_{tot} \frac{h}{t} f(w(t)) \end{aligned} \quad (4.1.7)$$

where $w = \frac{L-0.5H}{t}$.

For a doubly exposed hologram recorded at time t , we measured the size and velocity of every particle with diameter larger than $10 \mu m$. If there are N particles in a hologram, we can calculate $V_L(t)$, $w(t)$, and the corresponding probability density function, $f(w(t))$, according to the following equations:

$$V_L(t) = \sum_{i=1}^N d_i^3 \quad (4.1.8)$$

$$\bar{w}(t) = \frac{1}{N} \sum_{i=1}^N w_i \quad (4.1.9)$$

$$V_{tot} f(\bar{w}(t)) = V_L(t) \frac{t}{h} \quad (4.1.10)$$

Since w is observed directly from the holograms, it is not necessary to explicitly specify L and H in the above analysis, provided $H \ll L$, as it is.

Repeating the above computations for all holograms that were analyzed (typically 40 to 60 holograms for one sample), we got a curve of $V_{tot}f(w)$ versus w . We then integrated this curve to get V_{tot} , and normalized the $V_{tot}f(w)$ curve by V_{tot} to get the cumulative probability function, $F(w) = \int_0^w f(v)dv$.

Finally, the velocity range from 1×10^{-4} to 0.05 cm/sec was divided into 27 subranges in such a way to keep constant $\Delta \text{Log}(w_i) = \text{Log}(w_{i+1}) - \text{Log}(w_i)$. Hence, we have:

$$w_i \text{ (cm/sec)} = 10^{-4+0.1(i-1)}, \quad i = 1, 28 \quad (4.1.11)$$

Based on the $F(w)$ curve derived from the settling experiment, we applied an interpolation method was applied to get $F(w_i)$. The probability density function, $f(w_i)$ for a special velocity range, w_i to w_{i+1} , can then be calculated using the following equation:

$$f(w_i) = \frac{F(w_{i+1}) - F(w_i)}{w_{i+1} - w_i} \quad (4.1.12)$$

4.1.3.3 Conditional settling velocity distribution derived from the measurement of settling velocity

As mentioned before, a single settling analysis for one sample lasted for 48 *hr*. If more than one sample is withdrawn from the preceding coagulating experiment for

testing, some of them have to be stored for several days before the settling test, and the possible change of the samples during the storage is a major concern. Since it took only minutes to record holograms for size analysis, our experimental procedure was to record singly exposed holograms for all samples immediately after they were withdrawn from the coagulator. The settling measurements were then conducted after the size measurements. If it is assumed that the fall velocity distribution of particles within a particular size range, i.e. the conditional probability density function $f(w | d)$, does not change with time, the fall velocity distributions can be derived based on the independent measurements of size and fall velocities.

The analysis in Sec. 4.1.3.2 can be repeated for a small size range, d_j to d_{j+1} , to provide the conditional probability density functions for this size range. If there are M particles with diameter in the size range, d_j to d_{j+1} , inside a hologram, the corresponding equations to calculate the distributions are as:

$$V_{L,d_j}(t) = \sum_{i=1}^M d_i^3 \quad (4.1.13)$$

$$\bar{w}(t) = \frac{1}{M} \sum_{i=1}^M w_i \quad (4.1.14)$$

$$V_{tot,d_j} f(\bar{w}(t) | d_j) = V_{L,d_j}(t) \frac{t}{h} \quad (4.1.15)$$

$$f(w_i | d_j) = \frac{F(w_{i+1} | d_j) - F(w_i | d_j)}{w_{i+1} - w_i} \quad (4.1.16)$$

This resulting conditional probability density function, $f(w_i | d_j)$, will now be used in conjunction with the size distribution measured from the single exposure hologram to give fall velocity distributions of different samples.

4.1.3.4 Settling velocity distribution derived from the measurements of size and settling velocity

The fall velocity distribution of a sample can be derived from the separate measurements of sizes and velocities. The size distribution is calculated according to Eqn. 4.1.2, and the velocity distribution within a certain size range according to Eqn. 4.1.16. The combined results give the fall velocity distribution as follows:

$$f(w_i) = \sum_j f(w_i | d_j) p(d_j) (d_{j+1} - d_j) \quad (4.1.17)$$

This result now includes adjustments for the systematic biases of the hologram procedure. There are still, of course, the usual random sampling errors. This result is finally integrated to obtain cumulative distributions $F(w_i)$.

4.2 Experimental Results

Four sets of experiments using different sludges and different mixing processes were performed. The experimental conditions and related parameters in mixing and settling measurements are summarized in Table 4.2.1. Samples used in this study were the digested primary sludge (D.P.S.) from CSDOC and the effluent mixture (comprised of 46 % primary effluent and 54 % secondary effluent) from CSDLAC. Simple mixing, i.e., one dilution and one stirring speed for a short period, was used for particle coagulation in Runs 1 and 2. The coagulating reactor was used to simulate the special mixing history in the plume (plume mixing) in Runs 3 and 4.

Table 4.2.1 Summary of experimental parameters for the settling measurements of sludge and effluent particles (Concentrations given are suspended solids in the samples tested.)

No.	Sludge sample	Coagulation	Size distribution	Settling velocity measurement
1a	D.P.S. (CSDOC) ~ 25,000 mg/l	Simple mixing ~ 250 mg/l for 20 min	10 ⁵ : 1 dilution ~ 0.3 mg/l	10 ⁴ : 1 dilution in seawater ~ 2.5 mg/l
1b	Same as above	Same as above ~ 250 mg/l	—	10 ⁴ : 1 dilution in distilled water, ~ 2.5 mg/l
2	Effluent (CSDLAC) 56.5 mg/l	Simple mixing ~ 2.82 mg/l for 25 min	~ 0.47 mg/l	~ 0.47 mg/l
3	D.P.S. (CSDOC), Plume mixing			
		<i>t</i> = 0", 10000 mg/l	~ 0.2 mg/l	1.50 mg/l
		<i>t</i> = 20", 250 mg/l	~ 0.2 mg/l	2.74 mg/l
		<i>t</i> = 1'20", 60 mg/l	~ 0.2 mg/l	1.88 mg/l
		<i>t</i> = 2'30", 23 mg/l	~ 0.2 mg/l	—
		<i>t</i> = 3'50", 20 mg/l	~ 0.2 mg/l	—
		<i>t</i> = 5'40", 20 mg/l	~ 0.2 mg/l	2.47 mg/l
		<i>t</i> = 6'20", 20 mg/l	~ 0.2 mg/l	—
4	Effluent (CSDLAC), Plume mixing			
		<i>t</i> = 0", 58 mg/l	0.29 mg/l	2.9 mg/l
		<i>t</i> = 40", 2.14 mg/l	0.43 mg/l	—
		<i>t</i> = 1'20", 1.03 mg/l	1.03 mg/l	—
		<i>t</i> = 2'10", 0.56 mg/l	0.56 mg/l	0.56 mg/l
		<i>t</i> = 3'20", 0.70 mg/l	0.70 mg/l	—
		<i>t</i> = 4'30", 0.68 mg/l	0.68 mg/l	0.68 mg/l

4.2.1 Run 1—Digested primary sludge (CSDOC), simple mixing

The first run was conducted with digested primary sludge from the County Sanitation Districts of Orange County. It was done before the special reactor was built for simulating the mixing and dilution history in a plume; instead the mixing was done with a magnetic stirrer at constant dilution. The experimental conditions of this run were as follows: A sample of 20 ml D.P.S. was added to a flask with 2 l artificial seawater. The solids concentration of this suspension was 250 mg/l. This suspension was stirred with a magnetic stirrer for 20 min. Two samples were withdrawn and diluted with artificial seawater and distilled water respectively to a total dilution ratio of $10^4 : 1$ for settling velocity analysis. Another two samples were taken from these two diluted samples and diluted further to $10^5 : 1$ dilution in seawater and distilled water respectively for size distribution measurements.

4.2.1.1 Size distribution

Particle size measurements were performed for the sample diluted in seawater only. Sixty-five particles were observed in the 10-to-20 μm size range inside a volume of 0.40 cm^3 , 315 in the 20-to-40 μm size range inside a volume of 2.08 cm^3 , and 156 for diameter larger than 40 μm in a volume of 3.87 cm^3 . The probability density function $p(d)$ was calculated according to Eqn. 4.1.2. Instead of presenting the result as $p(d)$ versus d , it is plotted as $\frac{p(d)\Delta d}{\Delta(\text{Log } d)}$ versus $\text{Log } d$ (Figure 4.2.1). The total area under this curve is unity ($\sum p(d)\Delta d = 1$), and the area integrated over a particular size range represents the ratio of volume of particles in that size range

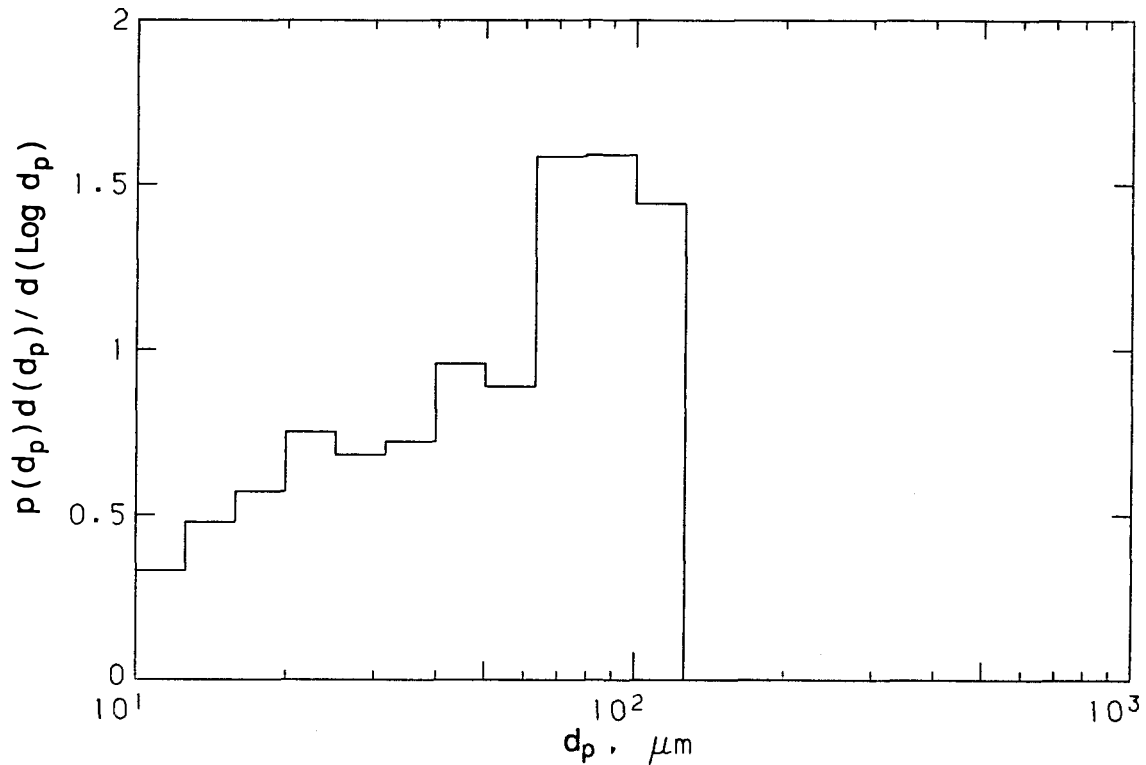


Figure 4.2.1 Size distribution ($d \geq 10 \mu m$) of the D.P.S. (CSDOC) after coagulation with a magnetic stirrer at 250 mg/l for 20 min , measured by holographic technique

to the total volume. The median diameter (for particles $> 10 \mu m$) falls between 50 to $63 \mu m$ in this case.

4.2.1.2 Run 1a—Settling velocity distribution measured in seawater

Thirty-six holograms were analyzed for the settling experiment of coagulated D.P.S. in seawater; the equivalent diameter and fall velocity of 755 particles were measured. The relationship of w versus d is plotted in logarithmic scale to cover the wide velocity and size ranges (Figure 4.2.2). The fall velocity distribution estimated

from the settling velocity measurements alone (according to Eqn. 4.1.8 to 4.1.12) is plotted in Figure 4.2.3. The result shows the 50% settling velocity for particles larger than $10 \mu m$ as $3.5 \times 10^{-3} \text{ cm/sec}$.

The conditional velocity distribution shown in Figure 4.2.4 was calculated on the basis of Eqn. 4.1.13 to 4.1.16, and $\frac{f(w | d) \Delta w}{\Delta(\text{Log } w)}$ was used instead of $f(w)$ in the figure to provide better illustration. For all size ranges, the velocity distribution covers a wide range and the median velocity increases with the size. The settling velocity distribution was derived from the size distribution (Figure 4.2.1) and velocity measurements (Figure 4.2.4) by use of Eqn. 4.1.17 is shown in Figure 4.2.5. The 50% fall velocity is about $1.8 \times 10^{-3} \text{ cm/sec}$ for the particles larger than $10 \mu m$.

4.2.1.3 Run 1b—Settling velocity distribution measured in fresh water

Thirty-eight holograms were analyzed for the settling test of the same sludge sample in fresh water and 643 particles were measured. The same procedures as in Sec. 4.2.1.2 were used to obtain different settling curves. Figure 4.2.6 shows the $w - d$ relationship, which is quite similar to that observed in seawater. Fall velocity distribution estimated from the settling test alone is shown in Figure 4.2.7, which gives the 50% velocity as $4 \times 10^{-3} \text{ cm/sec}$. The conditional fall velocity distributions are plotted in Figure 4.2.8. If we assume that the size distribution is the same as that in seawater, we can use the size distribution obtained in Sec. 4.2.1.1 to compute the velocity distribution as in Figure 4.2.9, which shows the 50% velocity as $2 \times 10^{-3} \text{ cm/sec}$.

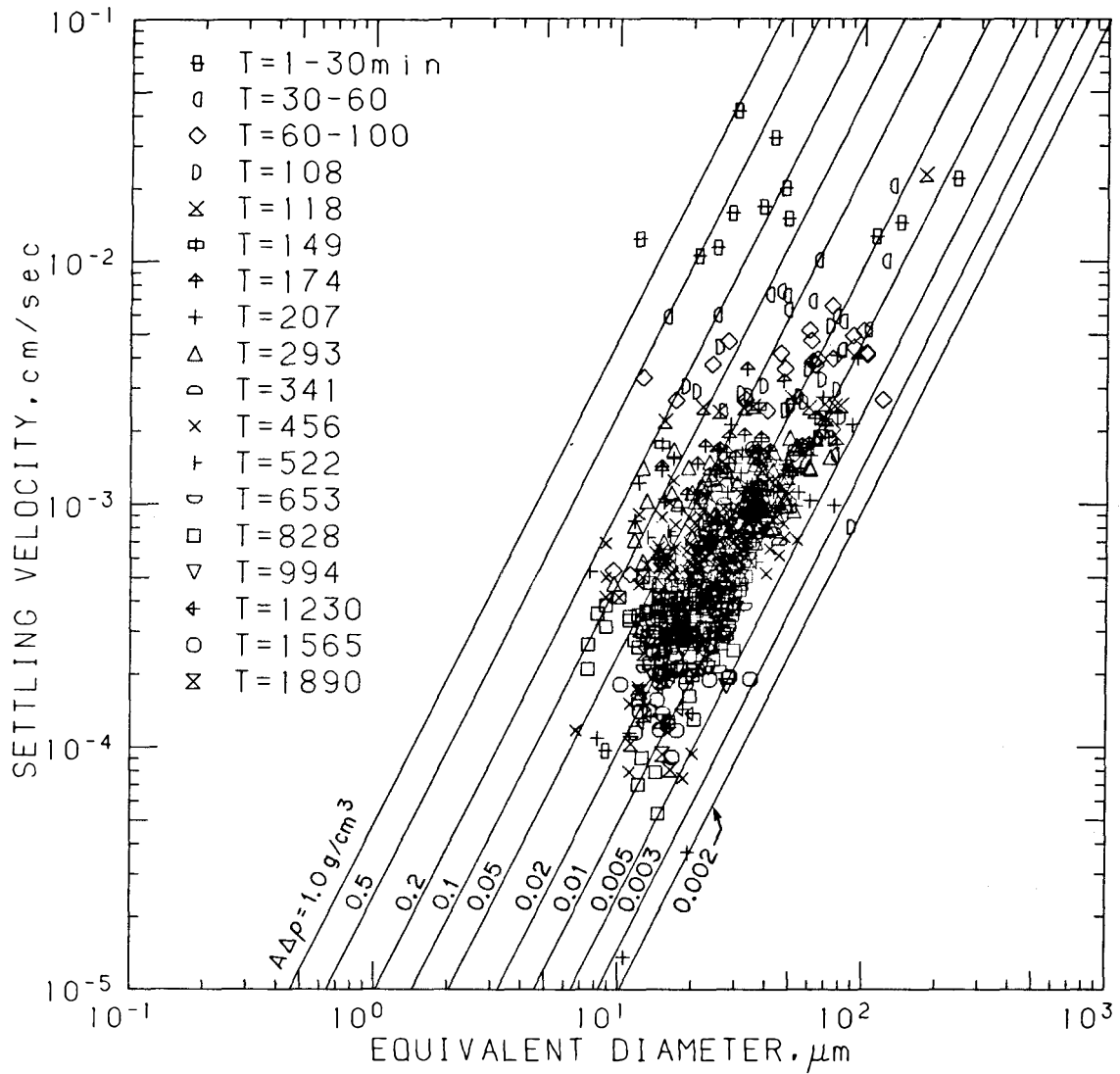


Figure 4.2.2 Settling velocity versus equivalent diameter for the D.P.S (CSDOC) measured in seawater after coagulation with a magnetic stirrer at 250 mg/l for 20 min

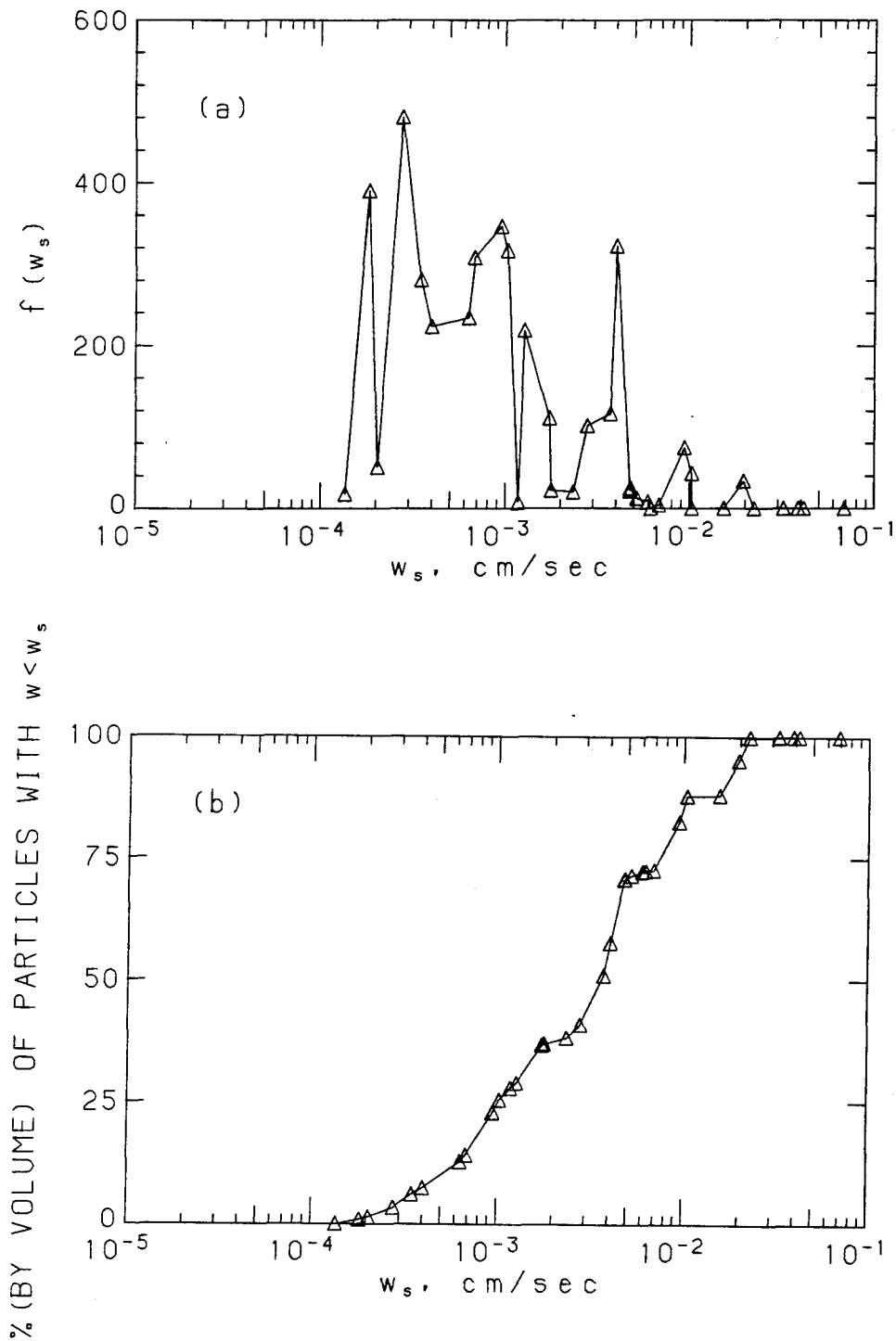


Figure 4.2.3 Settling velocity distribution ($d \geq 10\mu\text{m}$) of the D.P.S. (CSDOC) measured in seawater after coagulation with a magnetic stirrer at 250 mg/l for 20 min, derived from the settling measurement alone: (a) density distribution, (b) cumulative distribution

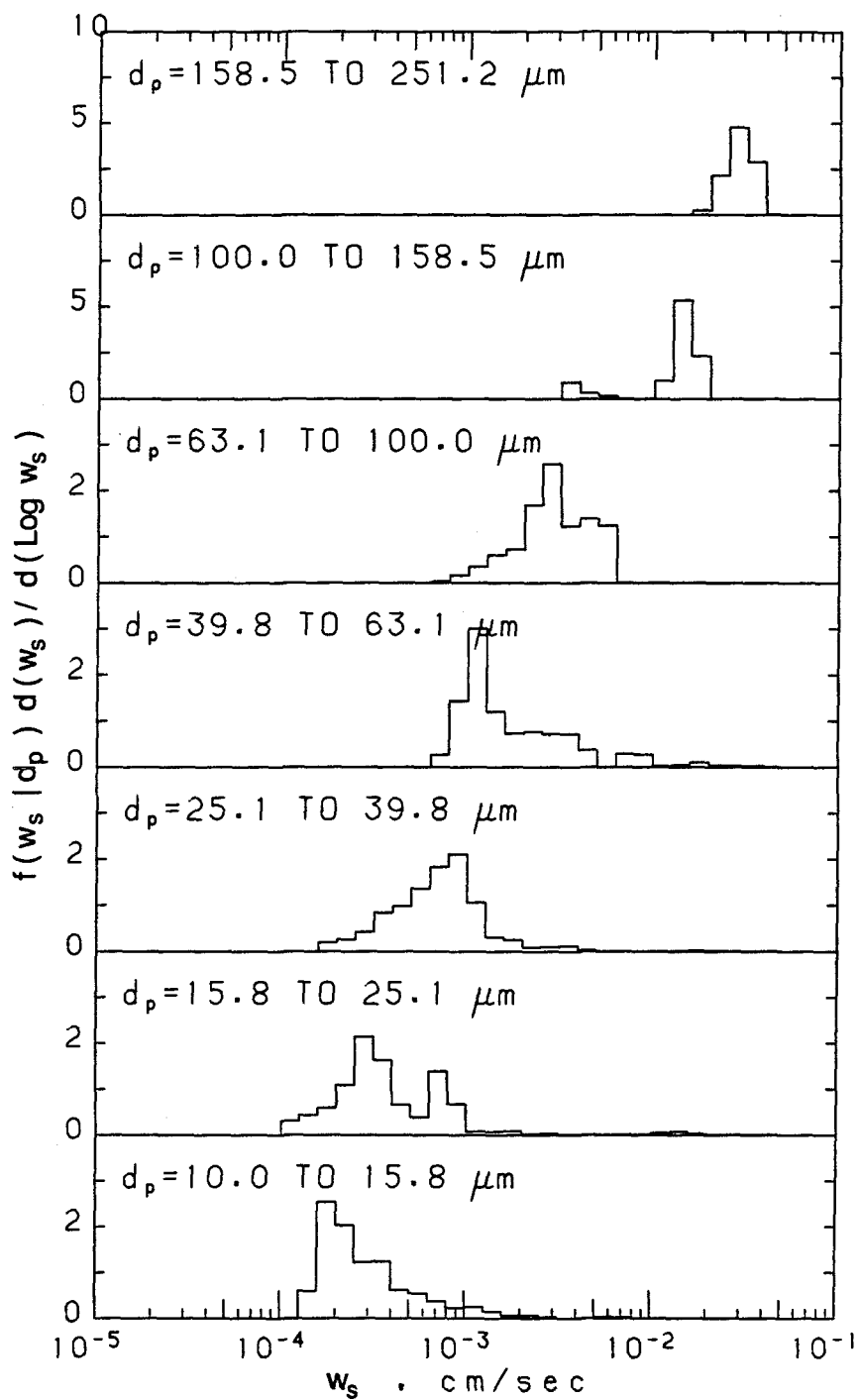


Figure 4.2.4 Conditional settling velocity distribution ($d \geq 10\mu\text{m}$) of the D.P.S. (CSDOC) measured in seawater after coagulation with a magnetic stirrer at 250 mg/l for 20 min

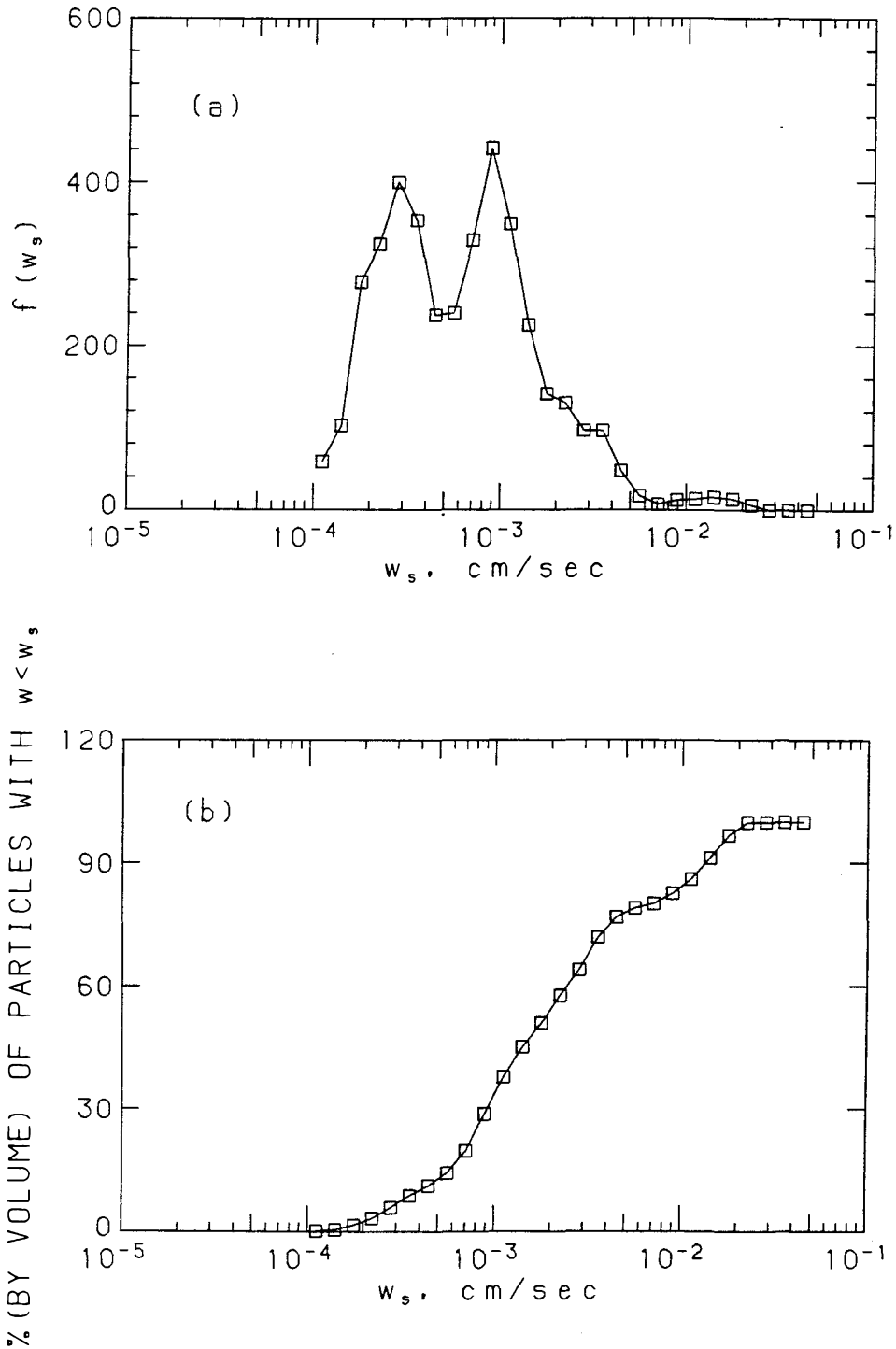


Figure 4.2.5 Settling velocity distribution ($d \geq 10\mu m$) of the D.P.S. (CSDOC) measured in seawater after coagulation with a magnetic stirrer at 250 mg/l for 20 min, derived from the measurements of both size and velocity: (a) density distribution, (b) cumulative distribution

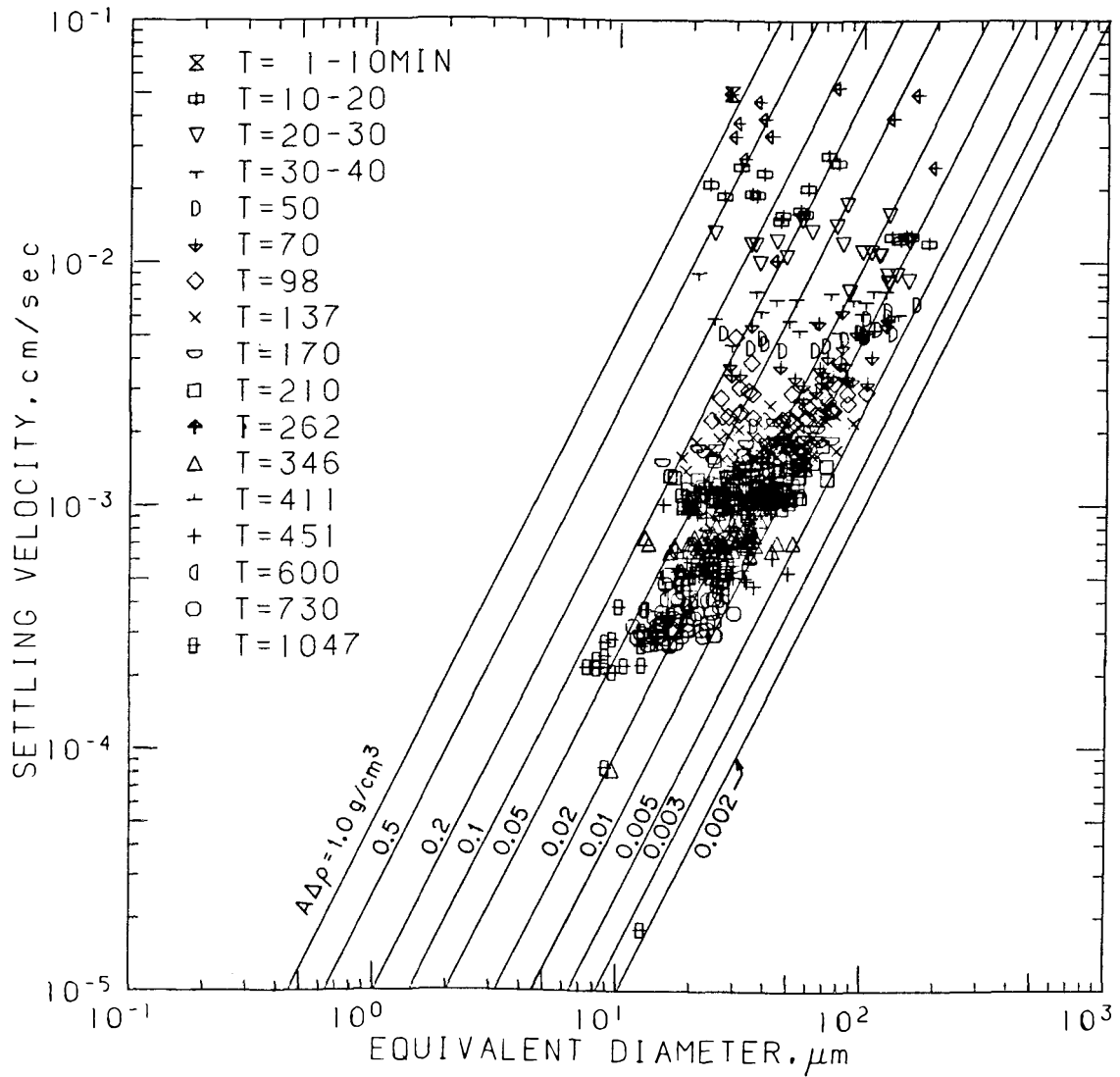


Figure 4.2.6 Settling velocity versus equivalent diameter for the D.P.S. (CSDOC) measured in fresh water after coagulation with a magnetic stirrer at 250 mg/l for 20 min

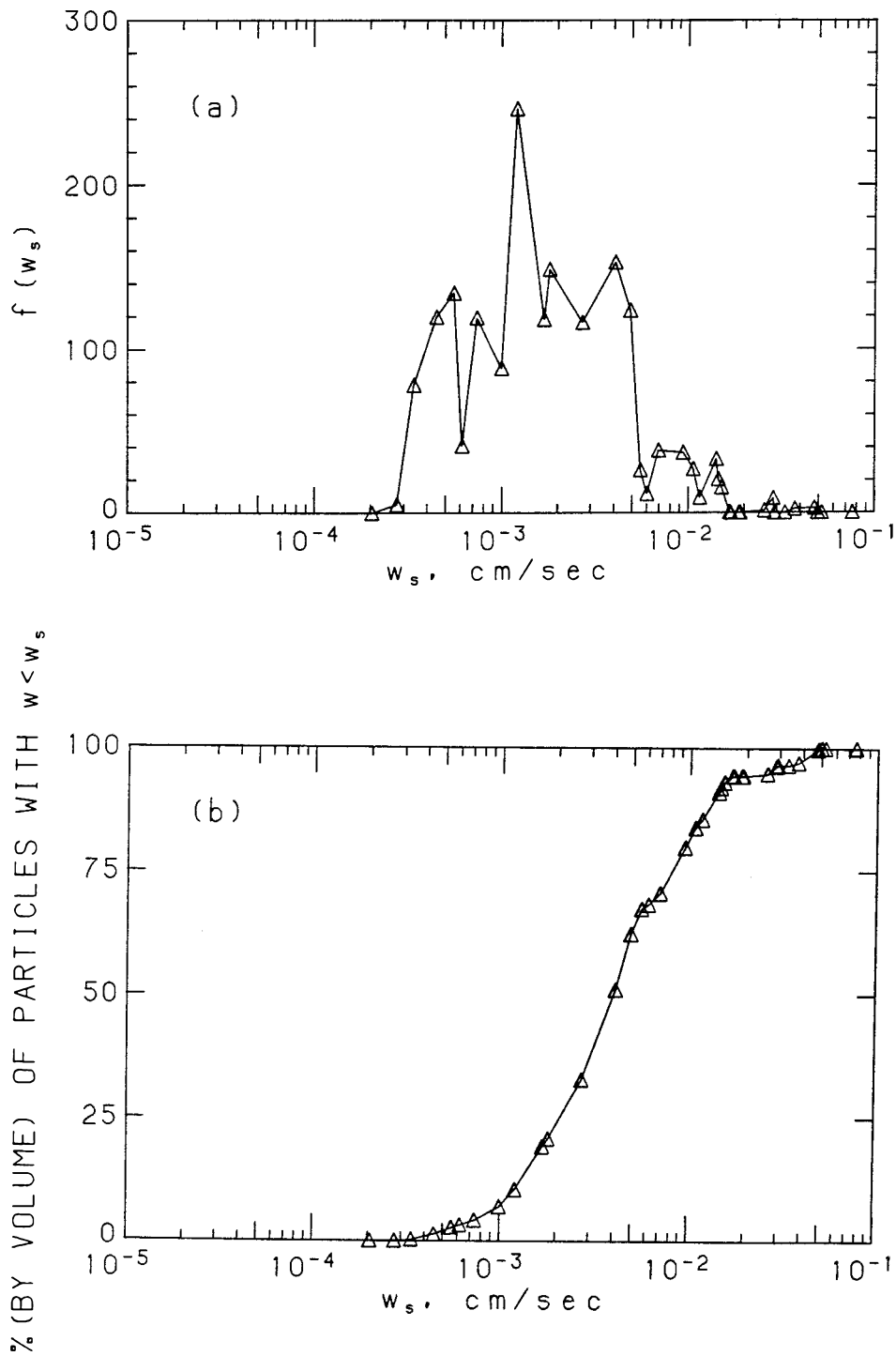


Figure 4.2.7 Settling velocity distribution ($d \geq 10\mu m$) of the D.P.S. (CSDOC) measured in fresh water after coagulation with a magnetic stirrer at 250 mg/l for 20 min, derived from the settling measurement alone: (a) density distribution, (b) cumulative distribution

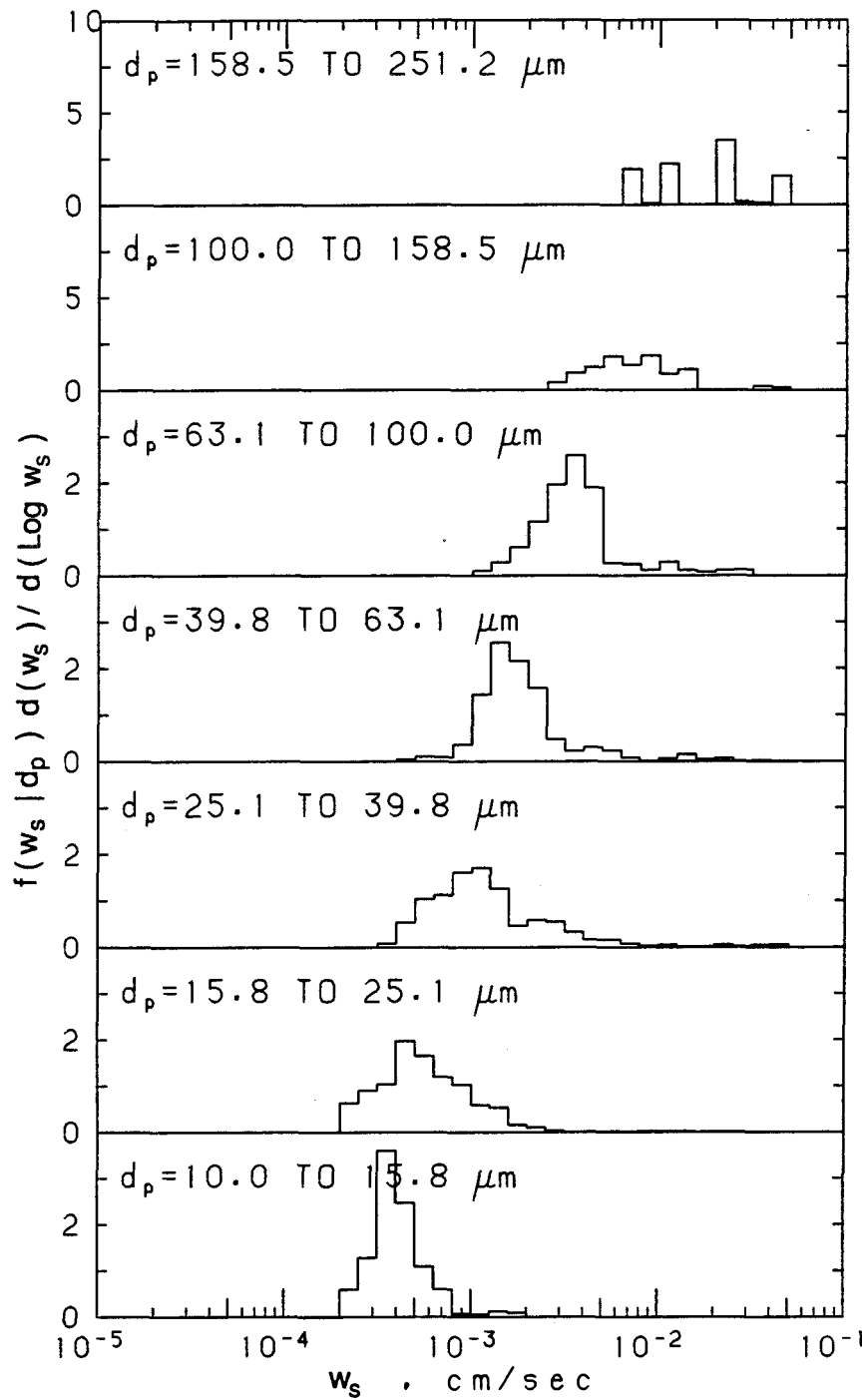


Figure 4.2.8 Conditional settling velocity distribution ($d \geq 10\mu\text{m}$) of the D.P.S. (CSDOC) measured in fresh water after coagulation with a magnetic stirrer at 250 mg/l for 20 min

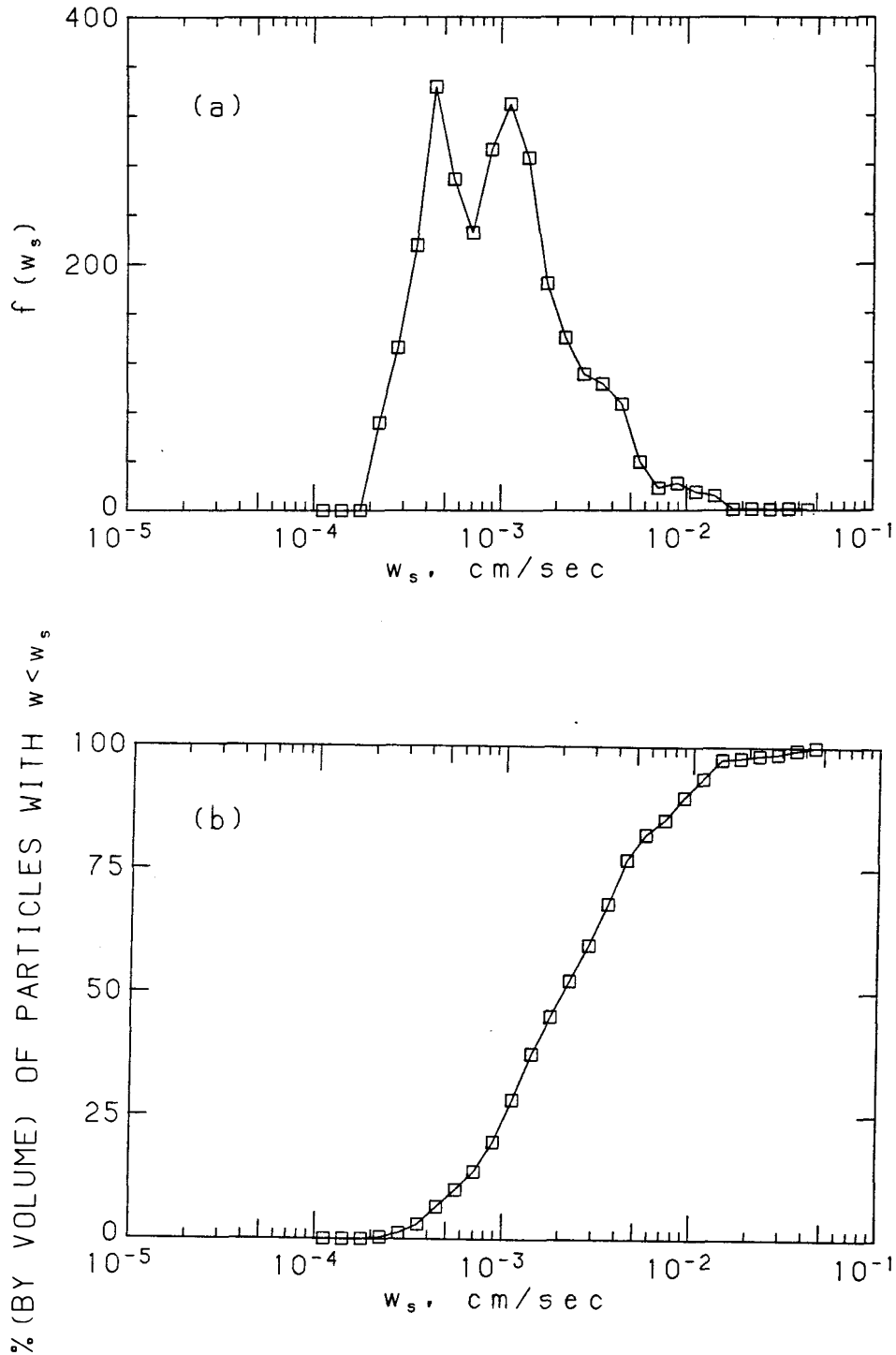


Figure 4.2.9 Settling velocity distribution ($d \geq 10\mu\text{m}$) of the D.P.S. (CSDOC) measured in fresh water after coagulation with a magnetic stirrer at 250 mg/l for 20 min, derived from the measurements of both size and velocity: (a) density distribution, (b) cumulative distribution

4.2.2 Run 2—Effluent (CSDLAC), simple mixing

The solids concentration of the effluent mixture was 57 mg/l . In this run, 52.5 ml effluent was first diluted with 1 l artificial seawater to a concentration of about 2.82 mg/l and stirred for 25 min with a magnetic stirrer. Samples were then withdrawn from this suspension and diluted to a total dilution of 100:1 for both velocity and size measurements.

4.2.2.1 Size distribution

A volume of 2.31 cm^3 was analyzed for particles of equivalent diameter from 10 to $20 \text{ }\mu\text{m}$, and 150 particles were observed. For particles larger than $20 \text{ }\mu\text{m}$, 179 particles were measured inside a volume of 10.16 cm^3 . The computed size distribution based on particle volume is shown in Figure 4.2.10. The median size is between 50 to $63 \text{ }\mu\text{m}$.

4.2.2.2 Settling velocity distribution

For the settling velocity distribution, 52 holograms were analyzed and 310 particles were measured. Figure 4.2.11 depicts the $w - d$ relationship, which roughly covers the same region of the graph as that covered by sludge particles. Figure 4.2.12 shows the fall velocity distribution derived from the settling measurements alone; the 50% velocity is $1 \times 10^{-2} \text{ cm/sec}$ for particles larger than $10 \text{ }\mu\text{m}$. Figure 4.2.13 shows the corresponding conditional velocity distributions for different size ranges. Figure 4.2.14 illustrates the velocity distribution derived from both the size and velocity measurements. A much smaller 50% velocity, $2.8 \times 10^{-3} \text{ cm/sec}$, is obtained.

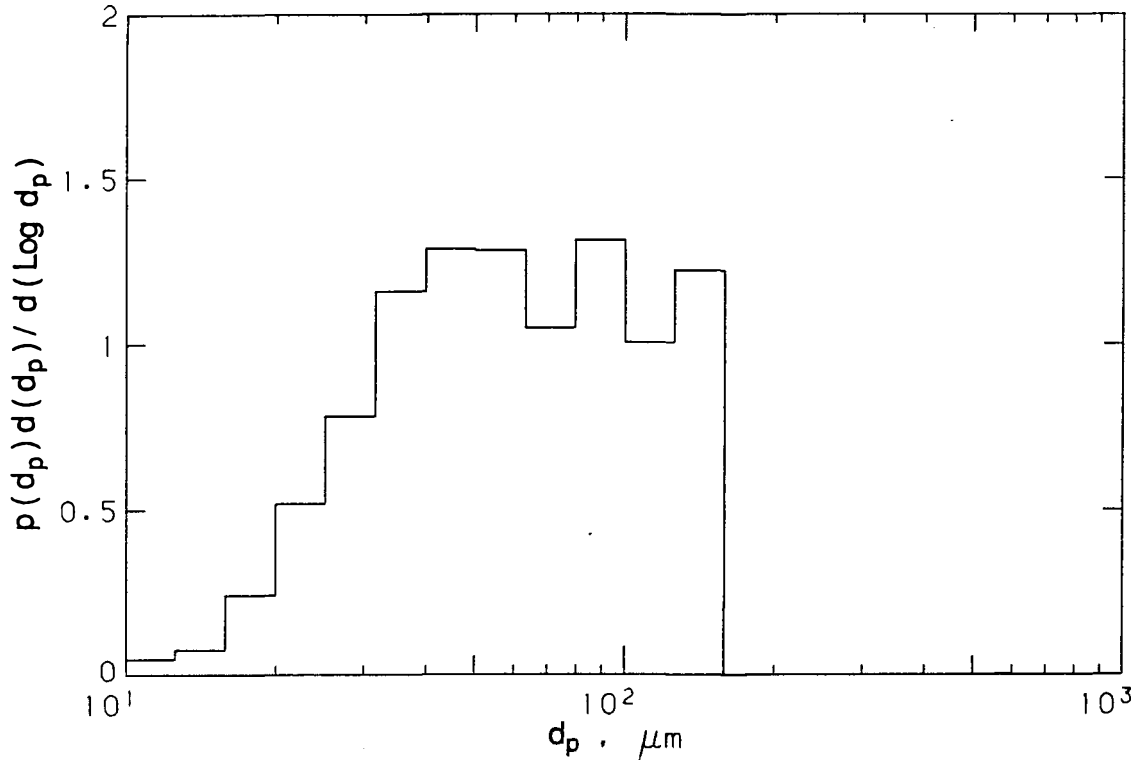


Figure 4.2.10 Size distribution ($d \geq 10 \mu\text{m}$) of the effluent (CSDLAC) after coagulation with a magnetic stirrer at 57 mg/l for 25 min , measured by holographic technique

4.2.3 Run 3—Digested primary sludge (CSDOC), plume mixing

The coagulation process used in Run 3 followed the calculations based on the buoyant jet equations with the input variables chosen approximately to correspond to a possible future deep sludge outfall for the Orange County (Figure 3.1.1 and 3.1.9). Coagulation was allowed to happen under the controlled condition in the coagulating reactor. The mixing scenario lasted for 6 min and 20 sec . To study the effect of the coagulation on the particle size distribution, a set of samples were taken from the reactor at intervals during the coagulating process ($t = 0''$, $20''$,

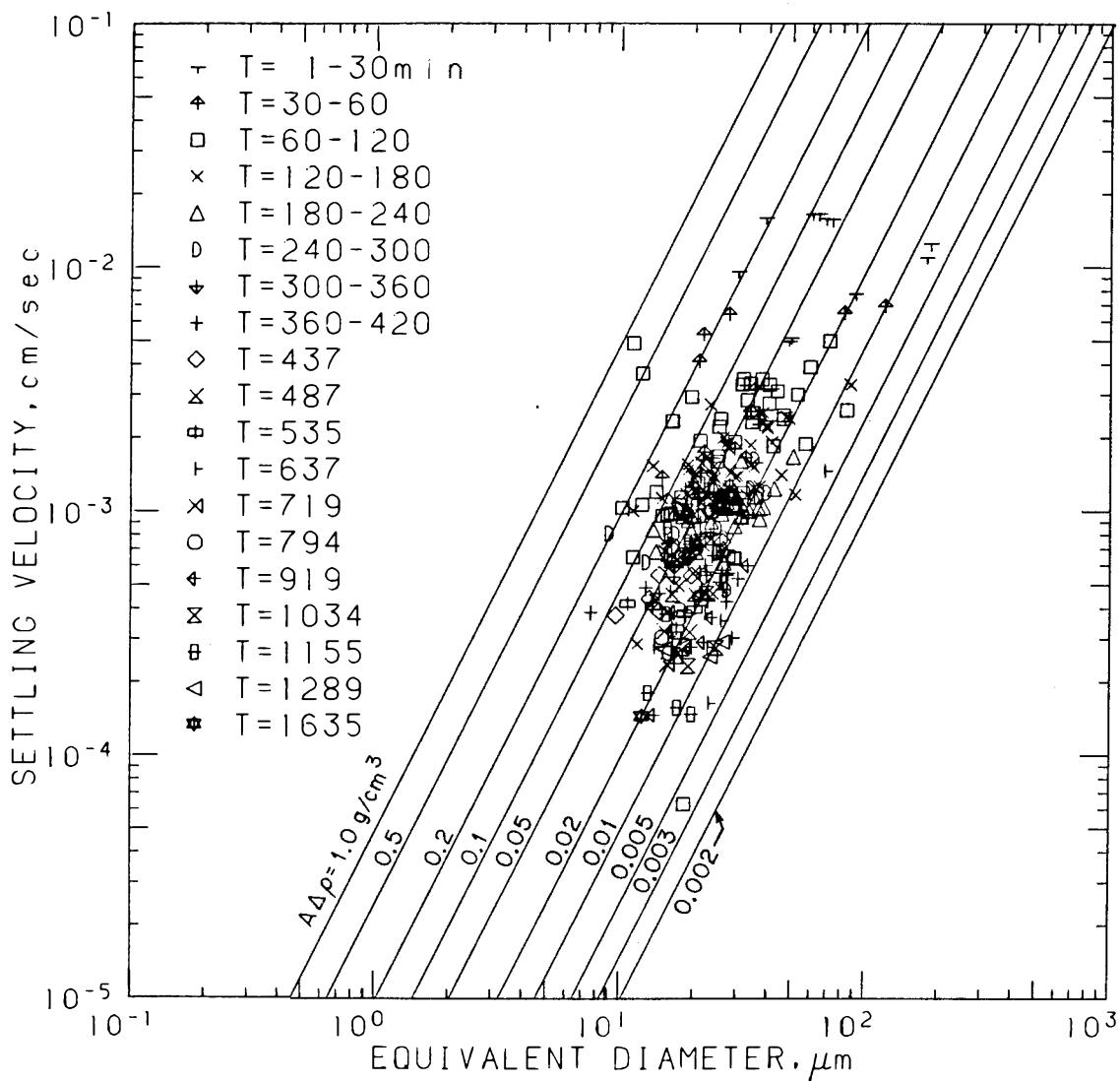


Figure 4.2.11 Settling velocity versus equivalent diameter for the effluent (CSD-LAC) measured in seawater after coagulation with a magnetic stirrer at 57 mg/l for 25 min

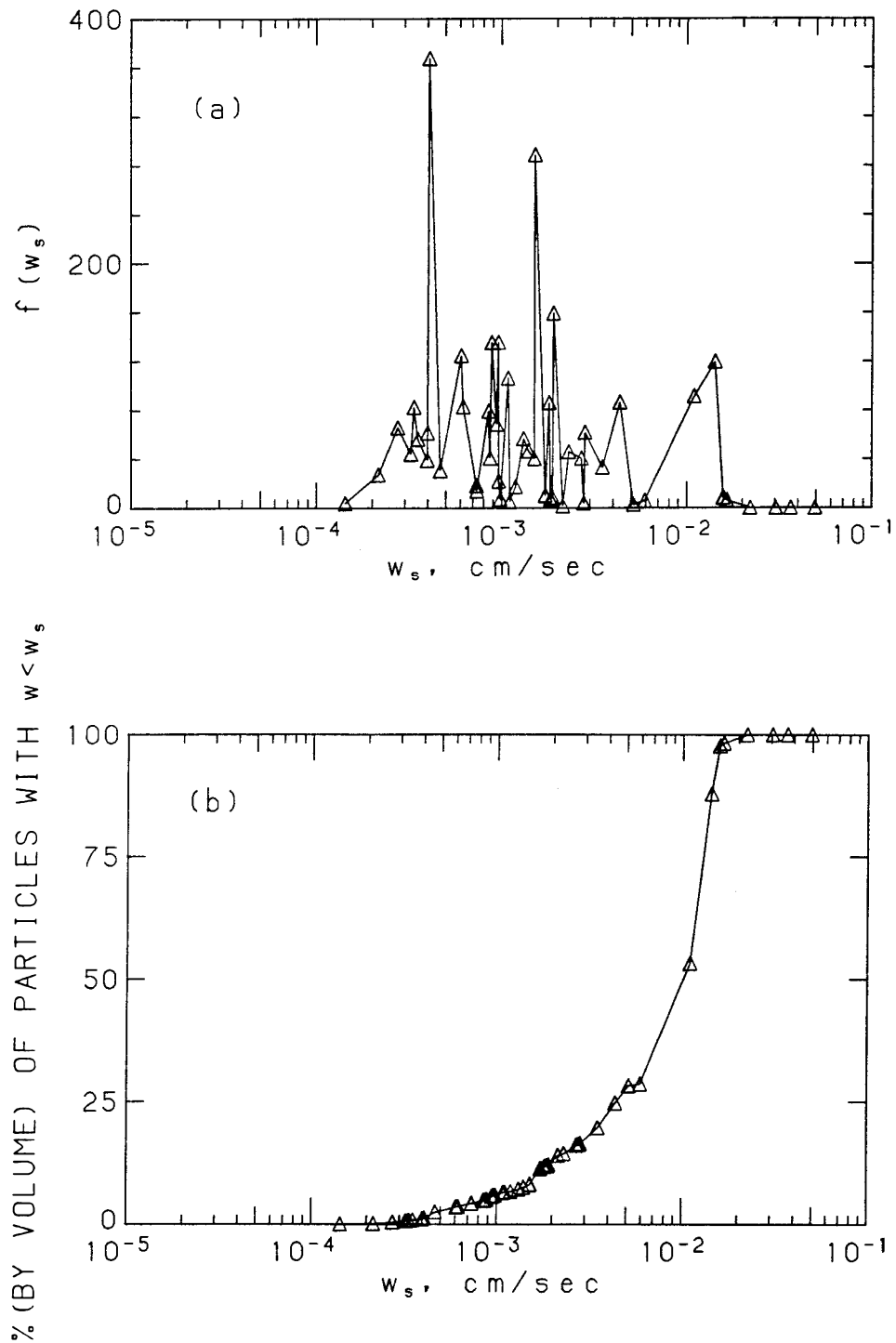


Figure 4.2.12 Settling velocity distribution ($d \geq 10\mu m$) of the effluent (CSDLAC) measured in seawater after coagulation with a magnetic stirrer at 57 mg/l for 25 min , derived from the settling measurement alone: (a) density distribution, (b) cumulative distribution

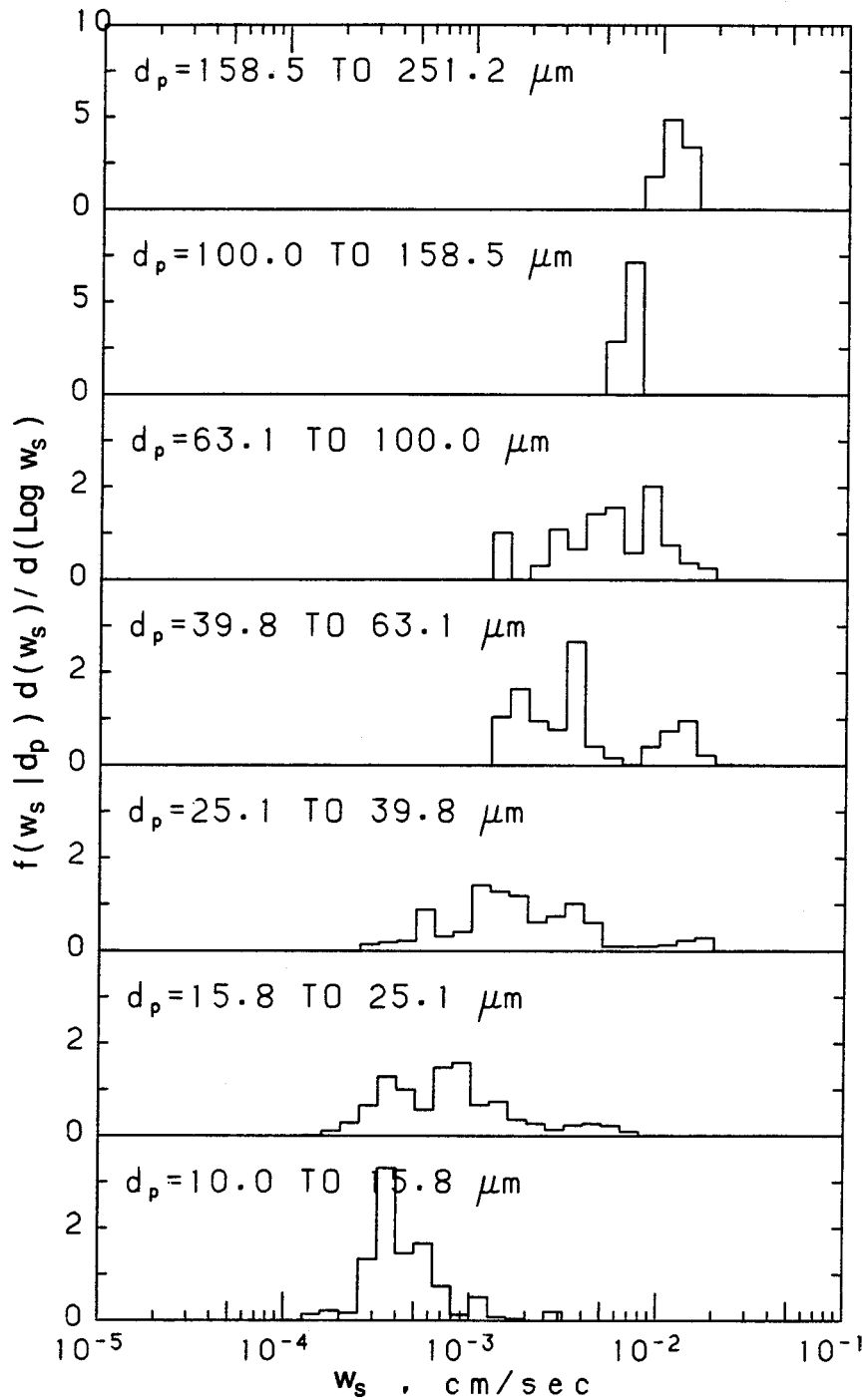


Figure 4.2.13 Conditional settling velocity distribution ($d \geq 10\mu\text{m}$) of the effluent (CSDLAC) measured in seawater after coagulation with a magnetic stirrer at 57 mg/l for 25 min

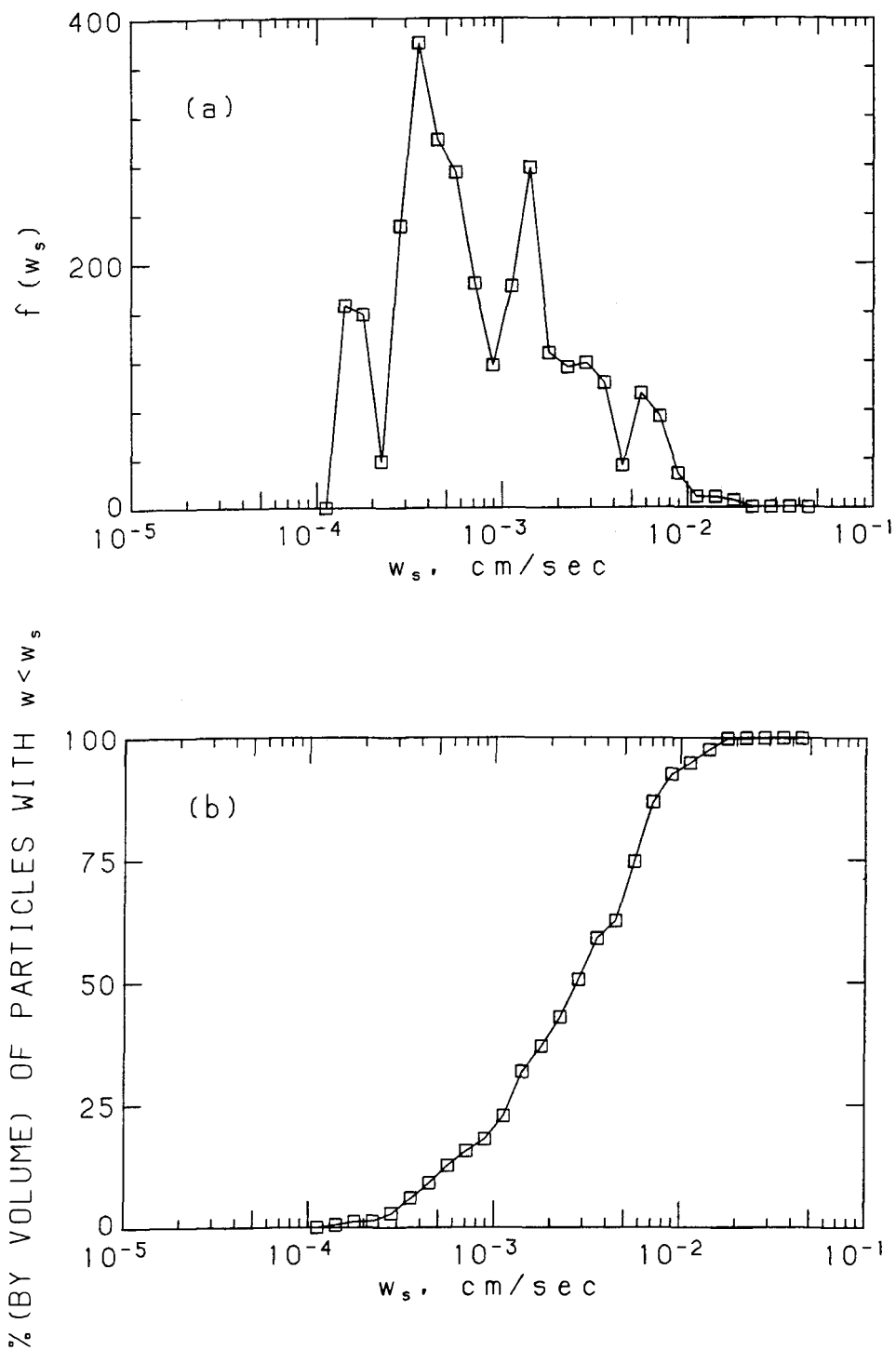


Figure 4.2.14 Settling velocity distribution ($d \geq 10\mu m$) of the effluent (CSDLAC) measured in seawater after coagulation with a magnetic stirrer at 57 mg/l for 25 min, derived from the measurements of both size and velocity: (a) density distribution, (b) cumulative distribution

1'20", 2'30", 3'50", 5'40", and 6'30"). All samples were diluted immediately to a concentration less than 2 *mg/l* with filtered artificial seawater. These samples were used for settling and filtration measurements. The samples used for size measurements with the holographic technique were prepared by further diluting the 2 *mg/l* samples to a concentration less than 0.5 *mg/l*.

Settling velocity measurements were performed for the samples withdrawn at 0", 20", 1'20", and 5'40". The solutions used to construct the density stratification inside the settling cells at $t = 0''$ were prepared by adding different amounts of sodium chloride to small volumes of deionized distilled water. For the rest of the samples, artificial seawater was used as the basis for preparing the solutions used to produce the stratification inside the settling cells. Since it took at least one week to analyze one set of settling data, only the holograms recorded for the samples withdrawn at 0" and 5'40" were examined.

4.2.3.1 Size distribution

Since the holographic camera system has a resolution limit of 10 μm , gravimetric analysis was used to examine the size change during the plume mixing for particles less than 10 μm . Each sample was filtered separately through five Nuclepore membranes of different pore sizes: 10 μm , 5 μm , 3 μm , 1 μm , and 0.4 μm . The mass collected on the membrane was kept in the range of 0.5 to 1 *mg* to avoid clogging effects while maintaining 90% accuracy in the weighing process.

The mass captured on each filter represents approximately the total mass of particles that are larger than the pore size of the filter. These filtration results were then used to construct the cumulative size distribution based on the mass of the

particles (Figure 4.2.15). Studying the size distributions obtained for samples extracted at different times from the reactor, we concluded that there is no significant size change through the coagulation process within the sampling error and the error range of the filtration technique. For all samples, the particles with diameter larger than $10 \mu m$ comprise about 60% of the total mass.

Seven singly exposed holograms recorded for samples withdrawn at different times during the mixing were analyzed. The examined volume, the number of particles measured, and the approximate dilution ratio are summarized in Table 4.2.2. Figure 4.2.16 shows the size distributions for particles larger than $10 \mu m$. The results, consistent with the filtration data, show very little change in particle size distributions at different times. The median size is around $25 \mu m$ for all samples.

4.2.3.2 Settling velocity distribution at $t = 0''$

For fall velocity analysis of a sample before dilution and mixing ($t = 0''$), 60 holograms were examined and 493 particles were measured. Figure 4.2.17 illustrates the $w - d$ relationship. The fall velocity distribution calculated directly from settling measurements is shown in Figure 4.2.18, which has a 50% velocity of $2.1 \times 10^{-3} \text{ cm/sec}$. The corresponding conditional probability density functions, $f(w_i | d_j)$, are depicted in Figure 4.2.19. The velocity distribution calculated based on Eqn. 4.1.17 is shown in Figure 4.2.20, which gives the 50% velocity as $7.6 \times 10^{-4} \text{ cm/sec}$.

4.2.3.3 Settling velocity distribution at $t = 5'40''$

For settling velocity analysis after the simulated plume dilution and mixing ($t = 5'40''$), 53 holograms were analyzed with 543 particles measured. The same

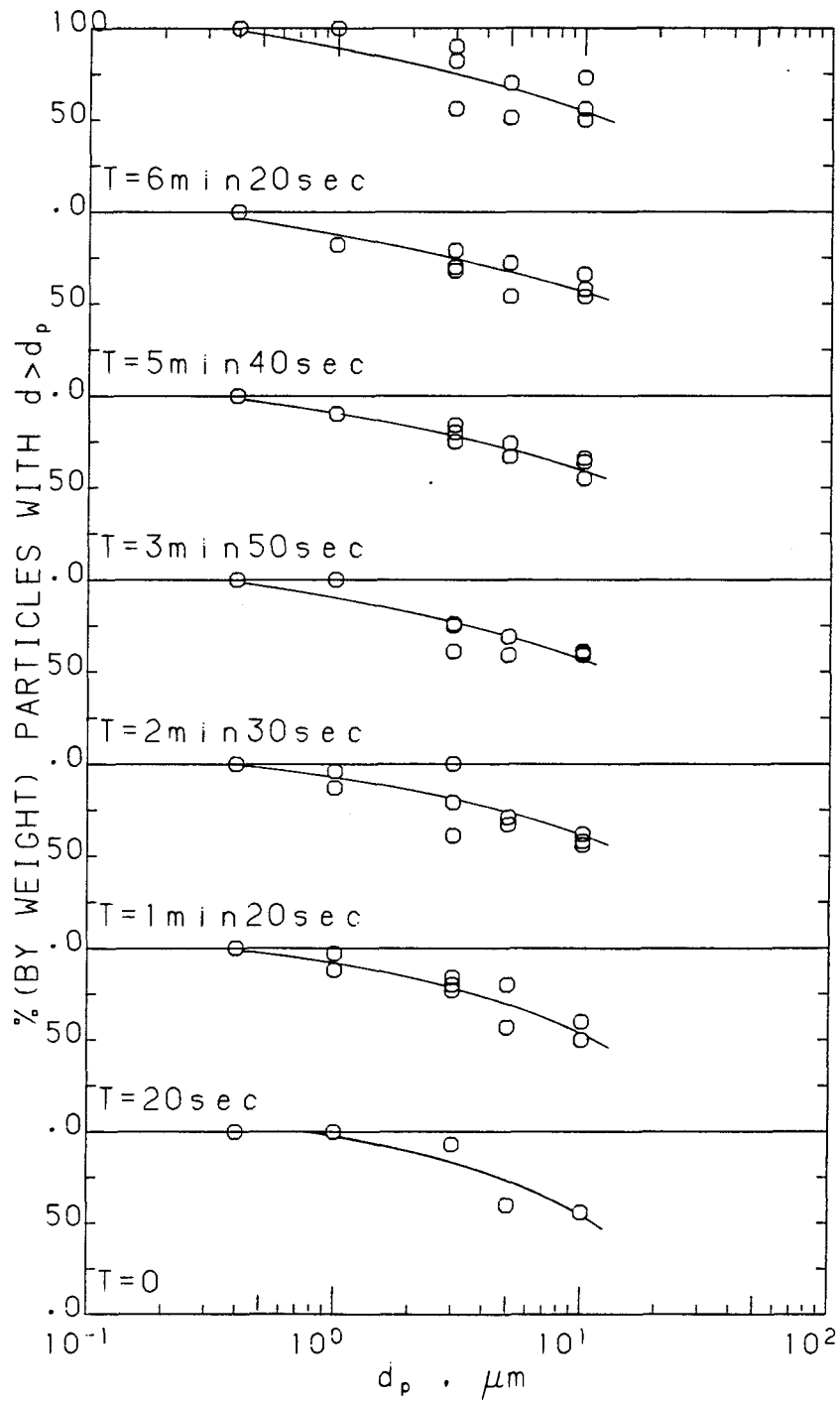


Figure 4.2.15 Size distributions ($d < 10 \mu m$) of the D.P.S.(CSDOC) at different times of plume mixing, measured by gravimetric technique

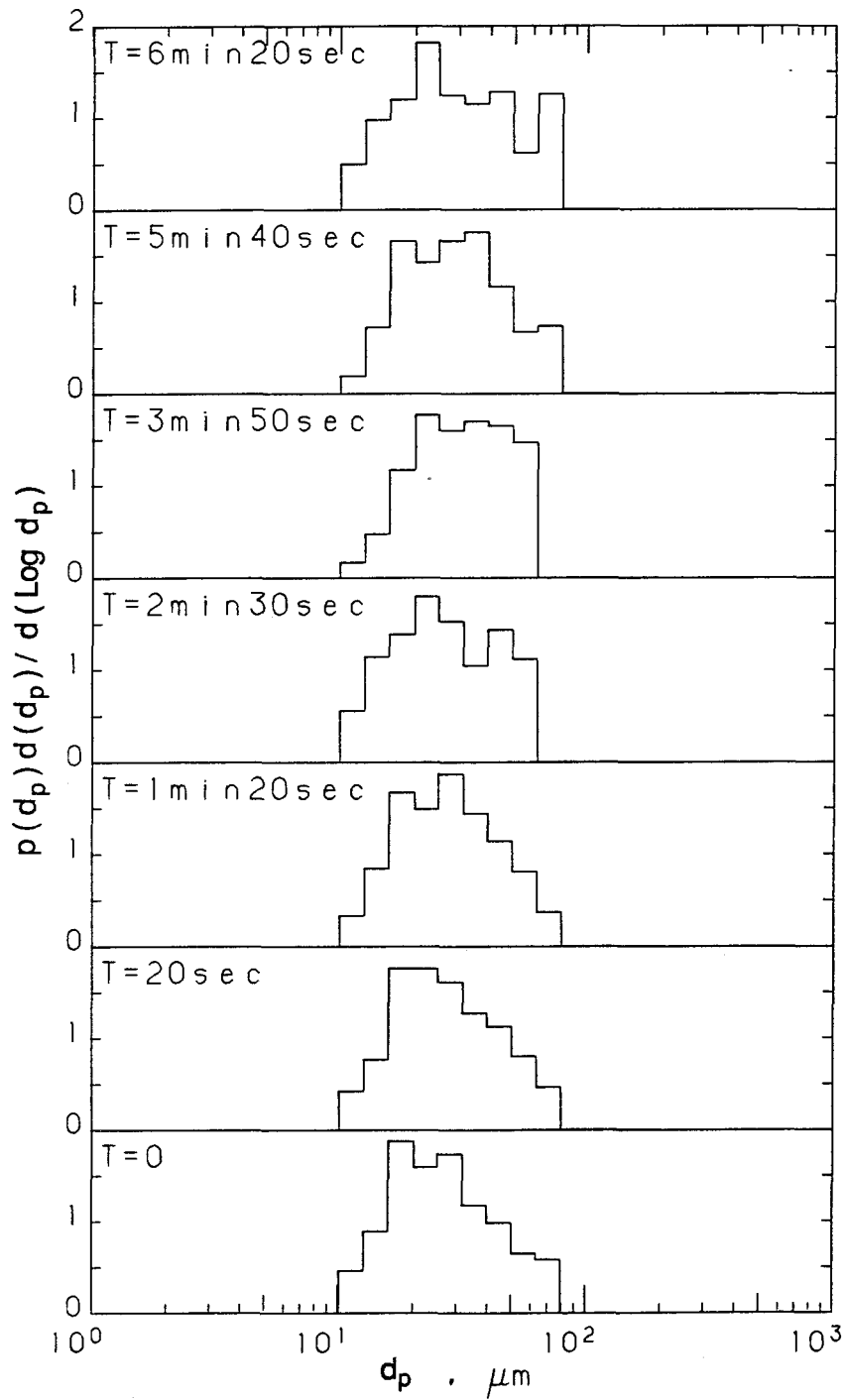


Figure 4.2.16 Size distributions ($d \geq 10 \mu\text{m}$) of the D.P.S.(CSDOC) at different times of plume mixing, measured by the holographic technique

Table 4.2.2 Summary of the number of particles and sample volume measured for the hologram recorded for each sample taken at different times during plume mixing experiment of the D.P.S. (CSDOC).

time	$10 \mu m \leq d \leq 20 \mu m$		$20 \mu m \leq d \leq 30 \mu m$		$d \geq 30 \mu m$		dilution ratio
	N	V (cm^3)	N	V (cm^3)	N	V (cm^3)	
0	133	0.281	185	1.537	92	4.390	1.2×10^5
20''	124	0.225	168	1.082	99	3.258	1.0×10^5
1'20''	124	0.263	154	1.073	94	3.239	1.0×10^5
2'30''	127	0.298	161	1.627	81	4.449	1.3×10^5
3'50''	94	0.285	146	0.928	99	2.381	6.2×10^4
5'40''	119	0.241	221	1.458	64	2.340	1.0×10^5
6'30''	137	0.350	159	1.576	82	4.138	1.3×10^5

procedures as in Sec. 4.2.3.2 were repeated to obtain different settling curves. Figure 4.2.21 shows the $w - d$ relationship, which is very similar to that observed at $t = 0''$. Fall velocity distribution from the settling experiment alone is shown in Figure 4.2.22, which gives a 50% velocity of $2 \times 10^{-3} \text{ cm/sec}$. The conditional fall velocity distributions are plotted in Figure 4.2.23. Together with the size distribution at 5'40'', we obtained the velocity distribution as in Figure 4.2.24, which shows a 50% velocity as $1 \times 10^{-3} \text{ cm/sec}$.

4.2.4 Run 4—Effluent (CSDLAC), plume mixing

The purpose of Run 4 was to simulate the ocean discharge process of the existing 120-in diameter effluent outfall of Los Angeles County by controlling the dilution and the mixing intensity inside the coagulating reactor (Figure 3.1.2). The solids concentration of the mixed effluent was only 58 mg/l; to provide enough particles for gravimetric and holographic measurements, the dilution ratio was slightly decreased and stopped at 100 after 190 sec (Figure 4.2.25). The solid line in Figure

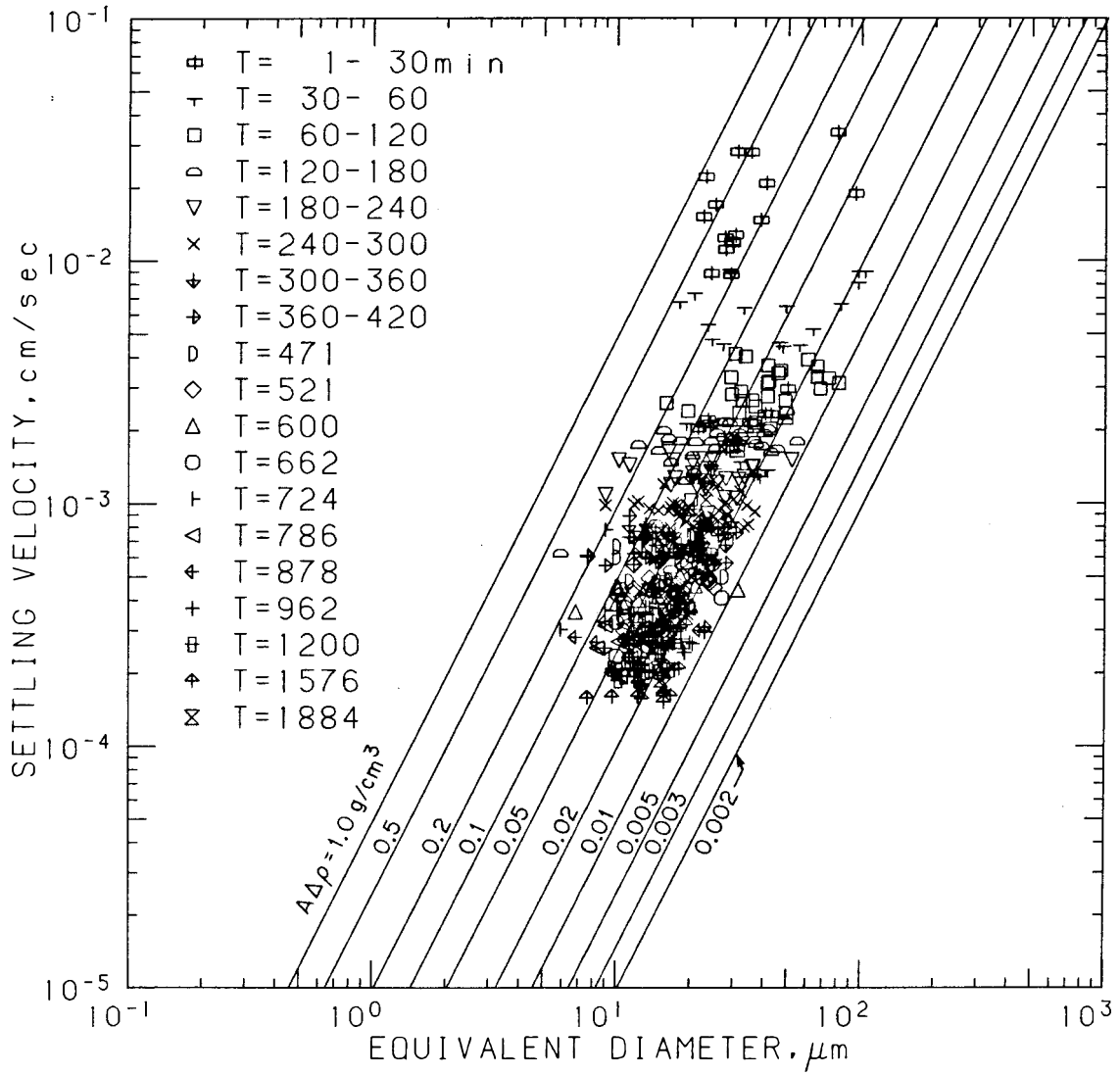


Figure 4.2.17 Settling velocity versus equivalent diameter for the D.P.S (CSDOC) measured in fresh water at $t = 0''$

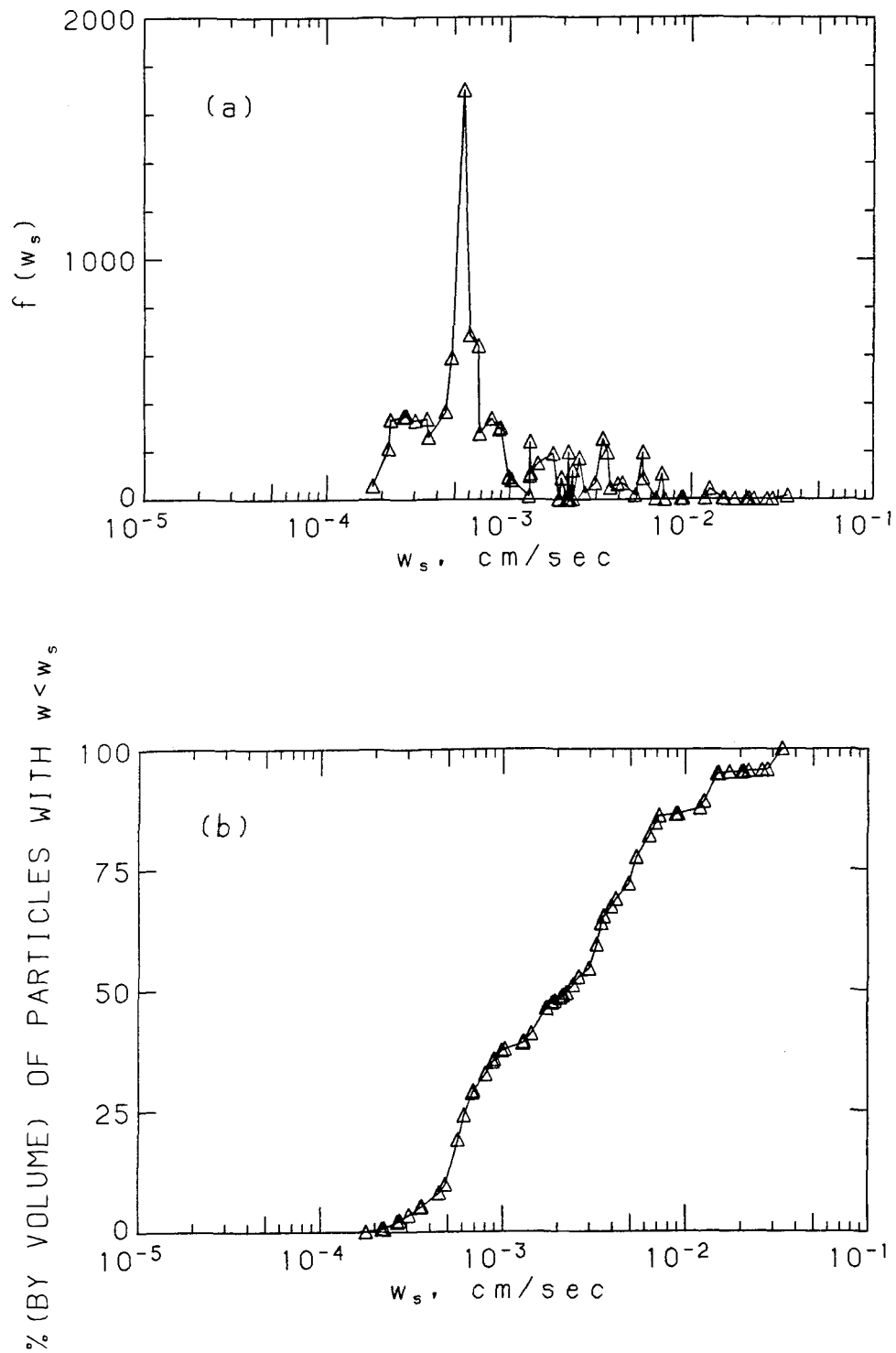


Figure 4.2.18 Settling velocity distribution ($d \geq 10 \mu m$) of the D.P.S. (CSDOC) measured in fresh water at $t = 0''$, derived from the settling measurement alone: (a) density distribution, (b) cumulative distribution

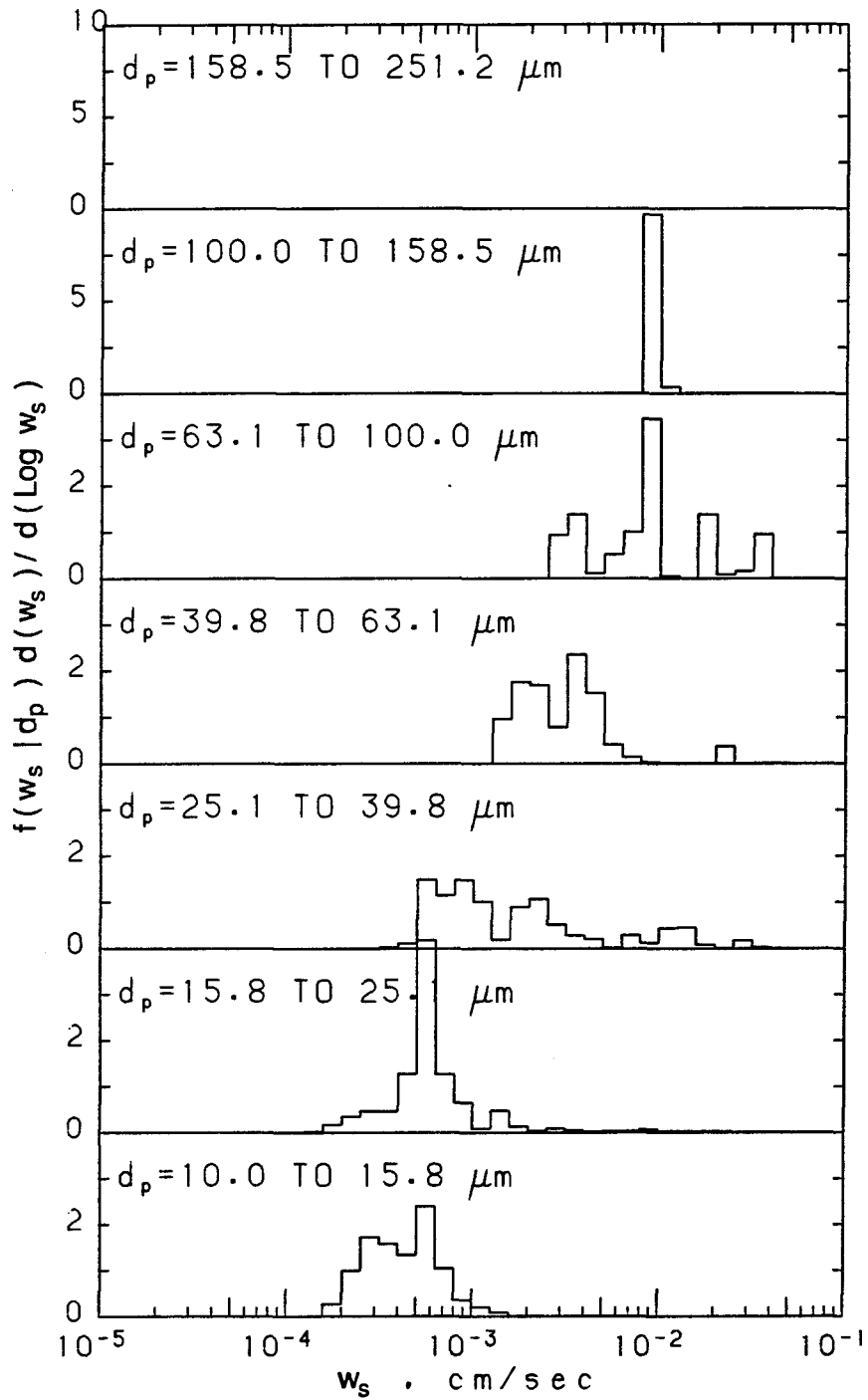


Figure 4.2.19 Conditional settling velocity distribution ($d \geq 10\mu\text{m}$) of the D.P.S. (CSDOC) measured in fresh water at $t = 0''$

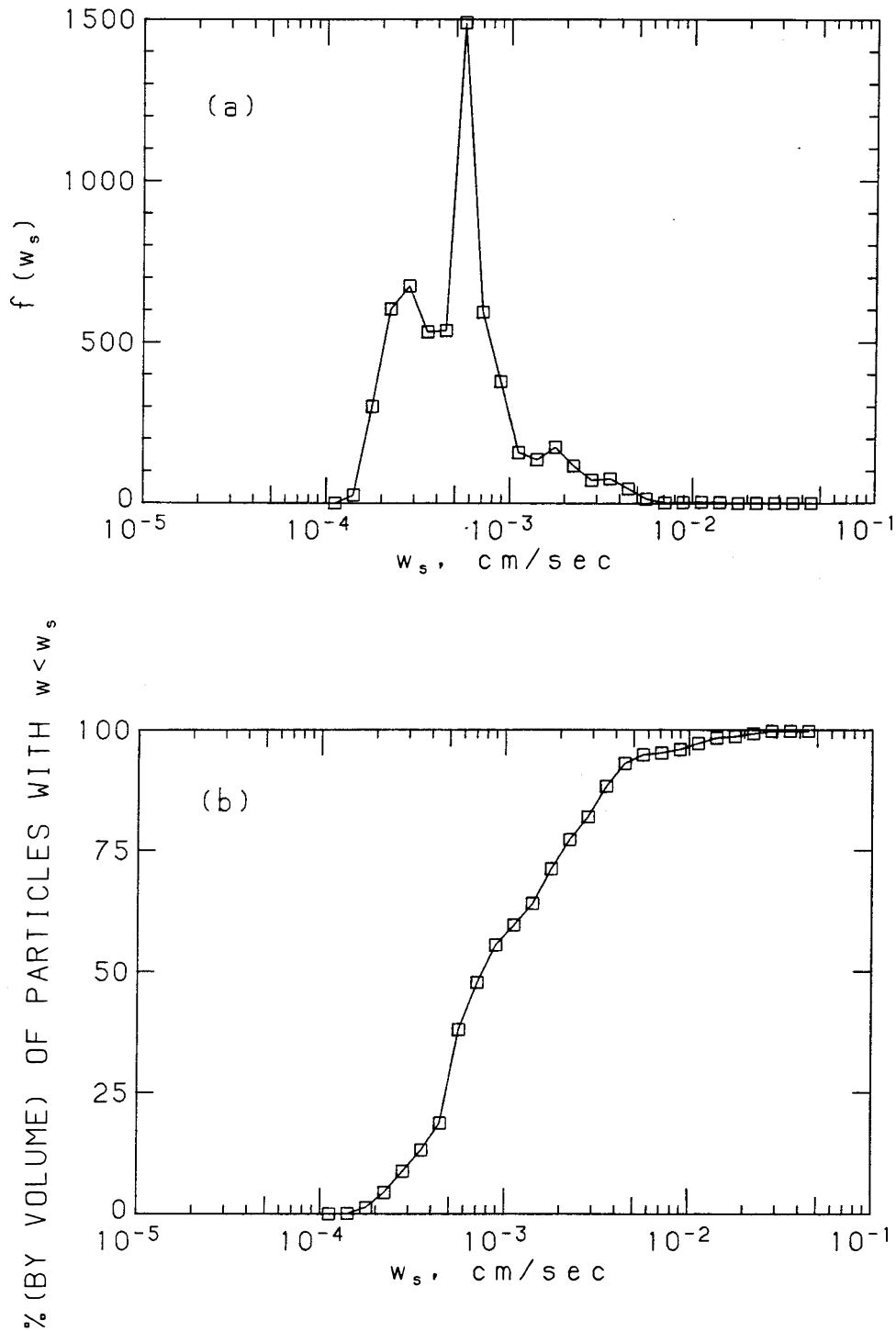


Figure 4.2.20 Settling velocity distribution ($d \geq 10\mu m$) of the D.P.S. (CSDOC) measured in fresh water at $t = 0''$, derived from the measurements of both size and velocity: (a) density distribution, (b) cumulative distribution

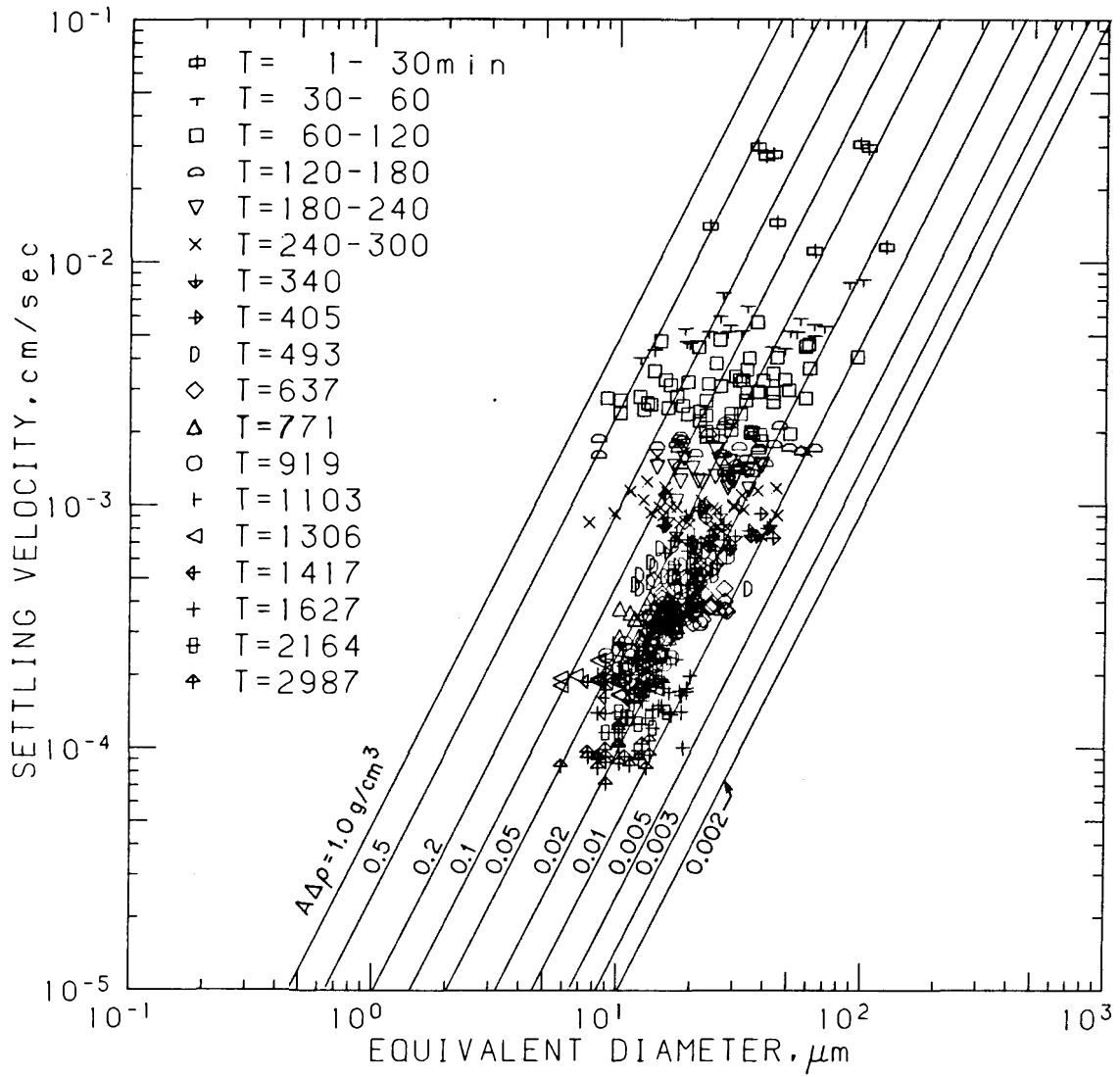


Figure 4.2.21 Settling velocity versus equivalent diameter for the D.P.S (CSDOC) measured in seawater at $t = 5'40''$

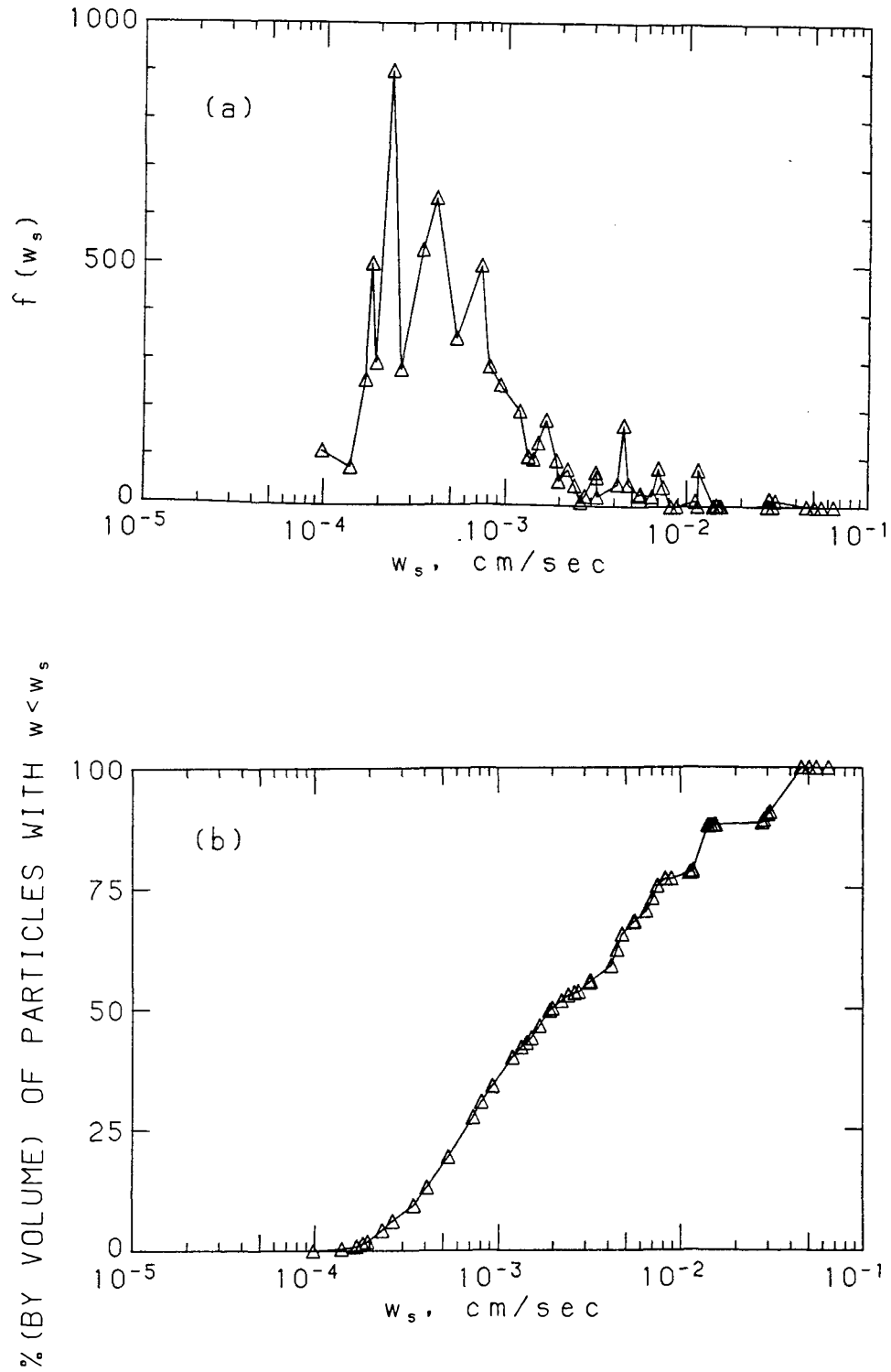


Figure 4.2.22 Settling velocity distribution ($d \geq 10\mu m$) of the D.P.S. (CSDOC) measured in seawater at $t = 5'40''$, derived from the settling measurement alone: (a) density distribution, (b) cumulative distribution

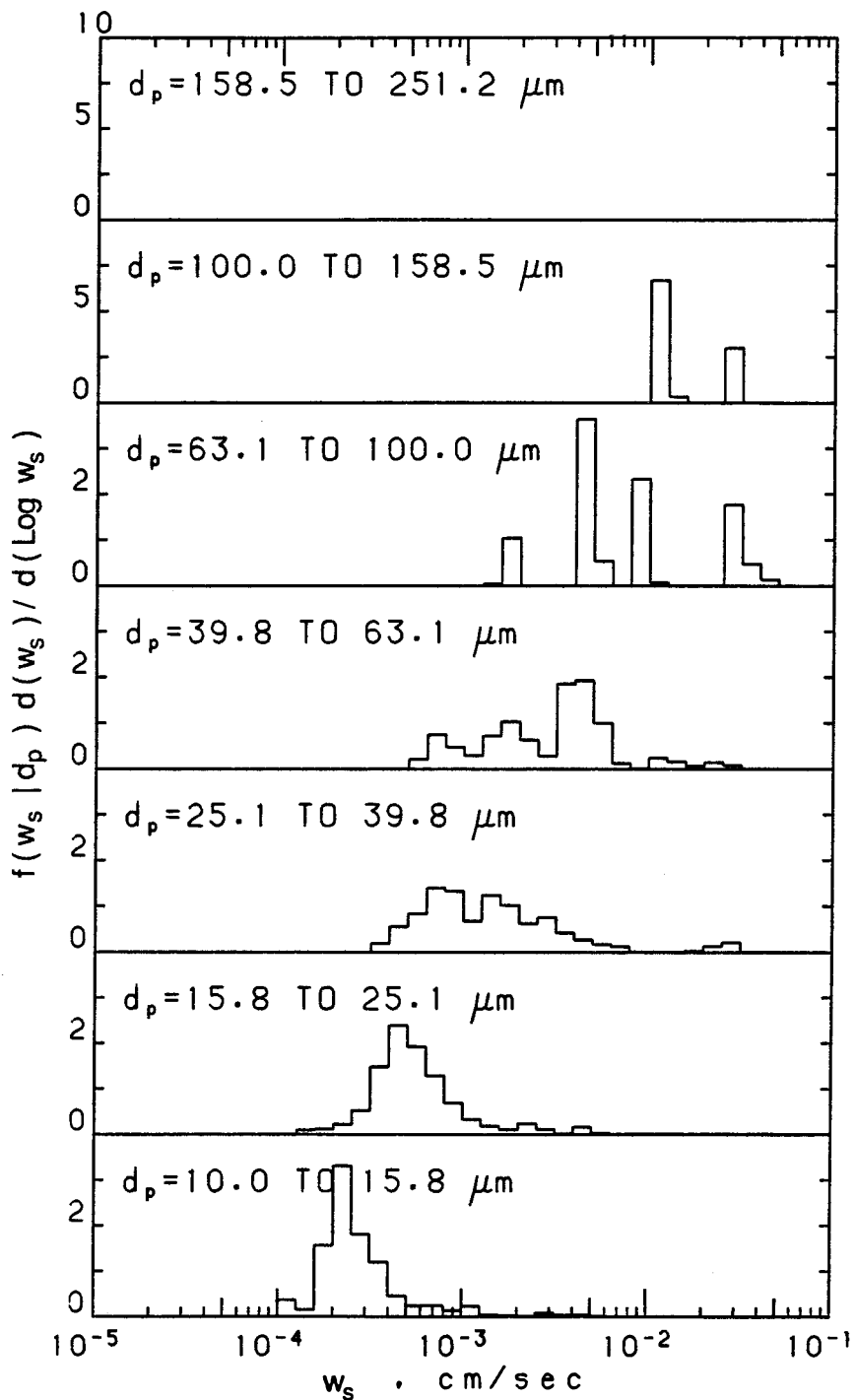


Figure 4.2.23 Conditional settling velocity distribution ($d \geq 10\mu\text{m}$) of the D.P.S. (CSDOC) measured in seawater at $t = 5'40''$

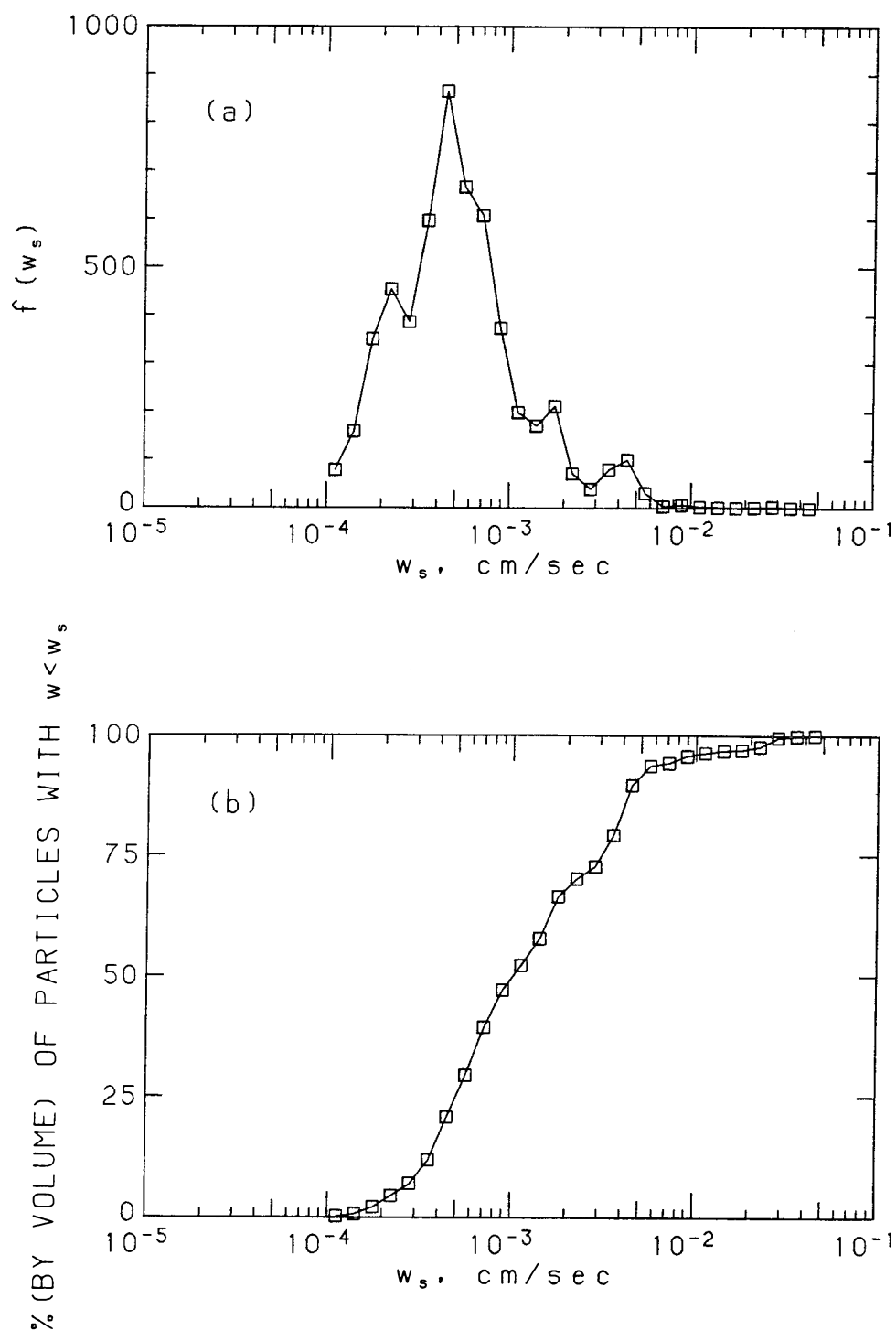


Figure 4.2.24 Settling velocity distribution ($d \geq 10\mu m$) of the D.P.S. (CSDOC) measured in seawater at $t = 5'40''$, derived from the measurements of both size and velocity: (a) density distribution, (b) cumulative distribution

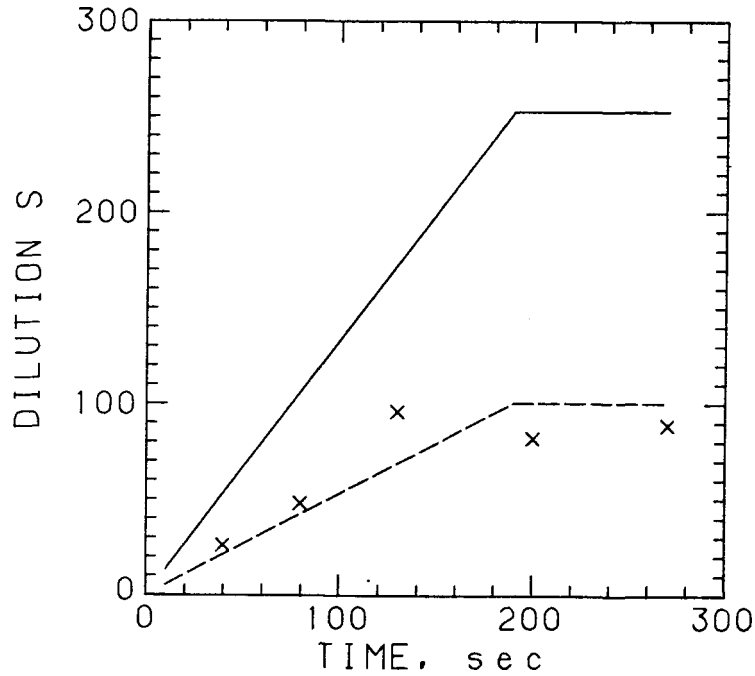


Figure 4.2.25 Revised dilution history of the plume mixing experiment for the effluent (CSDLAC): original design (—), revised design (- - -), and experiment measurements(x)

4.2.25 shows the original dilution schedule, the dash line the revised dilution schedule, and the crosses the experimental measurements. The stirring rate still followed the designed value, and the coagulating experiment lasted for 4 min 30 sec.

Six samples were withdrawn from the reactor at $t = 0''$, $40''$, $1'20''$, $2'10''$, $3'20''$, and $4'30''$. Dilutions measured for these samples are shown in Figure 4.2.25. These samples were analyzed for size distributions using both the holographic and filtration techniques. Settling velocity measurements were performed for the samples withdrawn at $0''$, $2'10''$, and $4'30''$. These settling tests were conducted only for a duration of 8 hr in the settling cell (48 hr in previous runs) in order to minimize the storage time, hence, the possible deterioration of other samples waiting to be tested. The measurable velocity range was then reduced to the range of 5×10^{-4}

to 0.05 cm/sec . Based on the previous settling velocity measurements, the volume fraction of the particles larger than $10 \mu\text{m}$ but with fall velocity from 1×10^{-4} to $5 \times 10^{-4} \text{ cm/sec}$ ranges from 2 to 15%. These particles were not measured in this experiment. Due to limited time, only the holograms recorded for the 4'30" sample were analyzed.

4.2.4.1 Size distribution

Since the solids concentrations of the effluent samples were too low to provide enough volume for multiple filtration processes with membranes of different pore sizes as described in Sec. 4.2.3.1, only $0.4 \mu\text{m}$ and $10 \mu\text{m}$ membranes were used here. The filtration results, which gave the percentage by weight of particles larger than $10 \mu\text{m}$, showed insignificant changes among samples taken at different times—about 20% solids by weight were larger than $10 \mu\text{m}$ for all samples.

Table 4.2.3 summarizes the volume examined, the number of particles measured, and the approximate dilution ratio for all the holograms analyzed. Figure 4.2.26 illustrates the size distributions based on particle volume for particles larger than $10 \mu\text{m}$ at different times. Again, no significant change in size distributions was observed. The median diameter ranges from 26 to $28 \mu\text{m}$.

4.2.4.2 Settling velocity distribution at $t = 4'30''$

For the settling experiment of the sample withdrawn at $t = 4'30''$, 59 holograms were analyzed and 97 particles were measured. The $w - d$ relationship as shown in Figure 4.2.27 is similar to those obtained in Runs 1, 2 and 3. If we assume that particles with velocity smaller than $5 \times 10^{-4} \text{ cm/sec}$ can be neglected, the velocity distributions for particles larger than $10 \mu\text{m}$ and the velocity distributions

Table 4.2.3 Summary of the number of particles and sample volume measured for the hologram recorded for each sample taken at different times during plume mixing experiment of the effluent (CSDLAC).

time	$10 \mu m \leq d \leq 20 \mu m$		$20 \mu m \leq d \leq 30 \mu m$		$d \geq 30 \mu m$		dilution ratio
	N	V (cm^3)	N	V (cm^3)	N	V (cm^3)	
0''	150	0.669	165	3.249	37	10.287	200
40''	239	0.759	149	2.667	35	6.373	130
1'20''	309	0.446	145	1.115	108	3.209	48
2'10''	145	0.233	140	1.339	77	4.115	57
2'10''	150	0.233	177	1.872	74	3.518	57
2'10''	162	0.233	170	1.287	83	3.331	57
3'20''	250	0.714	145	2.008	75	5.107	108
4'30''	150	0.268	164	1.607	90	4.341	86

for different size ranges are shown in Figures 4.2.28 and 4.2.29 respectively. Figure 4.2.28 shows the 50% velocity of $1.2 \times 10^{-3} \text{ cm/sec}$. The fall velocity distribution derived from both size and velocity measurements is presented in Figure 4.2.30, which shows the 50% velocity of $1 \times 10^{-3} \text{ cm/sec}$.

4.3 Summary

In summary, four sets of coagulating and settling experiments were performed using the digested primary sludge from CSDOC and the effluent from CSDLAC. Simple mixing with a magnetic stirrer was used for particle coagulation in the first two runs. Plume mixing, which was simulated inside a laboratory scale reactor, was used for the other two runs. These experiments illustrated the procedures for measuring the size distributions and the settling velocity distributions of effluent and sludge samples using the in-line holographic camera and the associated analysis system developed in this research.

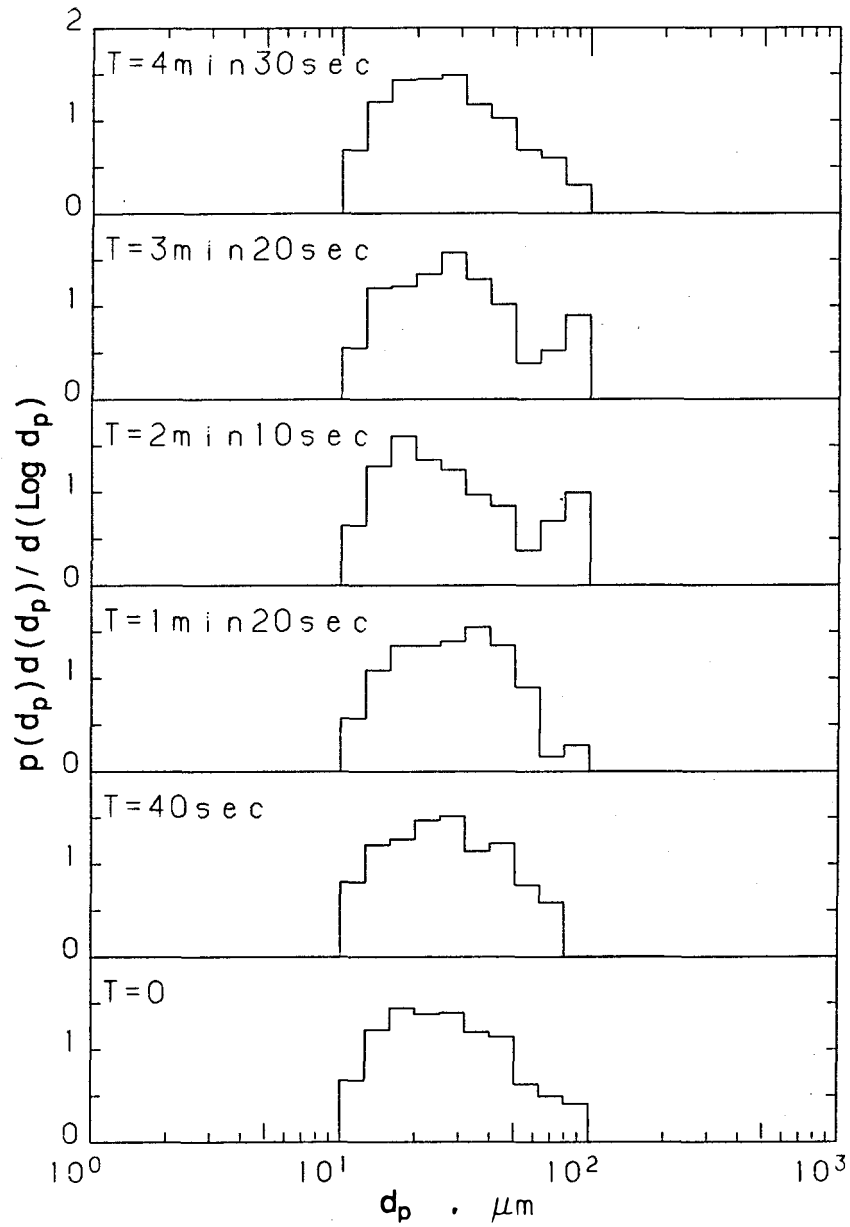


Figure 4.2.26 Size distributions ($d \geq 10 \mu\text{m}$) of the effluent (CSDLAC) at different times of plume mixing, measured by holographic technique

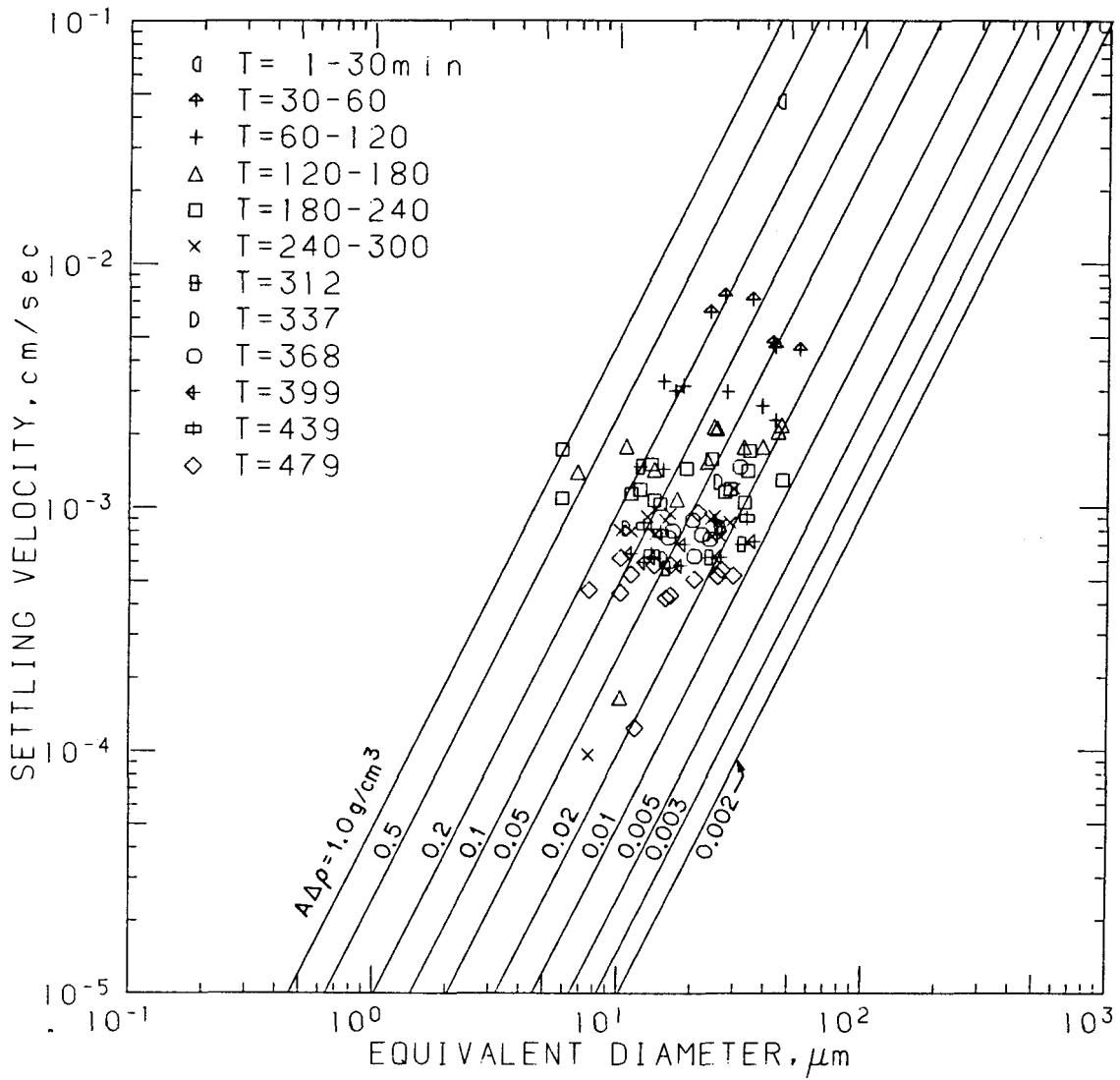


Figure 4.2.27 Settling velocity versus equivalent diameter for the effluent (CSD-LAC) measured in fresh water at $t = 4'30''$

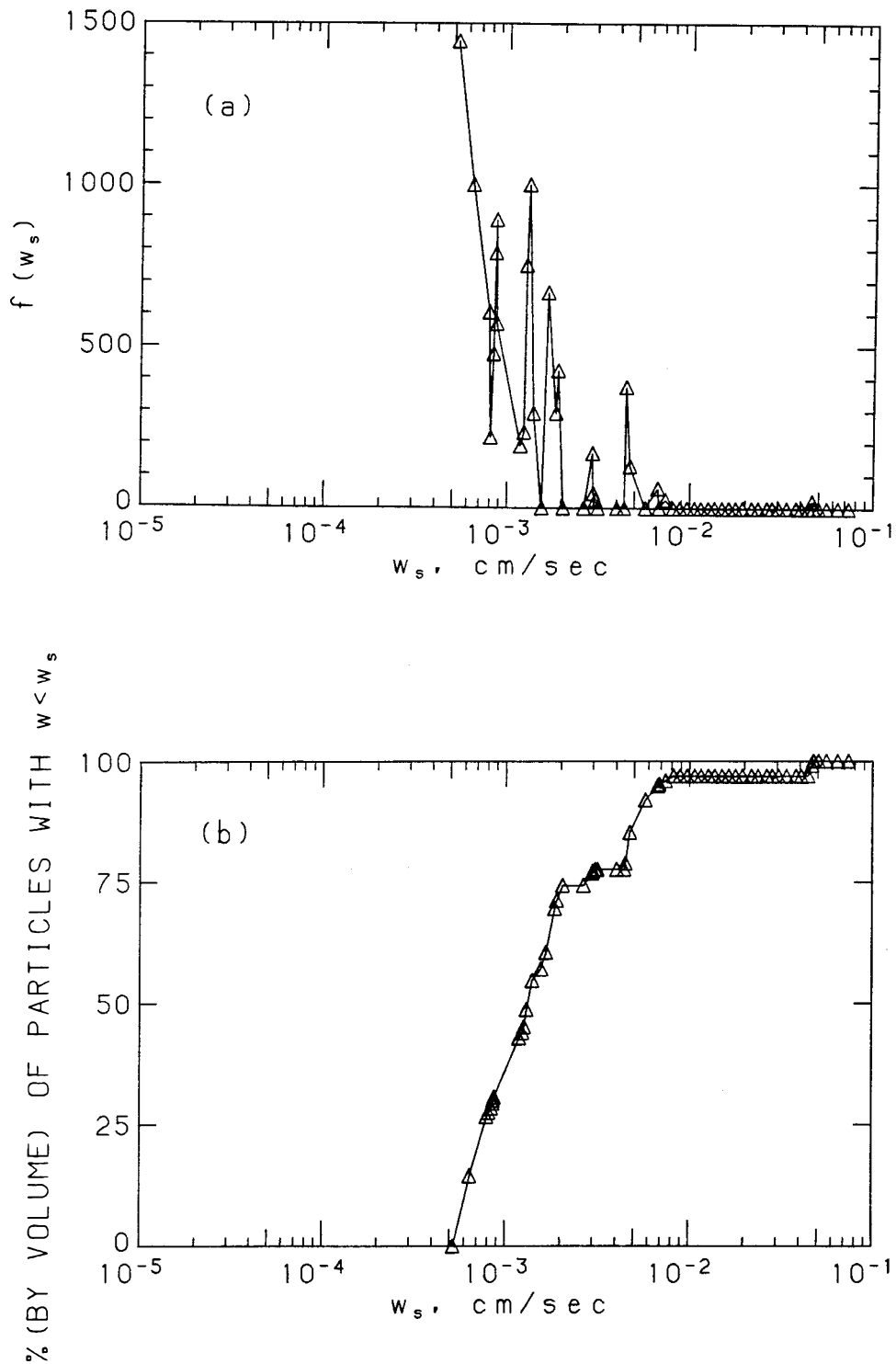


Figure 4.2.28 Settling velocity distribution ($d \geq 10\mu m$) of the effluent (CSDLAC) measured in fresh water at $t = 4'30''$, derived from the settling measurement alone: (a) density distribution, (b) cumulative distribution

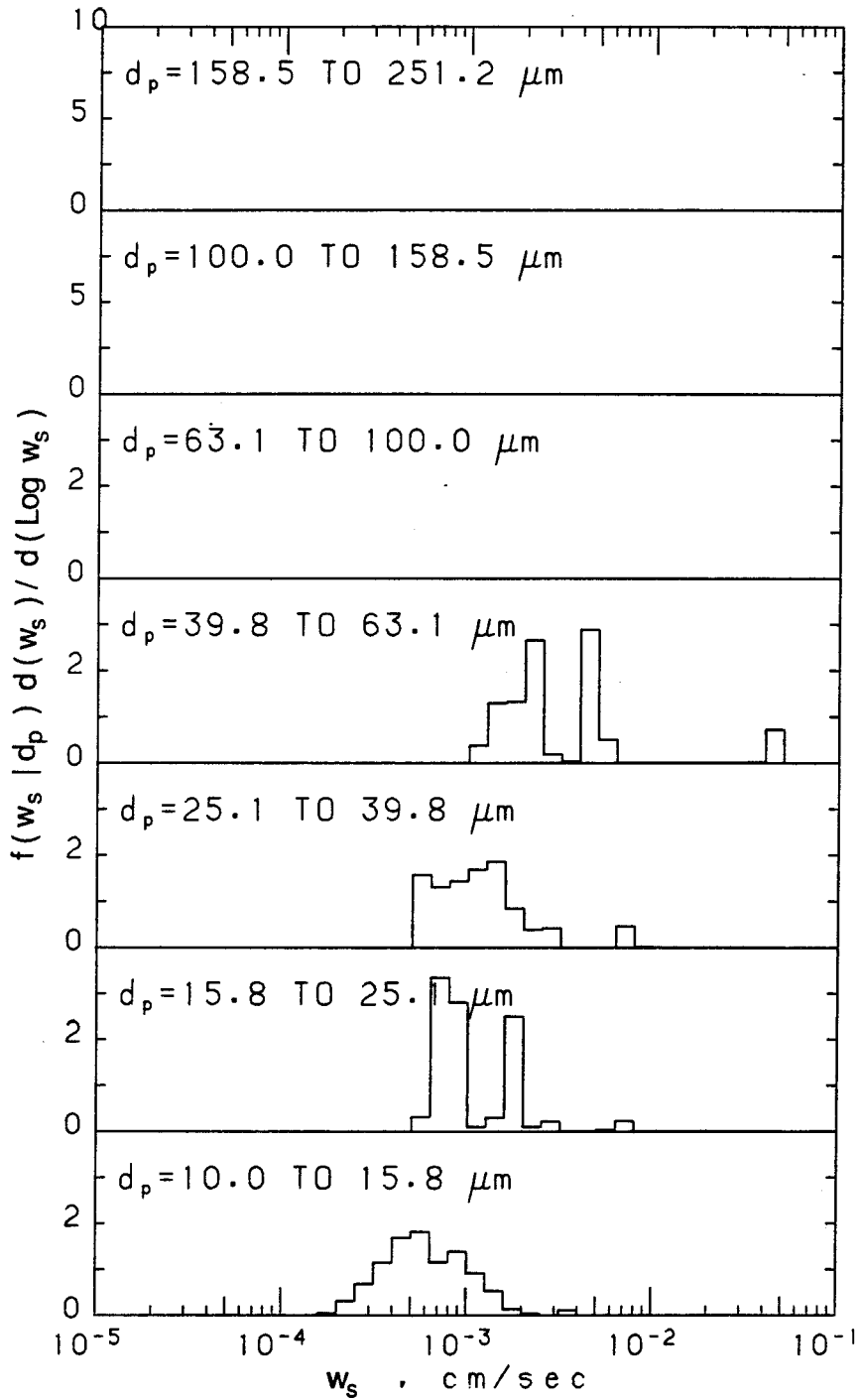


Figure 4.2.29 Conditional settling velocity distribution ($d \geq 10\mu\text{m}$) of the effluent (CSDLAC) measured in fresh water at $t = 4'30''$

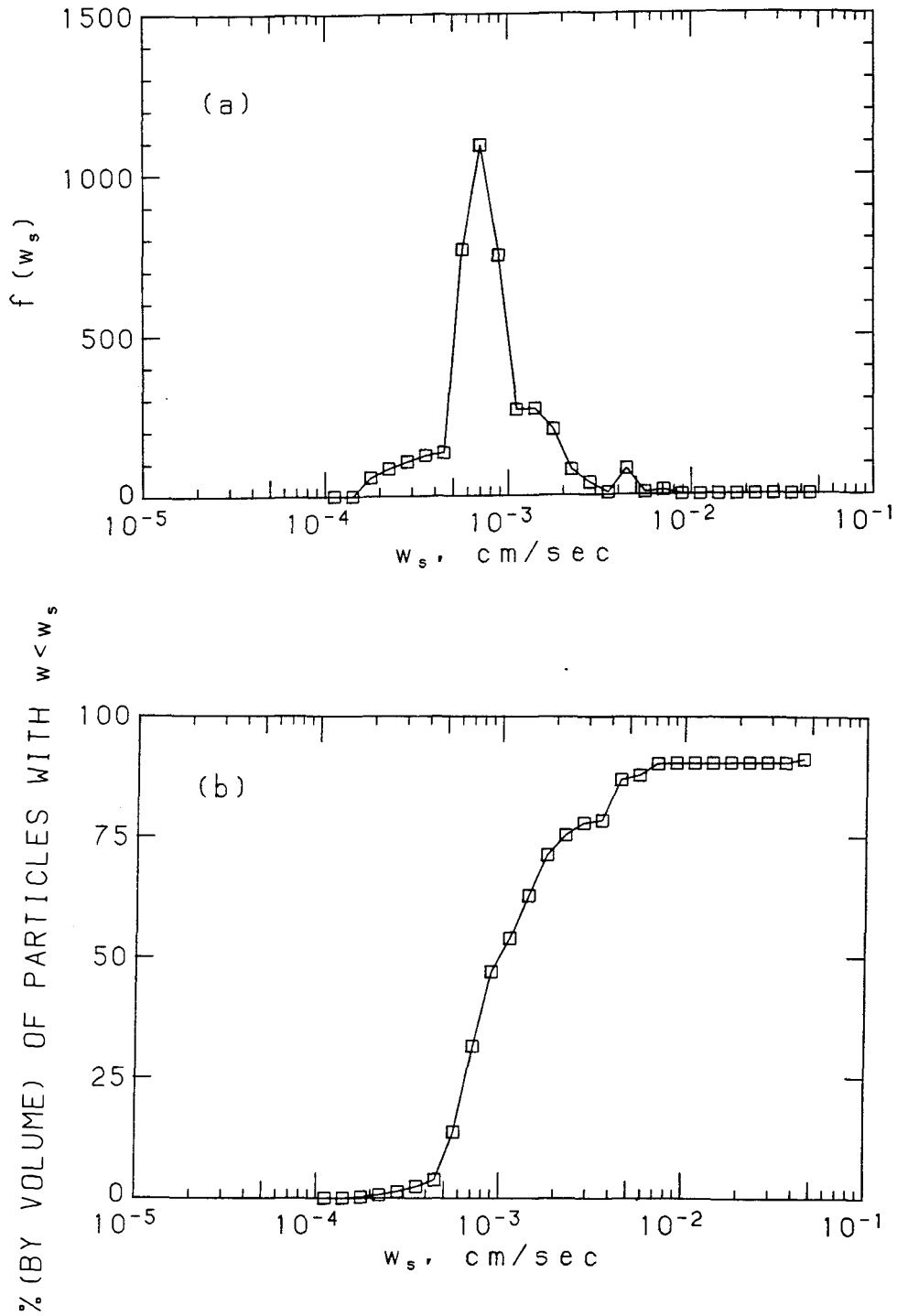


Figure 4.2.30 Settling velocity distribution ($d \geq 10\mu m$) of the effluent (CSDLAC) measured in fresh water at $t = 4'30''$, derived from the measurements of both size and velocity: (a) density distribution, (b) cumulative distribution

For size measurements with the holographic technique, equal-area diameter was used as the equivalent diameter for particle classification. Currently, the smallest equivalent diameter that can be analyzed using this holographic camera system is $10 \mu m$. Particles that are smaller than $10 \mu m$ have very small fall velocity ($\leq 1 \times 10^{-4} \text{ cm/sec}$). Hence, settling is no longer the controlling process in determining the fate of these particles. In order to determine the mass concentration of these unmeasured particles for proper interpretation of the measured fall velocity distribution of the particles, samples were filtered through $10 \mu m$ Nuclepore membranes.

It is concluded from our experimental results that there are no significant changes in the size distributions observed at different times during the simulated plume mixing. For the the digested primary sludge from CSDOC, the mass fraction of the particles larger than $10 \mu m$ remains roughly as 60 %, and the median diameter of these particles is around $25 \mu m$. For the effluent from CSDLAC, particles with diameter larger than $10 \mu m$ have a mass fraction of only 20 % and a median diameter of $27 \mu m$ through out the whole coagulation experiment. However, coagulation did modify the size distributions of the particles larger than $10 \mu m$ in the simple mixing cases (mixed with a magnetic stirrer at constant dilution for 20 min). The median diameter was increased to between 50 to $63 \mu m$ for both the digested primary sludge and the effluent.

The settling velocity analysis provides a measurable range of velocity from 1×10^{-4} to $5 \times 10^{-2} \text{ cm/sec}$. From the experimental observations, few particles with diameter *smaller* than $10 \mu m$ have fall velocity *faster* than $1 \times 10^{-4} \text{ cm/sec}$, and conversely practically no particles *larger* than $10 \mu m$ have fall velocity *smaller* than $1 \times 10^{-4} \text{ cm/sec}$; therefore, the lower limits of size measurement ($10 \mu m$) and

velocity measurement (10^{-4} *cm/sec*) are roughly equivalent for sewage and effluent particles.

The $w - d$ relationships are very similar among all the sewage and sludge particles that have been tested. Stokes' law is approximately confirmed by our observations—settling velocity increases with the square of the equivalent diameter, but we lack a direct measure of the effective particle density. Due to density or shape variations, fall velocities scatter over a factor of 50 for a single equivalent diameter.

Settling velocity distributions of particles larger than $10 \mu m$ can be derived from the settling measurement alone, or from the separate measurements of particle size and settling velocity. The latter procedure removes sampling biases, and is believed to be more accurate. The results are discussed in detail in the next chapter. The fall velocity distribution based only on the settling measurement always resulted in higher fall velocities than that derived from the measurements of both size and velocity. It may be because of sampling biases. Also, since holograms for measuring size distributions were recorded immediately after the samples were withdrawn from the reactor, while holograms for settling velocity measurements were recorded much later, the increase in fall velocity may be a result of the increase of particle size during the storage of samples before settling analysis.

5. DISCUSSION

In this chapter, the accuracy of various measurements, the limitations of the experimental technique, and the assumptions used in data analysis are discussed. Experimental results on particle coagulation and settling velocity analysis are discussed in detail and compared with other available data.

5.1 Limitations of the Experimental Technique

Several factors that may affect the applicability of the measuring technique such as the simplified assumptions used in data analysis, measurement errors, sampling errors are identified and discussed in the following sections.

5.1.1 Definition of the equivalent diameter

Scanning electron micrographs of sewage and sludge particles show that these particles do not have dense structures, but are loosely packed with many void spaces filled with water (Figure 5.1.1). The composition of sewage particles is also very complicated and heterogeneous. Furthermore, sewage particles do not have a well-defined edge and shape. They are basically irregular agglomerates of different kinds of solid substances in the sewage. All of these factors make it difficult to define

the size of particles during the size analysis. Moreover, the in-line holographic technique can be used only to observe the images of particles on the planes that are perpendicular to the optical axis of the illuminating light. The thickness of particles, i.e., the dimension of particles parallel to the optical axis, cannot be measured using the in-line holographic technique.

To provide a basis for interpretation and comparison of experimental data, the equivalent diameter, d_{equ} , was chosen to be the diameter of the circle that has the same area as that of the sewage particle on the image plane. This equal-area diameter was used for its simplicity and well-defined physical meaning.

For size analysis, it was assumed that the shape of a particle is independent of its size. Hence, the volume of a particle is proportional to the cube of its equivalent diameter. The lack of correlation between shape and size was confirmed by the experimental observations. For the thousands of particles examined by the holographic technique in our experiment, there is no preferential or dominant shape for any particle size range.

In correlating the settling velocities with particle sizes for nonspherical particles in Stokes' regime, the governing equation can be written as:

$$w = A \frac{g}{18\mu} \Delta\rho l_p^2 \quad (5.1.1)$$

where A is the shape factor of the particle; $\Delta\rho = \rho_p - \rho_f$, in which ρ_p is the effective density of particles, ρ_f is the density of the settling medium; and l_p is the characteristic length scale of particles. For sewage particles, the shape, density, and size vary significantly, and the observed settling velocities are affected by all these factors. The equivalent diameter, d_{equ} , is adopted as the characteristic length scale

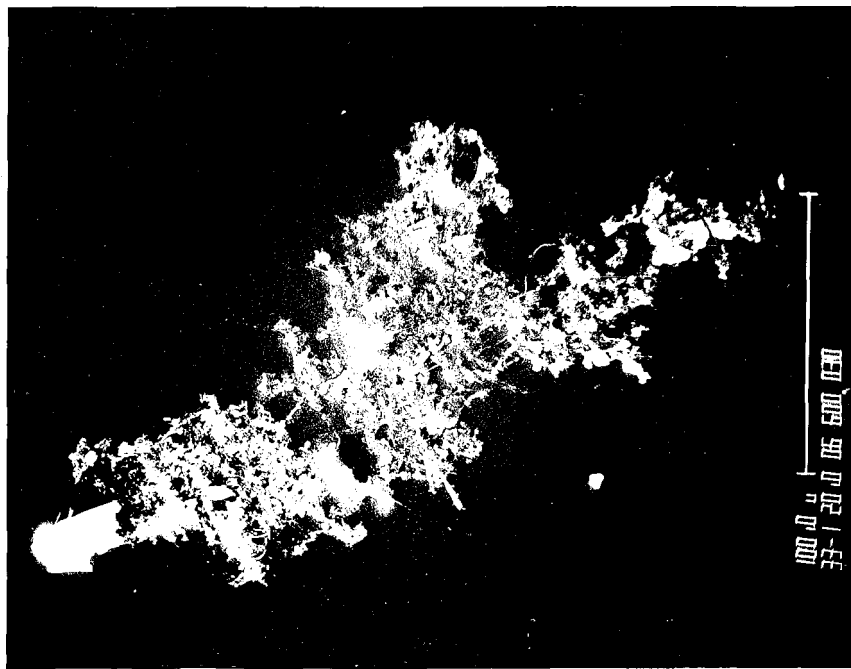
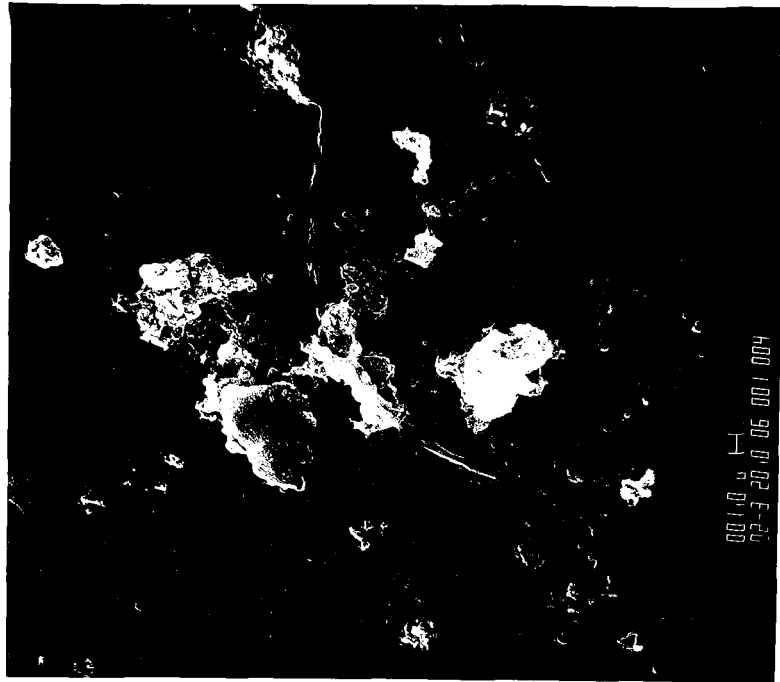


Figure 5.1.1 Scanning electron micrographs of sludge particles (digested primary sludge from the County Sanitation Districts of Orange County): (a) uncoagulated particles, (b) a coagulated particle

of the particles and the corresponding value of $A\Delta\rho$ was calculated as $\frac{18\mu w}{g d_{equ}^2}$. For perfect spheres, d_{equ} becomes the diameter and $A = 1$.

The shape factor A can be examined in more detail. For a nonspherical particle settling in Stokes' flow, the drag force F_D can be approximated by that of a sphere with diameter equal to the maximum dimension of the irregular particle (J. F. Brady, Caltech, private communication). If the maximum dimension measured on the image plane, i.e. len_v , is used as the maximum dimension, the drag force is:

$$F_D = 3\pi \mu len_v w \quad (5.1.2)$$

If it is also assumed that the volume of a particle is equal to $A_1 d_{equ}^3$, where A_1 is a proportionality constant (not known), the submerged weight of the particle is as follows:

$$F_G = A_1 d_{equ}^3 \Delta\rho g \quad (5.1.3)$$

From the force balance, i.e. $F_D = F_G$, the fall velocity becomes

$$w = \left(\frac{6}{\pi} A_1 \frac{d_{equ}}{len_v} \right) \frac{g}{18\mu} \Delta\rho d_{equ}^2 \quad (5.1.4)$$

and the shape factor A is $\frac{6}{\pi} A_1 \frac{d_{equ}}{len_v}$. However, plotting w versus $\left(\frac{d_{equ}}{len_v} \right)^{0.5} d_{equ}$ as suggested by Eqn. 5.1.4 instead of w versus d_{equ} as used in Chapter 4 does not eliminate the scatter of experimental data. From the measurements of sludge

and effluent particles, the median value of $\frac{d_{equ}}{len_v}$ is about 0.71 and A is $1.36A_1$ (see Appendix C). Lacking measurements of the third dimensions of particles, A_1 cannot be determined from the experimental data. Furthermore, the maximum dimension measured on the image plane, len_v , is not necessarily the maximum dimension of a particle in three dimension.

5.1.2 Particles with equivalent diameter smaller than $10 \mu m$

A substantial fraction of the particles in digested sludge and sewage effluent is smaller than $10 \mu m$. Faisst (1976, 1980) used a Coulter counter to measure the size distributions of the digested sludges from the County Sanitation Districts of Los Angeles County and the Hyperion treatment plant of the City of Los Angeles and concluded that 30 to 60 % of the particles (by volume) are smaller than $10 \mu m$. The size and fall velocity of these small particles cannot be measured accurately with the present holographic camera system due to inadequate resolution. However, since these particles, in general, have very small settling velocities ($< 1 \times 10^{-4} \text{ cm/sec}$), it may be sufficient to know only their total mass, which was measured by filtration.

The cutoff sizes of these two techniques, i.e. filtration and holography, are not exactly the same, but the difference is unknown. For example, some particles that are observed by the holographic technique may pass through the $10\text{-}\mu m$ Nuclepore membrane, and some particles that are retained on the membrane are not measured during hologram reconstruction.

5.1.3 Accuracy of the size distribution

The errors in the analysis of particle size distribution using the holographic technique come from two sources: the measurement errors and the sampling errors. The errors in measuring the size of individual particles certainly affect the distribution curve; so does the sampling process. In deriving the size distribution using Eqn 4.1.2, the volume concentrations of particles ($\frac{d^3}{V_d}$) in pre-determined size ranges were added, and the resulting volume concentrations in each size range were then normalized by the total volume concentration. Therefore, the errors in size measurement within each size range are not independent but affect each other. In order to estimate the errors in size distribution based on the errors in measuring the size of individual particles, a simple test was designed especially for this purpose.

An effluent sample (withdrawn at $t = 2'10''$ in Run 4) with suspended solids of 0.56 mg/l was used in these tests. This sample was divided in two, and a singly exposed hologram were recorded for each of them. Hologram A was analyzed three times. The number of particles measured and the volumes obtained are summarized in Table 4.2.3. The size distributions (based on particle volume) are plotted in Figure 5.1.2a. Figure 5.1.2b shows the size distribution measured for hologram B. The median diameter as measured from hologram A is within 26 to $29 \mu\text{m}$, and is $25 \mu\text{m}$ for hologram B. All these distribution curves are of similar shape. The maximum deviation in the probability density function $p(d_j)$ for each d_j range is roughly 0.05 .

5.1.4 Accuracy of the settling velocity distribution

Settling velocity distributions for different sewage particles were derived using Eqn. 4.1.8 to 4.1.12. This procedure comprises a sequence of summation, averaging, integration and normalization operations.

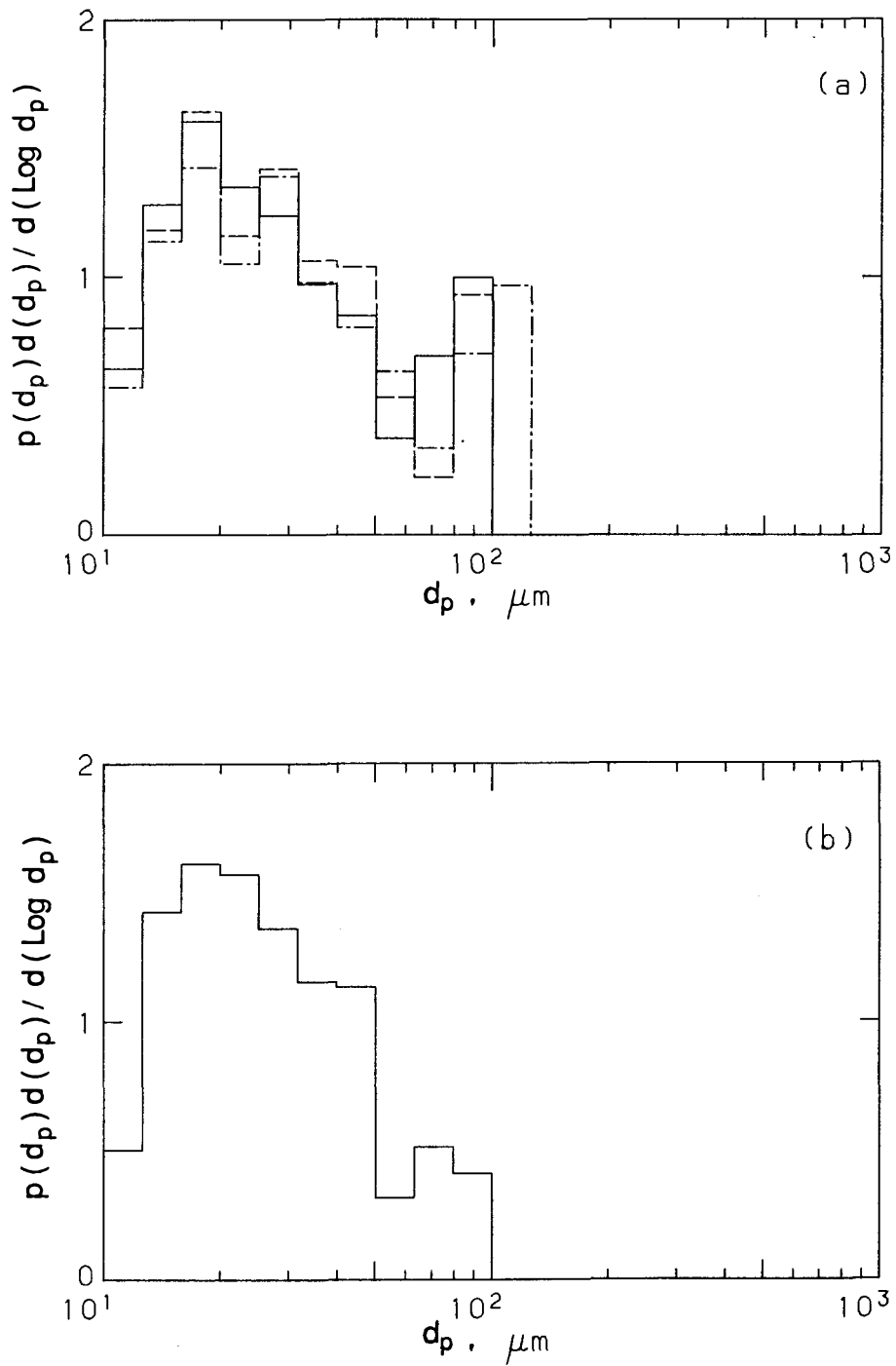


Figure 5.1.2 Size distributions ($d \geq 10 \mu\text{m}$) of the repeated measurements of the same sample from: (a) the same hologram, (b) a different hologram of the same sample

For Eqn. 4.1.10, the error in measuring the height of the sampling volume $\frac{\Delta h}{h}$ is estimated from the resolution of the micrometer ($10 \mu m$) and the vertical dimension of the film ($\sim 1.5 \text{ cm}$) to be less than 0.1 %. The error in time measurements, $\frac{\Delta t}{t}$, is less than 0.7 % for $t < 5 \text{ min}$ and 0.3 % for $t > 5 \text{ min}$. Hence, the error in the probability density function $f(w)$ is mainly due to the errors in measuring V_L (Eqn. 4.1.8). For a single particle, $\frac{\Delta d^3}{d^3}$ ($\propto 3 \frac{\Delta d}{d}$) is estimated to be approximately 15 %. If it is assumed that the errors of individual measurements are independent and normally distributed, the percentage errors of the summation of N measurements should decrease by a factor of $\frac{1}{\sqrt{N}}$. The number of particles measured inside each hologram (N) ranges from 1 to 50, and V_L , which is $\sum d^3$, should have an error of 2 to 15 %. The measuring error of individual values of w is from 3 to 13 % (Table 3.2.4), and, similarly, the errors of the average values should range from 13 down to less than 1 %.

In addition to errors in the measurements, errors introduced from the assumptions used to derive Eqn. 4.1.8 to 4.1.10 should also be considered. Two assumptions were made: that the fall velocity distribution $f(w)$ is independent of the initial positions of particles and that $f(w)$ calculated from the hologram recorded at time t can be approximated by the average $f(w)$ over the velocity range from $\frac{L - 0.5h - H}{t}$ to $\frac{L + 0.5h}{t}$ (which requires either that the particles are uniformly distributed over the volume Ha at the beginning of the settling test or that $f(w)$ varies slowly within the velocity range from $\frac{L - 0.5h - H}{t}$ to $\frac{L + 0.5h}{t}$, Figure 4.1.1).

The first assumption can only be satisfied if the number concentration of particles in the initial volume Ha (a is the cross section area of the settling cell) is large. This is probably true for small particles with high number concentration. However,

it is no longer true for large particles ($d > 63 \mu m$ and $w > 5 \times 10^{-3} \text{ cm/sec}$) as they do not appear in large quantities in test samples. Hence, the resulting velocity distribution curves can be significantly affected by the presence or absence of a few large particles. For example, the fall velocity distribution in Figure 4.2.12 is shifted to larger fall velocity range mainly due to the presence of two large particles ($d \sim 180 \mu m$) that account for almost 50 % of the total particle volume.

The second assumption represents basically an averaging process of the real fall velocity distribution. The velocity \bar{w} calculated from Eqn. 4.1.9 should fall in the range from $\frac{L - 0.5h - H}{t}$ to $\frac{L + 0.5h}{t}$ with a deviation $\Delta w = \frac{H + h}{t} \approx 0.5w$. The corresponding $f(\bar{w})$ from Eqn. 4.1.10 is the average of $f(w)$ over the range $w \pm 0.5\Delta w$. This suggests that the detailed shape of the distribution curve within Δw cannot be resolved.

From the above discussion, it can be concluded that the sharp changes in the probability density functions as observed in Figures 4.2.3, 4.2.7, 4.2.12, 4.2.18, 4.2.22, and 4.2.28 are not due to errors in measurements. They may, however, be caused by errors in sampling. If we repeat the settling measurements for the same sludge several times, the distributions obtained from each experiment will not be exactly the same, and the average of them should give a more representative result. Furthermore, the fall velocity distribution derived using both the settling velocity and particle size measurements gives a better estimate of the fall velocity distributions because the size distribution of particles is based on the single-exposure hologram and only the conditional distribution of fall velocity for given diameter is taken from the double-exposure holograms.

Improving the accuracy in measuring the settling velocity and equivalent diameter of individual particles would increase the accuracy of the fall velocity distribution somewhat, but cannot overcome sampling problems. In this regard it would help to modify the experimental setup by increasing the sampling volume (ha) and decreasing the initial thickness of the particle layer in the settling cell (H). Hence, for a certain velocity range w to $w + \Delta w$ at time t , all particles are in a volume of thickness of $H + t\Delta w \leq h$, and then they can all be captured in the sampling

volume. Therefore, $f(w)$ can be calculated for this velocity range as $\frac{\sum_w d^3}{\Delta w \sum_{tot} d^3}$.

5.1.5 Time limitation

It takes only minutes to record holograms for size distribution analysis, but two days to record holograms of settling velocity measurement of fall velocity down to 1×10^{-4} *cm/sec*. Using the present setup, we can work on only one sample at a time. Other samples, therefore, have to be stored for days before they can be analyzed. Although the concentration of samples was kept lower than 2 *mg/l* and samples were stored in a refrigerator to minimize deterioration, the size distribution may still change due to particle coagulation. The difficulties in preserving sample characteristics during storage and resuspending the particles for analysis without breaking their fragile structures limit the accuracy of the present technique.

Previous studies noticed the changes of size distributions for particle suspensions in seawater during storage. Peterson (1974) used a Coulter counter to study the change of particle size distributions as a function of storage time for water samples with volume concentrations of 0.3 to 4.0 *ppm* collected from Hermosa Beach Pier. He observed a 15 to 20 % increase in number concentrations for particles

ranging from 1 to 5 μm after 24 *hr* and explained the change as the results of aggregation of particles. Tennant *et al.* (1987) studied the size distributions of unagitated diluted sludge samples in seawater (1 to 10 *mg/l*) with a Coulter counter. They observed that the size distributions of the samples shifted noticeably to the coarse size range after overnight storage.

In this study, the samples used for velocity measurement have a concentration of about 2 *mg/l*. The storage time of samples ranged from 8 *hr* to several days. In the experiments for all four runs, we consistently observed a higher number fraction of large particles in settling velocity analysis than in size measurement. Since larger particles in general have faster fall velocity, this may explain why the fall velocity distributions derived from settling velocity measurement alone are consistently faster than those from the combined measurements of size and velocity (Figure 4.2.3 versus 4.2.5; 4.2.7 versus 4.2.9; 4.2.12 versus 4.2.14; 4.2.18 versus 4.2.20; 4.2.22 versus 4.2.24). Therefore, independent size measurement on fresh samples is necessary to provide the basis for determining velocity distributions that are not affected by the storage time of samples.

The changes in size distribution were also verified with the holographic technique for particles larger than 10 μm . One diluted effluent sample in seawater (withdrawn at $t = 4'30''$ in Run 4) with concentration of 0.68 *mg/l* was used in this test. Singly exposed holograms were recorded at 0'', 12 *hr*, 24 *hr*, and 36 *hr* after the sample was prepared. The measured size distributions at 0'' and 36 *hr* are shown in Figure 5.1.3. The volume fraction of particles in the 10 to 20 μm range decreased slightly while that in the 30 to 50 μm range increased. The median diameter shifted upward from 26 μm to 28 μm . The differences between these two size distributions are within the experimental error; hence it may indicate that

coagulation is not significant over this time period (36 *hr*) for the concentration of 0.68 *mg/l*.

This time limitation on settling velocity measurements can be eliminated by modifying the experimental setup to process several samples in parallel so that fresh samples can be analyzed immediately after they are withdrawn from the coagulator. According to Table 3.3.1, the time between recording two successive holograms increases with time and becomes longer than 6 *min* after 1 *hr*. This time duration is long enough for us to start recording holograms for another sample. The present holographic camera system can be modified into two separate units: one with the laser, the spatial filter, and the collimating lens to provide illuminating light, the other with settling cells and film holders to record holograms. We can then start recording the holograms for settling analysis for several samples one after another at 1 *hr* time delay in between. All the settling cells would be fixed during the tests, but the laser unit would need to be moved to provide the light source for recording holograms for different samples according to a predetermined schedule.

5.2 Degree of Coagulation

Results of the simulated plume mixing for both the proposed sludge disposal plan for CSDOC (Figures 4.2.15 and 4.2.16, Table 5.2.1) and the existing effluent outfall of CSDLAC (Figure 4.2.26, Table 5.2.2) suggest that the coagulation effect during the simulated plume mixing is negligible. Although the high ionic strength of the seawater provides favorable conditions for coagulation, actual coagulation may still be insignificant because of the small collision rate, or the short reaction time, or both.

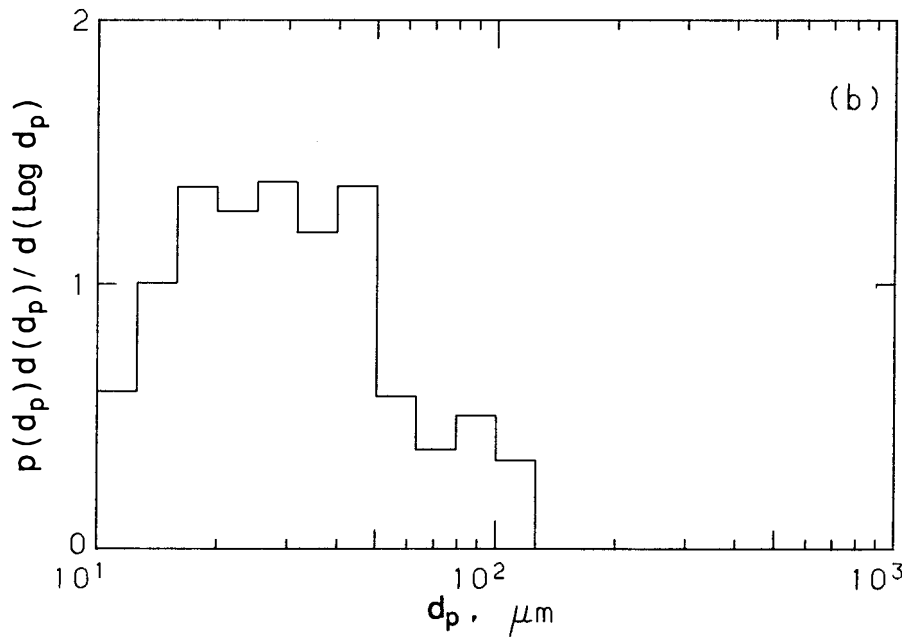
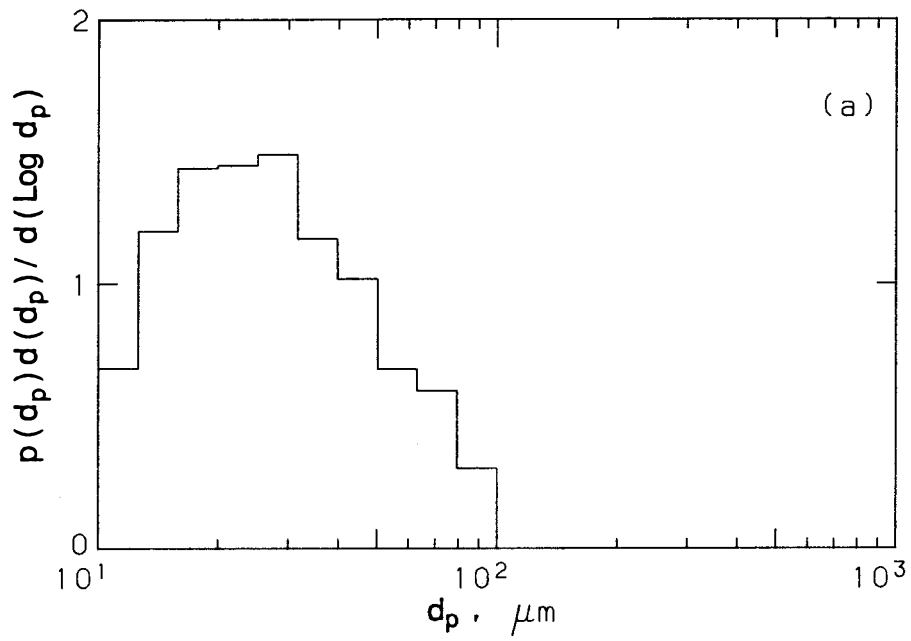


Figure 5.1.3 Size distributions ($d \geq 10 \mu\text{m}$) of a diluted effluent sample (0.68 mg/l) at different times: (a) $t = 0''$, (b) after being stored for 36 hr

Table 5.2.1 Summary of particle number concentrations (normalized to 1000:1 dilution) at different times during plume mixing experiment of the D.P.S. (CSDOC)

Size range (μm)	Particle number concentration, cm^{-3}						
	0'	20''	1'20''	2'30''	3'50''	5'40''	6'20''
10.0-12.6	2.1×10^4	2.0×10^4	1.5×10^4	2.1×10^4	5.3×10^3	2.4×10^4	2.0×10^4
12.6-15.8	1.8×10^4	1.6×10^4	1.6×10^4	2.1×10^4	6.8×10^3	2.5×10^4	2.0×10^4
15.8-20.0	2.0×10^4	1.9×10^4	1.6×10^4	1.3×10^4	8.6×10^3	1.6×10^4	1.2×10^4
20.0-25.0	8.4×10^3	9.6×10^3	7.2×10^3	8.0×10^3	6.1×10^3	2.6×10^3	9.0×10^3
25.0-31.6	4.6×10^3	4.5×10^3	4.6×10^3	3.4×10^3	2.8×10^3	1.4×10^3	3.0×10^3
31.6-39.8	1.6×10^3	1.8×10^3	1.8×10^3	1.2×10^3	1.5×10^3	6.8×10^2	1.4×10^3
39.8-50.1	6.3×10^2	8.0×10^2	7.4×10^2	8.5×10^2	7.1×10^2	2.5×10^2	8.3×10^2
50.1-63.1	2.0×10^2	2.7×10^2	2.8×10^2	3.0×10^2	3.4×10^2	6.4×10^1	1.9×10^2
63.1-79.4	8.5×10^1	9.0×10^1	6.2×10^1	1.3×10^2	2.6×10^1	4.0×10^1	1.9×10^2
79.4-100.	0	3.1×10^1	3.1×10^1	4.2×10^1	2.6×10^1	5.0×10^1	0
100.-126.	2.8×10^1	3.1×10^1	3.1×10^1	0	0	0	0
126.-158.	5.7×10^1	0	0	0	0	0	0
158.-200.	0	0	0	0	0	0	0

As mentioned in chapter 2, the dominant coagulation mechanism in a discharge plume is the turbulence shear. For the coagulation induced by turbulent shear, the collision rate, defined as the number of collisions between two particles per unit volume per unit time, is determined by the product of the particle concentrations and the square root of the ratio of energy dissipation rate to the viscosity of the fluid. Since both the particle concentration and the energy dissipation rate decrease dramatically over a very few minutes (Figures 3.1.1 and 3.1.2), the small particle concentration and low turbulence intensity later on may be non-conducive of any significant coagulation and maintain constant size distributions through the plume mixing.

Table 5.2.2 Summary of particle number concentrations (normalized to 100:1 dilution) at different times during plume mixing experiment of the effluent (CSDLAC)

Size range (μm)	Particle number concentration, cm^{-3}					
	0'	40''	1'20''	2'10''	3'20''	4'30''
10.0-12.6	180	190	140	200	150	200
12.6-15.8	160	140	120	260	150	170
15.8-20.0	100	79	75	170	75	100
20.0-25.0	47	43	36	66	42	53
25.0-31.6	27	22	19	36	24	27
31.6-39.8	10	8.6	10	14	10	10
39.8-50.1	4.9	4.5	4.8	6.2	4	5
50.1-63.1	1.3	1.4	1.6	1.8	0.8	1.3
63.1-79.4	0.5	0.6	0.2	0.6	0.5	0.8
79.4-100.	0.2	0	0.2	0.7	0.3	0.2
100.-126.	0	0	0	0.2	0	0
126.-158.	0.2	0	0.2	0	0	0.2
158.-200.	0	0.2	0	0	0	0

5.2.1 Comparison with Gibbs and Hopkins' experimental results

Gibbs and Hopkins (1984) performed experiments to study the effects of solids concentration and turbulence shear on the coagulation rate of sewage sludge in seawater. They used digested sewage sludge with the concentration of 85,600 mg/l from the City of Philadelphia. The sludge sample was diluted with filtered seawater with salinity of 32‰ to the volume ratios from 0.01 (856 mg/l) to 0.0002 (17.1 mg/l) before coagulation. Coagulation was conducted in a 1 l horizontal stirring device with two blades and the shear rate was measured by a torque meter. Particle size distributions at different times during coagulation were measured using the optical microscope technique.

The volumetric average diameter calculated from the size measurement of each sample was used as the representative floc size of a system to monitor the extent of coagulation. They concluded that the volumetric average diameters follow the equation $\ln(d_v) = kt + \ln(d_{v0})$, where d_v is the volumetric average diameter at time t , d_{v0} the volumetric average diameter at time 0, and k the rate constant, which increases with particle concentration and shear rate (Figure 5.2.1). They also studied the equilibrium time required for the average diameter (d_v) of a system under constant concentration and shear rate to reach a constant value. It was concluded that this equilibrium time decreases with increasing shear rates and particle concentrations (Figure 5.2.2).

The energy dissipation rates ($= \nu G^2$) used in Run 3 (Figure 3.1.1) are off the scale of G in Figure 5.2.1 for the first 3 *min* and then the rate constant k is less than $6 \times 10^{-3} \text{ min}^{-1}$ after 3 *min* according to Figure 5.2.1. This coagulation rate results in a change in the volumetric average diameter of less than 3 % for 4 *min*. According to Figure 5.2.2, the equilibrium time, which is about 80 *min* at 60 *sec* of plume simulation and longer than 100 *min* after 70 *sec*, is much longer than the simulation time used for D.P.S. (CSDOC) (6 *min* 20 *sec*), so coagulation is expected to be insignificant. Since particle number concentration in plume mixing for the effluent mixture from CSDLAC is at least 100 times less than that for D.P.S. (Table 5.2.2), the coagulation should not be significant either. The observation of negligible coagulation under the simulated mixing conditions in this study is consistent with Gibb and Hopkins's results.

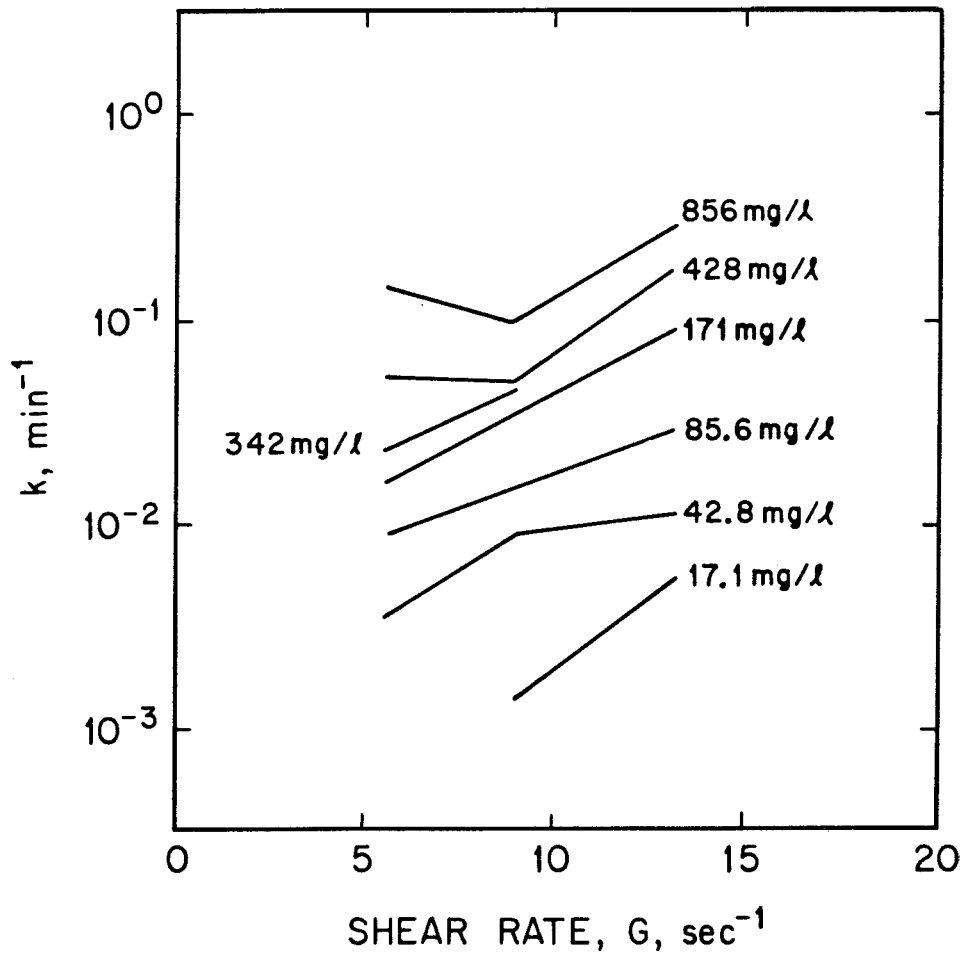


Figure 5.2.1 The relationship of the coagulation rate constant, k (min^{-1}), as a function of turbulent shear rate at different solids concentrations of sludge (from Gibbs, 1984)

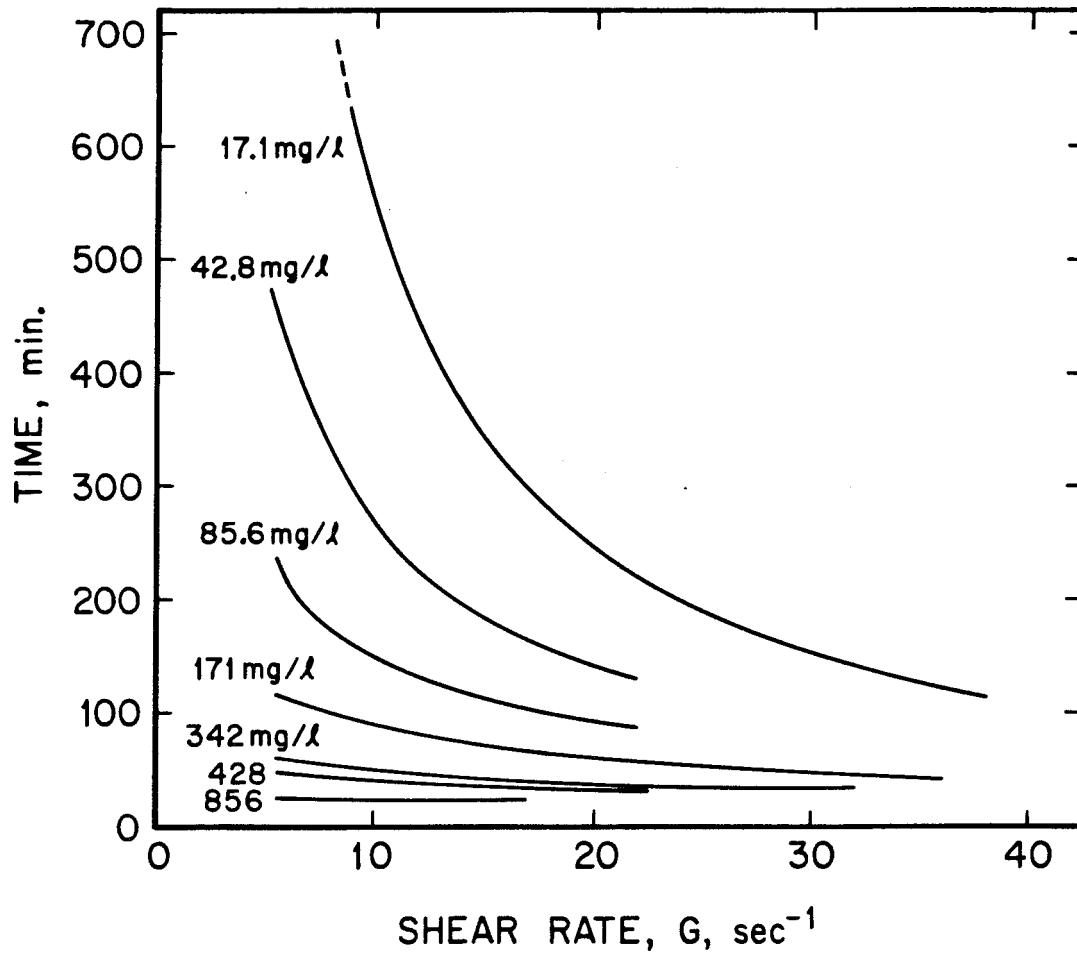


Figure 5.2.2 The relationship of the equilibrium time as a function of turbulent shear rate at different solids concentrations of sludge (from Gibbs, 1984)

5.2.2 Time scale of plume mixing

In our experiment, the mixing times of the plume simulation experiments for the D.P.S. (CSDOC) and the effluent (CSDLAC) were calculated based on the *centerline* velocity of the plume. If the *flux-weighted average* velocity is used instead, the coagulation time will be two times longer for the sludge (760 *sec* versus 380 *sec*) and $\sqrt{2}$ times longer for the effluent (382 *sec* versus 270 *sec*). Under this revised mixing condition, although the mixing time increases, the particle concentrations and energy dissipation rates are still very low except at the very beginning of the mixing experiment, and coagulation is still expected to be insignificant. Also in the case of sludge, the concentration in the plume is taken as average; if centerline concentration is preferred to correspond with the velocity assumption, then it is equivalent to reducing all dilutions by a factor of 1.78, or in practical terms, the effective initial suspended solids concentration becomes $\frac{10000}{1.78} = 5600 \text{ mg/l}$ ($\sim 64 \text{ tons/day}$).

5.3 Relationship between Particle Size and Fall Velocity

The w versus d relationships of both D.P.S. (CSDOC) and effluent (CSDLAC) under different mixing conditions do not show any significant difference (Figures 4.2.2, 4.2.6, 4.2.11, 4.2.17, 4.2.21 and 4.2.27). The data points in different plots scatter over roughly the same region on the plots. For comparison purpose, several straight lines were plotted on each w versus d graph. These lines were calculated according to the Stokes' law (Eqn 5.1.1) for particles with different $A\Delta\rho$ value as shown on the graph (A = shape factor =1 for spheres).

For both sludge and effluent samples, the data points cover a wide range of $A\Delta\rho$ from 0.002 to 0.5 g/cm^3 , with the median approximately 0.02 to 0.03 g/cm^3 . The

relationships between equivalent diameters and fall velocities are consistent with Stokes' law, i.e., $w \propto d_{equ}^2$. For any single equivalent diameter, the corresponding fall velocities range over a factor of 10 to 100 times. The range of errors from size and velocity measurements is only as wide as the plotting symbols in these graphs. Hence, the dispersion of the data is not due to experimental errors but due to the variations in density, shape, structure (porosity), and settling orientation of individual particles.

5.3.1 Shape of sewage particles

The shape of sewage and sludge particles is very irregular and complicated. There is no satisfactory way to define the shape factor that would apply to all particles. In this experiment, four different length scale (len_v , len_h , max_v , and max_h) and the square roots of the second moments about the principal axes ($\frac{\sigma_{major}}{d_{equ}}$ and $\frac{\sigma_{minor}}{d_{equ}}$) were calculated to provide rough estimates of particle shape (Appendix C). For example, Figure 5.3.1 shows some typical examples of $\frac{\sigma_{major}}{d_{equ}}$ and $\frac{\sigma_{minor}}{d_{equ}}$ for sludge and sewage particles (from Runs 3 and 4). Most of the observed particles have $\frac{\sigma_{major}}{\sigma_{minor}}$ smaller than 3, which suggests that the ratio of the longer dimension to the shorter one of particles is less than three. For a circle, $\frac{\sigma_{major}}{d_{equ}}$ and $\frac{\sigma_{minor}}{d_{equ}}$ are the same and equal 0.25; for an ellipse with semiaxes a and b , they are $\frac{1}{4}\sqrt{\frac{a}{b}}$ and $\frac{1}{4}\sqrt{\frac{b}{a}}$ respectively. For most sludge and effluent particles, $\frac{\sigma_{major}}{d_{equ}}$ is less than 0.75 and $\frac{\sigma_{minor}}{d_{equ}}$ is less than 0.3. Additional information on particle shape is included in Appendix C.

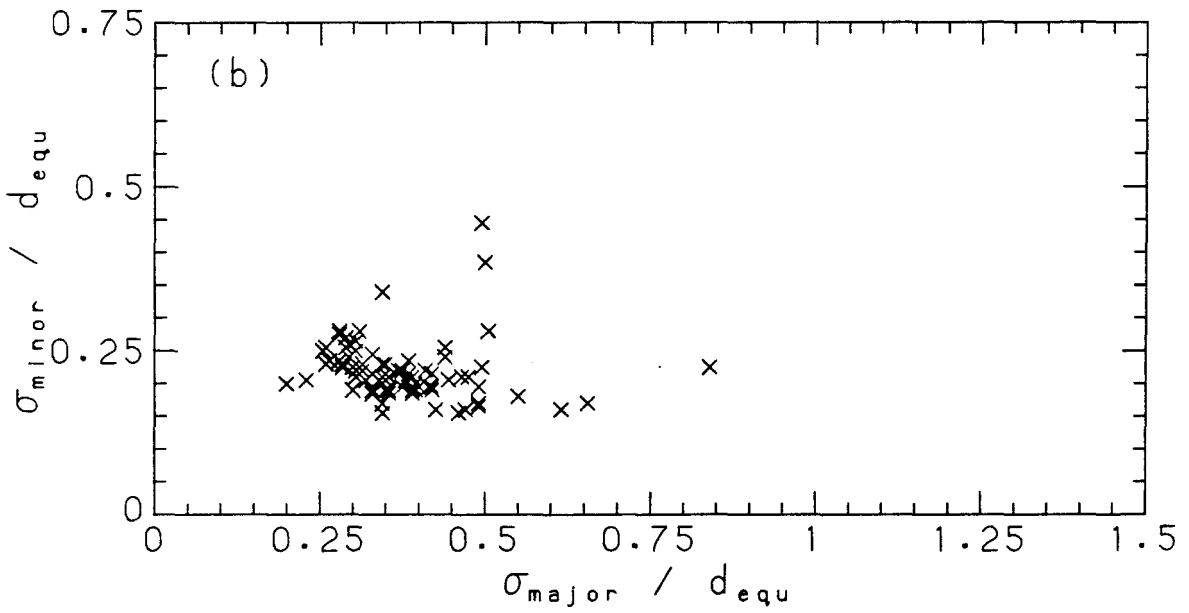
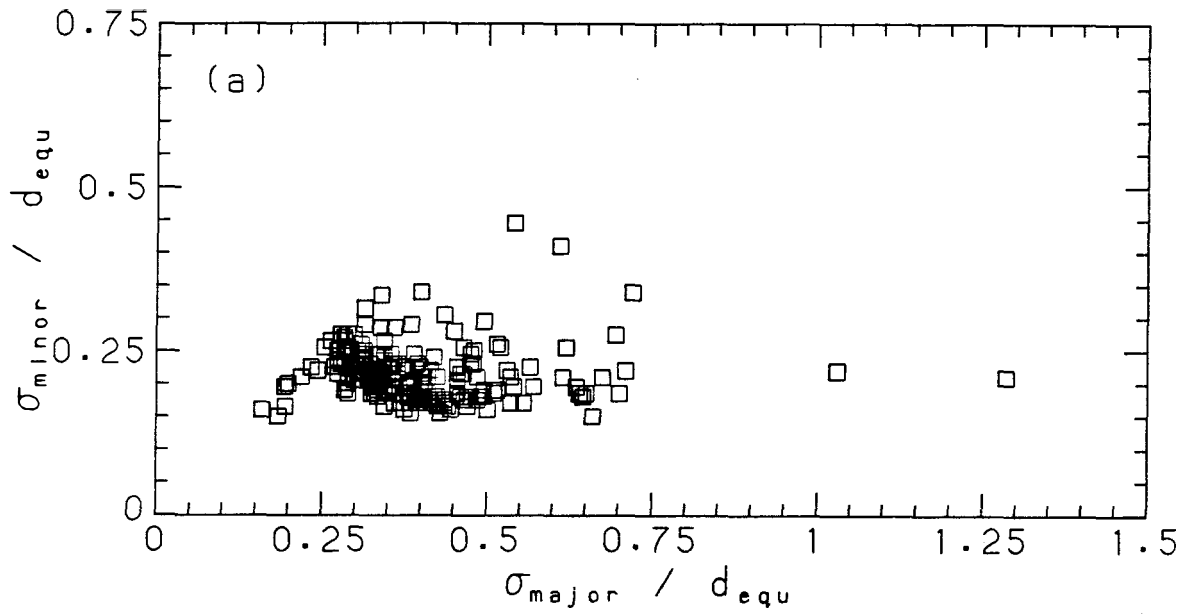


Figure 5.3.1 Examples of $\frac{\sigma_{major}}{d_{equ}}$ and $\frac{\sigma_{minor}}{d_{equ}}$ for sludge and sewage particles (a)

D.P.S. (CSDOC)—Run 3, (b) effluent (CSDLAC)—Run 4

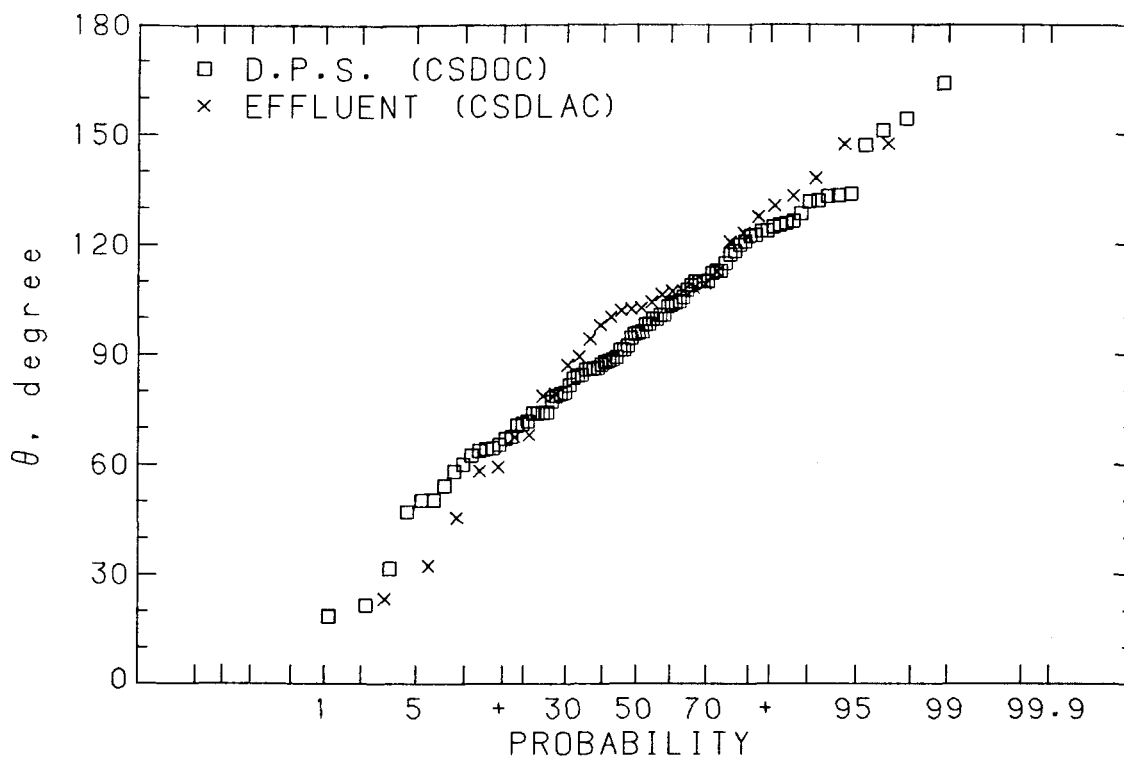


Figure 5.3.2 Orientation (in two-dimensional plane) of particles during settling (θ is the angle between the horizontal axis and the major principal axis of particles on the hologram plane which is perpendicular to the optical axis)

5.3.2 Orientation of particles during settling

The orientation of particles during settling can be examined by θ , the angle between the horizontal axis and the major principal axis of the particles (Appendix C). Particles with θ in the range from 45° to 135° outnumber particles with $\theta < 45^\circ$ or $\theta > 135^\circ$ by more than 6 to 1 (Figure 5.3.2). However, it is difficult to interpret the three-dimensional orientations of particles from the two-dimensional views.

5.3.3 Density of sludge particles

By comparing the settling velocities of the same kind of particles in settling mediums of different density (Run 1, Figure 4.2.2 versus 4.2.6), we concluded that the density of the settling medium (from 1.0056 to 1.0251 g/cm^3) does not alter the settling velocities significantly. This observation suggests that sewage particles in general have high void ratio, e (the ratio of the volume of void to the volume of the solid), and the density of the solid parts is much higher than the density of either seawater or fresh water, i.e., 1.0251 and 1.0056 g/cm^3 respectively.

When particles are introduced into a settling medium, the differences in the salt concentration of water inside and outside the particles create diffusion. Since the time scale of salt diffusion ($\frac{d^2}{D_s}$, D_s is the molecular diffusion coefficient of salt and equal to $1.3 \times 10^{-5} cm^2/sec$ at $20^\circ C$) is much smaller than that of settling ($\frac{d}{w}$) for the sewage particles, it can be safely assumed that the salt concentration inside the particle is always at equilibrium with that outside during settling. Hence, if ρ_{f1} is the density of seawater, ρ_{f2} the density of fresh water, ρ_s the density of the solid part of the particles, and e the void ratio of the particles, the product of the shape factor and the effective density of particles in these two media should be approximately equal and the following relationship holds:

$$\frac{\rho_s - \rho_{f1}}{1 + e} \cong \frac{\rho_s - \rho_{f2}}{1 + e} \cong \frac{0.01 - 0.05}{A} g/cm^3 \quad (5.3.1)$$

Faisst (1980) measured the densities of sludge particles using a Coulter counter to estimate the solid volume of particles and the filtration technique to estimate the mass of particles. He reported 1.37 g/cm^3 for Hyperion mesophilic sludge

and 1.69 g/cm^3 for CSDLAC's primary sludge. Therefore, we may assume $\rho_s \approx 1.5 \text{ g/cm}^3$, and with $A\Delta\rho \approx 0.02 \text{ g/cm}^3$ observed, we find the void ratio e must be approximately 23 to 24 for $A = 1$, i.e. 96 % of the volume is voids and 4 % solids.

However, for some of the particles smaller than $30 \mu\text{m}$, the minimum velocity observed is around $2 \times 10^{-4} \text{ cm/sec}$ in fresh water, and $5 \times 10^{-5} \text{ cm/sec}$ in seawater (Figures 4.2.2 and 4.2.6), indicating a factor of 4 difference in $A\Delta\rho$. Since the fluid density change is 0.02 g/cm^3 , the effective densities of particles should satisfy the following equation:

$$\frac{\rho_s - \rho_{f2}}{\rho_s - \rho_{f1}} \cong 4 \quad (5.3.2)$$

The above equations can be satisfied by particles of $\rho_s = 1.0316 \text{ g/cm}^3$ with porosity not determined. It suggests that some of these small particles may be relatively impervious to salt diffusion with much smaller values of solid density ρ_s .

5.3.4 Comparison with Gibb's measurements

Gibbs (1984) measured the settling velocities for individual sludge flocs after they were coagulated. Sludge samples at 100:1 dilution were coagulated in a blade-type mixer at shear rate of 2 sec^{-1} until the equilibrium state was reached, i.e., when the size distribution stopped changing. The coagulated samples were introduced to the top of a $15 \text{ cm} \times 1.2 \text{ m}$ settling column filled with seawater. A microscope with a pre-calibrated grid for sizing flocs was focused on the center of the column. From his observation, he concluded that the settling velocities of the sludge flocs increase with the size of the flocs (Figure 5.3.3). The regression lines of fall velocities and

sizes cut across the equal density lines, which indicates that the larger flocs are of progressively lower density.

Similar observations, the decrease of the floc density with the increase of the floc size, have been obtained for chemical flocs and natural aggregates either by directly measuring the floc density (Lagvankar and Gemmell, 1968) or by indirectly deriving the floc density from settling velocity measurements (Kajihara, 1971; Tambo and Watanabe, 1979; Kawana and Tanimoto, 1979). However, this phenomenon was not observed in this study. The reason may have to do with the different sizes and structures of sludge particles. Sludge particles used in Gibb's experiment are coagulated flocs mostly larger than $100 \mu m$, while the particles in this study are basically uncoagulated sewage particles mostly smaller than $100 \mu m$. Gibb's fall velocities are almost all larger than 0.05 cm/sec , while the measured fall velocities in our experiments are almost always smaller than 0.05 cm/sec . Another plausible explanation could be that convection currents in his settling column may have interfered with the velocity measurements at the lower end of the velocity range.

5.4 Settling Velocity Distribution

Due to the resolution limit, the present holographic camera system is unable to accurately measure the sizes for particles smaller than $10 \mu m$. However, their fall velocities still can be measured with 5 % accuracy. It is concluded from the settling velocity measurements that particles smaller than $10 \mu m$ generally have fall velocities slower than $1 \times 10^{-4} \text{ cm/sec}$. To construct the fall velocity distribution for one entire sample, it was then assumed that the settling velocities of these small particles are less than $1 \times 10^{-4} \text{ cm/sec}$. It was also assumed that the volume fraction measured by the holographic technique was roughly proportional to the

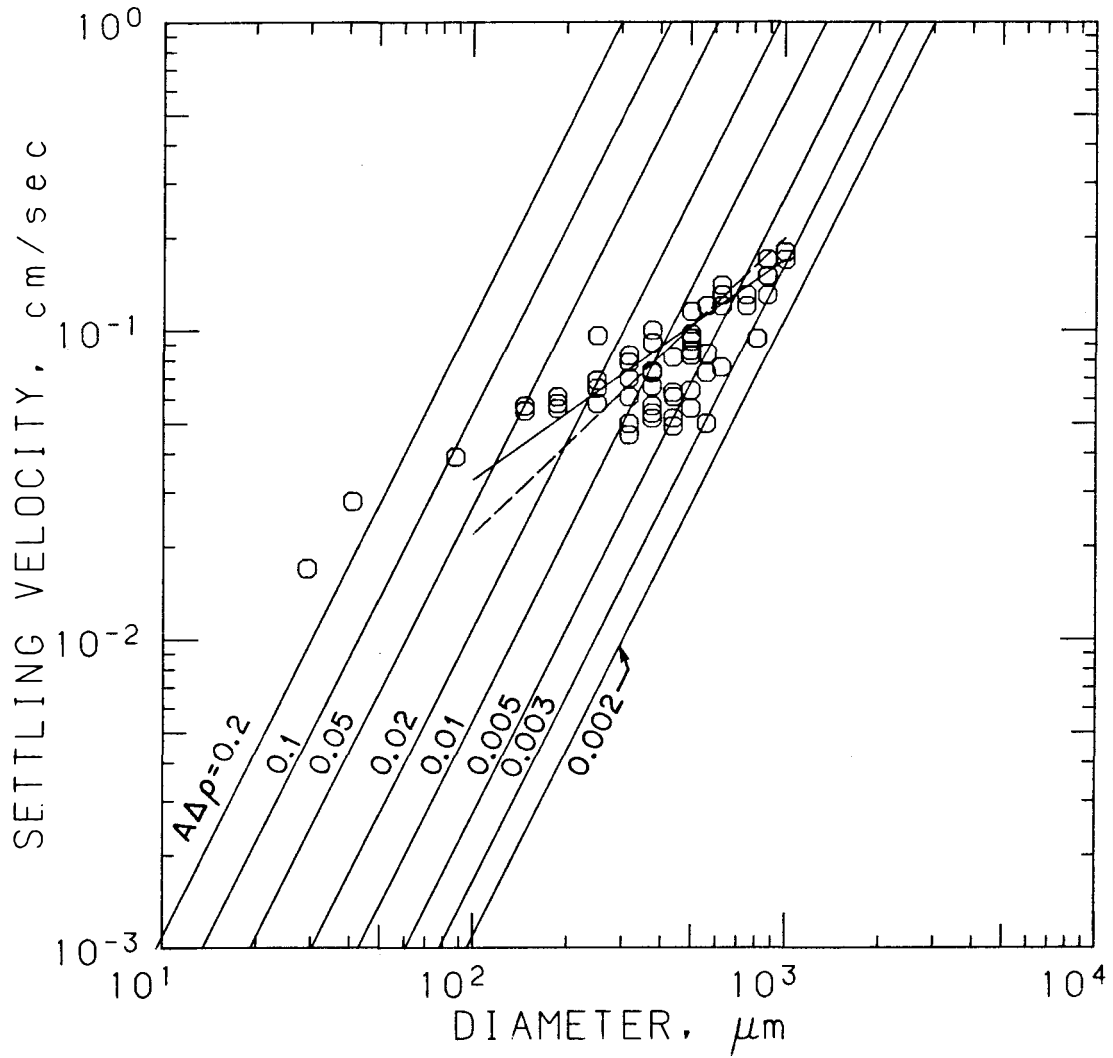


Figure 5.3.3 The relationship of settling velocity at 20°C and diameter of coagulated sludge flocs for anaerobic digested sludge from Wilmington; sludge was coagulated in seawater at a turbulent shear rate of 2 sec^{-1} (—) and 5 sec^{-1} (- - -) (from Gibbs, 1984)

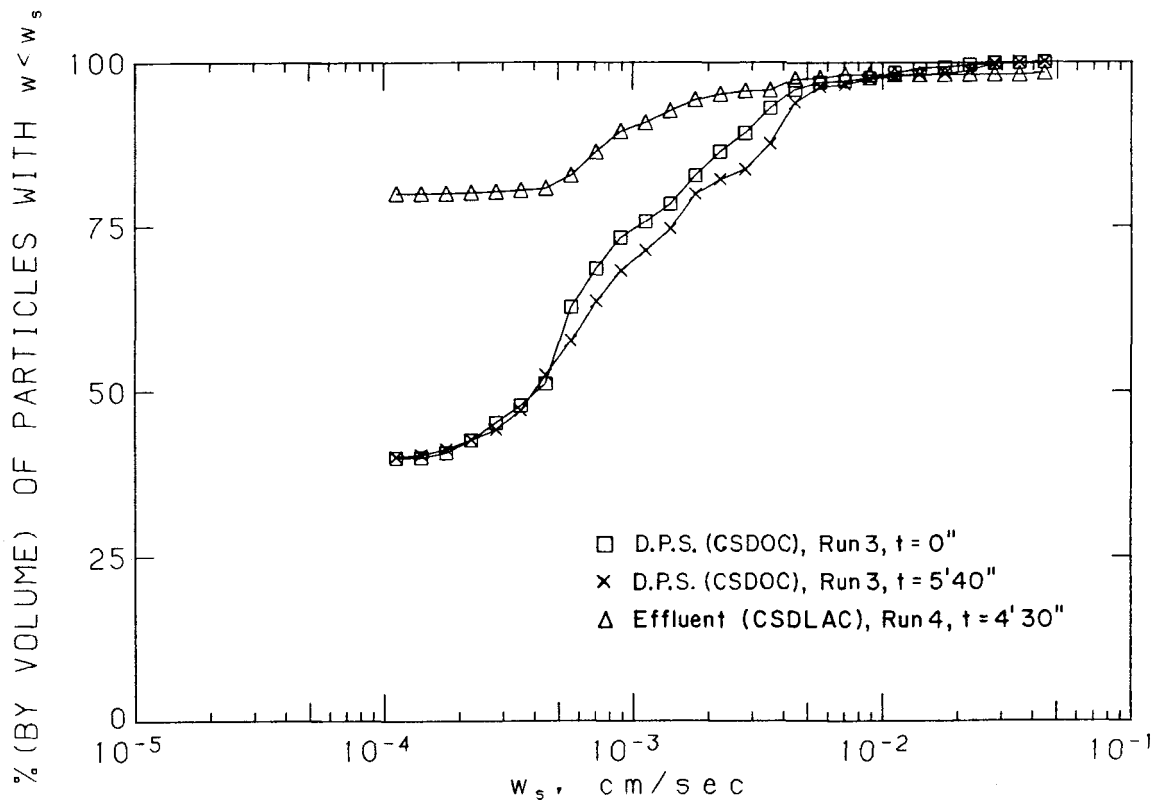


Figure 5.4.1 Settling velocity distributions for the entire sewage samples derived from the holographic measurements and the filtration analysis: Δ —effluent (CSDLAC, Run 4); \square —D.P.S. (CSDOC, Run 3, $t = 0''$); \times —D.P.S. (CSDOC, Run 3, $t = 5'40''$)

mass fraction measured by the filtration technique at the $10 \mu m$ cutoff. Figure 5.4.1 shows the derived fall velocity distributions for the entire size ranges for the D.P.S. (CSDOC) and the effluent (CSDLAC) based on the distributions derived from the measurements of size and velocity as well as the filtration analysis. Table 5.4.1 summarizes the fall velocity distributions for different samples. In the following, these results are compared with our settling column results and other available settling measurements for sludge and effluent particles.

Table 5.4.1 Summary of the settling velocity distributions for D.P.S.(CSDOC) and effluent (CSDLAC)

Run No.	Sample Description	Settling velocity distribution, <i>cm/sec</i>			
		25%ile	Median	75%ile	90%ile
Measurements by the holographic technique					
for $d \geq 10 \mu m$:					
1a	D.P.S., seawater	8.0×10^{-4}	1.5×10^{-3}	4.0×10^{-3}	1.3×10^{-2}
1b	D.P.S., fresh water	1.0×10^{-3}	2.0×10^{-3}	4.3×10^{-3}	9.0×10^{-3}
2	Effluent	1.1×10^{-3}	2.5×10^{-3}	5.5×10^{-3}	8.0×10^{-3}
3	D.P.S., $t = 0''$	5.0×10^{-4}	8.0×10^{-4}	2.0×10^{-3}	4.0×10^{-3}
3	D.P.S., $t = 5'40''$	5.2×10^{-4}	1.0×10^{-3}	2.5×10^{-3}	5.5×10^{-3}
4	Effluent, $t = 4'30''$	7.0×10^{-4}	1.0×10^{-3}	2.0×10^{-3}	7.0×10^{-3}
for the entire sample:					
3	D.P.S., $t = 0''$	$< 10^{-4}$	4.0×10^{-4}	1.0×10^{-3}	2.0×10^{-3}
3	D.P.S., $t = 5'40''$	$< 10^{-4}$	4.0×10^{-4}	1.5×10^{-3}	4.0×10^{-3}
4	Effluent, $t = 4'30''$	$< 10^{-4}$	$< 10^{-4}$	$< 10^{-4}$	10^{-3}
Measurements by the conventional settling column					
1 ^a	D.P.S., 182.4 <i>mg/l</i>	1.0×10^{-4}	1.0×10^{-3}	7.0×10^{-3}	3.0×10^{-2}
2 ^a	D.P.S., 211.4 <i>mg/l</i>	1.0×10^{-4}	1.0×10^{-3}	1.0×10^{-2}	1.0×10^{-1}
3 ^a	D.P.S., 245.4 <i>mg/l</i>	1.0×10^{-3}	2.0×10^{-2}	7.0×10^{-2}	3.0×10^{-1}
4 ^a	D.P.S., 240.6 <i>mg/l</i>	3.0×10^{-4}	1.0×10^{-2}	1.0×10^{-1}	2.0×10^{-1}
5 ^a	D.P.S., 224.5 <i>mg/l</i>	3.0×10^{-4}	2.0×10^{-2}	8.0×10^{-2}	4.0×10^{-1}
6 ^a	D.P.S., 201.9 <i>mg/l</i>	2.0×10^{-4}	1.0×10^{-3}	6.0×10^{-3}	4.0×10^{-2}
7 ^a	D.P.S., 36.9 <i>mg/l</i>	$\leq 1.0 \times 10^{-5}$	2.0×10^{-4}	3.0×10^{-3}	4.0×10^{-2}
8 ^a	D.P.S., 49.2 <i>mg/l</i>	1.0×10^{-4}	1.0×10^{-3}	1.0×10^{-2}	4.0×10^{-2}
9 ^a	D.P.S., 52.4 <i>mg/l</i>	1.0×10^{-4}	2.0×10^{-3}	1.0×10^{-2}	5.0×10^{-2}
1 ^b	D.P.S., 100:1	7.0×10^{-4}	4.0×10^{-3}	1.9×10^{-2}	6.5×10^{-2}
2 ^b	D.P.S., 100:1	1.2×10^{-4}	8.5×10^{-3}	2.5×10^{-2}	8.5×10^{-2}

a Selected experimental results from Appendix A

b Selected experimental results from Appendix B

5.4.1 Comparison with the measurements by conventional settling column

The fall velocity distributions measured by the holographic technique can be compared with those measured by the conventional settling column (Appendices A and B). Fall velocity distributions from 26 settling column tests with different sludge samples are summarized in Appendix A. In these runs, sludge samples were mixed with artificial seawater to desired dilution ratios and stirred thoroughly for less than one minute before they were introduced into the settling column. In Appendix B, three different pre-mixing procedures (lasting for 15 *min*, Figure 1.1 in Appendix B) were used to mix sludge-seawater suspensions before settling column tests to study the effects of the initial mixing on the apparent fall velocity distributions. It was concluded that higher solids concentration and longer mixing time in general result in faster settling velocities.

The settling column experiments were performed at 11°C for the fall velocity distributions summarized in Table 5.4.1 and Figure 5.4.2 from Appendix A. For all runs in Appendix B as well as the settling measurements using holographic technique, the water temperature was about 22°C. Temperature can affect velocities indirectly through the dynamic viscosity μ , i.e. $w \propto \frac{1}{\mu}$ in Stokes' regime. The dynamic viscosity μ of seawater with salinity 34‰ is 0.013472 $g \text{ sec}^{-1} \text{ cm}^{-1}$ at 11°C and 0.010210 $g \text{ sec}^{-1} \text{ cm}^{-1}$ at 22°C (Riley and Skirrow, 1975). Hence, the fall velocities in Appendix A should be timed by a factor of 1.3 when compared with the others.

The median fall velocities measured by the conventional settling column for the D.P.S. (CSDOC) are from 1×10^{-3} to 2×10^{-2} cm/sec at 100:1 dilution and

2×10^{-4} to 2×10^{-3} *cm/sec* at 500:1 dilution in Appendix A, and are from 4×10^{-3} to 8.5×10^{-3} *cm/sec* at 100:1 dilution in Appendix B (Table 5.4.1). These velocities are generally about one order of magnitude higher than the median velocities measured by the holographic technique. Fall velocity distributions from several selected runs in Appendices A and B (Runs 5, 6, 7 and 9 from Appendix A and 1 and 2 from Appendix B) are plotted in Figure 5.4.2, and the distributions obtained using holographic technique are also included in the same graph for comparison. These larger fall velocities observed in conventional settling column experiments may be due to the particle coagulation during settling (suspended solids concentration as 40 to 250 *mg/l*), or convection currents inside the column, or both.

5.4.2 Comparison with measurements by Faisst (1976, 1980)

Faisst (1976, 1980) performed experiments to measure the fall velocity distributions for different sludges with conventional settling columns at $10.5 \pm 0.5^\circ C$. The results are summarized in Figure 5.4.3 and Table 2 in Appendix A. Again, the fall velocities measured by holographic technique are noticeably lower. The differences of the velocity distributions obtained from the two techniques decrease with the increasing dilution ratios in the settling column, which implies that particle coagulation inside the settling column is the main reason for these differences.

5.4.3 Comparison with measurements by Gibbs (1984)

Gibbs (1984) studied the settling velocity distributions for coagulated sludges (the New Jersey Middlesex sludge and the digested sludge from the City of Philadelphia) with a 1.5 *m* long settling tube. Sludge samples were diluted with pre-filtered

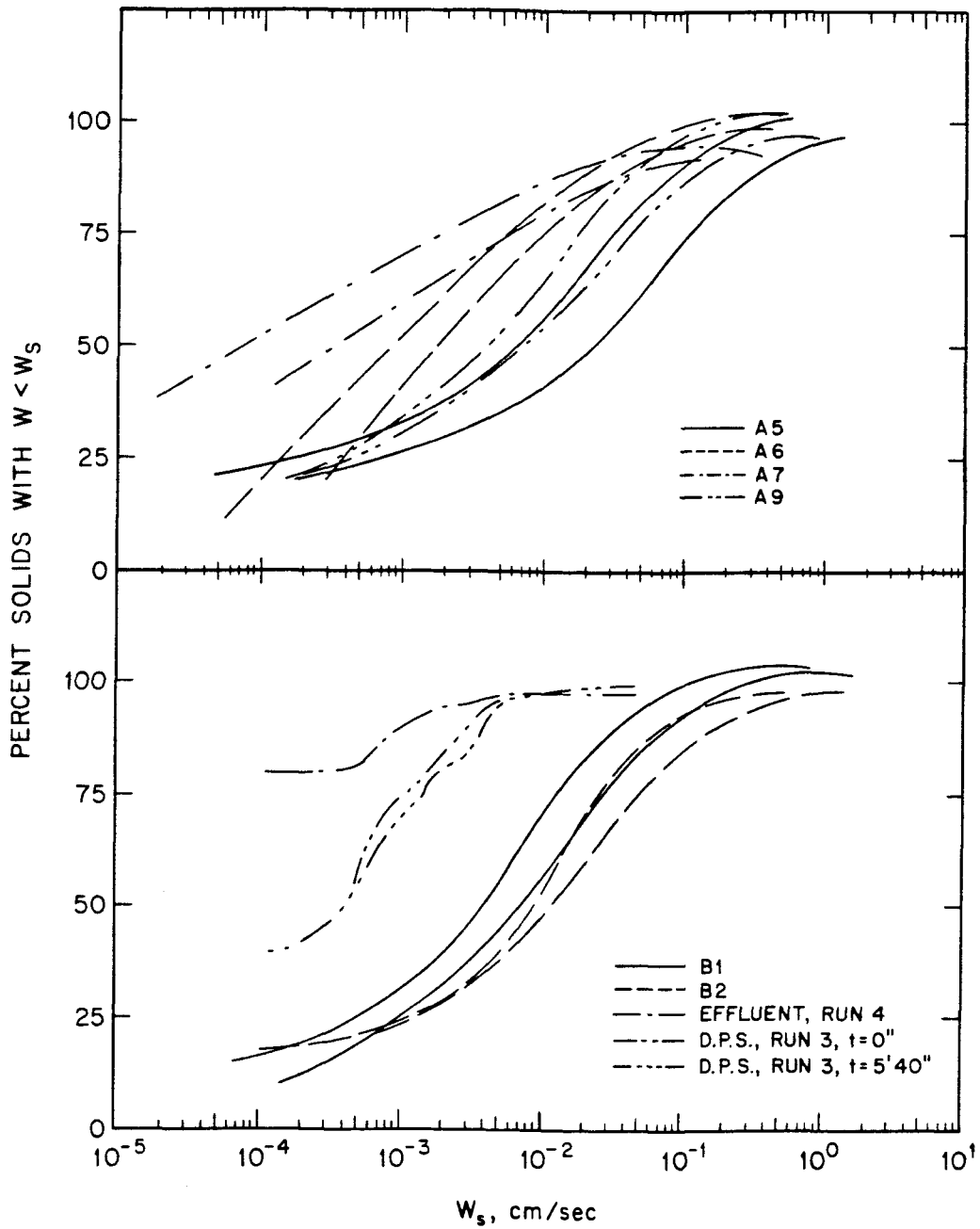


Figure 5.4.2 Settling velocity distributions of the D.P.S. (CSDOC) measured by the conventional settling column technique (each run has two lines representing the distributions measured at 60 and 120 cm from the bottom of the settling column): (a) selected results from Appendix A; (b) selected results from Appendix B compared with hologram results shown in Figure 5.4.1

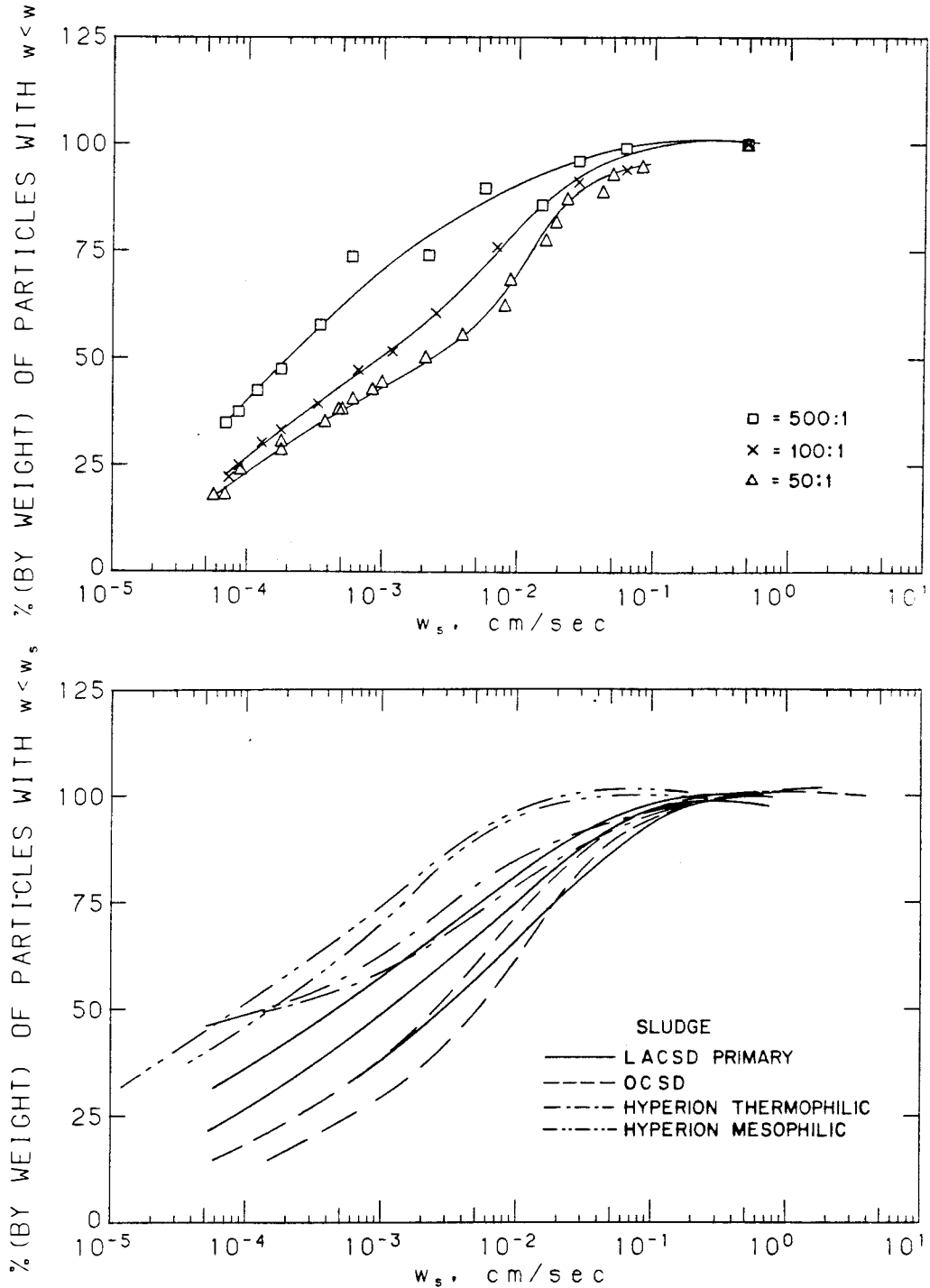


Figure 5.4.3 Settling velocity distributions for different sludge samples measured by Faisst (1976, 1980) with the settling column technique: (a) shallow column (2 l graduated cylinder), single-depth sampling at 15 cm below the surface; (b) tall column (171 cm), two-depth sampling at 30 and 90 cm from the bottom

seawater to a volume ratio from 0.002 to 0.009 (dilution from 500 to 110) and coagulated in a blade-type mixer at shear rate from 0 to 30 sec^{-1} to the equilibrium state when the size distributions stayed unchanged. The coagulated sludge samples were introduced from the top of the settling tube, and the mass of particles collected on a pan at the bottom of the tube was measured by an electrobalance at different times. The fall velocity distributions (Table 5.4.2) show median values ranging from 0.012 to 0.09.7 cm/sec for the Middlesex sludge and 0.056 to 0.13 cm/sec for the Philadelphia sludge, which are again significantly larger than those obtained in this study by as much as a factor of 100. Since the sludge particles measured in Gibb's experiment have been coagulated, they are larger in size and, therefore, should have faster fall velocities.

5.4.4 Comparison with the measurements by Ozturgut and Lavelle (1984)

Ozturgut and Lavelle (1984) derived the settling velocity distributions according to Stokes' law from the densities and sizes of sewage particles measured by experiments (see Sec 2.2.2). The sample used was the composite effluent from the Municipality of Metropolitan Seattle with suspended solids of 80 mg/l . The settling velocity distributions for particles smaller than 64 μm is shown in Figure 5.4.4. Particles larger than 64 μm (8.5 % by weight) are not included in this figure. Density measurement was performed only for the density range from 1.01 to 1.40 g/cm^3 . For particles with densities greater than 1.4 g/cm^3 (40 % by volume), two different densities were assumed in calculating fall velocities: 1.4 and 2.65 g/cm^3 .

If it is assumed that the larger particles have fall velocities larger than $5 \times 10^{-2} \text{ cm}/\text{sec}$ and the volume ratio is roughly proportional to the mass ratio, the

Table 5.4.2 Summary of the settling velocity distributions (by weight) for coagulated sludges: the New Jersey Middlesex sludge and the digested sludge from the City of Philadelphia by Gibbs (1984)

volume ratio	G <i>sec</i> ⁻¹	Settling velocity distribution, <i>cm/sec</i>		
		20%ile	Median	80%ile
A. New Jersey sludge				
0.005	0	8.9×10^{-2}	1.6×10^{-2}	3.4×10^{-2}
0.005	3	3.8×10^{-2}	9.7×10^{-2}	2.4×10^{-1}
0.005	6	1.0×10^{-2}	2.6×10^{-2}	6.8×10^{-2}
0.005	6	2.6×10^{-2}	5.1×10^{-2}	1.1×10^{-1}
0.005	9	3.7×10^{-2}	8.5×10^{-2}	1.7×10^{-1}
0.005	25	7.1×10^{-2}	1.2×10^{-2}	3.4×10^{-2}
0.005	30	2.9×10^{-2}	4.3×10^{-2}	7.3×10^{-2}
0.005	30	2.8×10^{-2}	4.0×10^{-2}	6.9×10^{-2}
0.007	30	2.2×10^{-2}	3.0×10^{-2}	4.6×10^{-2}
0.009	30	1.2×10^{-2}	1.8×10^{-2}	3.4×10^{-2}
B. Philadelphia sludge				
0.002	30	6.0×10^{-2}	9.9×10^{-2}	1.5×10^{-1}
0.003	30	5.4×10^{-2}	8.9×10^{-2}	1.7×10^{-1}
0.005	30	5.1×10^{-2}	1.3×10^{-1}	2.6×10^{-1}
0.007	30	3.4×10^{-2}	5.6×10^{-2}	9.7×10^{-2}
0.009	30	4.6×10^{-2}	9.3×10^{-2}	1.8×10^{-1}

median velocity is about 1.6×10^{-3} to 4.0×10^{-3} *cm/sec*, which is more than 10 times higher than that of the effluent from CSDLAC.

As mentioned in Sec. 2.2.2, a Coulter counter was used in their experiment to measure the volume of particles. A Coulter counter measures only the volume of the solid parts inside the flocs (Treweek and Morgan, 1977), hence underestimates the sizes of the flocs and their drag, and leads to calculated velocities which are too high. The possible breakage of particles during Coulter counter measurements can also introduce errors into size determination (Hunt, 1980; Gibbs, 1982). Finally, Ozturgut and Lavelle assumed that all particles are spherical in calculating the fall velocities for particles, while it is known that sewage particles are of very irregular shapes. Particles with the same density and volume, but different shape, may have different settling velocities.

5.4.5 Comparison with the measurements by Lavelle *et al* (1987)

Tennant *et al.* (1987) and Lavelle *et al.* (1987) adopted a similar two-stage experimental technique to determine settling velocities of sludge particles in seawater. Sludge particles were coagulated under controlled conditions that approximated a marine discharge site, and settling velocities were then measured in an environment where particle coagulation was curtailed by low solids concentration (≤ 10 *mg/l*).

They divided the experimental procedures into three steps: solids concentration measurements by filtration technique, size distribution measurements by sieve analysis, and separate settling velocity measurements for particles $> 63 \mu m$ and $< 63 \mu m$. The conventional settling column technique was used to measure settling velocities for coarse sludge particles ($> 63 \mu m$) in fresh water with initial concentration of ~ 200 *mg/l* and the test lasted for 15 *min*.

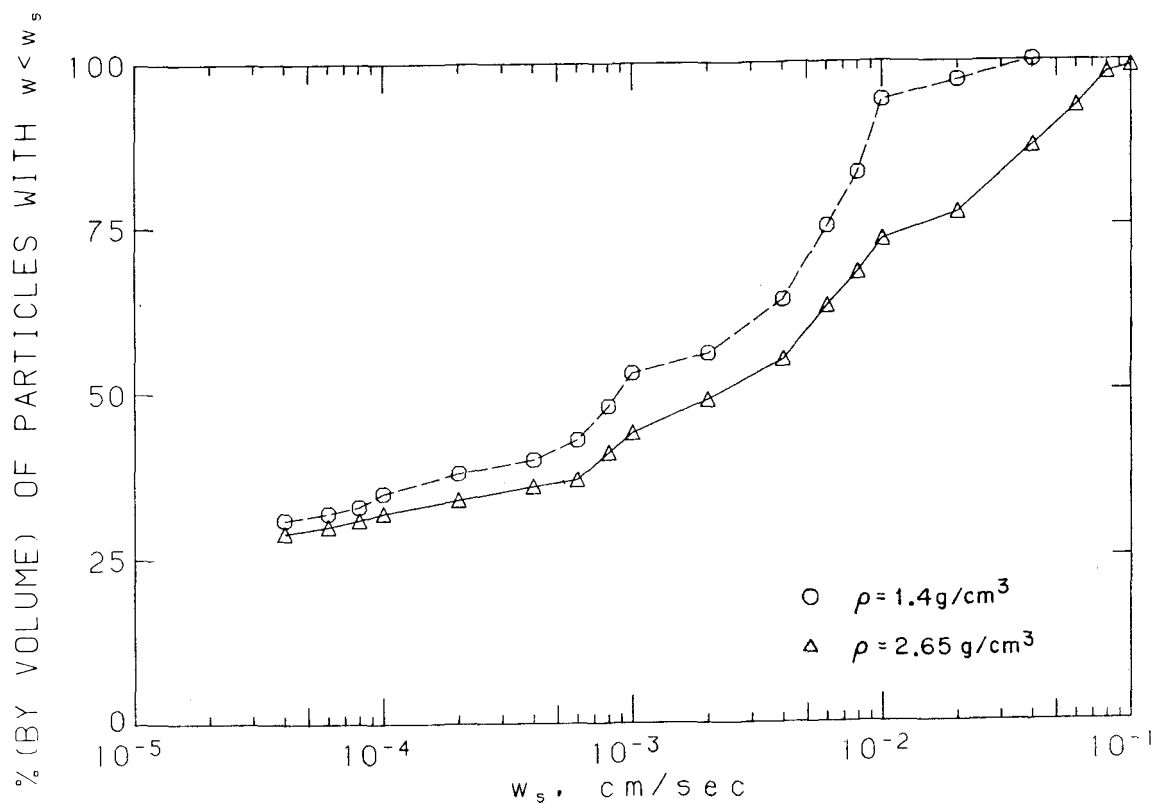


Figure 5.4.4 Settling velocity distribution ($d < 64 \mu m$) for the effluent sample from the Municipality of Metropolitan Seattle. This distribution is derived for settling velocities calculated according to Stokes' law with the measured densities and sizes of particles. The density of the heavy fraction (40% by volume), which is not measured, is assumed to be 1.4 g/cm^3 (O) and 2.65 g/cm^3 (Δ)(from Ozturgut and Lavelle, 1984)

For the fine fraction ($< 63 \mu m$), coagulation tests were performed inside a settling tube before settling velocities were measured. Sludge samples were placed in an empty settling tube, stirred with a magnetic stirrer at low speed when the water level was less than one-third of the height of the tube and with a perforated disk stirrer when the water level was higher. Filtered seawater was introduced into the settling tube to dilute the sludge samples in such a way as to produce a concentration of 500 mg/l within 2 min , 100 mg/l within 10 min , and 10 mg/l at the end of 30 min to simulate the mixing and dilution conditions at the discharge site. The settling tube was then transferred into a water bath ($24 \pm 0.02^\circ C$) and the sludge suspension was stirred overnight for temperature equilibration before starting the settling test. To start the settling experiment, the stirrer was stopped first and the sludge suspension was mixed gently with the disk stirrer. Settling velocity measurements basically followed the conventional settling column method for 24 hr , except that particle volume concentrations were measured for samples withdrawn from the tube by a Coulter counter instead of by gravimetric analysis.

Sludge samples from four treatment plants, West Point, Seattle; Hyperion, Los Angeles; Middlesex, New Jersey; Owls Head, New York, were analyzed in their experiments. The resulting settling velocity distributions for both coarse and fine fractions are shown in Figure 5.4.5. Particles with a diameter larger than $63 \mu m$ compose approximately 20 % by weight (18.9 % for West Point, 15.8 % for Hyperion, 14.6 % for Middlesex, and 47.3 % for Owls Head) of the sludge samples, and have a median velocity from 5×10^{-2} to $3 \times 10^{-1} \text{ cm/sec}$. The fine fraction of particles has a median velocity ranging from 8×10^{-4} to $2 \times 10^{-3} \text{ cm/sec}$. If both the coarse and fine fractions are considered, the median fall velocity ranges from 1×10^{-3} to $2 \times 10^{-2} \text{ cm/sec}$, and the 90 %ile is larger than $5 \times 10^{-2} \text{ cm/sec}$. Again, these

values are much higher than those observed in this study by about a factor of 10 based on all particle sizes.

In their coagulation process for the fine fraction of particles in sludge, the turbulent shear rate was not well defined and controlled. The coagulation time is much longer than that used in this study (370 *sec*) and particle concentrations as a function of coagulation time are much higher than those in our mixing experiment (Figure 3.1.9, 30 *mg/l* within 2 *min* and 10 *mg/l* at 6 *min*). Furthermore, their sludge samples were stirred overnight at a concentration of 10 *mg/l* before settling measurements, which might have induced more particle coagulation. In addition to the different characteristics of different sludges, this may explain the higher fall velocities observed in their study, since sludge particles had much more opportunity to coagulate and coagulated sludges have fast fall velocities.

5.4.6 Fractions of particles with fast settling velocities

Particles with large fall velocities in general would reach the sea bottom by settling within a relatively short period and tend to accumulate around the outfalls after discharge into the ocean. Slowly falling particles, for which settling is no longer the controlling transport process, can be diluted substantially and carried far away from the outfalls before they reach the ocean floor by diffusion. Hence, fast settling particles will cause stronger impact to the marine environment within a smaller region compared with slowly settling particles. The effects of an ocean discharge depend on the amount of particles in each category, so it is necessary to know the fractions of each in the discharged sludge or effluent mixture. The fractions (by mass or by volume) of particles with fall velocities larger than 0.01 *cm/sec* are summarized in Table 5.4.3 for the measurements performed in this study and the

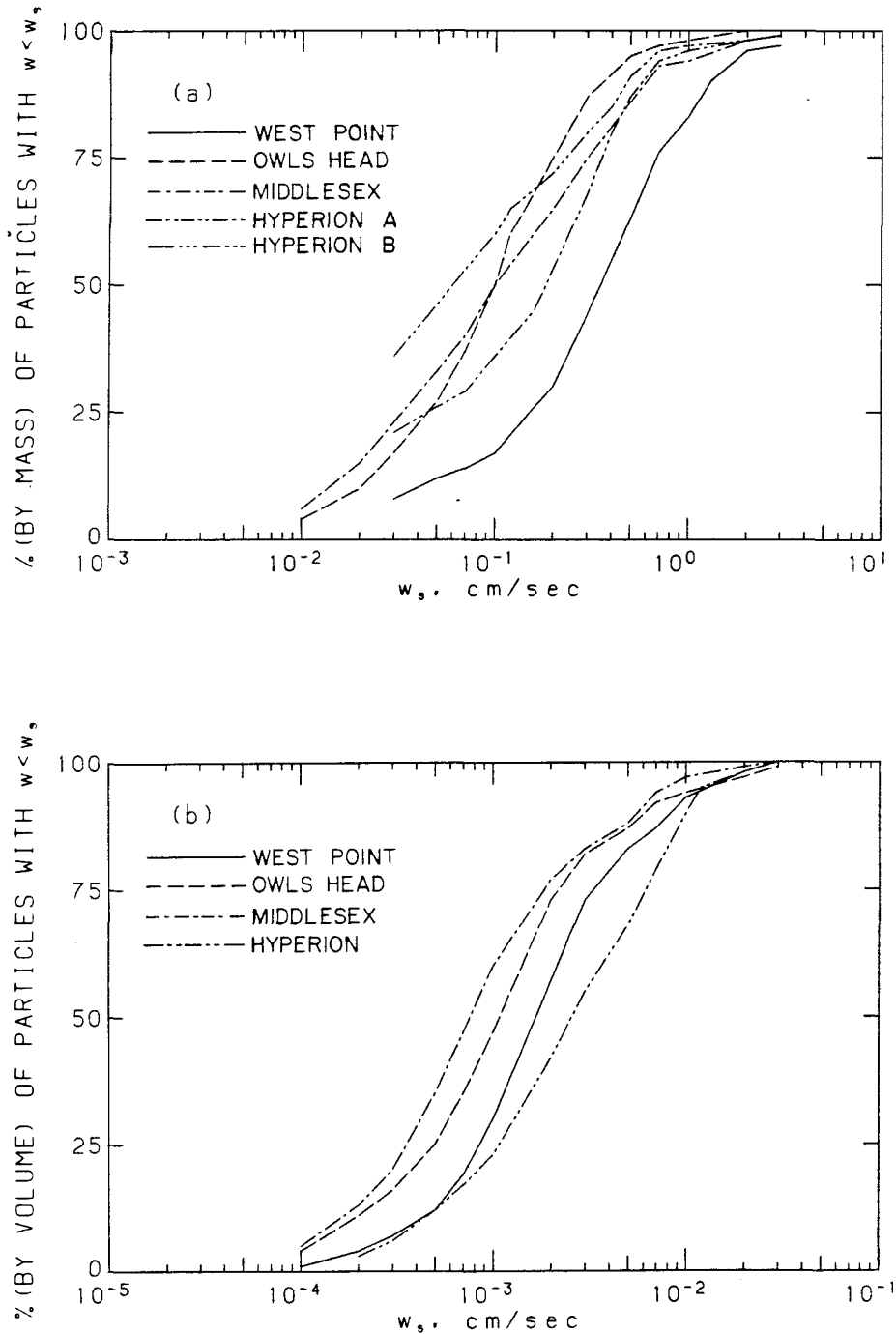


Figure 5.4.5 Settling velocity distributions for different sludges: (a) cumulative distributions by weight for the coarse fraction ($d > 63 \mu m$), (b) cumulative distributions by volume for the fine fraction ($d < 63 \mu m$) (from Lavelle *et al*, 1987)

related work by others. The fall velocity of 0.01 cm/sec (10 m/day) is chosen here as an indicator of the dividing line between fast and slow settling particles. The fractions of these fast settling particles are as low as 2 % in non-coagulated sludge samples (this study) and as high as 80 % in completely coagulated sludge samples (Gibbs, 1987).

5.5 Possible Field Application

The difficulties in faithfully simulating the particle coagulation for a discharge plume in the laboratory as well as the difficulties in preserving sample characteristics during transportation and storage bring the necessity for field observations. The holographic technique can be easily accommodated to measure particle size distributions in the field, but it is difficult to use it as an *in situ* method for measuring the fall velocity due to the lack of a stable platform.

A holographic camera system developed by O'Hern (1987) to study the concentration of cavitation nuclei in the ocean was applied to measurement of the particle size distributions above a sewage plume (O'Hern, 1987; O'Hern and Wang, forthcoming). Holograms were recorded at depths of 1, 3, 6, 12, 15, 21, 27, and 34 m at the location of the two CSDLAC sewage outfalls at Whites Point. In support of the holographic measurements, profiles of salinity, temperature and transmissivity were also measured. The number concentrations of particles increased dramatically at the same depth where the transmissivity decreased sharply ($\sim 25 \text{ m}$), indicating the upper edge of the submerged plume of sewage particles.

The measured number concentrations at the depth of 34 m were about $8 \times 10^3 \text{ cm}^{-3}$ for particles with diameter smaller than 20 μm and 250 cm^{-3} for particles with diameter between 20 and 100 μm . The particle number concentrations in the

Table 5.4.3 Summary of the fractions of particles with fall velocities larger than 0.01 *cm/sec* for different effluents and sludges

Sample description	Fractions
Measurements by the holographic technique	
for $d \geq 10 \mu m$:	
Run 1a—D.P.S., seawater	18 %
Run 1b—D.P.S., fresh water	13 %
Run 2—Effluent	7.0 %
Run 3—D.P.S., $t = 0''$	4.0 %
Run 3—D.P.S., $t = 5'40''$	4.3 %
Run 4—Effluent, $t = 4'30''$	9.0 %
for the entire sample:	
Run 3—D.P.S., $t = 0''$	2.4 %
Run 3—D.P.S., $t = 5'40''$	2.6 %
Run 4—Effluent, $t = 4'30''$	1.7 %
Measurements by the conventional settling column	
D.P.S. (CSDOC), 100:1 dilution	14 to 55 %
D.P.S. (CSDOC), 100:1 dilution, pre-mixed for 15 <i>min</i>	35 to 44 %
D.P.S. (CSDOC), 500:1 dilution	14 to 43 %
W.A.S. (CSDOC), 100:1 dilution	25 to 50 %
Mixture of 0.78 W.A.S. and 0.27 D.P.S. (CSDOC), 100:1 dilution	15 to 35 %
D.W.A.S. (CSDOC), 100:1 dilution	70 to 75 %
D.P.S. (CSDLAC), 100:1 dilution	30 to 37 %
D.P.S. (CSDLAC), 100:1 dilution, pre-mixed for 15 <i>min</i>	44 to 55 %
W.A.S. (CSDLAC), 100:1 dilution	50 to 60 %
Measurements by other researchers	
Faisst (1980):	
CSDLAC sludge, 50:1, 100:1, and 500:1 dilution	11 to 28 %
CSDOC sludge, 100:1 dilution	34 %
Hyperion thermophilic sludge, 100:1 dilution	20 %
Hyperion mesophilic sludge, 100:1 dilution	4 %
Gibbs (1984):	
New Jersey sludge, 111:1 to 200:1 dilution	≥ 80 %
Philadelphia sludge, 111:1 to 500:1 dilution	≥ 80 %
Ozturgut and Lavelle (1984):	
Effluent from the Municipality of Metropolitan Seattle	14 to 33 %
Lavelle <i>at al</i> (1987):	
Hyperion sludge	24 %
West Point sludge	24 %
Middlesex sludge	18 %
Owls Head sludge	50 %

water above the plume were similar to those obtained in the clean waters of the Long Point test site, which were about $2 \times 10^3 \text{ cm}^{-3}$ for particles with diameter smaller than $20 \mu\text{m}$, and from 20 to 90 cm^{-3} for particles with diameter between 20 and $100 \mu\text{m}$.

Size determinations by O'Hern's reconstruction system were obtained differently from those in this study. In his system, only a major and minor diameter were measured for non-circular objects. The volume was calculated by assuming either an ellipsoidal shape with the length of the third dimension as the geometric mean of the major and minor diameters, or a cylindrical shape with the base of the minor diameter and the height of the major diameter. The diameter of a sphere of equal volume was used as the diameter of particles in determining the size distributions.

The different definitions of particle sizes make it difficult to compare the size measurements from these two systems. Furthermore, the holograms were recorded in the field in August, 1985, while the plume mixing experiment with the effluent from CSDLAC was done in the laboratory in December, 1987. In the interim, plant improvements have reduced the effluent solids concentrations. There was no direct information on the suspended solids concentration of the effluent and the discharge flow rate at the precise time when the holograms were recorded, and, hence, direct comparisons of our results with the field data are difficult and will not be discussed here (for details see O'Hern and Wang, in preparation).

Applying the holographic system to determine settling velocities of particles in the field is much more difficult than size analysis, not only because it requires that the holographic equipment be completely isolated from the surface disturbances, but also because currents can cause the displacement of particles in addition to

settling. A holographic particle velocimeter was developed by Carder *et al.* (1982) to record *in situ* the sizes, shapes, orientations, and settling velocities of oceanic particles. His setup comprises a free-floating sediment trap equipped with an in-line holographic camera system to record holograms for particles falling into the sediment trap. Singly exposed holograms were recorded at preset time intervals. During reconstruction, coordinates relative to a reference point were determined for each particle and fall velocities were calculated from the measured displacements and time differences between two successive holograms.

This system is capable of measuring particle size from 15 to 250 μm , and fall velocity from 0.019 to 0.230 cm/sec . Densities of particles estimated from their settling velocities are from 1.37 to 5.10 g/cm^3 for the test done in the western Atlantic Ocean. These values are considerably higher than expected and may suggest that other processes, besides the settling, affect the movement of particles at the same time and the measured velocities are higher than the true fall velocities of particles.

This kind of submersible holographic system provides the *in situ* size distribution analysis and velocity measurement that are exempted from all the possible changes of sample characteristics due to sample collection. However, they require much more effort in design and construction and cost much more than a laboratory system of similar configuration. Once the instrument is lowered into the water, the performance of the system is so difficult to control that it may not record all the desired information. Working depth of the equipment is another concern. Hence, another possible field application without these difficulties is to bring the holographic camera system to a ship, to take samples from the ocean, and to record holograms for size distributions on board. However, it is still a big problem for fall velocity measurement due to the ship motion. With special caution in handling

samples, this method can minimize the changes of sample characteristic during sampling and avoid the aging of samples during transportation and storage.

6. SUMMARY AND CONCLUSION

6.1 Summary of Experimental Results

A new experimental technique for measuring fall velocities of sludge and effluent particles based on the holographic technique was developed in this study. Settling velocity distributions were derived from the size and velocity measurements using the holographic camera system. For sample processing before recording holograms for settling analysis, a small mixing tank was constructed to approximately simulate the dilution, mixing, and particle coagulation inside a discharge plume. Two marine outfall systems were selected for simulation: the proposed deep ocean sludge disposal outfall of the County Sanitation Districts of Orange County (CSDOC) and the existing effluent outfall system of the County Sanitation Districts of Los Angeles County (CSDLAC). Four sets of coagulation and settling experiments were performed with the digested primary sludge (D.P.S.) from CSDOC and the effluent mixture from CSDLAC. Important findings from this study are summarized in the following:

1. The holographic technique is feasible for determining the settling velocity and size distributions for particles larger than $10 \mu m$ for dilute suspensions of sludge or effluent at less than $2 mg/l$.
 - a) The effect of particle coagulation during the settling velocity measurements is eliminated by using samples of low particle concentration ($\leq 2 mg/l$).
 - b) The convection current induced by the temperature variation and by the act of introducing samples into the settling cell is minimized by a small density stratification ($\sim 0.07 m^{-1}$) of the water inside the settling cell.
 - c) The settling velocity range that can be measured by this holographic camera system is from 1×10^{-4} to $0.05 cm/sec$.
 - d) For size distribution measurements, measurable solids concentrations should be less than $0.5 mg/l$ for best results.
 - e) Multiple samples can be recorded on films within a short time for later analysis of the size distributions, which minimizes the possibility of changes of sample characteristics during storage.
 - f) The image analysis program, which provides detailed information on the size, shape, orientation and velocity of individual particles, improves the accuracy of measurements and saves considerably on the amount of time required for data analysis.

2. A laboratory apparatus (a continuous flow stirred tank reactor CFSTR) was designed to approximately simulate the mixing, dilution, and particle coagulation inside a discharge plume. The complicated structure of buoyant jets and the complex mechanics of coagulation cannot be reproduced by a

hydraulic model of a discharge plume. Therefore, a CFSTR was designed to produce the equivalent time history of particle concentration (or dilution) and energy dissipation rate. The dilution is very rapid at first, as in a turbulent plume, so that the concentration drops very quickly to low values. Mixing is simulated by a variable speed rotating paddle.

3. Results from the coagulation experiments show that the extent of coagulation of a mixing process depends on the time scale of mixing, and the time history of particle concentration and shear rate.

a) Under the simulated plume mixing conditions approximating the proposed sludge disposal for CSDOC (Run 3, 6'20'') and the existing effluent outfall for CSDLAC (Run 4, 4'30''), observed particle coagulation is small.

b) Significant coagulation is observed for sewage particles mixed by a magnetic stirrer at constant concentrations for a period of time as in Run 1 (D.P.S. from CSDOC, 250 *mg/l* for 20 *min*) and Run 2 (effluent mixture from CSDLAC, 2.82 *mg/l* for 25 *min*).

4. The settling characteristics, the relationships of particle size and fall velocity, are very similar for all the sewage and sludge particles measured in this study.

a) The trend of settling velocities versus diameter follows the Stokes' law: $w \propto d_{equ}^2$ but with considerable scattering.

b) The scatter patterns of data points shown on $w - d$ graphs from the settling measurements are similar for both the sludge and effluent samples. Data points cover a wide range of $A\Delta\rho$ from 0.002 to

0.5 g/cm^3 with the dominant value between 0.02 and 0.05 g/cm^3 , where A is a shape factor in Stokes' law (which is unity for spheres).

- c) For any given equivalent diameter, the corresponding fall velocities can vary by a factor of about 50. It suggests that the change in $A\Delta\rho$ is important for sludge and effluent particles.
5. The density of the settling medium (from 1.0056 to 1.0251 g/cm^3) does not alter significantly the settling velocities of the same sludge particles (Run 1, Figure 4.2.2 versus 4.2.6), which implies that sludge particles have very porous structures, and that the density of the solid parts is much higher than the density of both seawater and fresh water.
 6. The changes in the particle size distributions of samples diluted with artificial seawater after being stored for a certain period of time depend on both the particle concentration in the samples and the storage time.
 - a) The increase of settling velocity for diluted sludge samples with concentration from 0.5 to 2.5 mg/l stored for 1 to 6 days suggests that coagulation takes place during storage.
 - b) The size distributions remain practically unchanged for a diluted effluent sample (0.68 mg/l) stored for 36 hr.
 7. For particles larger than $10 \mu\text{m}$, the median fall velocity ranges from 0.0008 to 0.002 cm/sec for the digested primary sludge from CSDOC and from 0.001 to 0.0025 cm/sec for the effluent from CSDLAC. The 90-percentile velocity ranges from 0.004 to 0.013 cm/sec for the digested primary sludge from CSDOC and 0.007 to 0.008 cm/sec for the effluent (CSDLAC) (Table 5.4.1).

8. When all particles are considered, including those of equivalent diameter smaller than $10 \mu m$, the median fall velocity is 0.0004 cm/sec for the digested primary sludge from CSDOC and less than 0.0001 cm/sec for the effluent from CSDLAC. The 90-percentile velocity is from 0.002 to 0.004 cm/sec for the D.P.S. (CSDOC) and 0.001 cm/sec for the effluent (CSDLAC) (Table 5.4.1).
9. For particles larger than $10 \mu m$, the particles with settling velocity larger than 0.01 cm/sec account for 4 to 18 % by volume for the digested primary sludge from CSDOC and 7 to 9 % for the effluent from CSDLAC. For the entire sample, the mass fraction of the particles with fall velocity greater than 0.01 cm/sec is about 2.4 % for digested primary sludge from CSDOC and 1.7 % for the effluent (CSDLAC) (Table 5.4.3).

6.2 Recommendations for Future Work

6.2.1 Research

The settling characteristics (w vs. d) and the fall velocity distributions of the effluent and sludge particles depend on—among other things—the type of sewages, the treatment processes, and the discharging conditions. This study was based on two special kinds of sewage particles under special mixing conditions. Hence, the results may not be directly applicable to other sewage disposal systems. The fall velocity distributions of different sewage particles under different discharging conditions can be quite different and need to be studied on a case-by-case basis.

In this study, the simulation of the coagulation process inside a discharge plume is only a crude approximation. Among the many factors that affect the coagulation

process inside the discharge plume, only the coagulation time and the representative time history of particle concentration and turbulent shear were approximately simulated; however, these factors vary considerably from the center to the edge of the plume, making the validity of an overall plume description uncertain. Laboratory experiments that can simulate the mixing conditions more faithfully should be conducted to provide a better understanding of the coagulation process before performing field observations at a discharge site.

Furthermore, the presence of natural particles in the ocean was not considered in this study. These natural particles may interact with sewage particles and change the coagulation process and the settling characteristics of sewage particles. Hence, the effect of natural particles on the coagulation and settling of sewage particles should be studied in the future.

6.2.2 Improvements of the experimental technique

The present holographic camera system has a resolution limit of about $10 \mu m$ and the measurement errors increase dramatically near this limit (10 % in d_{equ}). The setup for fall velocity determination puts constraints on the measurable velocity range of 1×10^{-4} to 0.05 cm/sec . It takes two days to record the holograms for the fall velocity analysis, so the aging of samples becomes a serious concern. This setup also makes the derivation of fall velocity distributions complicated: several assumptions have to be made in calculating the distributions. Possible improvements of the experimental setup and procedures are summarized as follows.

Using lasers of higher power, or films of higher speed, or both, can decrease the exposure time in recording, hence, enable one to record fast moving particles.

An electronic shutter or pulse laser can be used for precisely controlling the exposure time and the time between double exposures on the same film. Also, the spatial resolution of the imaging devices, such as video camera, digitizing board and recording film can be increased to obtain sharper, clearer pictures. However, one has to note that the accuracy of size and velocity measurements for the effluent and sludge particles is not limited by that of the optical system, but is controlled by the sample preparation, handling and storage. Hence, the improvements of the experimental technique should be focused on developing better ways to prepare and preserve samples.

REFERENCES

- Argaman, Y. and W. J. Kaufman. 1970. Turbulence and flocculation. Journal of the Sanitary Engineering Division, Proceedings of the American Society of Civil Engineering, 96, SA2, 223-240.
- Batchelor, G. K. 1951. Pressure fluctuations in isotropic turbulence. Proc. Camb. Phil. Soc., 47, 359-374.
- Belz, R. A. and R. W. Menzel. 1979. Particle field holography at Arnold Engineering Development Center. Optical Engineering, 18, 3, 256-265.
- Bexon, R. 1973. Magnification in aerosol sizing by holography. Journal of Physics E : Scientific Instruments, 6, 245-248.
- Bexon, R., J. Gibbs, and G. D. Bishop. 1976. Automatic assessment of aerosol holograms. Journal of Aerosol Science, 7, 397-407.
- Birkner, F. B. and J. J. Morgan. 1968. Polymer flocculation kinetics of diluted colloidal suspension. Journal of the American Water Works Association, 60, 175-191.
- Boettner, E. A. and B. J. Thompson. 1973. Multiple exposure holography of moving fibrous particulate matter in the respiratory range. Optical Engineering, 12, 2, 56-59.
- Bradley, R. A. and R. B. Krone. 1971. Shearing effects on settling of activated sludge. Journal of the Sanitary Engineering Division, Proceedings of the American Society of Civil Engineering, 97, SA1, 59-79.
- Brenden, B. B. 1981. Miniature multiple-pulse Q-switched ruby laser holocamera for aerosol analysis. Optical Engineering, 20, 6, 907-911.
- Brooks, N. H. 1956. Memorandum to Hyperion Engineers on settling analyses of sewage effluents. July 5, 1956, 8 pp. Pasadena, California.

- Brooks, N. H., R. G. Arnold, R. C. Y. Koh, G. A. Jackson, and W. K. Faisst. 1985. Deep ocean disposal of sewage sludge off Orange County, California: a research plan. 2nd Ed. EQL report No. 21/2, Environmental Quality Laboratory, California Institute of Technology, Pasadena, California, 82 pp.
- Carder, K. L. 1979. Holographic microvelocimeter for use in studying ocean particle dynamics. Optical Engineering, 18, 5, 524-525.
- Carder, K. L. and D. J. Meyers. 1980. Holography of settling particles: shape parameters. Optical Engineering, 19, 5, 734-738.
- Carder, K. L., R. G. Steward, and P. R. Betzer. 1982. In situ holographic measurements of the sizes and settling rates of oceanic particulates. Journal of Geophysical Research, 87, C8, 5681-5685.
- Cartwright, S. L., P. Dunn, and B. J. Thompson. 1980. Particle sizing using far-field holography: new developments. Optical Engineering, 19, 5, 727-733.
- Caulfield, H. J., Ed. 1979. Handbook of Optical Holography. Academic Press, New York, New York, 638 pp.
- Chase, R. R. P. 1979. Settling behavior of natural aquatic particulates. Limnol. Oceanogr., 24, 3, 417-426.
- Clark, M. M. 1985. Critique of Camp and Stein's RMS velocity gradient. Journal of Environmental Engineering, 111, 6, 741-754.
- Cleasby, J. L. 1984. Is velocity gradient a valid turbulent flocculation parameter? Journal of Environmental Engineering, 110, 5, 875-897.
- Collier, R. J., C. B. Burckhardt, and L. H. Lin. 1971. Optical Holography. Academic Press, New York, New York, 605 pp.
- Delichatsios, M. A. and R. F. Probstein. 1975. Coagulation in turbulent flow: theory and experiment. Journal of Colloid and Interface Science, 51, 3, 394-405.
- Dubois, M., K. A. Gilles, J. K. Hamilton, P. A. Rebers and F. Smith. 1956. Colorimeter method for determination of sugars and related substances. Analytical Chemistry, 28, 350-356.
- Duedall, I. W., B. H. Ketchum, P. K. Park and D. R. Kester, Eds. 1983. Waste in the Ocean. vol. 1. Industrial and Sewage Wastes in the Ocean. John Wiley & Sons, New York, New York, 431 pp.

- Dyes, W. A., P. F. Kellen, and E. C. Klaubert. 1970. Velocity synchronized Fourier transform hologram camera system. Applied Optics, 9, 5, 1105-1112.
- Eastman Kodak Company. 1976. Kodak holographic plate, type 120-02 and Kodak holographic film (easter base) SO-173. Kodak Pamphlet No. P-311, Eastman Kodak Company, Rochester, New York, 4 pp.
- Eastman Kodak Company. Kodak high speed holographic film SO-253 (easter base) and special plates, type 131-01 and 131-02. Preliminary data, Eastman Kodak Company, Rochester, New York, 4 pp.
- Eastman Kodak Company. 1984. Characteristics of Kodak plates for scientific and technical applications. Kodak Publication No. P-140, Eastman Kodak Company, Rochester, New York.
- Ewan, B. C. R. 1979a. Holographic particle velocity measurement in the Fraunhofer plane. Applied Optics, 18, 5, 623-626.
- Ewan, B. C. R. 1979b. Particle velocity distribution measurement by holography. Applied Optics, 18, 8, 3156-3160.
- Faisst, W. K. 1976. Digested sewage sludge: characterization of a residual and modeling for its disposal in the ocean off Southern California. EQL Report No.13, Environmental Quality Laboratory, California Institute of Technology, Pasadena, California, 193 pp.
- Faisst, W. K. 1980. Coagulation of particulate in digested sludge. In *Particulate in Water: Characterization, Fate, Effects and Removal*. M. C. Kavanaugh and J. O. Leckie, Eds., *Advances in Chemistry Series 189*, American Chemical Society, Washington D. C., 259-282.
- Farley, K. J. 1984. Sorption and sedimentation as mechanisms of trace metal removal. Ph.D. Thesis, Massachusetts Institute of Technology, Cambridge, Massachusetts, 125 pp.
- Farley, K. J. and F. M. M. Morel. 1986. Role of coagulation in the kinetics of sedimentation. Environmental Science and Technology, 20, 2, 187-195.
- Fischer, H. B., E. J. List, R. C. Y. Koh, J. Imberger, and N. H. Brooks. 1979. *Mixing in Inland and Coastal Waters*. Academic Press, New York. 483 pp.

- Friedlander, S. K. 1977. *Smoke, Dust, and Haze*. Wiley-Interscience, New York, 317 pp.
- Fourney, M. E., J. H. Matkin, and A. P. Waggoner. 1969. Aerosol size and velocity determination via holography. Review of Scientific Instruments, 40, 2, 205–213.
- Foust, A. S., L. A. Wenzel, C. W. Clump, L. Maus, and L. Andersen. 1980. *Principles of Unit Operations*. John Wiley & Sons, New York, 768 pp.
- Gibbs, R. J. 1982. Particle dynamics of sewage sludge dumping in the ocean. In *Marine Pollution Paper Ocean'82*, Washington, D.C., 1058–1061.
- Gibbs, R. J. 1982. Floc stability during Coulter Counter size analysis. Journal of Sedimentary Petrology, 52, 2, 657–660.
- Gibbs, R. J. and M. J. Hopkins. 1984a. Effects of solids concentration and turbulence upon the coagulation rate of sewage sludge in seawater. In annual report to Office of Marine Pollution Assessment NOAA on particle dynamics of sewage sludge dumping in the ocean, R. J. Gibbs, Center for Colloidal Science, University of Delaware, Newark, Delaware.
- Gibbs, R. J. and M. J. Hopkins. 1984b. Equilibrium time and floc size of sewage sludge coagulated in sea water. In annual report to Office of Marine Pollution Assessment NOAA on particle dynamics of sewage sludge dumping in the ocean, R. J. Gibbs, Center for Colloidal Science, University of Delaware, Newark, Delaware.
- Gibbs, R. J. 1984. Particle dynamics of sewage sludge dumping in the ocean. annual report to Office of Marine Pollution Assessment NOAA, Center for Colloidal Science, University of Delaware, Newark, Delaware.
- Gladden, J. W. and R. D. Leighty. 1979. Recording Media. In *Handbook of Optical Holography*, H. J. Caulfield, Ed., Academic Press, New York, New York, 299–346.
- Günkel A. A. and M. E. Weber. 1975. Flow phenomena in stirred tanks. AIChE Journal, 21, 5, 931–946.
- Hausmann G. and W. Lauterborn. 1980. Determination of size and position of fast moving gas bubbles in liquids by digital 3-D image processing of hologram reconstructions. Applied Optics, 19, 20, 3529–3535.

- Herring, J. R. 1980. Wastewater particle dispersion in the Southern California offshore region. In *Particulate in Water: Characterization, Fate, Effects and Removal*. M. C. Kavanaugh and J. O. Leckie, Eds., *Advances in Chemistry Series 189*, American Chemical Society, Washington D. C., 283-304.
- Hidy, G. M. and J. R. Brock. 1970. *The Dynamics of Aerocolloidal Systems. The international reviews in aerosol physics and chemistry, volume 1*. Pergamon Press, Oxford. 379 pp.
- Hinze, J. O. 1975. *Turbulence*. McGraw-Hill Book Company, New York. 790 pp.
- Hopfinger, E. J. and J. A. Toly. 1976. Spatially decaying turbulence and its relation to mixing across density interfaces. *Journal of Fluid Mechanics*, 78, 1, 155-175.
- Hossain, M. S. and W. Rodi. 1982. A turbulence model for buoyant flows and its application to vertical buoyant jets. In *Turbulent Buoyant Jets and Plumes*. W. Rodi, Ed., Pergamon Press, New York, 121-179.
- Hunt, J. R. 1980. Coagulation in continuous particle size distributions; theory and experimental verification. Report No. AC-5-80, W. M. Keck Laboratory of Environmental Engineering Science, California Institute of Technology, Pasadena, California, 126 pp.
- Hunt, J. R. and J. D. Pandya. 1984. Sewage sludge coagulation and settling in seawater. *Environmental Science and Technology*, 18, 119-121.
- Ives, K. J. 1977. Experimental methods (2). In *The Scientific Basis of Flocculation*, part 1, K. J. Ives, Ed., Sijthoff and Noordhoff, Alphen an den Rijn, the Netherlands.
- Jackson, G. A. 1982. Sludge disposal in Southern California Basins. *Environmental Science and Technology*, 16, 11, 746-757.
- Kajihara, M. 1971. Settling velocity and porosity of large suspended particle. *Journal of the Oceanographical Society of Japan*, 27, 4, 158-162.
- Kavanaugh, M. C. and J. O. Leckie. Eds. 1980. *Particulates in Water, Characteristic, Fate, Effects and Removal*. American Chemical Society, Washington, D.C., 410 pp.
- Kawana, K. and T. Tanimoto. 1979. Suspended particles near the bottom in Osaka Bay. *Journal of the Oceanographical Society of Japan*, 35, 75-81.

- Koh, R. C. Y. 1982. Initial sedimentation of waste particulates discharged from ocean outfalls. Environmental Science and Technology, 16, 757–763.
- Koh, R. C. Y. 1983. Wastewater field thickness and initial dilution. Journal of Hydraulic Engineering, 16, 9, 1232–1240.
- Kurtz, R. L., H. Liu, and R. B. Owen. 1979. Holographic System. In Handbook of Optical Holography. H. J. Caulfield, Ed., Academic Press, New York, New York, 299–346.
- Lagvankar, A. L. and R. S. Gemmell. 1968. A size-density relationship for flocs. Journal of the American Water Works Association, 60, 9, 1040–1046.
- Lavelle, J. W., E. Ozturgut, E. T. Baker, D. Tennant, and S. Walker. 1987. Settling speeds of sewage sludge in seawater. Submitted for publication.
- Leentvaar, J. and T. S. J. Ywema. 1979. Some dimensionless parameters of impeller power in coagulation-flocculation processes. Water Research, 14, 135–140.
- Leentvaar, J. and M. Rebhun. 1983. Strength of ferric hydroxide flocs. Water Research, 17, 8, 895–902.
- Levins, D. M. and J. R. Glastonbury. 1972. Particle-liquid hydrodynamics and mass transfer in a stirred vessel, Part I—Particle-liquid motion. Trans. Inst. Chem. Engrs, 50, 32–41.
- Linden, P. F. 1971. Salt fingers in the presence of grid-generated turbulence. Journal of Fluid Mechanics, 49, 3, 611–624.
- List, E. J. and J. J. Morgan. 1984. Particle coagulation and ocean turbulence research. Report to Office of Ocean Assessment, National Ocean and Atmosphere Administration. Environmental Engineering Science, California Institute of Technology, Pasadena, California.
- Lo, T. Y. R. and W. J. Weber, Jr. 1984. Flocculent settling in quiescent system. Journal of Environmental Engineering Division, Proceedings of the American Society of Civil Engineering, 110, 174–189.
- Malyak, P. H. and B. J. Thompson. 1984. Particle displacement and velocity measurement using holography. Optical Engineering, 23, 5, 567–576.
- McLaughlin, R. T. 1958. On the mechanics of sedimentation in Artificial Basins. Ph.D. Thesis, California Institute of Technology, Pasadena, California, 196 pp.

- McLaughlin, R. T. 1959. The settling properties of suspensions. Journal of the Hydraulics Division, The American Society of Civil Engineering, 85, HY12, 9-41.
- Morel, F. M. M., J. C. Westall, C. R. O'Melia, and J. J. Morgan. 1975. The fate of trace metals in Los Angeles County wastewater discharge. Environmental Science and Technology, 9, 8, 756-761.
- Morel, F. M. M. and S. L. Schiff. 1983. Geochemistry of municipal waste in coastal waters. In Ocean Disposal of Municipal Wastewater: Impacts on the Coastal Environment. E. P. Myers, Ed., Sea Grant College Program, Massachusetts Institute of Technology, Cambridge, Massachusetts, 248-421.
- Myers, E. P. 1974. The concentration and isotopic composition of carbon in marine sediments affected by a sewage discharge. Ph.D. Thesis. California Institute of Technology, Pasadena, California, 179 pp.
- National Research Council, Board on Ocean Science and Policy, Commission on Physical Science, Mathematics, and Resources. 1984. Disposal of industrial and domestic wastes: land and sea alternatives. National Academy Press, Washington, D.C., 210 pp.
- O'Hern, T. J. 1987. Cavitation inception scale effects. I. Nuclei distributions in natural waters. II. Cavitation inception in a turbulent shear flow. Ph.D. Thesis. California Institute of Technology, Pasadena, California. 311 pp.
- O'Hern, T. J. and T. R. Wang. *In situ* holographic measurements of marine particle size distributions in a sewage plume. (in preparation).
- O'Shea, D. C., W. R. Callen, and W. T. Rhodes. 1978. Introduction to Lasers and Their Application. Addison-Wesley Publishing Company, Reading, Massachusetts, 276 pp.
- Ozturgut, E. and J. W. Lavelle. 1984. New method of wet density and settling determination for wastewater effluent. Environmental Science and Technology, 18, 947-952.
- Ozturgut, E. and J. W. Lavelle. 1986. Settling analysis of fine sedimentation in salt water at concentrations low enough to produce flocculation. Marine Geology, 69, 353-362.

- Papanicolaou, P. N. 1984. Mass and momentum transport in a turbulent buoyant vertical axisymmetric jet. Ph.D. Thesis. California Institute of Technology, Pasadena, California. 281 pp.
- Parker, D. S., W. J. Kaufman, and D. Jenkins. 1972. Floc breakup in turbulent flocculation process. Journal of the Sanitary Engineering Division, Proceedings of the American Society of Civil Engineering, 98, SA1, 79-99.
- Pavlou, S. P. and R. N. Dexter. 1979. Distribution of Polychlorinated Biphenyls (PCB) in estuarine ecosystem. Testing the concept of equilibrium partitioning in the marine environment. Environmental Science and Technology, 13, 1, 65-71.
- Payne, P. R., K. L. Carder, and R. G. Steward. 1984. Image analysis techniques for holograms of dynamic oceanic particles. Applied Optics, 23, 2, 204-210.
- Peterson L. L. 1974. The propagation of sunlight and the size distribution of suspended particles in a municipally polluted ocean water. Ph.D. Thesis. California Institute of Technology, Pasadena, California. 174 pp.
- Riley, J. P. and G. Skirrow. 1965. Chemical Oceanography. Academic Press, New York. vol. 1.
- Riley, J. P. and G. Skirrow. 1975. Chemical Oceanography. Academic Press, New York. vol. 2, 2nd ed.
- Rushton J. H., E. W. Costich, and H. J. Everett. 1950. Power characteristics of mixing impellers Part II. Chemical Engineering Progress, 46, 9, 467-404.
- Saffman, P. G. and J. S. Turner. 1956. On the collision of drops in the turbulent clouds. Journal of Fluid Mechanics, 1, 16-30.
- Schwartzberg H. G. and R. E. Treybal. 1968. Fluid and particle motion in turbulent stirred tanks. I&EC Fundamentals, 7, 1, 1-12.
- Stanton, A. C., H. J. Caulfield, and G. W. Stewart. 1984. An approach for automated analysis of particle hologram. Optical Engineering, 23, 5, 577-582.
- Stumm, W. and J. J. Morgan. 1981. Aquatic Chemistry. 2nd Ed. Wiley-interscience, New York, 780 pp.
- Tambo, N. and Y. Watanabe. 1979. Physical characteristics of flocs-I. the floc density function and aluminum floc. Water Research, 13, 409-419.

- Tambo, N. and H. Hozumi. 1979. Physical characteristics of flocs—II. strength of floc. Water Research, 13, 421–427.
- Tennant, D. A., S. L. Walker, J. W. Lavelle, and E. T. Baker. 1987. A practical manual for determining settling rates of ocean disposed sewage sludge. NOAA Technical Memorandum ERL PMEL-69, Pacific Marine Environmental Laboratory, Seattle, Washington, 29 pp.
- Tennekes, H. and J. L. Lumley. 1972. A First Course in Turbulence. The MIT Press, Cambridge, Massachusetts, 300 pp.
- Thomas, D. G. 1964. Turbulent disruption of flocs in small particle size suspensions. A.I.Ch.E. Journal, 10, 4, 517–523.
- Thompson, B. J., J. H. Ward, and W. R. Zinky. 1967. Application of hologram techniques for particle size analysis. Applied Optics, 6, 3, 519–526.
- Thompson, B. J. 1974. Holographic particle sizing technique. Journal of Physics E: Scientific Instruments, 7, 781–788.
- Thompson, B. J. 1979. Fraunhofer Holograms. In Handbook of Optical Holography. H. J. Caulfield, Ed., Academic Press, New York, New York, 157–163.
- Thompson, B. J. and P. Dunn. 1980. Advances in far-field holography—theory and application. Proc. SPIE, 215, 102–111.
- Thompson, S. M. and J. S. Turner. 1975. Mixing across an interface due to turbulence generated by an oscillating grid. Journal of Fluid Mechanics, 67, 2, 155–175.
- Tomi, D. T. and D. F. Bagster. 1978a. The behavior of aggregates in stirred vessels, Part I—theoretical considerations on the effect of agitation. Trans IChemE, 56, 1–8.
- Tomi, D. T. and D. F. Bagster. 1978b. The behavior of aggregates in stirred vessels, Part II—an experimental study of the flocculation of Galena in a stirred tank. Trans IChemE, 56, 9–18.
- Treweek, G. P. and J. J. Morgan. 1977. Size distributions of flocculated particles: application of electronic particle counters. Environmental Science and Technology, 11, 7, 707–714.
- Trolinger, J. D., W. M. Farmer, and R. A. Belz. 1968. Multiple exposure holography of time varying three-dimensional fields. Applied Optics, 7, 8, 1640–1641.

- Trolinger, J. D., R. A. Belz, and W. M. Farmer. 1969. Holographic techniques for the study of dynamic particle field. Applied Optics, 8, 5, 957-961.
- Trolinger, J. D. Particle field holography. 1975. Optical Engineering, 14, 5, 383-392.
- Valioulis, I. A. 1983. Particle collision and coalescence in fluids. Report No. KH-R-44, W. M. Keck Laboratory of Hydraulics and Water Resources, California Institute of Technology, Pasadena, California, 239 pp.
- Valioulis, I. A. and E. J. List. 1984. A numerical evaluation of the stochastic completeness of the kinetic coagulation equation. Journal of the Atmospheric Sciences, 41, 16, 2516-2529.
- van Duuren, F. A. 1968. Defined velocity gradient model flocculator. Journal of the Sanitary Engineering Division, Proceedings of the American Society of Civil Engineering, 94, SA4, 223-240.
- Wang, R. T., R. C. Y. Koh, and N. H. Brooks. 1984. Interpretation of sludge sedimentation measurements. In *Oceanic Processes in Marine Pollution*, vol. 6, Physical and Chemical Processes: Transport and Transformation, D.J. Baumgartner and I. W. Duedal, Eds. Krieger Publishing Company, Malabar, Florida (in press).
- Witherow, W. K. 1979. A high resolution holographic particle sizing system. Optical Engineering, 18, 3, 249-255.
- Wright, S. J. 1977. Effects of ambient crossflows and density stratification on the characteristic behavior of round turbulent buoyant jets. Report No. KH-R-36, W. M. Keck Laboratory of Hydraulic and Water Resources, Division of Engineering and Applied Science, California Institute of Technology, Pasadena, California, 254 pp.
- Wright, S. J. 1984. Buoyant jets in density-stratified crossflow. Journal of the Hydraulics Division, the American Society of Civil Engineering, 110, 5, 643-657.
- Yamate, G. and J. D. Stockham. 1979. Sizing particles using the microscope. In *Particle Size Analysis*, J. D. Stockham and E. G. Fochtman, Eds., Ann Arbor Science Publishing Inc., Ann Arbor, Michigan, 23-33.

Appendix A

Interpretation of Settling Column Measurements of Sludge

Theresa R. Wang, Robert C. Y. Koh and Norman H. Brooks

Environmental Quality Laboratory
California Institute of Technology
Pasadena, California

Abstract

1. Introduction
2. Experiment
 - 2.1 Materials and Methods
 - 2.2 Experimental Results and Discussion
3. Conceptual Model
 - 3.1 Description and Assumptions
 - 3.2 Governing Equations
 - 3.3 Solution Techniques
 - 3.4 Results and Discussion of the Conceptual Model
4. Comparison between Experiments and Model Predictions
 - 4.1 Comparison with Results from Couette-flow Reactor
 - 4.2 Comparison with Present Experimental Work
5. Summary and Conclusions

Acknowledgements

References

ABSTRACT

When sewage sludge is mixed with seawater at dilutions of 100:1 or 500:1, particle coagulation and settling occur simultaneously. If the suspension is placed in a standard sedimentation column used for measuring fall velocity distributions, the results cannot be interpreted as a fall velocity distribution if coagulation is significant.

This paper presents laboratory measurements for 26 tests of various sludges diluted in artificial seawater with results expressed as fall velocity distributions. A simple conceptual model of the combined processes of particle settling and coagulation demonstrates that it is not possible to separate these processes by analysis of sedimentation column data alone. The reason is that a multiplicity of different assumptions regarding settling and coagulation can lead to results which all agree reasonably with the measured data (concentration versus time at a fixed depth in the column).

The purpose of the conceptual model is to help illustrate why a unique interpretation is not possible. To determine settling rates correctly, a direct *in situ* measurement of particle velocity must be used (such as laser holography).

1. INTRODUCTION

The settling column is used extensively as an apparatus to measure fall-velocity distributions for various kinds of particles. The traditional way of data interpretation, which represents the results as a distribution curve of settling velocity, is valid only for nonflocculating particles. Interactions between settling and coagulation obscure the results when this technique is applied to coagulating particles such as sewage sludge. When samples are taken at a single depth in the column, the relative effects of particle settling and coagulation cannot be differentiated because the settling velocities are modified by coagulation between particles during the test. Despite the difficulties, results from a set of settling tests are still useful for comparison purposes. Such tests have been conducted for different types of sewage sludges from Plant No. 1 of the County Sanitation Districts of Orange County (CSDOC) and the Joint Water Pollution Control Plant of the County Sanitation Districts of Los Angeles County (CSDLAC).

The experimental results are first presented by the conventional method, that is, the apparent fall-velocity distributions, to permit comparison among them and with previous measurements (Faisst, 1976,1980). They are then used as examples to our conceptual model to show the non-uniqueness in possible data interpretations.

A simplified mathematical model including settling, coagulation and vertical diffusion is derived to demonstrate various ways to interpret the data. As is discussed in this chapter, either pure settling in association with a wide range of settling velocities or an n^{th} order coagulation together with a single fall velocity

can generate distribution curves of the same observed shape. Thus, it can be seen that there is not a unique method of interpreting data from a conventional settling column to give a clear picture of particle settling and coagulation.

2. EXPERIMENT

Two settling columns were used to measure the apparent fall-velocity distributions for sewage sludge diluted in seawater according to the simple settling theory. If $F(w_s)$ = cumulative distribution function (by weight); w_s = fall velocity; $c(z, t)$ = concentration at depth z below the surface at time t ; $c(z, 0) = c_0$ = initial concentration; then $F(w_s) = c(z_1, z_1/w_s)/c_0$, where z_1 is the sampling depth. In this section, the experimental techniques and materials is introduced, followed by the presentation and discussion of experimental data.

2.1. Materials and Methods

Two 10-liter plexiglass columns with five side-sampling ports were used as the settling apparatus (Fig. .1). All tests were run under quiescent conditions without shear. Filtered artificial seawater was used to eliminate the influence of various background solids in natural seawater in order to get consistent results. Sewage sludge samples from CSDOC and CSDLAC were first passed through a 0.5-mm nylon screen to remove coarse materials, some of which are floatable. This pretreatment of samples was necessary to avoid difficulty in transferring samples with pipettes and to reduce the amount of material floating to the surface during settling tests. This procedure was acceptable since it did not make significant change of total solids (TS), volatile solids (VS) and apparent fall-

velocity distribution (runs 13 and 14; runs 15 and 16), that is, less than a factor of 2 in w_s values at a given percentile. Settling experiments were started immediately after the pretreatment of all waste activated sludges. Digested primary sludges were stored in a refrigerator at 4°C for later use.

For each run, sludge samples were mixed with filtered artificial seawater to the desired dilution ratios. These diluted mixtures were poured or siphoned immediately into the apparatus. Siphoning is preferable because the pouring process entrains air bubbles which lift some attached particles to the surface. After the column was filled, small measured samples were withdrawn from two positions along the column with syringes at successive times (that is, 1, 2, 4, 8, 15, 30 min; 1, 2, 4, 8 hr; 1, 2, 4, 8 day). At the same time, elevations of water surface were recorded.

The volume of samples needed was determined by the technique used in solids concentration analysis. Two different techniques were used to measure the particle concentrations. One is the gravimetric method (Faisst, 1976,1980), which weighs the collected mass retained on the Nuclepore membrane (Nuclepore Corporation, Pleasanton, California) after filtration. The other detects the absorbances of chemically treated samples, which can be correlated with the mass concentration of particles (Dubois *et al.*, 1956; Bradely and Krone, 1971; Hunt, 1980; Hunt and Pandya, 1984). For gravimetric method, collection efficiency is a function of the amount of solids remaining on the membranes after filtration. Hence, sampling volumes of 10 ml to 500 ml were used to make the mass of collected particles fairly uniform. Samples of 10 ml were used for all runs with

the absorbance technique. All samples were transferred into well-covered beakers and stored in 4°C refrigerator for about 10 days. Then they were analysed either by filtration for gravimetric measurements or by treating with chemicals to develop color for spectrophotometry analysis. The gravimetric method was used for runs 1 - 22 and absorbance method was used for runs 23 - 26. The distribution curves, that is, normalized concentration $(c(z_1, z_1/w_s)/c_0)$ versus apparent fall velocity $(w_s = z_1/t)$, were then calculated from the particle concentrations, sample times and water depths according to the conventional method (see Faisst, 1976,1980).

2.2. Experimental Results and Discussion

The results for different sewage sludges and different samples of the same sewage-sludge streams were obtained by using the technique stated above. A summary of experimental parameters is shown in Table .1 and typical distribution curves are shown in Fig. .2. Experimental results of settling column under quiescent condition from Faisst (1980) are also included for comparative purpose in Table .2.

Similar to the results obtained by Faisst (1976,1980), the apparent fall-velocity distribution curves for the two different depths disagreed for all the tests (see Fig. .2 and Table .2). These differences are due to the fact that coagulation changes the size distribution and thus the fall-velocity distribution of particles. The values of settling velocity shown in Table .1 are the average of the fall velocities measured at these two depths.

Table 1. Summary of Sewage-sludge Settling Experimental Parameters^a

Run No.	Sludge Type	Temp	Sampling Date	Dilution Ratio	TS (%)	VS (%)	c ₀ (mg liter ⁻¹)	Height (cm)	Apparent Fall-Velocity Distribution (w _s , cm sec ⁻¹)			
									25%ile	Median	75%ile	90%ile
1 ^b	DPS	11 ⁰ C	7/17/82	100:1	2.40	53.9	182.36	158.0-175.0	1 X 10 ⁻⁴	1 X 10 ⁻³	7 X 10 ⁻³	3 X 10 ⁻²
2 ^b	DPS	11 ⁰ C	7/17/82	100:1	2.40	53.9	211.40	145.5-167.5	1 X 10 ⁻⁴	1 X 10 ⁻³	1 X 10 ⁻²	1 X 10 ⁻¹
3 ^b	DPS	11 ⁰ C	7/31/82	100:1	3.55	53.1	245.40	154.1-166.5	1 X 10 ⁻³	2 X 10 ⁻²	7 X 10 ⁻²	3 X 10 ⁻¹
4 ^b	DPS	11 ⁰ C	7/31/82	100:1	3.55	53.1	240.58	147.8-166.9	3 X 10 ⁻⁴	1 X 10 ⁻²	1 X 10 ⁻¹	2 X 10 ⁻¹
5	DPS	11 ⁰ C	7/31/82	100:1	3.55	53.1	224.50	143.4-156.7	3 X 10 ⁻⁴	2 X 10 ⁻²	8 X 10 ⁻²	4 X 10 ⁻¹
6	DPS	11 ⁰ C	9/7/82	100:1	2.27	54.7	201.88	149.0-165.0	2 X 10 ⁻⁴	1 X 10 ⁻³	6 X 10 ⁻³	4 X 10 ⁻²
7 ^b	DPS	11 ⁰ C	7/17/82	500:1	2.40	53.9	36.9	129.8-162.8	≤ 1 X 10 ⁻⁵	2 X 10 ⁻⁴	3 X 10 ⁻³	4 X 10 ⁻²
8 ^b	DPS	11 ⁰ C	7/31/82	500:1	3.55	53.1	49.18	123.3-165.0	1 X 10 ⁻⁴	1 X 10 ⁻³	1 X 10 ⁻²	4 X 10 ⁻²
9	DPS	11 ⁰ C	7/31/82	500:1	3.55	53.1	52.45	143.0-173.5	1 X 10 ⁻⁴	2 X 10 ⁻³	1 X 10 ⁻²	5 X 10 ⁻²
10 ^b	WAS	11 ⁰ C	9/7/82	100:1	0.313	60.4	12.69	105.9-166.0	1 X 10 ⁻³	1 X 10 ⁻²	2 X 10 ⁻¹	1
11	WAS	11 ⁰ C	11/16/82	100:1	0.36	61.3	24.04	98.1-162.5	2 X 10 ⁻³	4 X 10 ⁻³	1 X 10 ⁻²	2 X 10 ⁻²
12	DPS	11 ⁰ C	11/16/82	100:1	1.1	51.1	96.80	133.7-149.9	5 X 10 ⁻³	1 X 10 ⁻²	1 X 10 ⁻¹	≥ 1
13	CS1	11 ⁰ C	12/7/82	100:1	0.32	61.9	63.69	114.9-168.4	5 X 10 ⁻⁴	3 X 10 ⁻³	1 X 10 ⁻²	2 X 10 ⁻²
14 ^c	CS1	11 ⁰ C	12/7/82	100:1	0.32	61.0	65.14	119.5-144.3	4 X 10 ⁻⁴	2 X 10 ⁻³	7 X 10 ⁻³	1.5 X 10 ⁻²
15	CS1	11 ⁰ C	2/3/83	100:1	0.96	60.5	70.30	149.8-172.6	3 X 10 ⁻⁴	4 X 10 ⁻³	1 X 10 ⁻²	5 X 10 ⁻²
16 ^c	CS1	11 ⁰ C	2/3/83	100:1	0.96	60.5	79.85	151.3-169.7	2 X 10 ⁻⁴	2 X 10 ⁻³	1 X 10 ⁻²	5 X 10 ⁻²
17	CS1	11 ⁰ C	3/8/83	100:1	0.95	50.6	78.20	158.6	1 X 10 ⁻⁴	6 X 10 ⁻⁴	5 X 10 ⁻³	3 X 10 ⁻²
18	DWAS	25 ⁰ C	3/31/83	100:1	2.5	66.0	214.70	143.9-161.0	1 X 10 ⁻³	5 X 10 ⁻²	1 X 10 ⁻¹	3 X 10 ⁻¹
19	DWAS	11 ⁰ C	3/31/83	100:1	2.5	66.0	223.5	143.2-169.7	1 X 10 ⁻³	5 X 10 ⁻²	1 X 10 ⁻¹	4 X 10 ⁻¹
20	DPS	25 ⁰ C	3/31/83	100:1	1.5	50.5	110.00	153.7-166.4	2 X 10 ⁻³	5 X 10 ⁻³	2 X 10 ⁻²	5 X 10 ⁻²
21	DPS	11 ⁰ C	3/31/83	100:1	1.5	50.5	121.50	159.0-177.8	2 X 10 ⁻³	4 X 10 ⁻³	2 X 10 ⁻²	5 X 10 ⁻²
22	DPS	25 ⁰ C	3/31/83	100:1	1.5	50.5	116.6	150.4-166.2	2 X 10 ⁻³	6 X 10 ⁻³	3 X 10 ⁻²	5 X 10 ⁻²
23 ^d	Effluent	20 ⁰ C	7/13/83	100:1	-	-	-	157.0-161.0	^e 2 X 10 ⁻³	^e 1 X 10 ⁻²	^e 7 X 10 ⁻²	^e 1 X 10 ⁻¹
24 ^d	WAS	21 ⁰ C	8/-/83	100:1	-	-	-	156.2-161.1	4 X 10 ⁻³	2 X 10 ⁻²	7 X 10 ⁻²	4 X 10 ⁻¹
25 ^d	WAS	21 ⁰ C	12/5/83	200:1	-	-	-	155.3-159.5	1 X 10 ⁻³	1 X 10 ⁻²	5 X 10 ⁻²	5 X 10 ⁻¹
26 ^d	CS2	21 ⁰ C	12/5/83	2:1	-	-	-	157.9-162.2	1 X 10 ⁻³	4 X 10 ⁻³	2 X 10 ⁻²	2 X 10 ⁻¹

a Abbreviations are as follows: DPS, digested primary sludge; WAS, waste activated sludge;

CS1, combined sludge from CSDOC (0.78WAS & 0.27DPS); CS2, combined sludge from CSDLAC

(second effluent primary effluent WAS=200:160:0.9); DWAS, digested waste activated sludge;

TS, total solids (% by weight); VS, volatile solids, as percent of Total solids;

Runs 1-18 for sewage sludge from CSDOC; Runs 18-26 for sewage sludges from CSDLAC.

b Mixtures were filled by pouring, all others were filled by siphoning.

c Unprocessed, all others were passed through 0.5-mm nylon screen before tests.

d Absorbance method was used, all other runs were analyzed by gravimetric method.

e Solid concentrations were too low to be analyzed by absorbance method with satisfactory accuracy.

Table 2. Summary of Experimental Results of Settling Column Tests by Faisst (1980)

Run No.	Sludge Type	Dilution Ratio	Apparent Fall-Velocity Distribution (w_s , cm sec ⁻¹)			
			25%ile	Median	75%ile	90%ile
1 ^a	DPS(CSDLAC)	500:1	5×10^{-5}	5×10^{-4}	1×10^{-3}	1×10^{-2}
2 ^a	DPS(CSDLAC)	100:1	9×10^{-5}	9×10^{-4}	6×10^{-3}	3×10^{-2}
3 ^a	DPS(CSDLAC)	50:1	1×10^{-4}	2×10^{-3}	1×10^{-2}	5×10^{-2}
4 ^b	DPS(CSDOC)	100:1	2×10^{-4} -5×10^{-4}	3×10^{-3} -5×10^{-3}	1×10^{-2} -2×10^{-2}	5×10^{-2} -9×10^{-2}
5 ^b	Hyperion Thermophilic Sludge	100:1	$<< 10^{-5}$	1×10^{-4} -4×10^{-4}	4×10^{-3} -8×10^{-3}	3×10^{-2} -6×10^{-2}
6 ^b	Hyperion Mesophilic Sludge	100:1	$<< 10^{-5}$	9×10^{-5} -1×10^{-4}	1×10^{-3} -2×10^{-3}	5×10^{-3} -7×10^{-3}
7 ^b	DPS(CSDLAC)	100:1	7×10^{-5} -2×10^{-4}	1×10^{-3} -3×10^{-3}	1×10^{-2} -2×10^{-2}	4×10^{-2} -6×10^{-2}

a Shallow column (2-liter graduated cylinder), single-depth sampling at 15 cm from surface.

b Tall column (171 cm), two-depth sampling at 30 and 90 cm from bottom.

The apparent fall-velocity distributions were very similar for repeated tests with the same sewage-sludge samples at the same dilution (runs 1 and 2; runs 3,4 and 5; runs 8 and 9; runs 20 and 22). The quartile values of fall velocity vary by a factor of 2 or less with one exception.

For the same sewage-sludge sample, it was observed that the higher the initial dilution ratio, the lower the apparent settling velocities measured (runs 2 and 7, runs 3 and 8; runs 1,2 and 3 from Faisst 1980). Since the collision rate of particles decreases with concentration, the combined effect of coagulation and settling is less and lower apparent fall velocities result (Fig. .2(a) versus Fig. .2(b)).

The results were not similar for sewage sludge from the same source which were collected at different times, for example, runs 2 and 5 are both DPS (digested primary sludge) from CSDOC, but at different times (Fig. .2(a) versus Fig. .2(c)). Different types of sewage sludge refer to the sewage sludge from different treatment plants or those passed through different treatment processes. The distribution curves were distinct among the sewage sludges from CSDOC and CSDLAC, and also DPS and WAS (waste-activated sludge) from CSDOC (for example, runs 2 and 21 in Fig. .2(a) and Fig. .2(e); runs 2 and 11 in Fig. .2(a) and Fig. .2(d); runs 4 - 7 from Faisst 1980). The mechanisms which generate these differences are still unknown. These deviations among sewage sludge samples are expected because the characteristics of collected sewage, treatment processes, and operational conditions are different for different plants and at different sampling times.

Although most tests were done at 11°C, the temperature range from 11-25°C was used to test the temperature effects on the settling and coagulation of sewage sludge particles inside the settling column. The results were almost the same within this temperature range (runs 18 and 19; runs 20 and 21), that is, within a factor of 1.4 in w_s for a given percentile.

The average decrease of water depth in settling column was ~ 15 % by the end of each experiment due to the large sampling volume required for gravimetric analysis (runs 1-22, with maximum as 40% for run 11 and minimum as 7% for run 3). The effect due to decrease in water level was checked by running parallel experiments with two columns. Comparing the results for the two different cases, we can see the deviation is of a factor of 4 and cannot be neglected (Fig. 2(f)). Either a new measuring technique which requires smaller sampling volume or a settling column with larger cross-sectional area is recommended. Three runs (runs 2, 5 and 6) with surface level variation less than 10 % were used as inputs to our conceptual model.

3. CONCEPTUAL MODEL

Since there is not a direct way to isolate the information on settling velocities from the results of settling column tests, a simple conceptual model was developed to test the importance of coagulation before more complex experiments were designed and conducted. In this section, the description of the problem and basic assumptions of this model are introduced followed by the formulation and solution techniques. Some hypothetical results are included to illustrate the relative contribution from settling, coagulation and vertical diffusion. Finally,

comparisons between experimental data and model predictions are summarized and show that settling column data is insufficient for differentiating particle coagulation and settling.

3.1. Description and Assumptions

Sludge particles cover a wide size range ($\sim 1-100 \mu m$) (Faisst, 1976). Particles are apt to coagulate due to the high ionic strength and different fall velocities. Vertical diffusion resulting from the concentration gradient is another transfer process for particles in addition to settling and coagulation. Settling velocity is a function of density, size, shape, structure of individual particles, and fluid density and viscosity. Since coagulation can change the size distribution and the structure of flocs, it can modify fall velocity, and *vice versa*. The interactions are complicated. However, as a first step, several simplifying assumptions are made and summarized as follows:

1. Only two different kinds of particles are in this system. One is very fine from the original source which we will call the "original" particles; the other is a large one generated from coagulation of the original particles, and treated as "generated" particles.
2. The original particles are too small to settle during the time period of interest (that is, their fall velocity can be taken to be zero).
3. The generated particles have a sufficiently high fall velocity (that is, w_s) that we can neglect their further coagulation during their descent through the settling column.

4. The kinetics for the coagulation reaction can be represented by a n^{th} order reaction of the original particles, with the reaction constant α remaining the same throughout the whole experiment. If subscript 1 is used for original particles (and 2 for generated particles), the coagulation rate is expressed as

$$r_1 = - \frac{d c_1}{d t} = \alpha c_1^n \quad \text{mg litre}^{-1} \text{sec}^{-1} \quad 1$$

5. At the beginning, $t = 0$, there are no generated particles, and the original particles are uniformly distributed throughout the column.
6. The height of the column is much larger than its diameter so this model may be treated as a one-dimensional problem.

3.2. Governing Equations

A set of dimensionless equations are derived based on the assumptions above. If x is the distance measured from the bottom of the column, c_1 and c_2 are the dimensional concentrations for original and generated particles respectively; c_0 is the initial concentration of original particles; t is the dimensional time; H is the height of the water column; K and β are two dimensionless parameters defined as in equations 6 and 7, and the nondimensionalized variables $C_{1,2}$, ξ , τ are defined as

$$C_{1,2} = \frac{c_{1,2}}{c_0}, \quad \xi = \frac{x}{H}, \quad \tau = \frac{t}{H/w_s}, \quad 2$$

then the dimensionless equations for coagulation are, integrating equation 1:

$$C_1(\tau) = e^{-\beta\tau}, \quad n = 1 \quad 3$$

$$C_1(\tau) = [1 + (n - 1)\beta\tau]^{-\frac{1}{n-1}}, \quad n \neq 1 \quad 4$$

For mass conservation of the generated particles:

$$\frac{\partial C_2}{\partial \tau} = \frac{\partial C_2}{\partial \xi} + K \frac{\partial^2 C_2}{\partial \xi^2} + \beta C_1^n \quad 5$$

where

$$K = \frac{k}{H w_s} = \frac{\text{time scale of settling}}{\text{time scale of diffusion}} \quad 6$$

$$\beta = \frac{H c_0^{n-1} \alpha}{w_s} = \frac{\text{time scale of settling}}{\text{time scale of coagulation}} \quad 7$$

Initial condition (I.C.) is:

$$C_2(\xi, 0) = 0, \quad 0 \leq \xi \leq 1 \quad 8$$

Boundary conditions (B.C.) are:

$$\frac{\partial C_2(0,\tau)}{\partial \xi} = 0, \tau > 0 \quad 9$$

$$K \frac{\partial C_2(1,\tau)}{\partial \xi} + C_2(1,\tau) = 0, \tau > 0 \quad 10$$

3.3. Solution Techniques

First we consider the special case, $K = 0$, for which the equations for C_2 become:

$$\frac{\partial C_2}{\partial \tau} = \frac{\partial C_2}{\partial \xi} + \beta C_1^n \quad 11$$

$$I.C. \quad C_2(\xi,0) = 0, 0 \leq \xi \leq 1 \quad 12$$

$$B.C. \quad C_2(1,\tau) = 0, \tau > 0 \quad 13$$

It is noted that the equation for C_2 is that of a kinematic wave with a nonhomogeneous term given by the coagulation process. The equation can be

solved easily by superposition. The results are shown in equations 14 and 15.

$$C_i(\tau) = \begin{cases} [1 + \beta(n-1)(\tau - \rho)]^{\frac{1}{1-n}} & \text{if } \tau > \rho, n \neq 1 \\ 1 & \text{if } \tau < \rho, n \neq 1 \end{cases} \quad 14$$

$$C_i(\tau) = \begin{cases} e^{-\beta(\tau - \rho)} & \text{if } \tau > \rho, n = 1 \\ 1 & \text{if } \tau < \rho, n = 1 \end{cases} \quad 15$$

If $K \neq 0$, the complete equations including the diffusion term can be solved numerically. A computer program was written to do this using finite differences based on an implicit scheme.

3.4. Results and Discussions of the Conceptual Model

Some special cases with either fast or slow coagulation for $K = 0$ and $K \neq 0$ are presented to illustrate the relative importance among settling, coagulation and diffusion (Fig. 3(a) - Fig. 3(f)). These examples are calculated for $n = 2$; the parameters used and the associated physical conditions are summarized in Table 3.

Fig. 3(a) - 3(c) show three cases for $K = 0$ (no vertical diffusion) and three different values for the dimensionless coagulation parameter β . For small β (low coagulation rate, low initial concentration, short column and high fall velocity), the concentration is vertically uniform as in figure 3(a). Physically, this case corresponds to the instances when generated particles (C_2) settle

Table 3. List of Input Parameters for Example Results ($n = 2$)

Run No.	Dimensionless Coagulation Parameter $\beta = \frac{Hc_0\alpha}{w_s}$	Dimensionless Diffusion Parameter $K = \frac{k}{w_s H}$	Remarks
1	10^{-4}	0	No diffusion, slow coagulation / fast settling
2	1	0	No diffusion
3	10^4	0	No diffusion, fast coagulation / slow settling
4	10^{-4}	10^4	Rapid vertical diffusion
5	1	10^{-1}	-
6	10^4	10^{-4}	Rapid coagulation

immediately to the bottom and leave the water once they are produced by the coagulation of small particles. The concentration is represented almost exclusively by the non-settling particles (C_1). Since the initial concentration and the coagulation rate are the same for C_1 from the top of the column to the bottom, the concentration profile should remain uniform as predicted.

In contrast, Fig. .3(c) with relatively large β can be visualized as the situation when all the non-settling particles almost instantaneously coagulate to form C_2 . This becomes a simple settling test for particles with unique fall velocity. A kinematic wave propagates downward representing the front which separates clear water on top and particle-laden water at concentration c_0 below. Since the time is nondimensionalized by the fall time (time to fall a distance equal to the column height), the front reaches the bottom at a dimensionless time of unity. Figure .3(b) shows the case for an intermediate value of β . The concentration profiles as a function of time are in between those in Fig. .3(a) and .3(c) as expected. Fig. .3(d) - Fig. .3(f) present the situations with vertical diffusion. These can be compared with those in Fig. .3(a) - Fig. .3(c) to gauge the effects. For example, comparison of Fig. .3(e) and Fig. .3(b) clearly shows that diffusion smooths out the concentration profiles as expected. Also the proper boundary condition at the bottom can be imposed, which makes the concentration profiles vertical there. However, these examples were presented mainly to demonstrate the nature of the solutions and the sensitivity to the parameters β and K . The ranges used for illustration are probably more extreme than those that might be encountered in real problem.

4. COMPARISON BETWEEN EXPERIMENTS AND MODEL PREDICTIONS

In this section, we compare the model predictions with available laboratory experiments of sludge settling tests. It should be emphasized that our assumption of dual size particles provides a simplified model which is used only to demonstrate a different way of data interpretation. It is not intended to represent an exact description of the complicated mechanisms inside the settling column even if the predictions fit the experimental results. Two sets of experimental data are selected for illustration: one from Hunt and Pandya (1984), and the other summarized in Table 1.

Lo (1981), Lo and Weber (1984) and Farley (1984) have proposed different numerical models to describe the particle concentrations in settling columns. Lo and Weber deduced an empirical equation from the observed similarities between dynamic discrete settling (DDS, particles with fixed fall-velocity distribution settling under turbulence) and quiescent flocculent settling (QFS, coagulating suspension settling in quiescent environment) phenomenon. A parameter called "flocculation coefficient", and the discrete-equivalent (or effective) settling velocity are introduced to the governing equation for DDS in place of the turbulent mixing coefficient and real settling velocities. Farley derives a power law dependences of the mass removal rate of solids on mass concentration (that is, $dC/dt = -bC^n$, n from 1.3 - 2.3 depending on the concentration) from numerical simulation for a vertically homogeneous water column with spherical particles of constant density. For each cases, the experimental data can be fitted well by the proposed model.

Farley's model is a simplified explanation for some special case (uniform concentration, spherical particles, constant densities, etc.); and Lo's model is based on empirical observations without apparent physical meaning (artificial flocculation coefficient and discrete-equivalent settling velocities). Conventional settling column data are not sufficient to verify either model.

4.1. Comparison with Results from Couette Flow Reactor

Hunt and Pandya (1984) performed settling experiments with a flocculating dilute suspension of sewage sludge in a 15-cm high space between concentric rotating cylinders, and demonstrated empirically that the coagulation rate obeyed second order kinetics (that is, $n = 2$). Hunt also estimated the proportionality constant α and settling velocity w_s at several fluid shear rates G . By using Hunt's data and parameters, we could generate the output from our model, as illustrated in Fig. 4. The model predictions match Hunt's data well for the duration of his experiment (only about 60 minutes).

4.2. Comparison with Present Experimental Work

A plot of $1/C$ versus t similar to Fig. 4 should give a straight line if the second-order kinetics for coagulation reaction applies. Several runs shown in Table 1 are chosen to test this hypothesis. It is concluded that the data points from the settling column tests can hardly be fitted with straight lines for either short (~ 100 min) or long times ($\sim 10^4$ min). These deviations from second-order hypothesis may have two causes. First, the column we used is much longer than that used by Hunt (180 cm versus 15 cm). Secondly, settling tests

were conducted in a quiescent environment instead of one with laminar shear as in Hunt's experiments.

Since the second order kinetics of coagulation cannot be applied to our experimental data, different values of n and β are adjusted to best fit the experimental results by trial and error and linear regression. The dimensional form for equation 14 is as follows

$$\frac{c(t)}{c_0} = \left[1 + (n - 1) \alpha c_0^{n-1} \left(t - \frac{z}{w_s} \right) \right]^{\frac{1}{1-n}} \quad 16$$

The values of n and w_s are determined by requiring the plot of $(c(t)/c_0)^{1-n}$ versus $(t - z_1/w_s)$ to be as close as possible as a straight line. Three runs are chosen for comparison between experimental data and model prediction. One example of the fitted lines is shown in Fig. 5. The calculated parameters are summarized in Table 4. Normalized concentration and time are plotted for the results obtained from experiments and the model (in Fig. 6). The fitted values of n and w_s are much larger than expected. The maximum fall velocity observed during experiments is only of the order of 0.1 cm sec^{-1} . These results tell us, however, that pure settling is not the only way to explain the experimental data; n^{th} order coagulation with one fall velocity as described by this model can create the same result. Of course, we know there is not only a single fall-velocity, but based on this simple illustration, it can be concluded that other coagulation models can also be designed with multiple sets of particle sizes,

Table 4. List of Parameters Fitted by Numerical Model with $K = 0$

Run No.	c_0 <i>mg liter</i> ⁻¹	H <i>cm</i>	n	β	α <i>(liter / mg)</i> ⁿ⁻¹ <i>sec</i> ⁻¹	w_0 <i>cm sec</i> ⁻¹
2	211.4	167.5	3.85	0.0096	1.069×10^{-11}	0.79
5	224.5	156.7	4.35	0.0049	2.5×10^{-12}	0.6
6	201.88	165.0	2.68	0.00629	3.7×10^{-9}	0.725

and these could be adjusted to fit the data also. The work accomplished by Lo (1984) gives a good example. Thus we lack the information for a quantitative separation of settling and flocculation effects.

5. SUMMARY AND CONCLUSIONS

Efforts have been made to measure the fall-velocity distribution for sewage-sludge particles in seawater with the conventional settling column technique. Both settling and coagulation are observed to contribute to the downward transport of particles. Unfortunately, this technique is unable to provide separate information on the individual processes. In addition, if a large amount of water is withdrawn from the column to run the analysis, significant error is introduced (such as runs 10 and 11 for WAS with very small solids concentrations, runs 7 and 8 for high dilution). A solids-measuring technique with higher accuracy or a settling apparatus with larger cross section area and volume is expected to eliminate this problem.

A simple conceptual model has been developed to simulate a hypothesized settling and coagulation process of sewage-sludge particles in seawater for the settling column and to demonstrate an alternate interpretation of observed results, rather than simple settling. The expression of n^{th} order kinetics with a constant rate coefficient was assumed for the coagulating particles, and a single settling velocity was applied to the settling particles that were coagulated from the small ones. This model clearly did not cover all the processes and factors which may be involved inside the column. However, the model can predict results similar to those observed. It was concluded that second order kinetics as

suggested by Hunt, 1982ab, Hunt and Pandya, 1984 and Morel and Schiff, 1983 is not the only way to interpret observed data. Farley (1984) derived values of n other than 2 for different coagulating mechanics for a settling column with uniform particle concentration.

For more reliable fall velocity data, it is essential to design an *in situ* experimental setup capable of separating settling from coagulation in order to understand thoroughly the settling behavior of sewage sludge particles. Laboratory research is underway where coagulation in a reactor with controlled mixing is followed by direct fall velocity determination using holographic techniques.

ACKNOWLEDGMENTS

We acknowledge the U. S. National Oceanic and Atmospheric Administration (grant Nos. NA80RAD00055 and NA81RAC00153), the Sanitation Districts of Orange County, the Sanitation Districts of Los Angeles County and the Andrew W. Mellon Foundation for financial support, and thank T. Dichristina and K. Ng for assistance in the laboratory.

REFERENCES

Bradley, R. A. and R. B. Krone. 1971. Shearing effects on settling of activated sludge. Journal of the Sanitary Engineering Division , The American Society of Civil Engineering , 97 (SA1) , 59-79.

Dubois, M., K. A. Gilles, J. K. Hamilton, P. A. Rebers, and F. Smith. 1956. Colorimetric method for determination of sugars and related substances. Analytical Chemistry , 28 , 350-356.

Faisst, W. K. 1976. Digested sewage sludge: characterization of a residual and modeling for its disposal in the ocean off southern California. EQL Report No. 13, Environmental Quality Laboratory, California Institute of Technology, Pasadena, California, 193 pp.

Faisst, W. K. 1980. Coagulation of particulate in digested sludge. In Particulate in Water: Characterization, Fate, Effects and Removal. M. C. Kavanaugh and J. O. Leckie, Eds., Advances in Chemistry Series 189, American Chemical Society, Washington D. C., 259-282.

Farley, K. J. 1984. Sorption and sedimentation as mechanisms of trace metal removal. Thesis, Massachusetts Institute of Technology, Cambridge, Massachusetts, 125 pp.

Hunt, J. R. 1980. Coagulation in continuous particle size distribution: theory and experimental verification. Report No. AC-5-80, W. M. Keck Laboratory of

Environmental Engineering Science, California Institute of Technology, Pasadena, California, 126 pp.

Hunt, J. R. 1982a. Self-similar particle-size distributions during coagulation: theory and experimental verification. Journal of Fluid Mechanics , 122 , 169-185.

Hunt, J. R. 1982b. Particle dynamics in seawater: implications for predicating the fate of discharged particles. Environmental Science and Technology , 16 , 303-309.

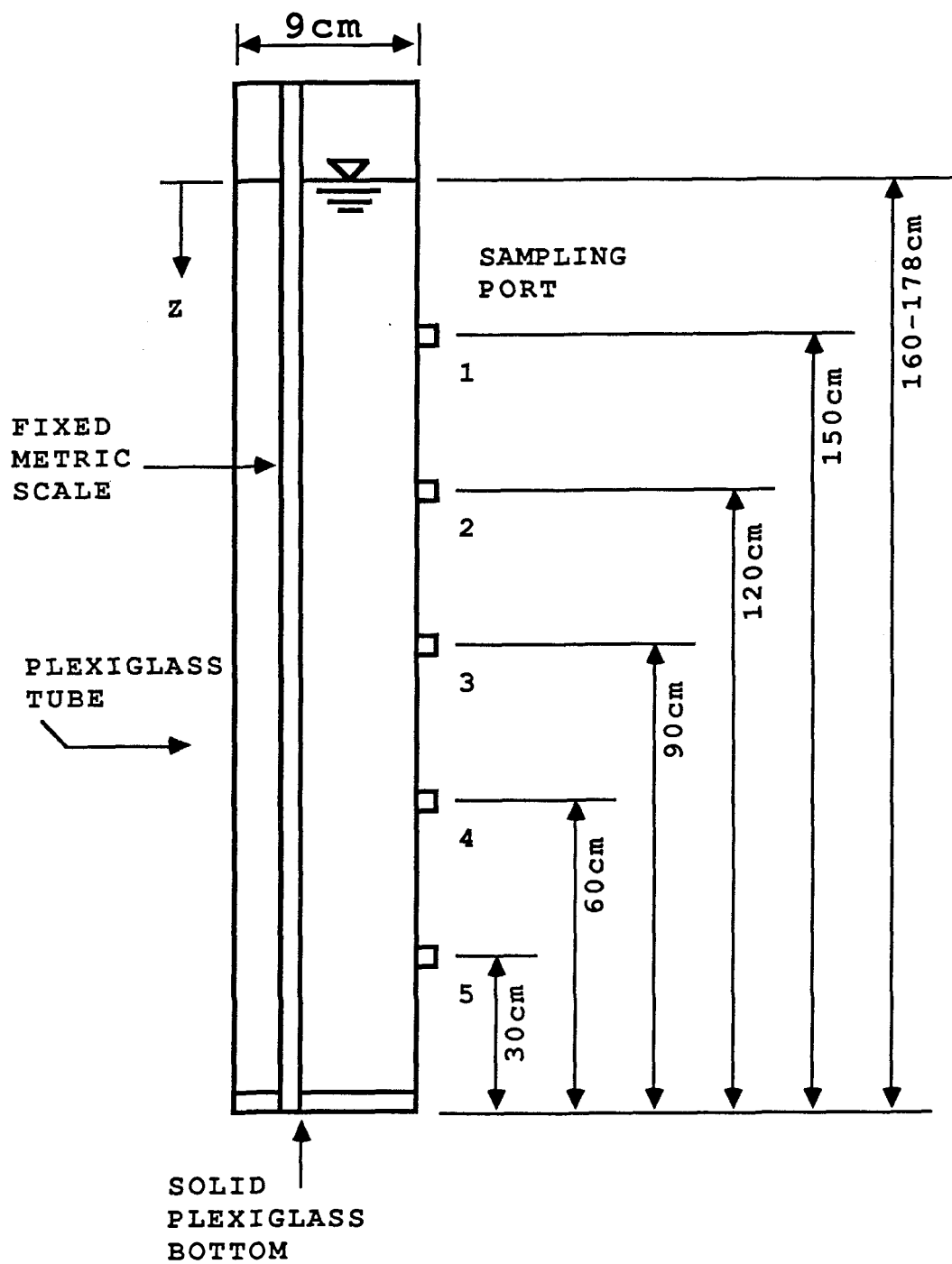
Hunt, J. R. and J. D. Pandya. 1984. Sewage sludge coagulation and settling in seawater. Environmental Science and Technology , 18 , 119-123.

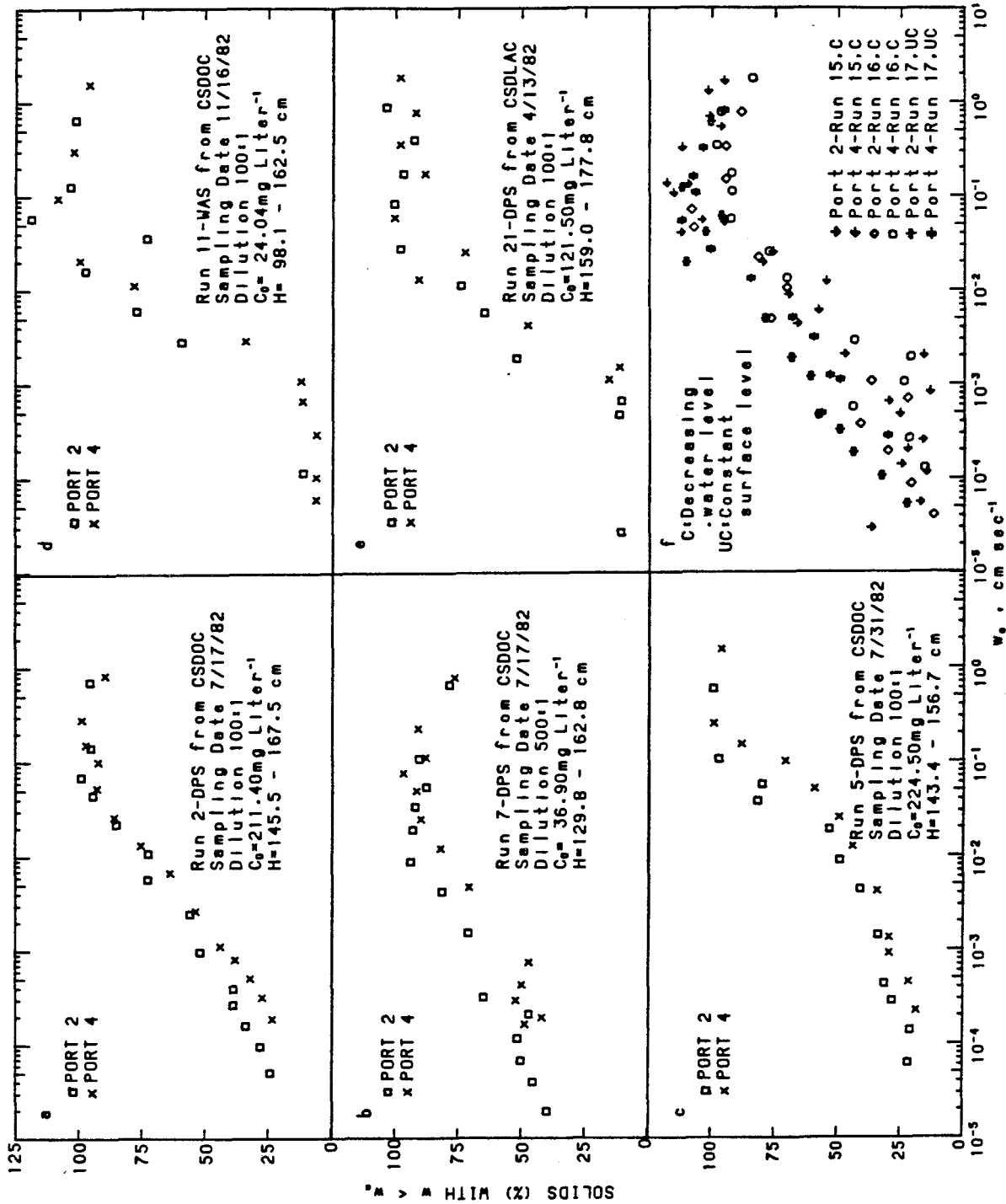
Lo, T. Y. R. 1981. A dynamic settling column for measurement of sedimentation of flocculent material under the influence of turbulence. Ph.D. Thesis, University of Michigan, Ann Arbor, Michigan, 274 pp.

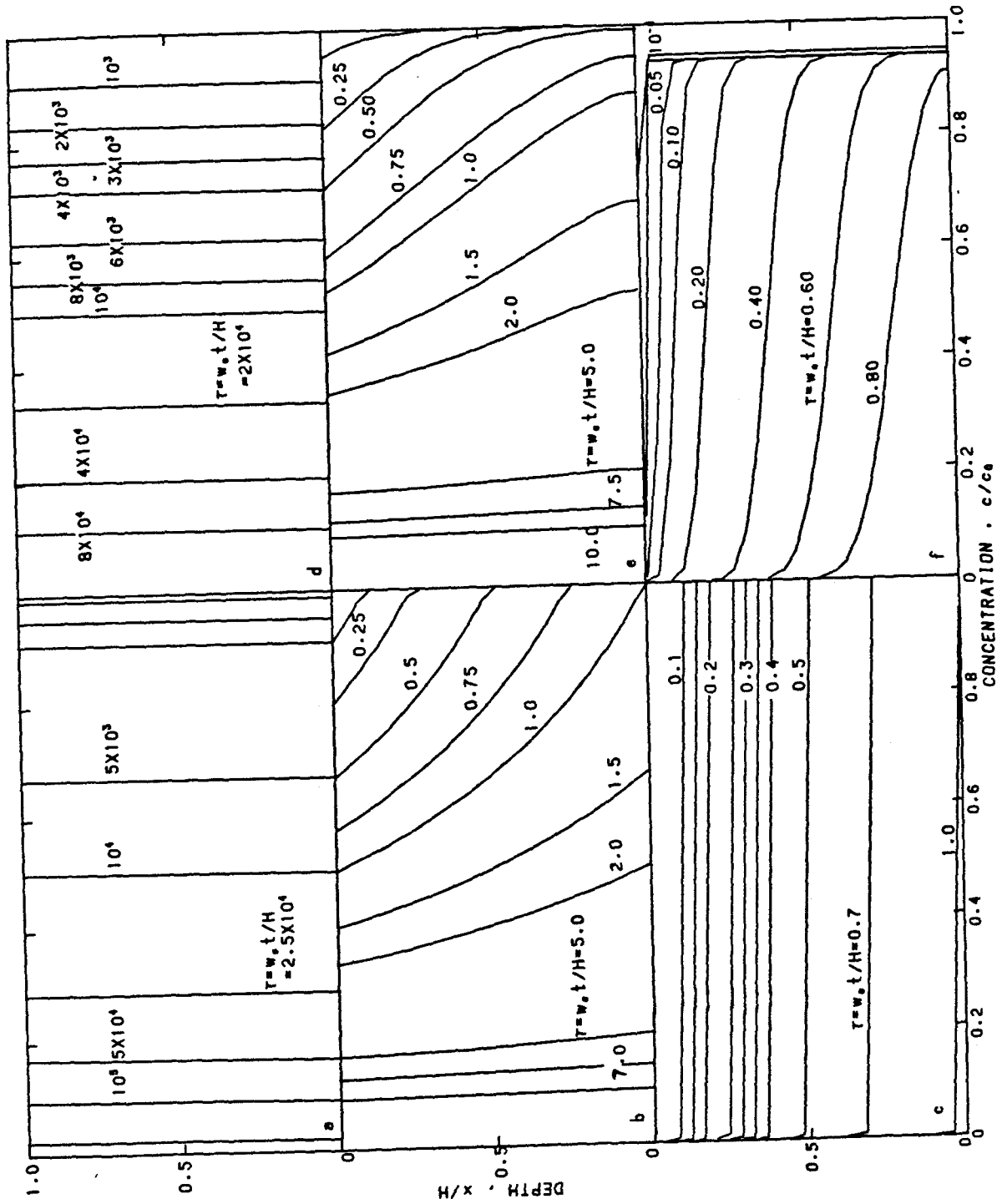
Lo, T. Y. R. and W. J. Weber, Jr. 1984. Flocculent Settling in quiescent system. Journal of Environmental Engineering , The American Society of Civil Engineering , 110 , 174-189.

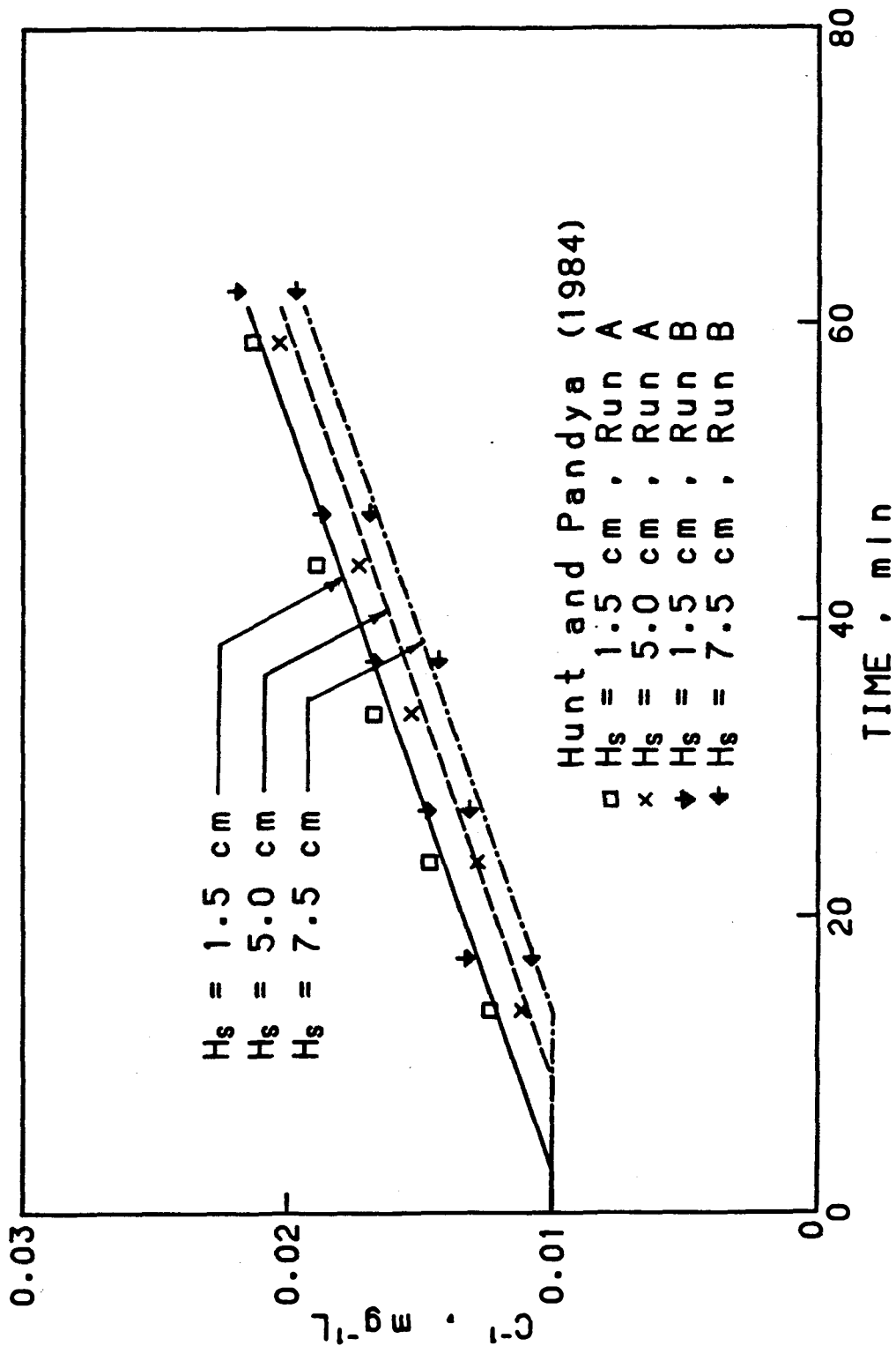
FIGURE LEGENDS

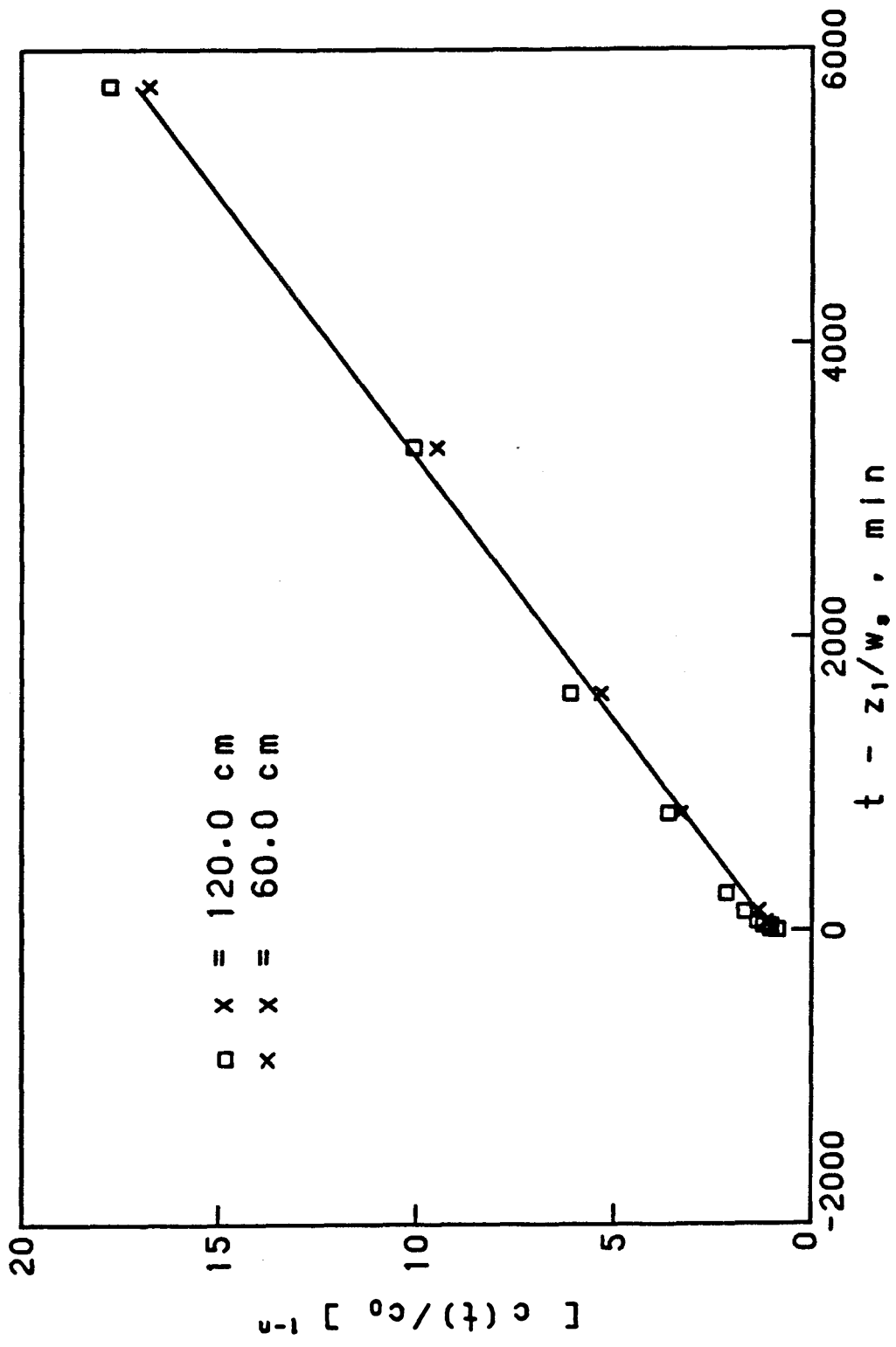
- Figure .1 Multiport settling column.
- Figure .2 Fall velocity distribution determined in a 1.8 m-high quiescent settling column (Table .1), for (a) run 2; (b) run 7; (c) run 5; (d) run 11; (e) run 21; (f) runs 15, 16 and run 17.
- Figure .3 Dimensionless concentration profiles in a quiescent settling column of height H with an initial uniform concentration c_0 . Time is nondimensionalized by the time to fall to a distance equal to column height. (see Table .3 and text for explanation), for (a) $\beta = 10^{-4}$, $K = 0$; (b) $\beta = 1$, $K = 0$; (c) $\beta = 10^4$, $K = 0$; (d) $\beta = 10^{-4}$, $K = 10^4$; (e) $\beta = 1$, $K = 0.1$; (f) $\beta = 10^4$, $K = 10^{-4}$.
- Figure .4 Comparison of numerical model with experimental results from Hunt and Pandya (1984).
- Figure .5 Best fit straight line determined empirically by iterating n , w_s , α for run 5 in Table .1.
- Figure .6 Time history of concentration decrease and comparison with model prediction using values n , w_s , α as determined in Fig. .5.

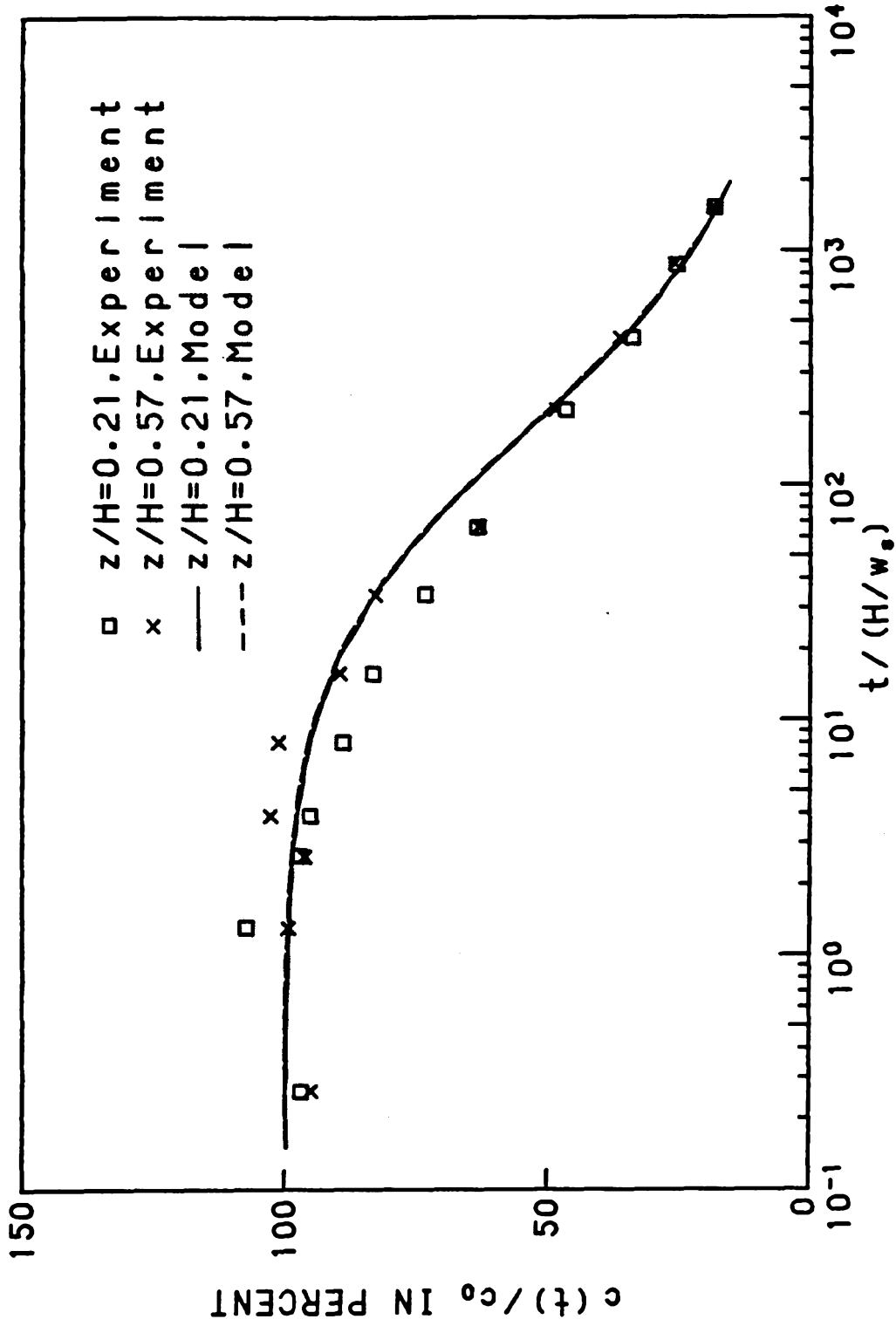












Appendix B

Effects of Initial Mixing on the Apparent Fall Velocity Distributions Using Conventional Settling Column Techniques

1.1 Objective

Coagulation of sludge particles is observed during quiescent settling column experiments (Faisst, 1976, 1980 and Wang *et al.* in press). Sludge particles grow by collision and attachment as they travel to the bottom of the settling column. Hunt and Pandya (1984) conducted a set of similar experiments with and without shear in a concentric-rotating-cylindrical device and they found that the rate of coagulation of sludge followed a second order kinetics, i.e., $dC/dt = -\alpha C^2$. Our experimental data however do not follow a linear relationship between the inverse concentration of particles and the elapse time. There are several factors, such as the dimensions of the settling apparatus and the mixing conditions, which might contribute to this discrepancy. The procedure of premixing sludge with seawater is expected to be a controlling process among these factors.

Sludge particles are destabilized once they are introduced into seawater and the coagulation takes place. Mixing conditions and the particle concentration in mixture determine the rate and the extent of coagulation in the initial mixing stage, and also, the subsequent settling process within the settling apparatus. The work

presented in this chapter is the result of a study of the effects of the initial mixing conditions on the settling-coagulating behavior of sludge particles.

1.2 Procedure

The pre-mixing procedure for our previous runs was as follows (Wang *et al.* in press). The sludge-seawater suspension was stirred thoroughly when the two were combined. The mixing time was always less than one minute and stirring speed was not specified. It was concluded from earlier results that this simple pre-mixing did not make significant differences for the same sludge samples (see Wang *et al.* in press).

In order to investigate the effects of initial mixing during the preparation of sludge samples, three simple pre-mixing techniques, Case A, Case B and Case C, were investigated to determine their effects on coagulation and the subsequent results for conventional settling-column experiments. The differences between these three techniques are illustrated in Fig. 1.1. Both the rate of introducing the seawater to the sludge to form a mixture (i.e., slopes of these curves) and the stirring time are varied.

Case A is simply the instantaneous mixing of sludge and artificial seawater at constant speed for a short period. A 100 *ml* sludge sample was added to a container which contain 9900 *ml* seawater. This mixture was stirred immediately with a stirring bar (0.9 *cm* dia. X 43.5 *cm* long) at a speed of 110 ± 10 *rpm* for fifteen minutes.

Case B is designed to simulate the mixing process inside a discharge plume. A 100 *ml* sample of sludge is introduced into an empty vessel. Seawater is transferred into the vessel at increasing flow rates which are calculated based on the entrainment

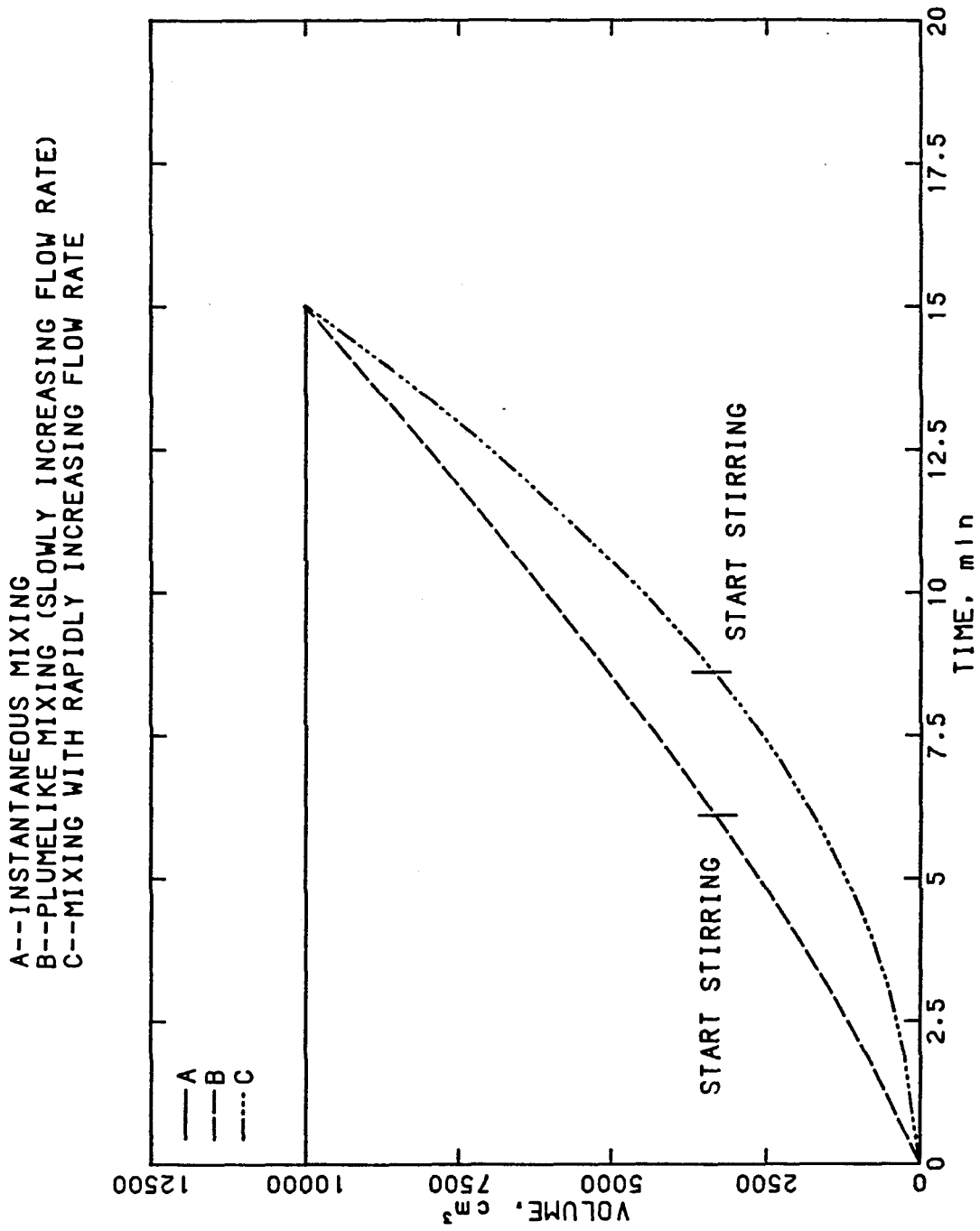


Figure 1.1 Sample volume as function of time for three different initial mixing scenarios.

of a simple axisymmetric plume. The total volume in this container as a function of time is shown in Fig. 1.1 as curve B. Once the container is about one-third full (about 6 minutes from the start), the mixture is stirred, as in Case A, for 9 minutes.

Case C starts with a lower rate of dilution than Case B (i.e., lower dilution ratio and higher solids concentration), but ends at the same concentration and volume after 15 minutes. The technique used for Case C is similar to that for Case B with the following exceptions: a smaller volume of seawater at the outset, faster increasing flow rates and shorter mixing periods (curve C in Fig. 1.1).

1.3 Results and Discussion

Two tests were conducted with Case A and Case C for digested primary sludge (D.P.S.) from County Sanitation Districts of Orange County (CSDOC) to examine pre-mixing effects for the two extreme cases. Then, Cases A and B were compared by using D.P.S. from County Sanitation Districts of Los Angeles County (CSDLAC). Results were analyzed and presented as apparent fall-velocity distributions in Figs. 1.2 to 1.7. The experimental parameters are summarized in Table 1.1. The results will be discussed below.

1.3.1 Case A vs. Case C, (D.P.S. from CSDOC, runs 1 and 2)

(Figs. 1.2 and 1.3)

The combined settling-coagulating behaviors are different for runs 1 and 2. Particles in run 2 tend to settle a little faster. The difference between the distribution curves at two depths are also smaller in this case (i.e., run 2). This observation indicates that the extent of coagulation during the initial mixing is higher in Case

Table 1.1 Summary of Experimental Parameters for Investigation of Initial Mixing on Coagulation and Sedimentation in Settling Column Experiments

Run No.	1	2	3	4	5	6
Sludge Source	D.P.S. (CSDOC)	D.P.S. (CSDOC)	D.P.S. (CSDLAC)	D.P.S. (CSDLAC)	D.P.S. (CSDLAC)	D.P.S. (CSDLAC)
Dilution	100:1	100:1	100:1	100:1	100:1	100:1
C_o , mg/l	—	—	232.9	210.3	226.5	217.6
A_o	3.143	3.286	3.676	3.428	3.261	3.172
H , cm	157.2-162.8 160.0 ± 1.8%	166.2-171.7 169.0 ± 1.6%	160.0-164.9 162.4 ± 1.5%	160.3-165.0 162.6 ± 1.5%	160.7-179.8 171.2 ± 5%	159.8-165.9 162.8 ± 2%
Mixing	A (15 min)	C (15 min)	A (15 min)	B (15 min)	B (15 min)	A (1 min)
25%ile w cm/sec	4.3×10^{-4} - 1.0×10^{-3}	1.2×10^{-3} - 1.2×10^{-3}	5.0×10^{-4}	$< 10^{-3}$	1.0×10^{-4} - 1.2×10^{-3}	1.0×10^{-4}
50%ile w cm/sec	4.0×10^{-3} - 7.0×10^{-3}	7.0×10^{-3} - 1.0×10^{-2}	1.2×10^{-2}	1.0×10^{-2} - 2.0×10^{-2}	1.0×10^{-2} - 2.0×10^{-2}	4.2×10^{-3} - 2.0×10^{-2}
75%ile w cm/sec	1.3×10^{-2} - 2.5×10^{-2}	2.0×10^{-2} - 3.0×10^{-2}	6.0×10^{-2}	3.0×10^{-2} - 5.0×10^{-2}	4.0×10^{-2} - 5.2×10^{-2}	2.2×10^{-3} - 6.0×10^{-2}
90%ile w cm/sec	4.0×10^{-2} - 9.0×10^{-2}	6.0×10^{-2} - 1.1×10^{-1}	2.0×10^{-1}	7.0×10^{-2} - 1.0×10^{-1}	1.0×10^{-1}	7.2×10^{-2} - 1.0×10^{-1}

A = Instantaneous mixing

B = Plumelike mixing (slowly increasing flow rate)

C = Mixing with rapidly increasing flow rate

C than in Case A. Since the solids concentrations are always higher in Case C, this technique provides a better environment for coagulation.

1.3.2 Case A vs. Case B, (D.P.S. from CSDLAC, runs 3 to 5)

(Figs.1.4-1.6)

Run 3 was premixed as Case A, while runs 4 and 5 were pre-mixed as Case B but with different initial concentrations and water heights in the settling columns. Results from runs 4 and 5 are nearly the same; in run 5 the faster settling at an early stage for the experiment might be due to the somewhat higher particle concentration. The differences between Case A and Case B are not as significant as those between Case A and Case C. The instantaneous mixing (run 3) gives the largest apparent fall-velocity distribution and the closest results for two sampling depths.

1.3.3 Case A for different mixing times (D.P.S. from CSDLAC, run 3 vs. 6)

(Figs 1.4 and 1.7)

Run 6 was pre-mixed in Case A but for a shorter period (1 *min* vs. 15 *min*). As expected the coagulation is observed to be closer to completeness for the longer mixing time.

1.4 Conclusion

It can be concluded from these six runs of settling-column tests that initial mixing does cause differences in the subsequent settling-coagulating behavior of sludge inside the settling column. Both particle concentration and stirring time are critical factors. In general, higher solids concentration and longer mixing time produce faster coagulation, provided that the other factors remain roughly the same.

D.P.S. (CSDOC), 100:1
INSTANTANEOUS MIXING (CASE A, 15MIN)

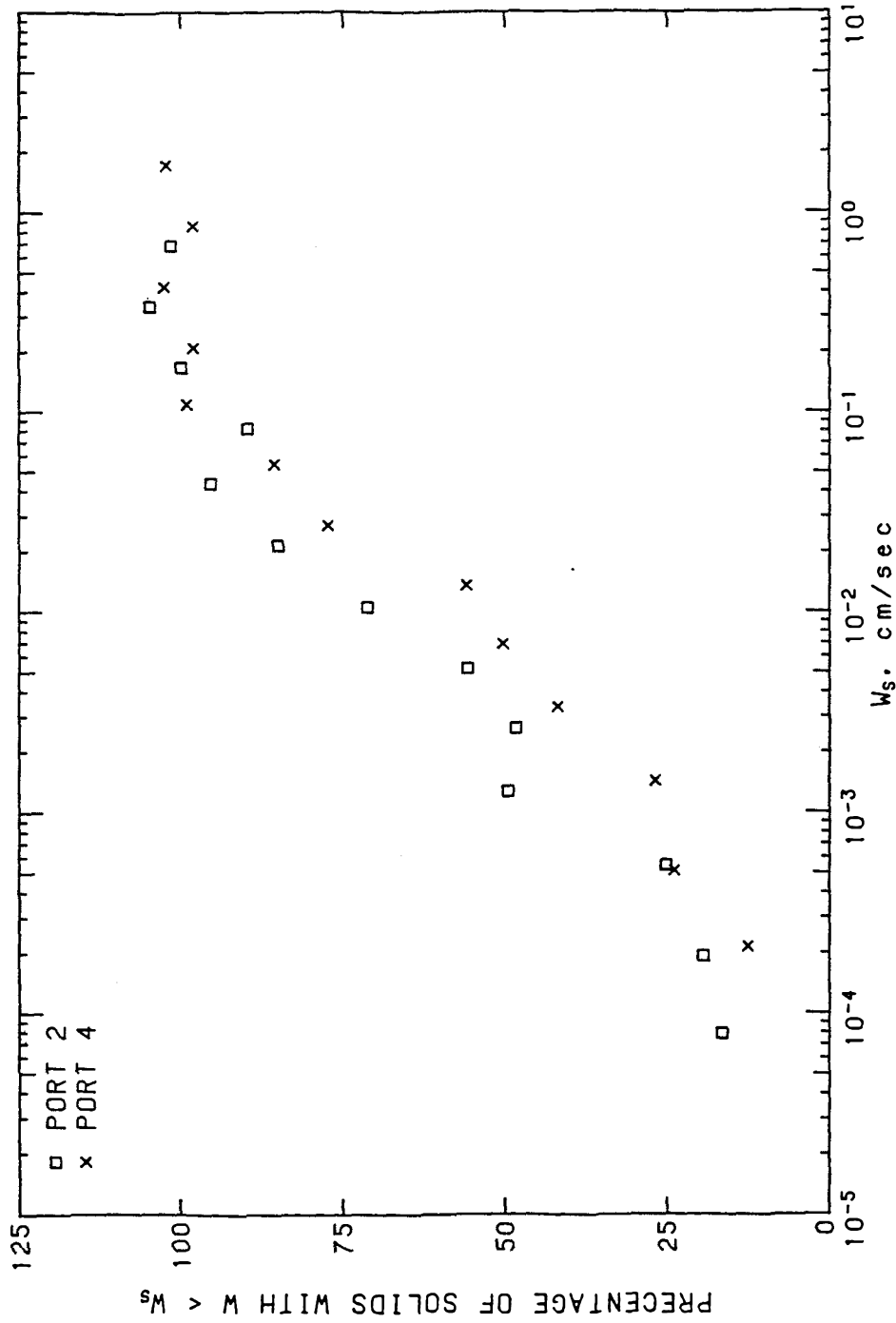


Figure 1.2 Apparent fall velocity distribution for Run 1. See Table 1.1 for further details.
Ports 2 and 4 are two sampling ports along column with Port 2 about 38.0 cm and
Port 4 98.0 cm below water surface.

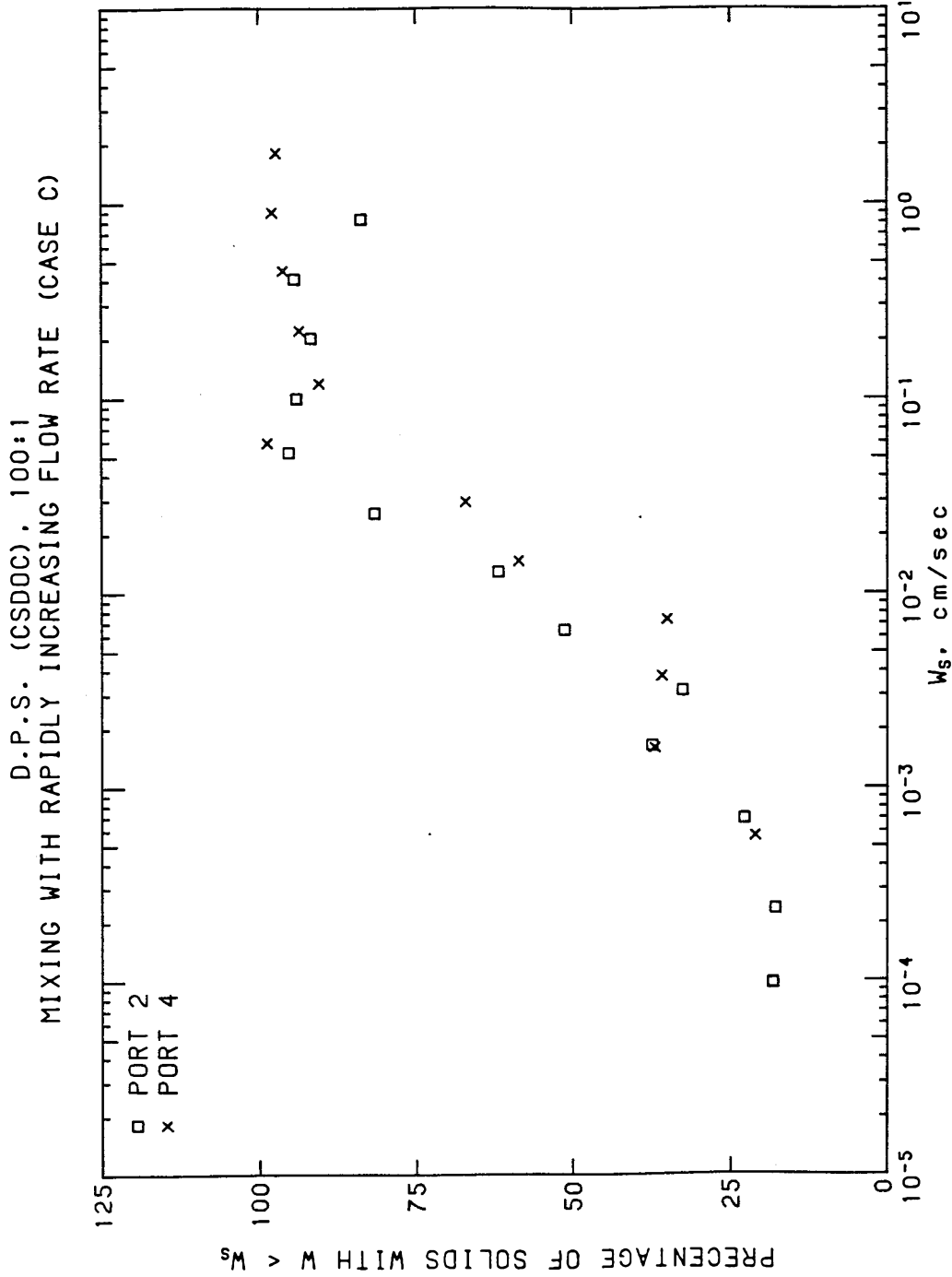


Figure 1.3 Apparent fall velocity distribution for Run 2. See Table 1.1 for further details.
Ports 2 and 4 are two sampling ports along column with Port 2 about 47.0 cm and
Port 4 107.0 cm below water surface.

D.P.S. (CSDLAC), 100:1, $C_0=232.9\text{mg/L}$
INSTANTANEOUS MIXING (CASE A, 15 MIN)

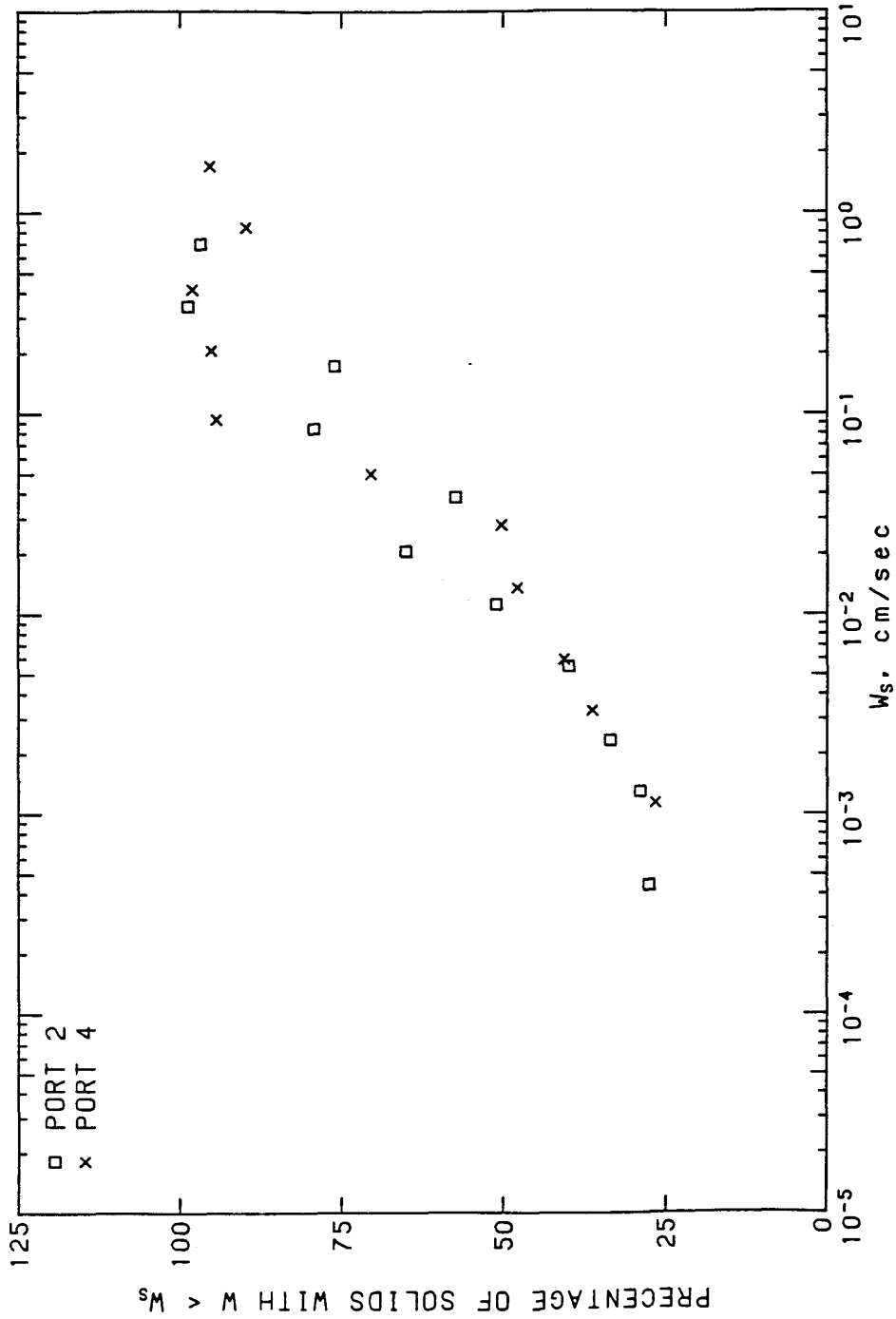


Figure 1.4 Apparent fall velocity distribution for Run 3. See Table 1.1 for further details.
Ports 2 and 4 are two sampling ports along column with Port 2 about 40.0 cm and
Port 4 100.0 cm below water surface.

D.P.S. (CSDLAC). 100:1. $C_0=210.3\text{mg/L}$. PLUMELIKE MIXING

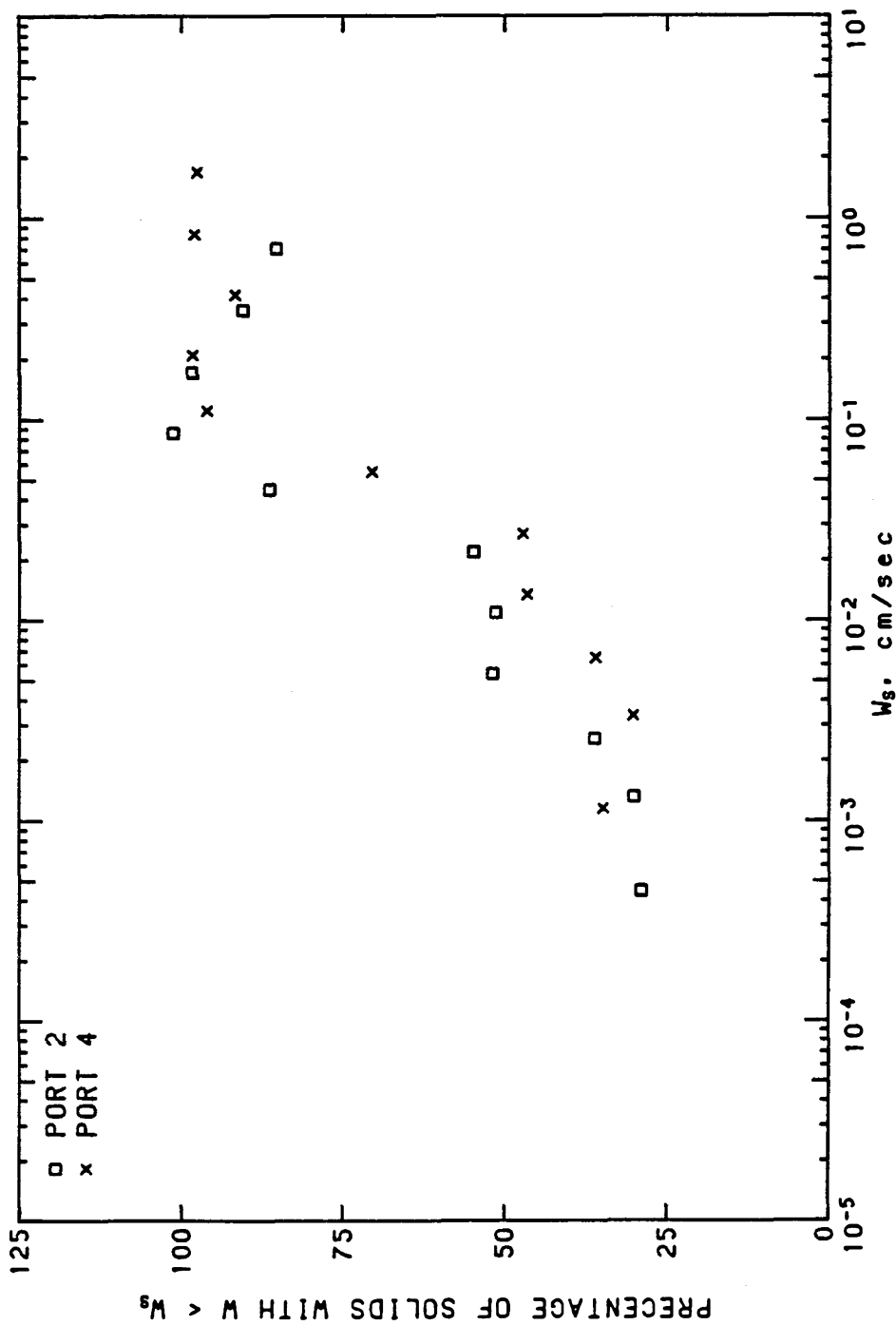


Figure 1.5 Apparent fall velocity distribution for Run 4. See Table 1.1 for further details. Ports 2 and 4 are two sampling ports along column with Port 2 about 40.0 cm and Port 4 100.0 cm below water surface.

D.P.S. (CSDLAC), 100:1, $C_0=226.5\text{mg/L}$, PLUMELIKE MIXING

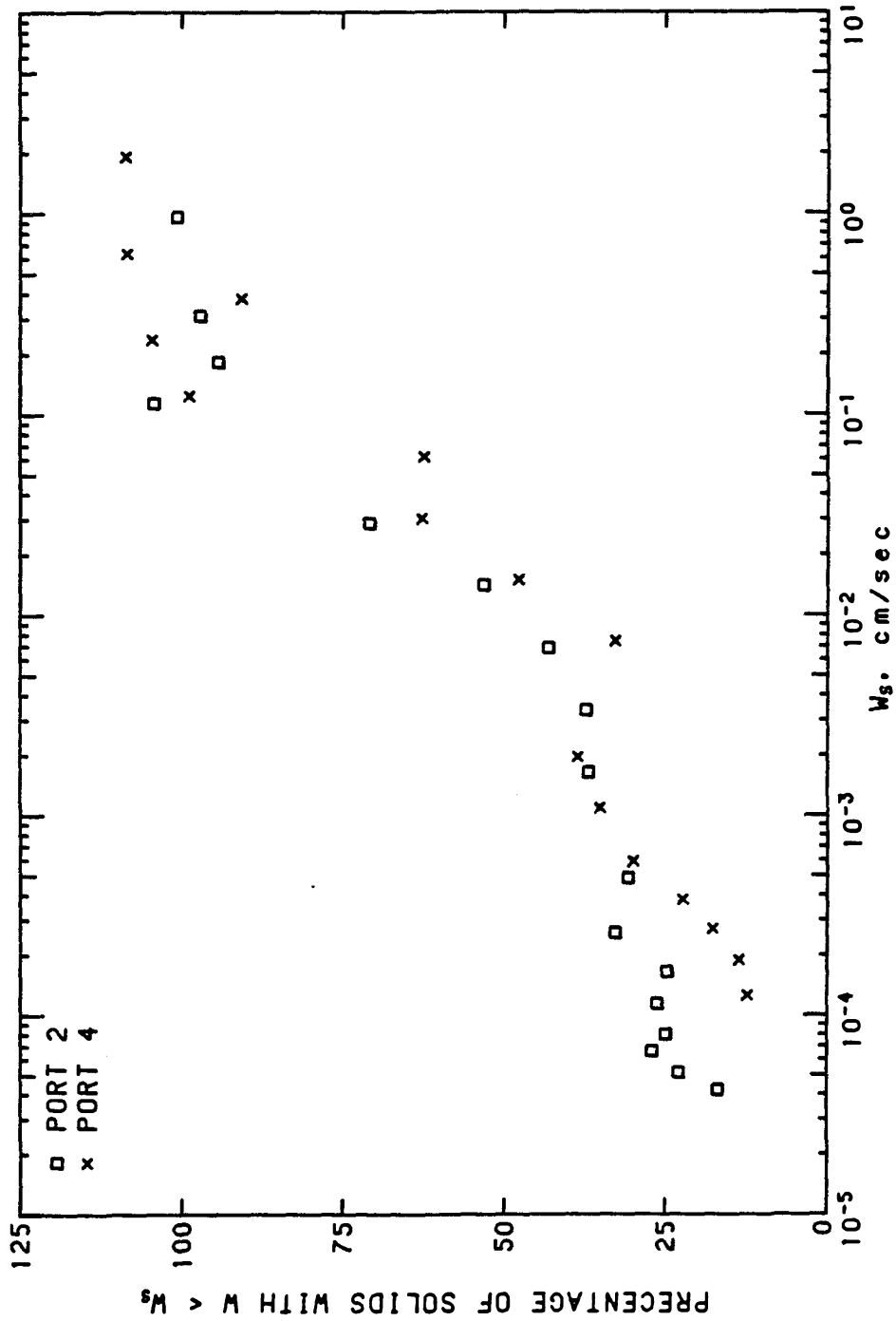


Figure 1.6 Apparent fall velocity distribution for Run 5. See Table 1.1 for further details. Ports 2 and 4 are two sampling ports along column with Port 2 about 49.0 cm and Port 4 109.0 cm below water surface.

D.P.-S. (CSDLAC), 100:1, $C_0=217.6\text{mg/L}$
INSTANTANEOUS MIXING (CASE A, 1 MIN)

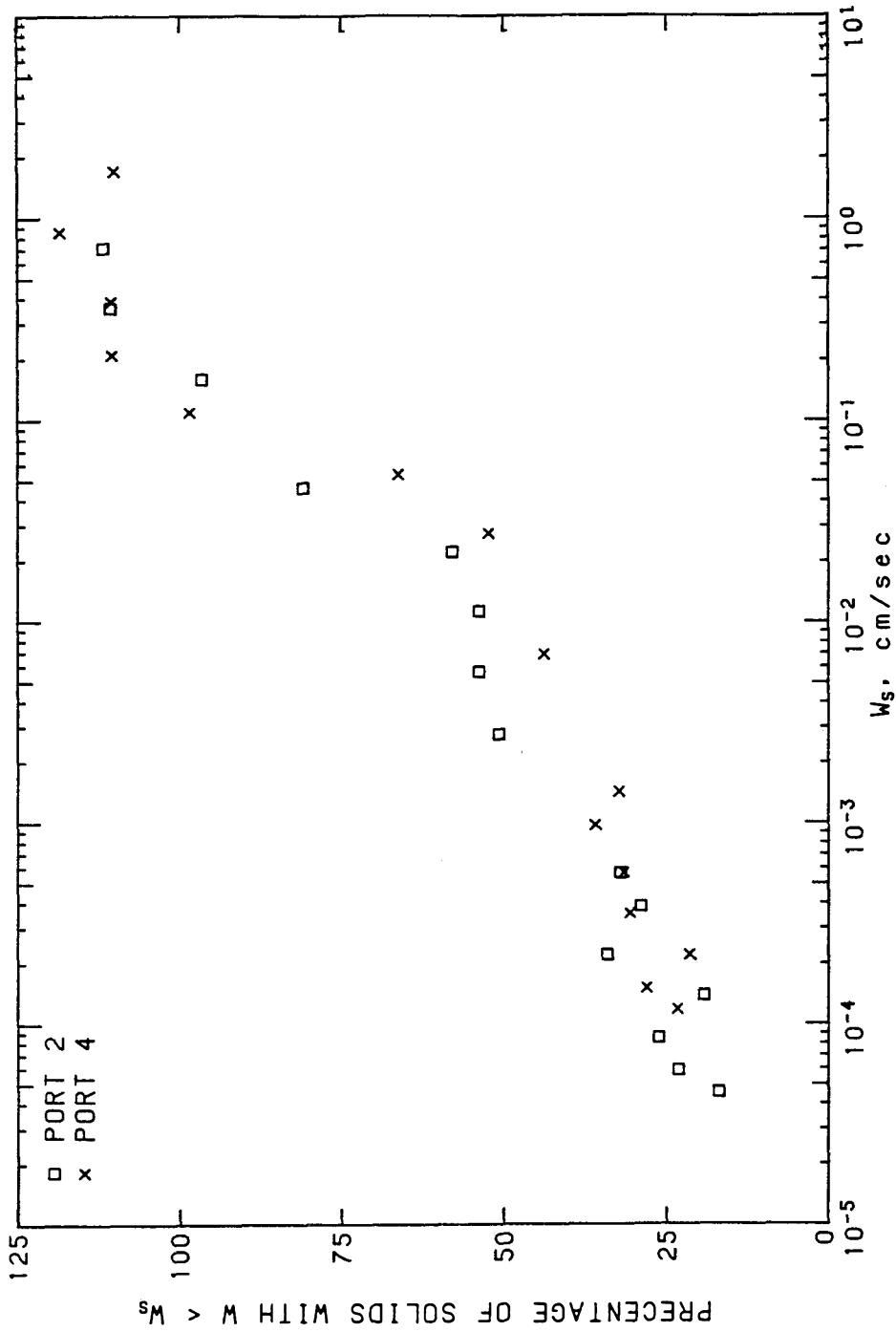


Figure 1.7 Apparent fall velocity distribution for Run 6. See Table 1.1 for further details. Ports 2 and 4 are two sampling ports along column with Port 2 about 41.0 cm and Port 4 101.0 cm below water surface.

Higher particle concentration provides an explanation for the faster sedimentation rate of run 2 compared to run 1. Longer stirring time might suggest a larger apparent fall velocity of run 3. However, the differences between runs 3, 4, and 5 are not large enough for a firm conclusion to be drawn. In order to define the effects of initial mixing more precisely, further experiments are required.

1.5 Reference

- Faisst, W. K. 1976. Digested sewage sludge: characterization of a residual and modeling for its disposal in the ocean off Southern California. EQL Report No.13, Environmental Quality Laboratory, California Institute of Technology, Pasadena, California, 193 pp.
- Faisst, W. K. 1980. Coagulation of particulate in digested sludge. In Particulate in Water: Characterization, Fate, Effects and Removal. M. C. Kavanaugh and J. O. Leckie, Eds., Advances in Chemistry Series 189, American Chemical Society, Washington D. C., 259-282.
- Hunt, J. R. and J. D. Pandya. 1984. Sewage sludge coagulation and settling in seawater. Environmental Science and Technology, 18, 119-121.

Appendix C. Particle Image Analysis

In this Appendix, the formulas used to calculate the area, the centroid, the equal-area diameter, the directions of the principal axes, the maximum and minimum dimensions along the principal axes, and the second moments in the principal directions are summarized.

The preprocessing steps (digitization, quantization and thresholding, see Section 3.2.2) create a binary image of values 1 or 0 defined on a two-dimensional grid of size $N_x \times N_y$. In this system, $N_x = N_y = 140$. The image function is written as:

$$I(x, y) = \begin{cases} 1, & \text{object;} \\ 0, & \text{background.} \end{cases} \quad (\text{C.1})$$

The area A_p is the sum of the number of pixels of nonzero (object) values as

$$A_p = \sum_{x=1}^{N_x} \sum_{y=1}^{N_y} I(x, y) \quad (\text{C.2})$$

and the coordinates of the centroid (the center of mass of the nonzero object region), (\bar{x}, \bar{y}) , is

$$\bar{x} = \frac{\sum_{x=1}^{N_x} \sum_{y=1}^{N_y} xI(x,y)}{\sum_{x=1}^{N_x} \sum_{y=1}^{N_y} I(x,y)} = \frac{\sum_{x=1}^{N_x} \sum_{y=1}^{N_y} xI(x,y)}{A_p}$$

$$\bar{y} = \frac{\sum_{x=1}^{N_x} \sum_{y=1}^{N_y} yI(x,y)}{\sum_{x=1}^{N_x} \sum_{y=1}^{N_y} I(x,y)} = \frac{\sum_{x=1}^{N_x} \sum_{y=1}^{N_y} yI(x,y)}{A_p}$$
(C.3)

The equal-area diameter, d_{equ} , is the diameter of the circle that has the same area of the particle being observed (Figure C.1),

$$d_{equ} = \sqrt{\frac{4A_p}{\pi}}$$
(C.4)

To compute the directions of the principal axes, it is required to first compute higher order moments μ_{20} , μ_{11} , and μ_{02} according to the following equations:

$$\mu_{pq} = \sum_{x=1}^{N_x} \sum_{y=1}^{N_y} (x - \bar{x})^p (y - \bar{y})^q I(x,y)$$
(C.5)

Then the angle, θ , between the principal axes and the x-axis is calculated as

$$\theta = \frac{1}{2} \tan^{-1} \left(\frac{2\mu_{11}}{\mu_{20} - \mu_{02}} \right)$$
(C.6)

The angle θ obtained may be with respect to either the major principal axis or the minor principal axis. One way to determine a unique orientation of the major

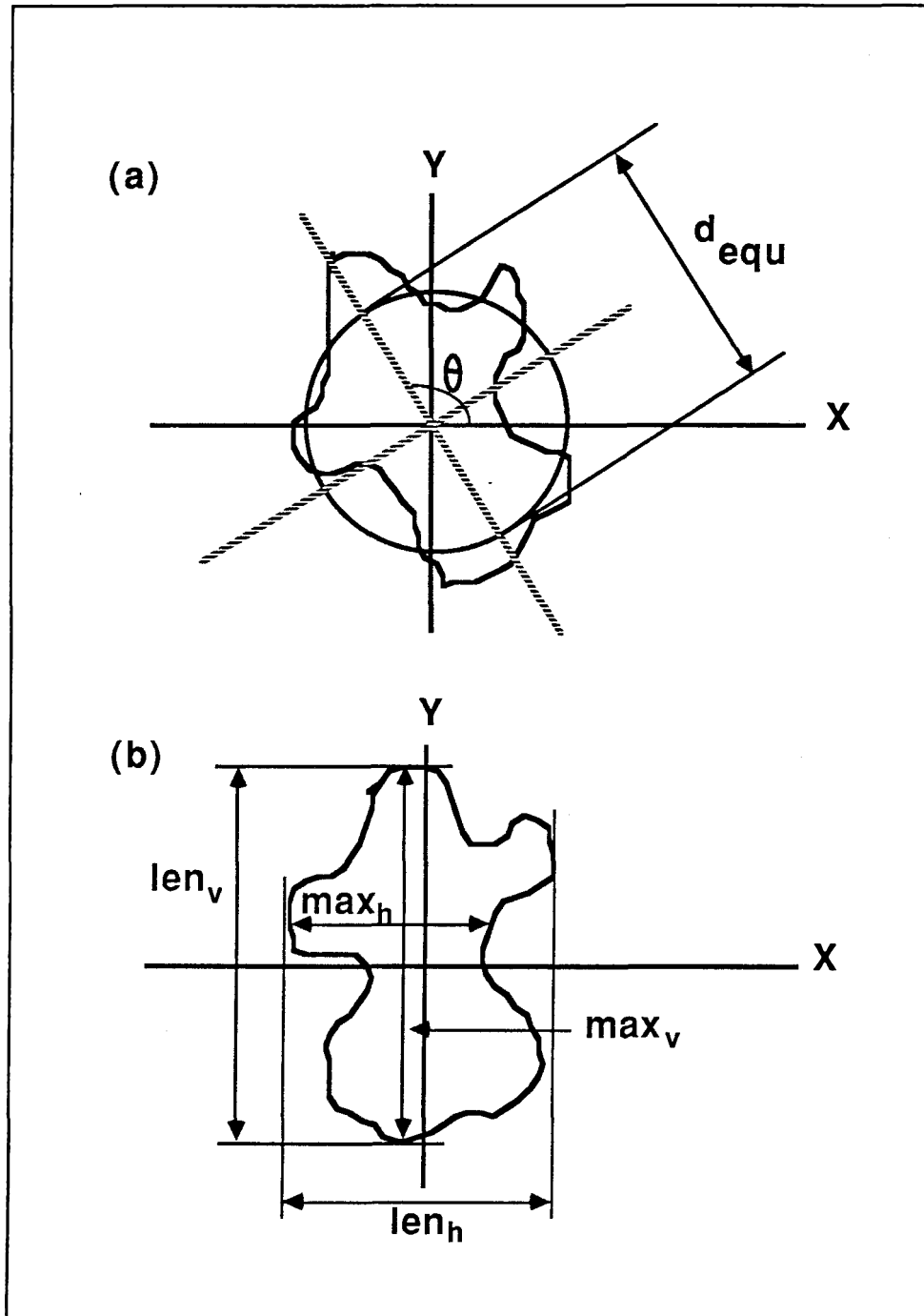


Figure C.1 Definitions of the equivalent diameter d_{equ} , the angle θ , and the other length scales used to characterize the shape of particle images

principal axis is to set the additional constraints that $\mu'_{30} > 0$ and $\mu'_{20} > \mu'_{02}$ where primed quantities denote normalized moments measured in the rotated coordinate system with principal axes as coordinate axes (Figure C.1). If the angle of the minor axis is located, then 90° is added ($\theta < 90^\circ$) or subtracted ($\theta > 90^\circ$) from θ to give the angle between the major axis and the x-axis.

There are four length scales along the directions of the principal axes which measure the “elongateness” of particles along these directions (Figure C.1). To calculate these four length scales, the image of the object is first rotated clockwise by θ so that the major and minor axes align with the x and y axes, respectively. If an object point has a coordinate (x, y) , then after rotation the new coordinate (x', y') is

$$(x', y') = (x - \bar{x}, y - \bar{y}) \begin{pmatrix} \cos\theta & -\sin\theta \\ \sin\theta & \cos\theta \end{pmatrix} + \left(\frac{N_x}{2}, \frac{N_y}{2} \right) \quad (\text{C.7})$$

The vertical and horizontal dimensions, len_v and len_h , of the rectangular bounding box which encloses the image of a particle are two important length scales. They are computed as follows: Start from the centroid and count the number of object (nonzero) pixels in the direction perpendicular to the principal axes. If the number is not zero, increment the dimension by one. Now, move away from the centroid along the direction of the principal axes, and repeat the counting procedure as described above until a point is reached where the count drops to zero. This implies that we have reached the end of the object in the direction of the principal axis and the current dimension count is the length of the object along the principal directions.

We can also define max_v and max_h to be the lengths of the longest scan lines contained in a particle along the directions of the principal axes. Note that for spherical particles, len_v is the same as max_v and len_h is the same as max_h . However, for irregular particles, these two pairs of length scales may or may not be the same.

Finally, the second moments in the principal directions, σ^2 , measure the “spread” of the object in the principal axis directions. The square roots of the moments, σ_{major} and σ_{minor} , are computed as

$$\begin{aligned}\sigma_{major} &= \sqrt{\frac{1}{A_p} \sum_{x'=1}^{N_x} \sum_{y'=1}^{N_y} I(x', y') \left(y' - \frac{N_y}{2}\right)^2} \\ \sigma_{minor} &= \sqrt{\frac{1}{A_p} \sum_{x'=1}^{N_x} \sum_{y'=1}^{N_y} I(x', y') \left(x' - \frac{N_x}{2}\right)^2}\end{aligned}\tag{C.8}$$

The measured data for samples in Run 3 ($t = 0''$) and Run 4 ($4'30''$) are summarized in Tables C.1 and C.2 respectively. The different length scales, d_{equ} , len_v , len_h , max_v , and max_h , as well as σ_{major} and σ_{minor} can be used to characterize particle shape. For example, Figure C.2 shows the ratios of the maximum dimension (len_v) to d_{equ} versus d_{equ} with the median value of about 1.4. The aspect ratio of particles can be estimated by $\frac{len_v}{len_h}$, $\frac{max_v}{max_h}$, and $\frac{\sigma_{major}}{\sigma_{minor}}$; results are shown in Figures C.3, C.4, and C.5, which all give the aspect ratio less than 2 for most of the particles.

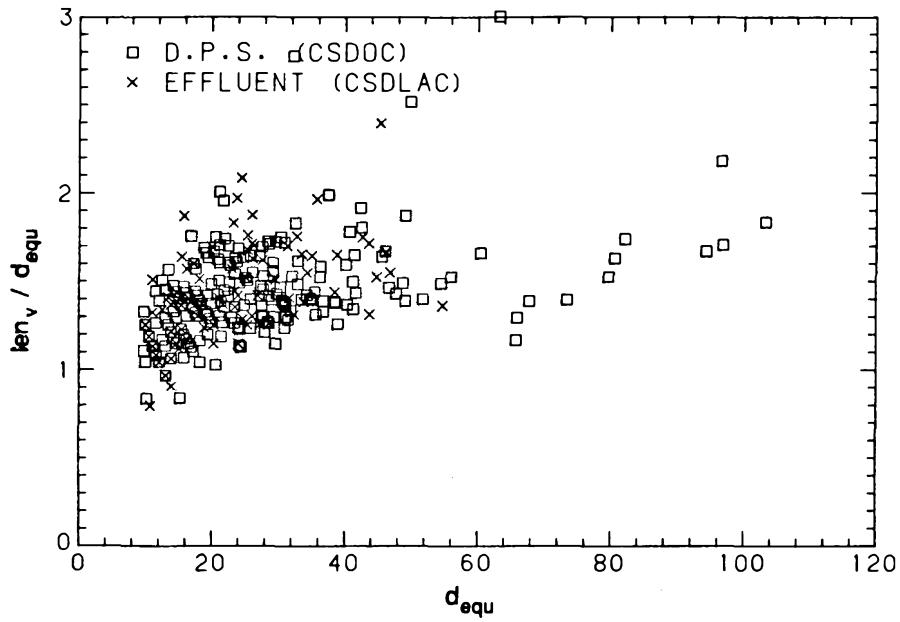


Figure C.2 $\frac{len_v}{d_{equ}}$ versus d_{equ} for D.P.S (CSDOC)—Run 3, $t = 0''$ (\square), and effluent (CSDLAC)—Run 4, $t = 4'30''$ (\times)

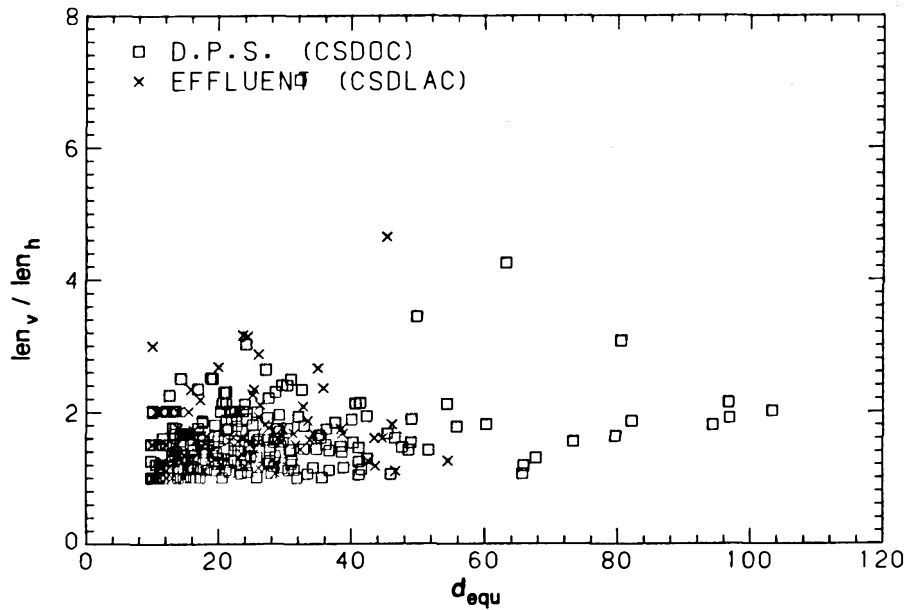


Figure C.3 $\frac{len_v}{len_h}$ versus d_{equ} for D.P.S (CSDOC)—Run 3, $t = 0''$ (\square), and effluent (CSDLAC)—Run 4, $t = 4'30''$ (\times)

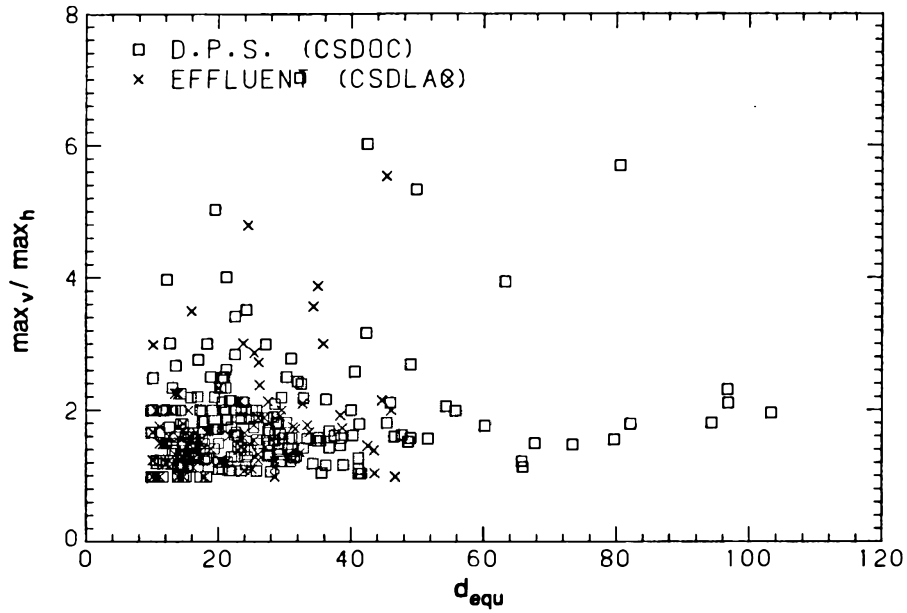


Figure C.4 $\frac{\max_v}{\max_h}$ versus d_{equ} for D.P.S (CSDOC)—Run 3, $t = 0''$ (\square), and effluent (CSDLAC)—Run 4, $t = 4'30''$ (\times)

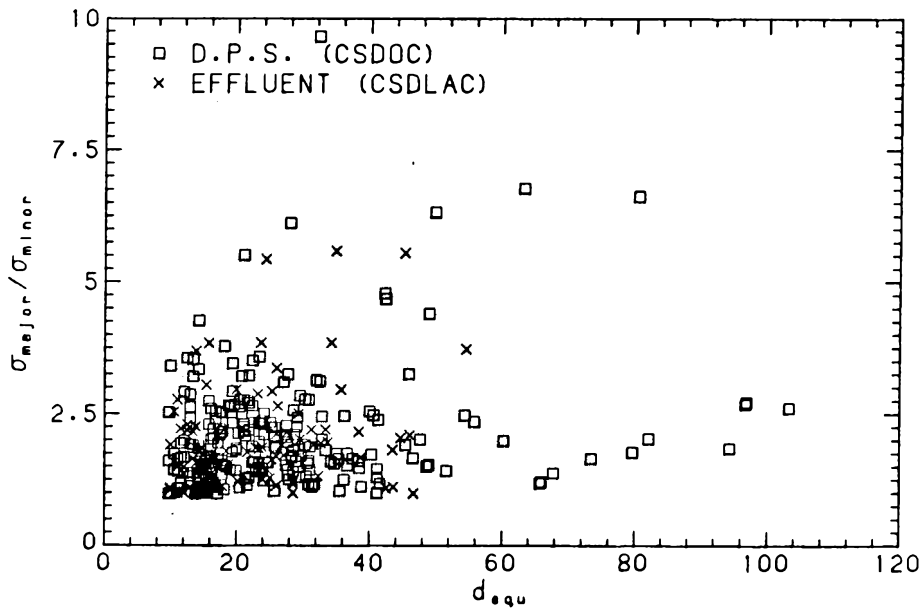


Figure C.5 $\frac{\sigma_{major}}{\sigma_{minor}}$ versus d_{equ} for D.P.S (CSDOC)—Run 3, $t = 0''$ (\square), and effluent (CSDLAC)—Run 4, $t = 4'30''$ (\times)

Table C.1 Summary of the experimental data for Run 3—D.P.S. (CSDOC) at $t = 0$.

A_p	d_{equ}	w	θ	$\frac{\sigma_{major}}{d_{equ}}$	$\frac{\sigma_{minor}}{d_{equ}}$	$\frac{len_v}{d_{equ}}$	$\frac{len_h}{d_{equ}}$	$\frac{max_v}{d_{equ}}$	$\frac{max_h}{d_{equ}}$
1361.07	37.56	1.33×10^{-3}	102.93	0.37	0.22	1.99	1.09	1.30	0.81
1957.64	49.84	2.96×10^{-3}	85.92	0.88	0.14	2.52	0.73	2.35	0.44
453.69	24.03	2.12×10^{-3}	71.96	0.41	0.17	1.68	0.80	1.50	0.71
1415.51	42.45	2.33×10^{-3}	133.19	1.03	0.22	1.36	1.05	1.80	0.30
435.54	23.55	2.21×10^{-3}	82.40	0.40	0.17	1.54	0.90	1.45	0.73
952.75	34.83	2.16×10^{-3}	21.67	0.36	0.23	1.40	0.98	1.23	0.80
1279.41	40.36	2.33×10^{-3}	50.25	0.34	0.19	1.37	0.89	1.11	0.69
753.13	30.97	2.80×10^{-2}	95.78	0.43	0.16	1.72	0.69	1.72	0.62
4981.52	79.64	3.37×10^{-2}	107.49	0.34	0.19	1.52	0.94	1.28	0.83
970.90	35.16	2.79×10^{-2}	125.15	0.32	0.19	1.39	0.85	1.15	0.73
417.39	23.05	2.21×10^{-2}	70.50	0.31	0.22	1.29	0.93	1.20	0.83
1297.55	40.65	2.08×10^{-2}	126.27	0.44	0.17	1.78	0.84	1.63	0.63
499.06	25.21	1.70×10^{-2}	60.81	0.37	0.16	1.52	0.85	1.35	0.68
753.13	30.97	1.70×10^{-3}	103.42	0.34	0.21	1.38	0.96	1.10	0.82
6986.83	94.32	1.89×10^{-2}	67.58	0.36	0.19	1.67	0.93	1.42	0.79
1170.52	38.61	1.47×10^{-2}	64.28	0.31	0.20	1.38	1.00	1.22	0.77
399.25	22.55	1.52×10^{-2}	69.49	0.35	0.19	1.41	0.94	1.23	0.75
598.85	27.56	1.87×10^{-3}	103.96	0.34	0.22	1.36	0.87	1.15	0.88
598.87	27.61	1.24×10^{-2}	128.30	0.47	0.23	1.31	1.08	1.31	0.77
725.90	30.40	1.27×10^{-2}	91.13	0.44	0.16	1.68	0.70	1.75	0.70
362.95	21.50	2.04×10^{-3}	65.21	0.34	0.17	1.38	0.80	1.29	0.69
689.61	29.63	1.18×10^{-2}	31.58	0.29	0.22	1.15	1.00	1.15	0.94
680.53	29.44	1.20×10^{-2}	109.74	0.35	0.19	1.30	0.87	1.30	0.80
607.94	27.82	1.11×10^{-2}	59.99	0.31	0.23	1.46	1.00	1.23	0.92
617.02	28.03	1.68×10^{-3}	133.61	0.31	0.25	1.22	1.14	1.07	0.99
671.46	29.17	8.73×10^{-3}	120.71	0.38	0.17	1.56	0.80	1.38	0.77
462.76	24.27	8.83×10^{-3}	84.10	0.28	0.23	1.14	0.96	1.14	0.96
7363.39	96.82	9.03×10^{-3}	86.20	0.49	0.18	1.71	0.89	1.71	0.81
8375.12	103.26	9.00×10^{-3}	79.54	0.47	0.18	1.84	0.91	1.65	0.85
435.54	23.55	1.49×10^{-3}	15.67	0.32	0.20	1.26	0.90	1.17	0.81
290.36	19.23	2.12×10^{-3}	67.18	0.44	0.17	1.66	0.67	1.33	0.67
662.39	29.04	8.88×10^{-3}	84.04	0.33	0.20	1.39	0.88	1.25	0.88
644.24	28.64	9.18×10^{-3}	78.60	0.34	0.19	1.41	0.89	1.34	0.82
7340.70	96.68	8.11×10^{-3}	74.19	0.51	0.19	2.18	1.01	1.67	0.73
1161.45	38.46	1.28×10^{-3}	99.56	0.34	0.21	1.38	0.94	1.22	0.83
254.07	17.99	6.74×10^{-3}	67.76	0.34	0.21	1.42	0.94	1.30	0.94
798.49	31.89	1.48×10^{-3}	58.05	0.40	0.34	1.34	1.34	1.13	0.87
1887.35	49.02	6.49×10^{-3}	73.91	0.32	0.21	1.39	0.91	1.30	0.82
1034.41	36.29	1.31×10^{-3}	125.65	0.36	0.28	1.59	1.05	1.24	1.05
5290.03	82.07	6.63×10^{-3}	122.42	0.37	0.19	1.74	0.94	1.35	0.75
852.94	32.95	6.39×10^{-3}	96.09	0.46	0.19	1.62	0.90	1.55	0.71
335.73	20.68	7.32×10^{-3}	87.37	0.47	0.18	1.75	0.82	1.75	0.82
399.25	22.55	2.07×10^{-3}	103.17	0.37	0.23	1.41	1.13	1.23	0.94
408.32	22.80	1.21×10^{-3}	80.01	0.34	0.22	1.50	0.84	1.40	0.84
1333.85	41.21	1.37×10^{-3}	133.00	0.28	0.28	1.35	1.29	1.13	1.09
1660.51	45.98	4.59×10^{-3}	47.17	0.56	0.17	0.93	0.88	1.67	0.79
3139.53	63.22	5.22×10^{-3}	112.76	0.88	0.13	3.00	0.70	1.99	0.50
435.54	23.55	5.45×10^{-3}	129.31	0.51	0.26	1.17	1.00	1.54	0.81

A_p	d_{equ}	w	θ	$\frac{\sigma_{major}}{d_{equ}}$	$\frac{\sigma_{minor}}{d_{equ}}$	$\frac{len_v}{d_{equ}}$	$\frac{len_h}{d_{equ}}$	$\frac{max_v}{d_{equ}}$	$\frac{max_h}{d_{equ}}$
489.99	24.98	1.39×10^{-3}	102.56	0.35	0.22	1.37	1.02	1.20	0.86
462.76	24.27	1.42×10^{-3}	85.18	0.38	0.18	1.49	0.79	1.40	0.70
580.72	27.19	4.53×10^{-3}	94.38	0.45	0.14	1.64	0.62	1.64	0.55
2449.93	55.85	4.48×10^{-3}	89.15	0.43	0.18	1.49	0.84	1.52	0.76
1787.54	47.71	4.43×10^{-3}	100.60	0.43	0.21	1.43	0.98	1.38	0.85
471.84	24.51	4.74×10^{-3}	84.09	0.40	0.22	1.13	1.04	1.13	0.87
3411.75	65.91	3.66×10^{-3}	97.98	0.31	0.25	1.29	1.10	1.10	0.97
725.90	30.40	4.13×10^{-3}	88.53	0.38	0.20	1.47	0.84	1.40	0.77
317.58	20.11	1.03×10^{-3}	39.35	0.31	0.22	1.38	1.06	1.06	0.95
880.16	33.48	4.03×10^{-3}	163.73	0.47	0.25	1.27	1.21	1.40	0.89
1705.87	46.60	3.52×10^{-3}	65.39	0.34	0.20	1.47	0.92	1.33	0.82
1333.85	41.21	3.14×10^{-3}	154.14	0.34	0.23	1.50	1.03	1.03	0.93
2849.17	60.23	3.91×10^{-3}	104.39	0.40	0.20	1.66	0.92	1.38	0.78
4228.39	73.37	3.28×10^{-3}	123.51	0.32	0.19	1.39	0.90	1.16	0.79
1624.21	45.48	3.44×10^{-3}	70.58	0.38	0.20	1.64	0.99	1.36	0.75
1361.07	41.63	3.17×10^{-3}	124.62	0.34	0.28	1.43	1.28	1.08	1.02
680.53	29.44	2.81×10^{-3}	92.29	0.31	0.20	1.30	0.94	1.16	0.87
5090.40	80.50	3.13×10^{-3}	63.80	0.69	0.10	1.63	0.53	0.74	0.13
671.46	29.24	3.31×10^{-3}	71.05	0.62	0.25	1.61	0.94	1.10	0.73
3393.60	65.73	3.32×10^{-3}	150.95	0.27	0.22	1.16	1.10	1.07	0.87
1342.92	41.35	3.70×10^{-3}	77.14	0.42	0.17	1.65	0.77	1.39	0.77
780.35	31.52	2.37×10^{-3}	146.88	0.29	0.25	1.28	1.15	1.22	0.94
998.12	35.65	2.66×10^{-3}	131.82	0.28	0.27	1.32	1.32	1.08	1.01
1860.13	48.67	2.64×10^{-3}	109.85	0.34	0.22	1.49	1.05	1.14	0.75
834.79	32.60	2.64×10^{-3}	109.75	0.50	0.16	1.83	0.79	1.57	0.65
3602.30	67.72	2.98×10^{-3}	71.76	0.34	0.25	1.38	1.07	1.23	0.82
807.57	32.07	2.89×10^{-3}	87.81	0.54	0.17	1.53	0.80	1.46	0.60
353.88	21.23	7.42×10^{-4}	92.09	0.40	0.17	1.61	0.70	1.40	0.70
199.62	15.94	2.59×10^{-3}	75.09	0.29	0.19	1.20	0.80	1.20	0.80
299.44	19.53	2.40×10^{-3}	159.50	0.62	0.21	1.09	0.98	1.20	0.55
1333.85	41.21	2.76×10^{-3}	91.16	0.31	0.24	1.35	1.09	1.19	0.93
1887.35	49.02	2.36×10^{-3}	98.21	0.66	0.15	1.39	0.74	1.87	0.69
1034.41	36.29	2.08×10^{-3}	86.01	0.42	0.17	1.52	0.88	1.52	0.70
1406.44	42.32	2.03×10^{-3}	85.78	0.67	0.14	1.36	0.70	1.91	0.61
1061.63	36.77	2.51×10^{-3}	100.67	0.34	0.22	1.16	1.04	1.33	0.93
1061.63	36.77	2.15×10^{-3}	109.96	0.34	0.19	1.39	0.99	1.27	0.75
607.94	27.82	2.19×10^{-3}	112.70	0.32	0.22	1.30	1.07	1.23	0.84
653.31	28.84	2.15×10^{-3}	95.44	0.72	0.34	1.40	0.81	1.48	0.81
762.20	31.15	1.79×10^{-3}	74.06	0.41	0.22	1.37	1.10	1.30	0.82
508.13	25.44	1.69×10^{-3}	142.26	0.41	0.18	1.50	0.92	1.17	0.67
344.80	20.95	1.80×10^{-3}	92.60	0.68	0.21	1.32	0.92	1.42	0.71
1261.26	40.07	1.95×10^{-3}	108.77	0.44	0.17	1.60	0.85	1.49	0.75
689.61	29.63	1.68×10^{-3}	88.08	0.47	0.17	1.73	0.72	1.58	0.72
172.40	14.82	1.65×10^{-3}	43.44	0.31	0.29	1.29	1.15	0.87	0.87
235.92	17.33	6.30×10^{-4}	101.73	0.41	0.21	1.60	0.99	1.48	0.74
163.33	14.42	8.27×10^{-4}	117.62	0.36	0.19	1.48	0.88	1.18	0.59
1188.67	38.90	1.73×10^{-3}	119.79	0.29	0.25	1.26	1.10	1.10	0.93
2322.89	54.38	1.81×10^{-3}	122.18	0.38	0.16	1.49	0.70	1.29	0.62
117.96	12.26	1.75×10^{-3}	9.22	0.22	0.11	1.04	0.69	1.04	0.52
753.13	30.97	1.61×10^{-3}	83.48	0.29	0.25	1.24	1.03	1.10	0.89

A_p	d_{equ}	w	θ	$\frac{\sigma_{major}}{d_{equ}}$	$\frac{\sigma_{minor}}{d_{equ}}$	$\frac{len_v}{d_{equ}}$	$\frac{len_h}{d_{equ}}$	$\frac{max_v}{d_{equ}}$	$\frac{max_h}{d_{equ}}$
290.36	19.23	1.24×10^{-3}	17.60	0.32	0.22	1.33	1.00	1.33	0.77
852.94	32.95	1.29×10^{-3}	114.79	0.46	0.22	1.49	1.03	1.29	0.90
226.85	16.99	1.51×10^{-3}	87.06	0.53	0.22	1.75	1.00	1.38	0.62
480.91	24.75	1.50×10^{-3}	61.01	0.39	0.25	1.63	1.12	1.29	0.69
208.70	16.30	1.64×10^{-3}	86.10	0.37	0.22	1.30	0.92	1.17	0.79
81.66	10.20	1.51×10^{-3}	0.00	0.29	0.09	1.25	0.62	1.25	0.62
372.03	21.76	1.53×10^{-3}	125.24	0.51	0.19	1.96	0.98	1.47	0.69
99.81	11.27	1.44×10^{-3}	150.74	0.44	0.31	1.13	0.94	0.94	0.56
989.04	35.49	1.41×10^{-3}	79.17	0.34	0.20	1.44	0.90	1.20	0.78
2096.05	51.66	1.51×10^{-3}	64.47	0.34	0.24	1.40	0.99	1.24	0.79
353.88	21.23	1.18×10^{-3}	120.22	0.77	0.14	1.21	0.70	2.01	0.50
299.44	19.53	5.01×10^{-4}	123.39	0.33	0.19	1.42	0.87	1.09	0.76
435.54	23.55	9.06×10^{-4}	117.10	0.64	0.18	1.09	0.90	1.36	0.73
598.87	27.61	1.06×10^{-3}	123.60	0.40	0.17	1.70	0.77	1.31	0.69
744.05	30.78	1.05×10^{-3}	87.07	0.33	0.21	1.38	0.97	1.32	0.83
607.94	27.82	1.27×10^{-3}	54.16	0.38	0.19	1.30	0.92	1.30	0.76
816.64	32.25	1.20×10^{-3}	62.53	0.82	0.09	2.78	0.40	2.78	0.40
145.18	13.60	4.36×10^{-4}	150.00	0.31	0.22	1.25	0.94	1.10	0.79
217.77	16.65	1.19×10^{-3}	51.88	0.46	0.20	1.15	0.89	1.40	0.89
254.07	17.99	8.85×10^{-4}	113.21	0.69	0.28	1.07	0.71	1.30	0.71
263.14	18.30	9.50×10^{-4}	64.80	0.34	0.22	1.04	0.93	1.04	0.81
208.70	16.30	9.32×10^{-4}	14.18	0.30	0.20	1.30	0.92	1.30	0.92
417.39	23.05	1.04×10^{-3}	106.94	0.31	0.22	1.29	0.93	1.20	0.74
254.07	17.99	9.27×10^{-4}	92.90	0.31	0.23	1.30	0.94	1.18	0.94
617.02	28.03	9.00×10^{-4}	18.58	1.28	0.21	0.99	0.00	1.22	0.00
145.18	13.60	9.52×10^{-4}	94.64	0.31	0.09	1.10	0.62	1.25	0.47
526.28	25.89	8.52×10^{-4}	101.35	0.48	0.23	1.40	1.07	1.15	0.74
172.40	14.82	2.94×10^{-4}	168.47	0.32	0.22	1.29	0.87	1.00	0.87
108.89	11.77	9.91×10^{-4}	9.22	0.28	0.25	1.09	1.09	1.09	0.90
181.48	15.20	7.76×10^{-4}	67.50	0.22	0.21	0.84	0.84	0.84	0.84
635.17	28.44	8.98×10^{-4}	118.09	0.40	0.23	1.05	0.90	1.27	0.82
526.28	25.89	1.20×10^{-3}	44.81	0.29	0.28	1.24	1.24	1.07	0.99
217.77	16.65	9.63×10^{-4}	57.70	0.52	0.25	1.02	1.02	1.15	0.89
535.35	26.11	9.36×10^{-4}	105.53	0.40	0.22	1.55	0.98	1.23	0.81
698.68	29.83	1.04×10^{-3}	81.55	0.35	0.20	1.43	0.93	1.36	0.86
117.96	12.26	1.02×10^{-3}	7.09	0.57	0.19	1.04	0.52	1.39	0.35
299.44	19.53	3.49×10^{-4}	132.37	0.46	0.19	1.09	0.87	1.31	0.76
925.53	34.33	8.21×10^{-4}	50.17	0.45	0.28	1.42	1.24	1.12	0.93
381.10	22.03	6.96×10^{-4}	11.74	0.37	0.17	1.45	0.77	1.45	0.68
381.10	22.03	7.65×10^{-4}	24.87	0.71	0.22	1.16	0.00	1.36	0.00
199.62	15.94	7.14×10^{-4}	77.93	0.50	0.18	0.94	0.80	1.47	0.67
526.28	25.89	7.86×10^{-4}	108.06	0.41	0.18	1.64	0.82	1.48	0.74
462.76	24.27	8.03×10^{-4}	7.65	0.56	0.22	1.05	0.35	1.23	0.35
372.03	21.76	1.33×10^{-3}	50.08	0.29	0.25	1.27	1.17	1.08	0.98
235.92	17.33	7.56×10^{-4}	124.61	0.26	0.26	1.11	1.11	0.99	0.99
362.95	21.50	7.90×10^{-4}	126.74	0.28	0.22	1.19	0.99	1.09	0.89
317.58	20.11	1.29×10^{-3}	110.44	0.35	0.19	1.49	0.95	1.27	0.74
136.11	13.16	8.23×10^{-4}	112.50	0.31	0.23	1.29	0.97	0.97	0.81
208.70	16.30	7.38×10^{-4}	54.60	0.50	0.19	1.04	0.79	1.17	0.79
208.70	16.30	7.46×10^{-4}	60.04	0.31	0.22	1.30	0.92	1.04	0.79

A_p	d_{equ}	w	θ	$\frac{\sigma_{major}}{d_{equ}}$	$\frac{\sigma_{minor}}{d_{equ}}$	$\frac{len_v}{d_{equ}}$	$\frac{len_h}{d_{equ}}$	$\frac{max_v}{d_{equ}}$	$\frac{max_h}{d_{equ}}$
635.17	28.44	7.56×10^{-4}	99.56	0.50	0.29	1.73	1.13	1.42	0.75
163.33	14.42	7.60×10^{-4}	61.32	0.38	0.12	1.48	0.59	1.33	0.59
136.11	13.16	7.26×10^{-4}	48.75	0.54	0.44	1.46	1.13	0.97	0.81
136.11	13.16	7.42×10^{-4}	58.00	0.47	0.25	1.29	0.97	1.13	0.81
263.14	18.30	6.83×10^{-4}	52.81	0.70	0.19	1.16	0.81	1.39	0.47
99.81	11.27	8.10×10^{-4}	22.50	0.30	0.28	1.13	1.13	0.94	0.75
235.92	17.33	3.58×10^{-4}	99.16	0.34	0.20	1.35	0.86	1.23	0.86
335.73	20.68	9.46×10^{-4}	132.65	0.25	0.22	1.03	1.03	0.93	0.82
408.32	22.80	3.10×10^{-4}	96.95	0.41	0.17	1.59	0.84	1.50	0.75
444.62	23.79	5.01×10^{-4}	99.61	0.42	0.18	1.61	0.81	1.52	0.71
127.03	12.72	2.34×10^{-4}	91.53	0.41	0.12	1.50	0.67	1.50	0.50
308.51	19.82	6.68×10^{-4}	86.94	0.51	0.19	1.18	0.86	1.29	0.75
335.73	20.68	6.12×10^{-4}	66.90	0.49	0.17	1.75	0.82	1.54	0.62
734.98	30.59	7.59×10^{-4}	117.15	0.38	0.29	1.39	1.25	1.18	0.83
190.55	15.58	7.65×10^{-4}	84.92	0.32	0.20	1.37	0.82	1.37	0.82
435.54	23.55	5.84×10^{-4}	40.88	0.61	0.41	1.63	1.54	1.09	1.00
108.89	11.77	6.23×10^{-4}	35.89	0.23	0.14	1.09	0.73	0.90	0.73
190.55	15.58	6.01×10^{-4}	133.49	0.28	0.28	1.23	1.10	1.10	0.95
353.88	21.23	6.89×10^{-4}	93.93	0.41	0.17	1.71	0.81	1.50	0.81
163.33	14.42	6.71×10^{-4}	41.74	0.56	0.13	1.03	0.74	1.33	0.74
244.99	17.66	6.25×10^{-4}	94.96	0.39	0.19	1.33	0.73	1.33	0.73
607.94	27.82	5.69×10^{-4}	131.50	0.63	0.19	1.15	0.92	1.53	0.92
163.33	14.42	5.75×10^{-4}	63.43	0.29	0.21	1.33	0.88	1.18	0.88
172.40	14.82	5.94×10^{-4}	15.24	0.35	0.19	1.44	0.87	1.29	0.87
353.88	21.23	6.34×10^{-4}	52.11	0.54	0.19	1.00	0.90	1.30	0.50
127.03	12.72	7.10×10^{-4}	115.59	0.31	0.22	1.17	1.00	1.17	0.67
263.14	18.30	6.28×10^{-4}	45.34	0.28	0.26	1.16	1.04	0.93	0.93
190.55	15.58	6.34×10^{-4}	89.23	0.30	0.23	1.23	0.95	1.23	0.95
172.40	14.82	5.69×10^{-4}	74.02	0.34	0.22	1.44	0.87	1.00	0.87
526.28	25.89	7.38×10^{-4}	94.32	0.38	0.20	1.40	0.90	1.40	0.74
353.88	21.23	6.29×10^{-4}	67.08	0.37	0.17	1.50	0.81	1.40	0.60
399.25	22.55	6.84×10^{-4}	92.20	0.65	0.19	1.33	0.85	1.61	0.47
381.10	22.03	5.53×10^{-4}	62.95	0.51	0.19	1.74	0.87	1.36	0.77
317.58	20.11	7.37×10^{-4}	68.20	0.31	0.22	1.27	1.06	1.16	0.95
453.69	24.03	5.43×10^{-4}	83.15	0.32	0.22	1.24	0.98	1.24	0.88
72.59	10.00	6.00×10^{-4}	80.78	0.35	0.14	1.33	0.88	1.33	0.67
72.59	10.00	6.65×10^{-4}	103.28	0.35	0.14	1.33	0.88	1.33	0.67
244.99	17.66	6.45×10^{-4}	66.32	0.41	0.19	1.45	0.96	1.45	0.73
199.62	15.94	6.22×10^{-4}	124.19	0.28	0.23	1.20	1.07	1.20	0.80
190.55	15.58	4.72×10^{-4}	69.63	0.34	0.20	1.37	0.82	1.10	0.69
163.33	14.42	6.24×10^{-4}	131.71	0.34	0.34	1.33	1.03	0.88	0.74
90.74	10.75	4.42×10^{-4}	45.00	0.42	0.24	0.99	0.99	1.19	0.99
299.44	19.53	4.47×10^{-4}	96.73	0.64	0.19	0.98	0.55	1.63	0.32
399.25	22.55	6.10×10^{-4}	78.25	0.47	0.17	1.70	0.85	1.61	0.56
163.33	14.42	4.69×10^{-4}	118.47	0.48	0.25	1.03	1.03	1.18	1.03
99.81	11.27	4.78×10^{-4}	87.97	0.24	0.14	1.13	0.75	0.94	0.75
644.24	28.64	7.01×10^{-4}	73.86	0.32	0.23	1.26	0.96	1.26	0.82
326.66	20.39	5.07×10^{-4}	90.17	0.46	0.22	1.67	0.83	1.46	0.62
208.70	16.30	4.88×10^{-4}	46.51	0.28	0.23	1.17	1.04	1.17	0.79
381.10	22.03	6.31×10^{-4}	124.91	0.34	0.26	1.36	1.07	1.25	0.96

A_p	d_{equ}	w	θ	$\frac{\sigma_{major}}{d_{equ}}$	$\frac{\sigma_{minor}}{d_{equ}}$	$\frac{len_v}{d_{equ}}$	$\frac{len_h}{d_{equ}}$	$\frac{max_v}{d_{equ}}$	$\frac{max_h}{d_{equ}}$
589.80	27.40	4.99×10^{-4}	66.98	0.36	0.17	1.48	0.77	1.32	0.70
281.29	18.92	5.87×10^{-4}	82.97	0.44	0.17	1.69	0.68	1.69	0.68
762.20	31.15	4.41×10^{-4}	112.07	0.35	0.25	1.30	1.02	1.16	0.82
199.62	15.94	3.58×10^{-4}	128.64	0.49	0.21	0.80	0.80	1.07	0.67
344.80	20.95	4.58×10^{-4}	97.65	0.43	0.17	1.63	0.71	1.52	0.61
72.59	10.00	4.57×10^{-4}	135.00	0.31	0.31	1.33	1.33	0.88	0.88
226.85	16.99	4.48×10^{-4}	103.15	0.46	0.18	1.75	0.75	1.38	0.50
154.25	14.01	4.61×10^{-4}	37.47	0.23	0.22	1.07	1.07	0.91	0.91
272.21	18.62	4.19×10^{-4}	125.02	0.28	0.19	1.38	0.92	1.03	0.80
226.85	16.99	3.86×10^{-4}	133.67	0.28	0.25	1.13	1.00	1.00	0.87
172.40	14.82	4.83×10^{-4}	165.92	0.32	0.19	1.29	0.87	1.29	0.72
208.70	16.30	4.63×10^{-4}	99.07	0.39	0.20	1.43	0.92	1.30	0.79
72.59	10.00	3.87×10^{-4}	71.67	0.23	0.14	1.11	0.88	1.11	0.67
244.99	17.66	4.40×10^{-4}	60.47	0.54	0.21	1.57	0.85	1.33	0.85
317.58	20.11	3.79×10^{-4}	59.01	0.34	0.18	1.38	0.85	1.27	0.85
136.11	13.16	4.49×10^{-4}	34.61	0.33	0.12	0.81	0.64	0.97	0.64
117.96	12.26	4.01×10^{-4}	37.71	0.22	0.13	1.04	0.69	1.04	0.69
81.66	10.20	4.50×10^{-4}	116.67	0.39	0.00	0.83	0.42	1.04	0.42
644.24	28.64	8.52×10^{-4}	84.30	0.43	0.17	1.71	0.75	1.56	0.75
172.40	14.82	4.15×10^{-4}	60.72	0.38	0.22	1.29	0.87	1.00	0.72
90.74	10.75	3.80×10^{-4}	60.48	0.29	0.20	1.19	0.99	0.99	0.80
81.66	10.20	3.49×10^{-4}	0.00	0.16	0.16	0.83	0.83	0.83	0.83
108.89	11.77	3.24×10^{-4}	41.19	0.31	0.26	1.26	1.09	1.09	1.09
190.55	15.58	3.27×10^{-4}	83.54	0.34	0.25	1.23	0.95	1.10	0.82
172.40	14.82	3.72×10^{-4}	128.20	0.29	0.25	1.15	1.15	1.00	0.72
136.11	13.16	3.47×10^{-4}	94.17	0.25	0.10	1.13	0.64	1.13	0.49
108.89	11.77	3.56×10^{-4}	88.40	0.39	0.20	1.45	0.90	1.45	0.73
181.48	15.20	3.49×10^{-4}	162.31	0.34	0.22	1.40	0.84	1.12	0.84
254.07	17.99	3.35×10^{-4}	91.14	0.47	0.22	1.42	0.94	1.42	0.94
217.77	16.65	3.66×10^{-4}	132.40	0.28	0.23	1.15	0.89	1.02	0.76
145.18	13.60	3.69×10^{-4}	71.67	0.41	0.21	1.57	0.94	1.25	0.79
208.70	16.30	3.13×10^{-4}	121.00	0.41	0.20	0.92	0.79	1.30	0.79
163.33	14.42	4.09×10^{-4}	11.73	0.31	0.25	1.33	1.03	1.03	0.88
136.11	13.16	3.77×10^{-4}	67.50	0.34	0.12	1.29	0.64	1.29	0.64
254.07	17.99	3.93×10^{-4}	15.31	0.35	0.22	1.42	0.94	1.07	0.71
154.25	14.01	4.11×10^{-4}	81.86	0.25	0.25	1.22	1.07	1.07	0.91
145.18	13.60	3.74×10^{-4}	107.18	0.46	0.13	1.25	0.62	1.25	0.62
154.25	14.01	2.70×10^{-4}	39.56	0.37	0.28	1.22	1.07	0.91	0.91
326.66	20.39	2.65×10^{-4}	46.47	0.31	0.22	1.25	1.04	1.25	0.94
181.48	15.20	2.65×10^{-4}	71.19	0.35	0.19	1.40	0.84	1.12	0.70
172.40	14.82	2.54×10^{-4}	90.13	0.32	0.25	1.15	1.15	1.15	0.72
244.99	17.66	3.04×10^{-4}	90.65	0.40	0.19	1.45	0.73	1.33	0.73
308.51	19.82	2.69×10^{-4}	83.86	0.31	0.22	1.29	0.96	1.08	0.86
190.55	15.58	3.14×10^{-4}	87.84	0.31	0.18	1.37	0.82	1.37	0.82
263.14	18.30	2.76×10^{-4}	94.64	0.41	0.22	1.39	0.93	1.28	0.81
154.25	14.01	2.65×10^{-4}	103.92	0.29	0.27	1.22	1.07	0.91	0.91
172.40	14.82	2.63×10^{-4}	72.19	0.34	0.23	1.15	0.87	1.15	0.87
145.18	13.60	2.82×10^{-4}	125.78	0.30	0.23	1.25	0.94	0.94	0.79
181.48	15.20	2.82×10^{-4}	22.50	0.27	0.22	1.12	0.84	0.98	0.84
145.18	13.60	2.43×10^{-4}	107.27	0.36	0.20	1.41	0.94	1.25	0.62

A_p	d_{equ}	w	θ	$\frac{\sigma_{major}}{d_{equ}}$	$\frac{\sigma_{minor}}{d_{equ}}$	$\frac{len_v}{d_{equ}}$	$\frac{len_h}{d_{equ}}$	$\frac{max_v}{d_{equ}}$	$\frac{max_h}{d_{equ}}$
190.55	15.58	2.57×10^{-4}	45.87	0.28	0.22	1.23	0.95	0.95	0.95
172.40	14.82	2.24×10^{-4}	117.79	0.52	0.22	1.15	0.87	1.15	0.87
181.48	15.20	2.55×10^{-4}	109.57	0.28	0.28	1.12	1.12	0.84	0.84
272.21	18.62	2.53×10^{-4}	133.56	0.25	0.25	1.14	1.14	1.03	1.03
281.29	18.92	2.44×10^{-4}	85.37	0.41	0.19	1.24	0.79	1.35	0.79
208.70	16.30	2.62×10^{-4}	135.00	0.25	0.24	1.04	1.04	0.92	0.92
181.48	15.20	2.29×10^{-4}	97.77	0.33	0.29	1.40	0.98	1.26	0.84
199.62	15.94	2.55×10^{-4}	42.80	0.25	0.20	1.07	0.94	0.94	0.94
145.18	13.60	2.74×10^{-4}	69.43	0.31	0.12	1.25	0.62	1.25	0.62
99.81	11.27	3.53×10^{-4}	119.32	0.35	0.23	1.33	1.13	1.33	0.75
99.81	11.27	2.60×10^{-4}	52.48	0.23	0.23	1.13	1.13	0.94	0.94
99.81	11.27	2.44×10^{-4}	4.17	0.34	0.22	1.33	0.94	1.33	0.75
163.33	14.42	2.40×10^{-4}	60.86	0.35	0.21	1.48	0.88	1.18	0.74
190.55	15.58	2.58×10^{-4}	80.34	0.29	0.20	1.23	0.82	0.95	0.69
235.92	17.33	2.67×10^{-4}	94.22	0.37	0.22	1.60	0.99	1.35	0.86
117.96	12.26	1.87×10^{-4}	76.72	0.32	0.22	1.39	0.87	1.04	0.69
99.81	11.27	2.25×10^{-4}	85.93	0.30	0.28	1.13	1.13	0.94	0.75
127.03	12.72	2.17×10^{-4}	78.75	0.35	0.29	1.17	1.17	1.00	1.00
199.62	15.94	2.06×10^{-4}	141.95	0.34	0.21	1.34	0.94	1.20	0.80
199.62	15.94	2.11×10^{-4}	28.05	0.37	0.17	1.47	0.80	1.34	0.67
127.03	12.72	2.15×10^{-4}	61.26	0.47	0.33	1.17	1.17	1.00	1.00
172.40	14.82	2.02×10^{-4}	47.74	0.35	0.22	1.29	0.87	1.15	0.72
90.74	10.75	1.94×10^{-4}	11.79	0.37	0.22	1.38	0.99	1.38	0.80
90.74	10.75	1.96×10^{-4}	139.07	0.35	0.25	1.38	1.19	1.19	0.80
108.89	11.77	2.07×10^{-4}	99.22	0.22	0.00	1.09	0.36	1.09	0.36
217.77	16.65	2.06×10^{-4}	155.60	0.29	0.25	1.15	1.15	1.02	1.02
117.96	12.26	2.11×10^{-4}	68.05	0.36	0.22	1.39	1.04	1.22	0.69
136.11	13.16	2.02×10^{-4}	14.85	0.42	0.20	1.29	0.97	1.29	0.81
81.66	10.20	1.87×10^{-4}	3.99	0.23	0.14	1.04	0.83	1.04	0.83
263.14	18.30	3.90×10^{-4}	96.08	0.70	0.17	1.39	0.70	1.63	0.58
145.18	13.60	2.06×10^{-4}	74.99	0.34	0.09	1.41	0.62	1.41	0.47
117.96	12.26	2.05×10^{-4}	76.72	0.28	0.28	1.04	1.04	0.87	0.87
81.66	10.20	2.05×10^{-4}	45.00	0.29	0.09	1.25	0.62	1.25	0.62
81.66	10.20	2.06×10^{-4}	85.83	0.22	0.14	1.04	0.83	1.04	0.62
117.96	12.26	2.17×10^{-4}	42.35	0.32	0.25	1.22	1.04	1.04	0.87
117.96	12.26	2.06×10^{-4}	76.72	0.27	0.26	1.04	1.04	1.04	0.87
244.99	17.66	2.97×10^{-4}	159.18	0.34	0.20	1.45	0.85	1.21	0.85
190.55	15.58	1.53×10^{-4}	110.93	0.26	0.21	1.10	0.95	1.10	0.95
127.03	12.72	1.76×10^{-4}	119.14	0.34	0.22	1.34	1.00	1.17	0.67
408.32	22.80	2.96×10^{-4}	121.69	0.37	0.23	1.12	1.03	1.12	0.84
117.96	12.26	1.82×10^{-4}	85.78	0.35	0.28	1.22	1.04	1.04	0.87
217.77	16.65	1.62×10^{-4}	69.78	0.32	0.29	1.28	0.89	1.02	0.64
217.77	16.65	3.07×10^{-4}	85.62	0.29	0.27	1.28	0.89	1.02	0.89
117.96	12.26	1.61×10^{-4}	48.73	0.35	0.14	1.39	0.69	1.22	0.69
235.92	17.33	2.07×10^{-4}	42.80	0.36	0.25	1.11	0.99	0.99	0.86
290.36	19.23	3.17×10^{-4}	107.47	0.40	0.23	1.55	1.00	1.11	0.77
145.18	13.60	3.09×10^{-4}	97.99	0.31	0.22	1.25	0.94	1.25	0.79
190.55	15.58	1.62×10^{-4}	75.70	0.34	0.20	1.23	0.82	1.23	0.82
263.14	18.30	3.09×10^{-4}	163.66	0.52	0.23	0.93	0.70	1.16	0.81
190.55	15.58	1.95×10^{-4}	114.92	0.30	0.26	1.10	0.95	0.95	0.82

A_p	d_{equ}	w	θ	$\frac{\sigma_{major}}{d_{equ}}$	$\frac{\sigma_{minor}}{d_{equ}}$	$\frac{len_v}{d_{equ}}$	$\frac{len_h}{d_{equ}}$	$\frac{max_v}{d_{equ}}$	$\frac{max_h}{d_{equ}}$
254.07	17.99	2.09×10^{-4}	138.88	0.28	0.24	1.18	1.18	0.94	0.94
127.03	12.72	1.69×10^{-4}	67.50	0.22	0.22	1.00	1.00	0.83	0.83
181.48	15.20	1.88×10^{-4}	88.35	0.35	0.19	1.40	0.84	1.40	0.70
190.55	15.58	1.77×10^{-4}	87.49	0.23	0.22	1.10	0.95	0.82	0.82

Table C.2 Summary of the experimental data for Run 4—Effluent (CSDLAC) at $t = 4'30''$.

A_p	d_{equ}	w	θ	$\frac{\sigma_{major}}{d_{equ}}$	$\frac{\sigma_{minor}}{d_{equ}}$	$\frac{len_v}{d_{equ}}$	$\frac{len_h}{d_{equ}}$	$\frac{max_v}{d_{equ}}$	$\frac{max_h}{d_{equ}}$
1615.14	45.35	4.63×10^{-2}	94.12	0.61	0.11	2.39	0.51	2.35	0.43
961.82	34.99	7.12×10^{-3}	59.35	0.53	0.09	1.46	0.55	1.64	0.43
435.54	23.55	6.31×10^{-3}	105.08	0.35	0.19	1.45	0.90	1.26	0.81
571.65	26.98	7.39×10^{-3}	23.34	0.35	0.19	1.42	0.79	1.34	0.71
1488.10	43.53	4.53×10^{-3}	100.11	0.44	0.24	1.72	1.08	1.37	0.98
2341.04	54.60	4.43×10^{-3}	107.12	0.84	0.22	1.37	1.09	1.37	0.19
1424.59	42.59	4.73×10^{-3}	67.44	0.50	0.44	1.75	1.40	1.10	0.75
598.87	27.61	2.98×10^{-3}	147.20	0.42	0.19	1.62	0.93	1.31	0.62
226.85	16.99	3.00×10^{-3}	113.04	0.37	0.22	1.38	1.00	1.00	0.75
263.14	18.30	3.15×10^{-3}	73.04	0.47	0.21	1.51	0.93	1.16	0.70
1161.45	38.46	2.60×10^{-3}	89.30	0.44	0.20	1.44	0.83	1.38	0.72
181.48	15.20	3.29×10^{-3}	58.28	0.26	0.23	1.12	0.98	1.12	0.98
1497.18	43.66	2.27×10^{-3}	58.32	0.29	0.26	1.32	1.12	0.93	0.88
181.48	15.20	1.43×10^{-3}	148.50	0.31	0.22	1.12	0.84	1.12	0.84
1669.58	46.11	2.17×10^{-3}	102.26	0.39	0.19	1.66	0.93	1.48	0.74
499.06	25.21	2.10×10^{-3}	93.00	0.50	0.38	1.52	0.68	0.85	0.76
154.25	14.01	1.43×10^{-3}	87.17	0.28	0.12	1.22	0.61	1.07	0.61
90.74	10.75	1.77×10^{-3}	0.00	0.25	0.10	1.19	0.60	1.19	0.60
1569.77	44.71	2.04×10^{-3}	120.62	0.39	0.19	1.52	0.95	1.43	0.67
1179.59	38.75	1.77×10^{-3}	108.06	0.35	0.21	1.65	0.99	1.43	0.82
235.92	17.33	1.08×10^{-3}	106.74	0.40	0.19	1.60	0.74	1.11	0.74
417.39	23.05	1.54×10^{-3}	100.95	0.41	0.22	1.57	1.01	1.29	0.93
471.84	24.51	2.13×10^{-3}	105.94	0.70	0.13	1.91	0.61	2.09	0.44
81.66	10.20	1.65×10^{-4}	31.72	0.29	0.27	1.25	1.25	1.04	1.04
825.72	32.42	1.76×10^{-3}	97.80	0.30	0.22	1.32	0.92	1.25	0.92
154.25	14.01	1.07×10^{-3}	121.36	0.47	0.21	1.37	0.91	1.37	0.61
898.31	33.82	1.41×10^{-3}	78.63	0.40	0.20	1.38	0.88	1.26	0.75
644.24	28.64	1.19×10^{-3}	137.95	0.25	0.25	1.26	1.19	1.04	1.04
453.69	24.03	1.57×10^{-3}	101.80	0.35	0.19	1.42	0.88	1.33	0.80
145.18	13.60	1.50×10^{-3}	29.14	0.34	0.20	1.41	0.94	1.25	0.94
580.72	27.19	1.15×10^{-3}	32.34	0.44	0.25	1.25	1.10	1.02	0.70
1714.95	46.73	1.29×10^{-3}	79.17	0.34	0.34	1.55	1.41	1.05	1.05
99.81	11.27	1.14×10^{-3}	94.07	0.34	0.23	1.13	0.94	1.13	1.13
281.29	18.92	1.44×10^{-3}	59.45	0.32	0.20	1.24	0.90	1.13	0.79
843.86	32.78	1.04×10^{-3}	147.30	0.42	0.22	1.75	0.85	1.37	0.65
117.96	12.26	1.18×10^{-3}	85.93	0.26	0.25	1.04	1.04	1.04	0.87
925.53	34.33	1.70×10^{-3}	112.58	0.65	0.17	1.24	0.75	1.55	0.44
172.40	14.82	1.03×10^{-3}	11.48	0.38	0.20	1.44	0.87	1.29	0.72
644.24	28.64	1.19×10^{-3}	106.18	0.28	0.23	1.26	1.04	1.12	0.96
689.61	29.63	1.19×10^{-3}	102.58	0.34	0.17	1.51	0.87	1.44	0.72
81.66	10.20	8.02×10^{-4}	13.62	0.26	0.14	1.25	0.83	1.04	0.62
644.24	28.64	8.66×10^{-4}	104.15	0.28	0.23	1.26	1.04	1.19	0.96
154.25	14.01	7.74×10^{-4}	84.69	0.30	0.19	0.91	0.76	0.76	0.76
208.70	16.30	9.40×10^{-4}	110.27	0.26	0.23	1.17	1.04	1.04	0.92
453.69	24.03	7.58×10^{-4}	87.24	0.28	0.22	1.15	0.98	1.07	0.98
99.81	11.27	7.98×10^{-4}	104.94	0.37	0.14	1.51	0.75	1.33	0.75
535.35	26.11	8.47×10^{-4}	130.43	0.37	0.22	1.63	1.06	0.98	0.74
480.91	24.75	9.18×10^{-4}	92.43	0.31	0.21	1.29	0.86	1.29	0.86

A_p	d_{equ}	w	θ	$\frac{\sigma_{major}}{d_{equ}}$	$\frac{\sigma_{minor}}{d_{equ}}$	$\frac{len_v}{d_{equ}}$	$\frac{len_h}{d_{equ}}$	$\frac{max_v}{d_{equ}}$	$\frac{max_h}{d_{equ}}$
190.55	15.58	8.89×10^{-4}	106.75	0.33	0.22	1.37	0.82	1.10	0.82
444.62	23.79	8.92×10^{-4}	67.71	0.52	0.14	1.97	0.62	1.88	0.62
535.35	26.11	7.56×10^{-4}	127.49	0.41	0.19	1.72	0.89	1.38	0.74
136.11	13.16	9.14×10^{-4}	80.78	0.23	0.20	0.97	0.97	0.97	0.81
190.55	15.58	5.64×10^{-4}	87.02	0.55	0.18	1.64	0.82	1.64	0.82
789.42	31.70	7.04×10^{-4}	123.01	0.37	0.19	1.41	0.94	1.27	0.74
117.96	12.26	1.47×10^{-3}	52.36	0.19	0.13	1.04	0.69	1.04	0.69
426.47	23.30	6.22×10^{-4}	55.46	0.49	0.17	1.83	0.92	1.37	0.64
535.35	26.11	8.30×10^{-4}	109.18	0.46	0.14	1.87	0.65	1.55	0.57
508.13	25.44	8.25×10^{-4}	108.10	0.38	0.23	1.67	1.17	1.34	0.75
181.48	15.20	6.14×10^{-4}	5.00	0.33	0.19	1.40	0.84	1.40	0.84
90.74	10.75	8.22×10^{-4}	0.00	0.10	0.10	0.80	0.80	0.80	0.80
508.13	25.44	1.27×10^{-3}	87.93	0.47	0.16	1.76	0.75	1.67	0.58
199.62	15.94	7.52×10^{-4}	91.57	0.62	0.16	1.87	0.80	1.87	0.54
317.58	20.11	8.86×10^{-4}	64.01	0.46	0.16	1.70	0.63	1.49	0.63
372.03	21.76	7.72×10^{-4}	112.99	0.33	0.19	1.37	0.88	1.27	0.79
435.54	23.55	7.38×10^{-4}	151.37	0.31	0.22	1.36	1.00	1.17	0.81
217.77	16.65	8.00×10^{-4}	57.70	0.38	0.22	1.40	0.89	1.28	0.76
326.66	20.39	6.29×10^{-4}	47.27	0.29	0.24	1.15	1.04	1.15	0.94
771.27	31.34	1.46×10^{-3}	133.11	0.42	0.19	1.70	1.02	1.42	0.81
1007.19	35.81	7.24×10^{-4}	107.22	0.49	0.17	1.97	0.83	1.78	0.60
272.21	18.62	7.03×10^{-4}	74.20	0.50	0.28	1.38	1.14	1.14	0.69
254.07	17.99	5.75×10^{-4}	96.51	0.29	0.25	1.30	1.18	1.07	1.07
535.35	26.11	6.24×10^{-4}	45.44	0.31	0.26	1.30	1.14	1.23	0.98
99.81	11.27	6.46×10^{-4}	76.72	0.28	0.28	1.13	1.13	0.94	0.94
127.03	12.72	5.93×10^{-4}	77.80	0.30	0.13	1.34	0.67	1.00	0.50
154.25	14.01	6.19×10^{-4}	129.85	0.39	0.21	1.22	0.91	1.22	0.76
145.18	13.60	6.47×10^{-4}	93.99	0.44	0.20	1.25	0.94	1.41	0.62
172.40	14.82	7.85×10^{-4}	36.09	0.28	0.28	1.15	1.15	1.00	1.00
880.16	33.48	9.02×10^{-4}	87.01	0.42	0.19	1.65	0.89	1.47	0.82
127.03	12.72	8.38×10^{-4}	57.52	0.50	0.22	1.17	1.00	1.34	0.83
190.55	15.58	4.24×10^{-4}	93.51	0.31	0.22	1.23	0.95	1.23	0.82
326.66	20.39	5.06×10^{-4}	127.82	0.31	0.25	1.25	1.04	1.04	0.83
81.66	10.20	4.45×10^{-4}	76.72	0.31	0.28	1.25	1.25	1.04	0.83
108.89	11.77	1.24×10^{-4}	137.65	0.34	0.16	0.90	0.73	1.09	0.73
81.66	10.20	6.19×10^{-4}	67.50	0.29	0.00	1.25	0.42	1.25	0.42
208.70	16.30	5.79×10^{-4}	0.68	0.31	0.23	1.17	0.92	1.17	0.92
508.13	25.44	5.21×10^{-4}	8.46	0.34	0.21	1.25	0.92	1.17	0.75
544.43	26.33	5.54×10^{-4}	68.04	0.43	0.16	1.70	0.81	1.53	0.64
680.53	29.44	5.24×10^{-4}	101.88	0.49	0.19	1.45	0.94	1.52	0.80
208.70	16.30	4.35×10^{-4}	0.00	0.37	0.22	1.57	0.92	1.30	0.92
99.81	11.27	5.30×10^{-4}	55.58	0.35	0.23	1.33	1.13	1.13	0.75
154.25	14.01	5.79×10^{-4}	48.04	0.43	0.12	1.07	0.61	1.07	0.61
353.88	21.23	9.51×10^{-4}	118.05	0.33	0.25	1.40	1.11	1.11	0.90